NAZARBAYEV UNIVERSITY

AIRBORNE PARTICULATE MATTER IN ASTANA, KAZAKHSTAN: POTENTIALLY TOXIC ELEMENTS, LUNG BIOACCESSIBILITY, AND RISK ASSESSMENT

by
Akmaral Agibayeva

Submitted in partial fulfillment

of the requirements for the degree of Doctor of Philosophy in Civil Engineering

February, 2024

AIRBORNE PARTICULATE MATTER IN ASTANA, KAZAKHSTAN: POTENTIALLY TOXIC ELEMENTS, LUNG BIOACCESSIBILITY, AND RISK ASSESSMENT

by
Akmaral Agibayeva

Submitted in partial fulfillment of the requirement for the degree of

Doctor of Philosophy in Civil Engineering

School of Engineering and Digital Sciences

Civil and Environmental Engineering Department

Nazarbayev University

February, 2024

Supervised by

Prof. Mert Guney

Prof. Ferhat Karaca

Prof. Egemen Avcu

Declaration

I declare that the research contained in this thesis, unless otherwise formally indicated within the text, is the author's original work. The thesis has not been previously submitted to this or any other university for a degree and does not incorporate any material already submitted for a degree.

Signature:

Akmaral Agibayeva

Date:

BLANK

Abstract

The degradation of air quality remains one of the most critical environmental concerns. Exposure to airborne pollutants is extensively associated with various health conditions, including respiratory and cardiovascular diseases, and premature death. The health risks of air pollution have been linked to particulate matter (PM) and its constituents. Potentially Toxic Elements (PTEs) in atmospheric PM are a critical factor contributing to its toxicity. This doctoral thesis addresses multiple aspects of air quality in Astana, Kazakhstan, offering a holistic understanding of the local air pollution situation through (1) analysis of PM and gaseous pollutant concentration; (2) proposing a modification to the toxicity assessment of PM-bound PTEs via *in vitro* lung bioaccessibility; (3) the assessment of health risk due to inhalation exposure to PM using bioaccessible concentration of PTEs; (4) morphological characterization of PM; (5) source identification; (6) studying precipitation chemistry and its role in air pollution; and (7) assessment of the public knowledge, perception and attitude towards local air quality in Astana. The methodological framework involved primary data analysis (342 PM samples collected in Astana, Kazakhstan from 2021 to 2023) and air pollution data obtained from monitoring stations located in the city (S1-S6) in 2018-2020. Annual and 24-hour mean concentrations of $PM_{2.5}$, $PM_{2.5-10}$, and gaseous pollutants (SO_2, CO, NO_2, NO, and HF) were, in general, higher than established national and international (World Health Organization (WHO)) maximum permissible levels (e.g., for $PM_{2.5}$ annual mean of 29.7 $\mu g/m^3$ in 2018-2019; and 24-hour mean of 28.7 $\mu g/m^3$ (maximum: 534 $\mu g/m^3$) for $PM_{2.5}$ and 226 $\mu g/m^3$ (maximum: 1,564 $\mu g/m^3$) for $PM_{2.5-10}$, respectively, in 2021-2023). To simulate real-life inhalation exposure to PM-bound PTEs, the assessment was conducted through optimization of *in vitro* lung bioaccessibility testing in simulated lung fluids (SLF) (i.e., modified Gamble's solution (GS) and Artificial Lysosomal Fluid (ALF)). For a modification of commonly established methodology, a large set of PTEs (Cd, Co, Cr, Cu, Mn, Ni, Pb, Sb, V, and Zn) has been investigated using seven distinct formulations of GS, one ALF on two reference materials (SRM 2691 and BGS 102). The bioaccessibility of the selected PTEs generally increased in modified GS with the incorporation of 5% DPPC (phospholipid) (e.g., from 2.87% to 8.35% for V in BGS 102), 0.25% cholesterol (e.g., from 27.3% to 31.5% for Cr in SRM 2691), and 5% DPPC + 0.5% cholesterol (e.g., from 43.5% to 51.5% for Cu in BGS 102). Therefore, using DPPC + cholesterol may be recommended for routine bioaccessibility testing. The effect of the tested solid-to-liquid ratio (S/L) was sample and element-specific. Overall, a lower S/L led to a higher

bioaccessibility % in ALF. For all PTEs, the peak bioaccessibility was reached at a 4-week extraction, suggesting a longer testing duration when feasible. The optimized parameters for *in vitro* bioaccessibility were later applied for inhalation bioaccessibility of selected PTEs (i.e., Cd, Co, Cr, Cu, Fe, Mn, Ni, Pb, V, and Zn) in $PM_{2.5}$ collected in Astana, Kazakhstan. The highest bioaccessible concentration was observed for Fe (mean: 16,229 mg/kg, range: (906-30,419 mg/kg) and V (mean: 10,725 mg/kg, range: (687-27,092 mg/kg). The inhalation Health Risk Assessment (HRA) using a bioaccessible concentration of PTEs in $PM_{2.5}$ revealed acceptable carcinogenic and non-carcinogenic risks for adult and children exposure, although the maximum Cancer Rate (CR) for adults was slightly higher (1.01×10^{-6}) than the established United States Environmental Protection Agency (U.S. EPA) threshold ($HIc > 1 \times 10^{-6}$). Scanning Electron Microscopy (SEM) analysis determined several major PM particle groups, including bioaerosols, coal fly ash (CFA), dust (natural or construction), and soot particles. Irregularly shaped, small-sized particles of CFA are associated with respiratory conditions and neurodevelopmental disorders, while soot particles of complex shapes can penetrate deeply into the respiratory system. In precipitation analysis, the mean concentration of major ions (i.e., F^-, Cl^-, NO_2^-, NO_3^-, SO_4^{2-}, PO_4^{3-}, K^+, Na^+, NH_4^+, Ca^{2+}, Mg^{2+}) remained within permissible levels for groundwater, drinking, and surface water. However, in April, the highest F^- concentration (1.82 mg/L) exceeded the WHO limit for drinking water (1.5 mg/L). The concentration of most heavy metals (i.e., Cd, Co, Cr, Cu, Mn, Pb) was below WHO's maximum permissible levels, except for V, which exhibited the highest average concentration of 108 µg/L in precipitation samples across four seasons. The chemical analysis of PM and precipitation revealed common sources, including coal/liquid fuel combustion and vehicular exhaust. $PM_{2.5}$ concentration modeling via Multiple Linear Regression (MLR) and Machine Learning (ML) Random Forest (RF) algorithms revealed PM_{10} and CO as major predictors of $PM_{2.5}$ concentration. A real-life pollution scenario using Conditional Bivariate Probability Function (CBPF) analysis also suggested a substantial contribution of coal-heated power plant activity (CHPPs) and coal combustion from residential heating, coupled with emissions from internal combustion engine vehicles. Structural equation modeling (SEqM) was employed to investigate the causal relationship between perceived air quality, environmental literacy, and willingness to pay (WTP) for environmental protection. The age, education, and health status of the participants significantly affected ($p < 0.001$) their level of environmental knowledge and awareness. The SEqM analysis indicates that knowledge is the major determinant in improving public awareness and perception of local air pollution (path value = 0.626). The findings of the current research

work can assist healthcare professionals and environmental researchers in public health-related decision-making and establishing feasible air quality guidelines.

Acknowledgments

I would like to express my sincere gratitude to the incredible people whose support and encouragement helped me to reach this milestone:

To my supervisor, Prof. Mert Guney, whose guidance, patience, and unique teaching method made me the professional I am today. Your insights, experience, work ethic, and personality made all the difference. I would like to thank my internal supervisor, Prof. Ferhat Karaca, for the guidance, support, and strong belief in my abilities. I also express my gratitude to my external supervisor, Prof. Egemen Avcu, who navigated me professionally throughout my Ph.D. journey. I express particular gratitude to our head of department, Prof. Jong Kim, who gave me the opportunity to be a part of the Department of Civil and Environmental Engineering and for being a great example of leadership.

The biggest shoutout goes to my husband, Olzhas, for being my rock. Your love, constant support, and belief in me got me through the multiple challenges I faced along the way. I would not have made it without you.

I am endlessly grateful to my parents for showing me that education is a hard one but the most valuable asset and that knowledge is the only thing no one can take from you. I would like to extend a special thanks to my sister, Madina, for being my constant inspiration and giving me emotional strength through this academic journey.

I want to thank my mother-in-law for her support and help throughout my graduate program, especially during the first part of my Ph.D. studies.

I would like to thank my son, who, without realizing it, is my biggest motivation and whose curiosity has no limits. I also apologize for working sometimes when you asked me to play instead.

Thanks to all my students, who taught me as much as I taught them and who gave me the motivation to continue my work.

I would like to give special thanks to my colleagues, who became my closest friends.

Lastly, a big thanks to my dearest friends who I was lucky to have beside me.

Contents

BLANK

LIST OF TABLES

LIST OF FIGURES

LIST OF SYMBOLS

***In vitro* lung bioaccessibility**

m_{bio} Bioaccessible mass

C_{bio}	Bioaccessible concentration

Conditional Bivariate Probability Function (CBPF)

$\Delta\theta$	Wind sector
Δu	Wind speed interval
C_i	Pollutant concentration
r	Wind speed
θ	Wind direction
β_0	The overall mean of response
s	Isotropic smooth function
$u_i \; and \; \vee_i$	Wind covariates
$\overline{u}$	Mean wind speed
ε_i	The *i*th residual
r	Correlation coefficient

PM concentration prediction model

Δx	The concentration difference between the observed $PM_{2.5}$ and the threshold level
$PAF_{i,g}$	Population attributable fraction of disease or disability group *i* for a population group *g*
$RR_{i,g}$	Population attributable fraction of disease or disability group *i* for a population group *g*
β	Exposure-response coefficient

Knowledge, Perception and Attitude (KAP) about air pollution

χ^2	Chi-squared statistic

LIST OF ACRONYMS AND DEFINITIONS

A

AC	Acenaphthene
ACY	Acenaphthylene
ADD	Average daily dose
ALF	Artificial Lysosomal Fluid
ANN	Artificial neural networks
ANTH	Anthracene
API	Air pollution index
ARIMA	Autoregressive integrated moving average
AT	Average time
ATP	Adenosine triphosphate
B	
B[a]A	Benzo[a]anthracene
B[a]P	Benzo[a]pyrene
B[b]F	Benzo[b]fluoranthene
B[k]F	Benzo[k]fluoranthene
B[ghi]P	Benzo[g,h,i]perylene
BEAS-2B	Human bronchial epithelial cell line
BSA	Bovine serum albumin
BTEX	Benzene, toluene, ethylbenzene, and xylene
C	
CBF	Conditional Bivariate Function
CBPF	Conditional Bivariate Probability Function
CC-SEM	Computer-controlled SEM
CFA	Coal fly ash
CSF	Cancer slope factor
CHPP	Coal-heated power plant
CHRY	Chrysene
CMB	Chemical Mass Balance
COHb	Carboxyhemoglobin
COPD	Chronic obstructive pulmonary disorder
CR	Carcinogenic risk

CV	Cross-validation
CV-MSE	Cross-validation of mean squared error
CXCL8	Interleukin 8
CYPs	Cytochromes P450 proteins
D	
D[ah]A	Dibenz[a,h]anthracene
DCFH-DA	Dichlorodihydrofluorescein diacetate
DFC	Dichlorodihydrofluorescein
DI	Deionized water
DL	Detection limits
DPPC	1,2-dipalmitoyl-sn-glycero-3-phosphocholine
E	
EC	Electrical conductivity
EC	Exposure concentration (may be abbreviated as ECON or Econ)
ED	Exposure duration
EDS	Energy-dispersive X-ray spectroscopy
ED-XRF	Energy dispersive X-ray fluorescence
EF	Enrichment factor (If crustal add *c* as subscript (EF_c)
EF	Exposure frequency
F	
FE-SEM	Field-Emission SEM
FLTH	Fluoranthene
FLU	Fluorene
FTIR	Fourier-transform infrared spectroscopy
G	
GS	Gamble's solution
Gpx	Glutathione peroxidase
GR	Greatest repeatability
H	
HA	Hyaluronic acid

HHRA	Human Health Risk Assessment
HBE	Human bronchial epithelial cell line
HI	Hazard index
HO-1	Heme oxygenase 1
HPB	High blood pressure
HQ	Hazard quotient
I	
IA	Index of agreement
IC	Ion chromatography
ICP	Inductively coupled plasma
ICP-MS	Inductively coupled plasma mass spectrometry
ICP-OES	Inductively coupled plasma-atomic (optical) emission spectroscopy
IL-1β	Interleukin-1β
IL-6	Interleukin-6
IND	Indeno[1,2,3-*c,d*]pyrene
IUR	Inhalation unit risk
J	
J774 cell	Macrophage-like J774 cell lines
K	
KAP	Knowledge, perception and attitude
L	
LCR	Lifetime cancer risk
M	
MAE	Mean absolute error
MCI	Monthly calculation index
MCS	Monte Carlo simulation
ML	Machine learning
MLR	Multiple linear regression
N	
NAD(P)H	Nicotinamide adenine dinucleotide phosphate

NAP	Naphthalene
ND	Natural dust
NME	Normalized mean error
NME	Normalized mean error
NMR	Nuclear Magnetic Resonance spectroscopy
NO·	Nitric oxide radical
NQO1	NAD(P)H quinone oxidoreductase 1
Nrf2	Nrf2 signaling pathway
P	
PA	Atmospheric pressure
PA	Prediction accuracy
PAF	Population attributable fraction
PCA	Principal component analysis
PGE	Platinum group elements
PHEN	Phenanthrene
PM	Particulate Matter
PMF	Positive matrix factorization
PTE	Potentially Toxic Elements
PTFE	Polytetrafluoroethylene
PVDF	Polyvinylidene fluoride
PYR	Pyrene
R	
RAW 264.7	Murine macrophage cell line
RF	Radiofrequency coil
RF	Random forest
RH	Relative humidity
RMSE	Root mean square error
ROS	Reactive oxygen species
RR	Relative risk

RSD	Relative standard deviation
S	
SA	Source apportionment
SELF	Simulated Epithelial Lung Fluid
SEM	Scanning Electron Microscopy
SEqM	Structural Equation Modeling
SLF	Simulated lung fluid
S/L ratio	Solid-to-liquid ratio
SODs	Superoxide dismutases
SR-XRF	Synchrotron radiation XRF
SRM	Standard Reference Material
T	
T	Temperature
TEM	Transmission Electron Microscopy
TNF-alpha	Tumor Necrosis Factor alpha
TSP	Total suspended particles
V	
VIF	Variance inflation factor
W	
WD-XRF	Wavelength dispersive XRF
WD	Wind direction
WHO	World Health Organization
WS	Wind speed
WTP	Willingness-to-pay
X	
XRD	X-ray Diffraction
XRF	X-ray fluorescence
XPS	X-ray spectrometry
Y	
YLD	Years of Life Lost due to Disability
YLL	Years of Life Lost due to premature death

CHAPTER 1: INTRODUCTION

1.1. Research background and novelty

Atmospheric particulate matter (PM) can be described as an aerosol comprised of small solid or liquid particles of varying sizes and chemical compositions. It is widely accepted that PM quantity and quality are critical indicators of the air pollution problem. The presence of PM in the air may compromise human health and ecosystem stability, induce changes in weather patterns and the climate, and impair atmospheric visibility (IPCC, 2013). Depending on the formation mechanism, PM can be categorized as either primary (directly emitted by a source) or secondary (formed in the atmosphere through chemical reactions) and may experience additional changes in their physicochemical properties. The critical parameter that influences its fate in the atmosphere and during human exposure is the particle size, which is often characterized by aerodynamic diameter (d) corresponding to the actual diameter of a perfect sphere particle with unit density exhibiting the same aerodynamic properties. U.S. Environmental Protection Agency (U.S. EPA, 1999b) defines airborne particles with d less than 100 μm as total suspended particles (TSP), which can be further classified as PM_{10} (d less than 10 μm), coarse PM (d in the range of 2.5-10 μm), $PM_{2.5}$ or fine PM (d less than 2.5 μm), and $PM_{0.1}$ or ultra-fine PM (d less than 0.1 μm) (de Kok et al., 2006).

Many countries put an upper limit on the allowable PM mass concentration levels, including both PM_{10} and $PM_{2.5}$, as a response to public concerns and numerous literature confirming the adverse health effects of PM. According to the estimates presented by Chuang et al. (2011), approximately 2.1 million deaths are a direct result of exposure to

fine PM. The list of human health effects caused by airborne PM includes but is not limited to, chronic lung and cardiovascular diseases, nonlethal heart attacks, asthma, limited lung function, and breathing difficulties (Kim et al., 2015). In 2015, the International Agency for Research on Cancer (IARC) expert board on outdoor air pollution unanimously decided to include PM in the group of carcinogenic air pollutants (Loomis et al., 2013). Though the direct correlation between PM levels and adverse health impact is established, the knowledge of the exact ways atmospheric particulate matter affects human health is still limited.

One of the major determinants of PM toxicity is the physicochemical characteristics of the particles. Physical characteristics, including particle size, shape, surface area, and solubility, determine the toxicity level induced by PM exposure. Finer PM fractions have shown more significant deposition in the respiratory tract and the ability to penetrate deeper into the alveoli (Farina et al., 2011; Kelly & Fussell, 2012), resulting in accumulation of reactive oxygen species (ROS) and induction of oxidative stress. PM can also cause systemic inflammation by increasing the number of inflammatory markers and inflammatory cells (e.g. lymphocytes and macrophages) (Pardo et al., 2020; Ren et al., 2020; Wu et al., 2018; Yang et al., 2018). Chemical composition is another critical parameter contributing to PM toxicity. Potentially toxic elements (PTEs) (e.g. heavy metals) in the PM matrix reduce cell viability (Feng et al., 2020; Figliuzzi et al., 2020; Pardo et al., 2020) by disrupting cellular functions and inducing inflammatory response and apoptotic mechanisms (Figliuzzi et al., 2020; Jan et al., 2020; Könczöl et al., 2011).

When assessing the health risks associated with PM-bound PTEs health assessors traditionally rely on total PTEs concentrations which can lead to an overestimation of health impact (Guney et al., 2017; Liu et al., 2019). Recent methodology, commonly known as *in vitro* bioaccessibility, involves the estimation of the bioavailable fraction of a contaminant accessible for uptake in the respiratory system which can provide a more accurate risk evaluation (Guney et al., 2017). Physiologically based conditions in the human body are reproduced using simulated lung fluids (SLFs), such as Gamble's solution (GS) and artificial lysosomal fluid (ALF) (Ren et al., 2020). The wide range of SLF composition, applied physiological parameters and contaminant mobilization factors emphasize the need for a standardized lung bioaccessibility protocol for measuring elemental solubility in SLFs.

In Kazakhstan, rapid population growth, fast economic development, and resource exploration have led to the deterioration of air quality. In 2019, Kazakhstan was ranked 29th among the world's most polluted countries. Moreover, the National Air Quality Monitoring System lacks publicly available air monitoring data for the majority of Kazakhstani cities. Most cities in Kazakhstan exceed the annual air pollution permissible level established by the World Health Organization's (WHO) guidelines (Assanov et al., 2021). Astana, the capital city of Kazakhstan, is characterized by severe climate conditions with prolonged and harsh winters, resulting in a six-month-long heating season. Elevated levels of air pollutants (e.g., PM, SO_2, NO_2, CO) are frequent during the heating period. For instance, $PM_{2.5}$ concentrations can reach between 100-200 μg/m^3 on winter days (Assanov et al., 2021). The estimated annual premature mortality rate related to PM exposure in Kazakhstan is 8,134 cases (Kerimray et al., 2020).

The prior studies conducted in Kazakhstan on air quality include transportation-related air emissions in Almaty (Carlsen *et al.,* 2018); tropospheric NO_2 concentrations based on satellite measurements (Darynova *et al.,* 2018); benzene, toluene, ethylbenzene, and xylene (BTEX) concentrations and ratios in Almaty (Baimatova *et al.,* 2016); availability and quality of air pollution data in Kazakhstan (Russell *et al.,* 2018); and, general pollution characterization in Almaty (Nazhmetdinova *et al.,* 2017). Kerimray et al. (2018) established the relationship between the recent increase in the population of Astana. Baimatova (2014) studied the concentrations of 16 priority Polycyclic Aromatic Hydrocarbons (PAHs), selected heavy metals, and inorganic salts on the PM in Almaty. Adil'bayeva et al. (2016) estimated the prevalence of air pollution using data from geochemical snow surveys. Lyu et al. (2018) determined the main indicators of atmospheric air pollution in different districts of Almaty. Kerimray *et al.,* 2020 addressed the impact of COVID-19 restrictions on the air pollution levels of Almaty. The current research work is a comprehensive analysis of air quality in Astana, Kazakhstan, investigating multiple aspects in air pollution, that have not been done in prior literature. Moreover, modifications to the proposed *in vitro* lung bioaccessibility will assist in a more accurate estimation of PM toxic potential.

1.2 Aim and objectives

The objectives of this thesis project include:

1) to evaluate spatial and temporal variations of $PM_{2.5}$, $PM_{2.5\text{-}10}$, PM_{10}, SO_2, HF, CO, NO, and NO_2 in Astana, Kazakhstan (October 2018 – May 2023) and suggest MLR and RF-based pollutant concentration prediction models.

2) to enhance *in vitro* method for the estimation of lung bioaccessibility of selected PTEs by conducting *in vitro* experiments using modified SLFs (GS and ALF) and two SRMs (SRM 2691 and BGS 102);

3) to assess human health risks associated with PM exposure through analysis of the link between health risk and PM morphology; calculation of DALYs and application of U.S. EPA framework for inhalation risk assessment due to $PM_{2.5}$ exposure using bioaccessible concentration of PTEs;

4) to evaluate the dispersion patterns of pollutant levels and suggest potential air pollution emission sources via CBPF, morphological characterization, and precipitation analysis;

5) to evaluate the relationship between knowledge, perception, and attitude of Astana's general public towards local air quality via structural equation modeling (SEqM) approach.

The major research questions of the thesis are "What is the current state of air quality in Astana and is it associated with any adverse health effects?"

1.3 Research significance

The current dissertation is an interdisciplinary analysis of air quality in Astana, Kazakhstan. While prior local studies provided valuable insights into PM mass concentration, pollutant distribution, and potential emission sources, this work extends beyond by comprehensively addressing multiple dimensions of air pollution in the region. Due to the large dependence on coal combustion in energy production of

Kazakhstani cities coupled with the issue of limited air quality monitoring and management framework, it is imperative to conduct a comprehensive PM characterization and health risk assessment in the region. Moreover, the current dissertation covers the topic of elemental solubility of PM-bound in lung fluids and suggests potential modifications to the existing *in vitro* bioaccessibility method. The available literature on PM bioaccessibility from various emission sources remains limited, and lacking in Kazakhstan, emphasizing the significance of further research in this area. The bioaccessibility data was further utilized for inhalation health risk assessment which will aid health professionals, policymakers, and governmental institutions in making informed decisions for proactive air pollution mitigation strategies. Moreover, the current work includes the forecasting of PM concentration in Astana, Kazakhstan, and source apportionment, which is valuable for the region of limited publicly available air monitoring data. Lastly, the focus is driven not only to the estimation of the level of ambient air pollutants and related environmental effects but also to the social aspect of air pollution-related topics which is usually neglected. In Kazakhstan, the level of knowledge and awareness among the general public about air pollution may remain considerably low. The findings of the current dissertation are expected to assist healthcare professionals, environmental researchers, and governmental institutions in evaluating the decision-making process concerning healthcare, disease prevention, and health promotion in Astana's urban population.

1.4 Outline

Chapter 1 consists of the background of the research, objectives, and significance of the Thesis. The rest of the thesis is organized as follows:

Chapter 2 consists of a literature review on the physicochemical characteristics of PM and selected PM characterization techniques and toxicological analysis.

Chapter 3 describes the applied methodology including *in vitro* lung bioaccessibility, human health risk assessment (HHRA), PM morphological analysis, PM source identification, and population survey on local air quality.

Chapter 4 presents the results and discusses the findings of the particulate air pollution analysis. It includes findings on the solubility of PTEs in lung fluid, analysis of carcinogenic and non-carcinogenic health risks utilizing bioaccessible PTEs concentration, Scanning Electron Microscopy (SEM) micrographs of PM particles and source identification, PM concentration forecasting results, and findings from Structural Equation Modeling (SEqM) analysis for. The identification of leading factors in population awareness about air pollution.

Chapter 5 includes conclusions of the current thesis, as well as limitations and recommendations for future research.

CHAPTER 2: LITERATURE REVIEW

2.1 Physicochemical characteristics and common sources of PM

Contemporary epidemiological research faces the challenge of establishing causal relationships between the elemental composition of PM, cellular processes, and the progression of related health conditions (Vargas Buonfiglio & Comellas, 2020). Consequently, toxicological investigations can complement these studies by offering insights into the mechanisms that underlie observed health effects (Akhtar et al., 2011). Studies on PM toxicity suggest that airborne particles have the capacity to induce a cellular response by elevating the levels of reactive oxygen species (ROS), disrupting cellular oxidative potential, and inducing oxidative stress (Pardo et al., 2020; Ren et al., 2020; Wu et al., 2018; Yang et al., 2018) (Figure 2.1).

Furthermore, exposure to PM is associated with increased production of inflammatory markers and the buildup of inflammatory cells (e.g., eosinophils, neutrophils, macrophages, and lymphocytes) (Cáceres et al., 2020; Chan et al., 2019). The health hazard posed by atmospheric particulates is linked to both their physical attributes and chemical makeup (Bakand et al., 2012). Although the chemical toxicity of PM has been thoroughly studied, less emphasis has been put on the effect of the physical properties on the biological response to the exposure.

2.1.1 Cytotoxic and inflammatory potential of different size fractions of PM

Fine fractions of PM (e.g., $PM_{2.5}$, $PM_{0.1}$) are suggested to exhibit a higher toxic potential due to their ability to deeply penetrate the pulmonary alveoli and persist in the

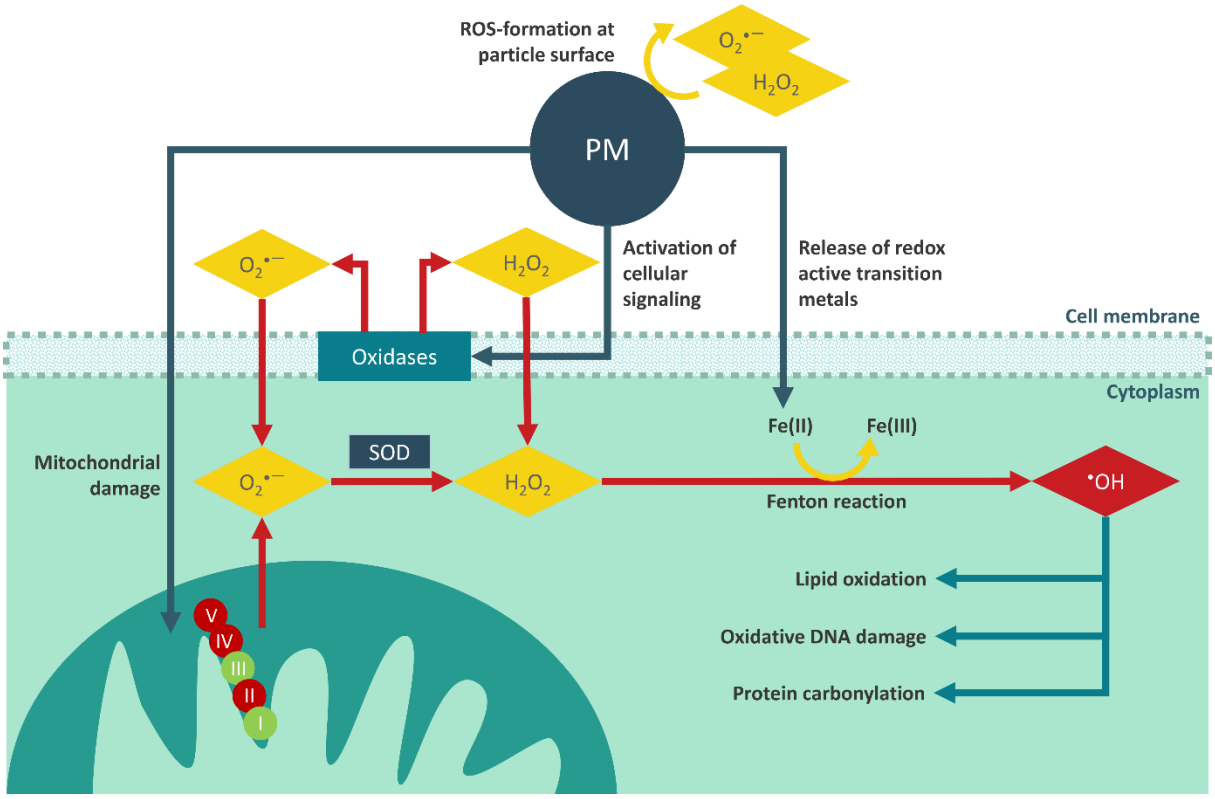

Figure 2.1: The cellular response model to PM exposure entails that PTEs bound to PM trigger the generation of free radicals through the Fenton reaction. This leads to the initiation of cellular signaling pathways, ultimately resulting in damage to both cellular and mitochondrial structures. The free radical defense mechanism involves the activation of NAD(P)H quinone oxidoreductase 1 (NQO1) and cytochromes P450 (CYPs) proteins (adapted from Yadav & Phuleria, 2020)

respiratory system (Farina et al., 2011; Kelly & Fussell, 2012). Additionally, although smaller particles increase the overall particle count, they do not contribute substantially to the total particle mass. This characteristic is more associated with larger particulates (Cassee et al., 2013; Kelly & Fussell, 2012). Exposure to fine PM increases plasma viscosity leading to acute cardiovascular events (e.g., myocardial infarction) (Aztatzi-Aguilar et al., 2018; Farina et al., 2011). Finer particles also induce greater

inflammatory response per unit particle mass due to larger surface area, higher reactivity, content of organic carbon and s, and high surface area to volume ratio (Aztatzi-Aguilar et al., 2018; Xue et al., 2019). The formation of particle aggregates results in phagocytic dysfunction of alveolar macrophages, and infiltration into the lower respiratory tract (Bakand et al., 2012). Extensive research has consistently highlighted the increased inflammatory potential of $PM_{2.5}$ in comparison to larger size fractions (Cassee et al., 2013; Feng et al., 2020; Kelly & Fussell, 2012). The study by Thomson et al. (2015) documented an inflammatory response triggered by $PM_{0.5\text{-}2.5}$ in macrophage-like J774 cell lines. Furthermore, both short-term and prolonged exposure to $PM_{2.5}$ and $PM_{0.1}$ can activate the Nrf2 molecular pathway, signifying the presence of oxidative stress, which was not evident for coarse PM fractions (Aztatzi-Aguilar et al., 2018).

The lower toxic potential of larger particles can be explained by general unresponsiveness due to the clearance mechanisms (Aztatzi-Aguilar et al., 2018) and deposition in the upper portion of the respiratory tract (e.g., bronchial tree) (Guney et al., 2016). However, investigation of PM-induced cytotoxic effects revealed that accumulation of tumor necrosis factor-α (TNF-alpha) (an inflammatory mediator) after PM_{10} exposure was notably higher than $PM_{2.5}$, indicating greater inflammatory response (Farina et al., 2011; Jan et al., 2020). Moreover, a study conducted by Aztatzi-Aguilar et al. (2018) found an association between the highest expression of heme oxygenase 1 (HO-1), an antioxidant enzyme serving as a cellular oxidative stress marker, with PM_{10} exposure. Additionally, Huang et al. (2011) reported that exposure to $PM_{2.5\text{-}10}$ resulted in

a more distinctive gene expression pattern, whereas patterns observed with $PM_{2.5}$ and $PM_{0.1}$ exposures showed similarities.

2.1.2 Relation of particle morphology to the toxic potential of PM

Morphological features of PM particles are among the crucial determinants of PM-induced cytotoxic effect. Primary particles are classified into the following structures: (i) shell-core structure with multiple spherical nuclei concentrically oriented making up the "outer core" and "inner core" with randomly oriented layers; (ii) turbostratic structure with nonaligned basal planes; (iii) purely turbostratic structures and (iv) fullerenoid (onion-shaped) structures (Ghadikolaei et al., 2020; Wang et al., 2020) (Figure 2.2). The ability of particulates to exhibit not only distinct morphologies but also assemble into chain-like or grain-like structures has been well documented in the literature (e.g., soot from diesel exhaust) (Ault et al., 2012; Qian et al., 2020; Wang et al., 2020).

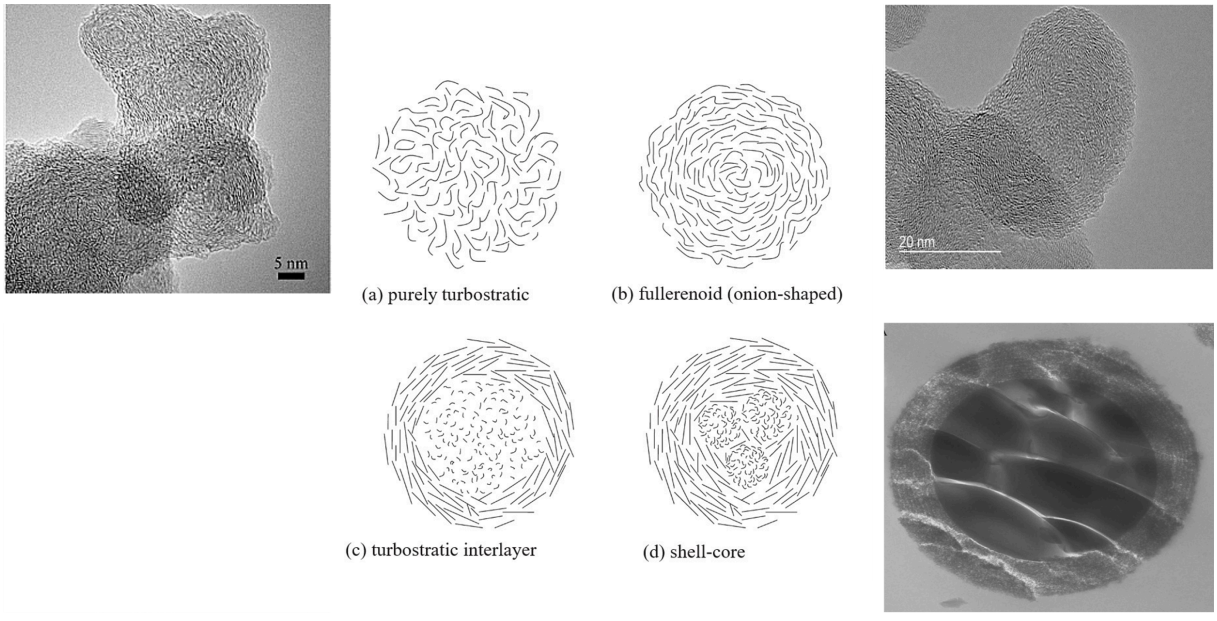

Figure 2.2: Simplified diagram depicting the internal structure of primary particles and TEM images of selected structures (Reproduced from Zhou et al., 2015 with permission from *Applied Energy;* Reproduced from Zhou et al., 2015 with the permission of *The Journal of Geophysical Research;* Gritti et al., 2010 with the permission of *The Journal of Chromatography A*; Ghadikolae et al., 2020 with the permission of *Fuel)*.

Typically, anthropogenic combustion processes at high temperatures, such as industrial combustion, generate spherical particles (González et al., 2017). A recent review, Wang et al., 2020, explored the interactions of barrel-, disk-, and rod-shaped particles with cellular structures. The review highlighted that barrel- and disk-shaped micro/nanoparticles can interfere with the structure of the 1,2-dipalmitoyl-sn-glycero-3-phosphocholine (DPPC) monolayer, the primary phospholipid of pulmonary surfactant (Figure 2.3). Barrel-shaped particles, due to their larger contact area, can induce more structural damage to the lung surfactant. In contrast, rod-shaped particles disrupt alveolar structure by penetrating more effectively,

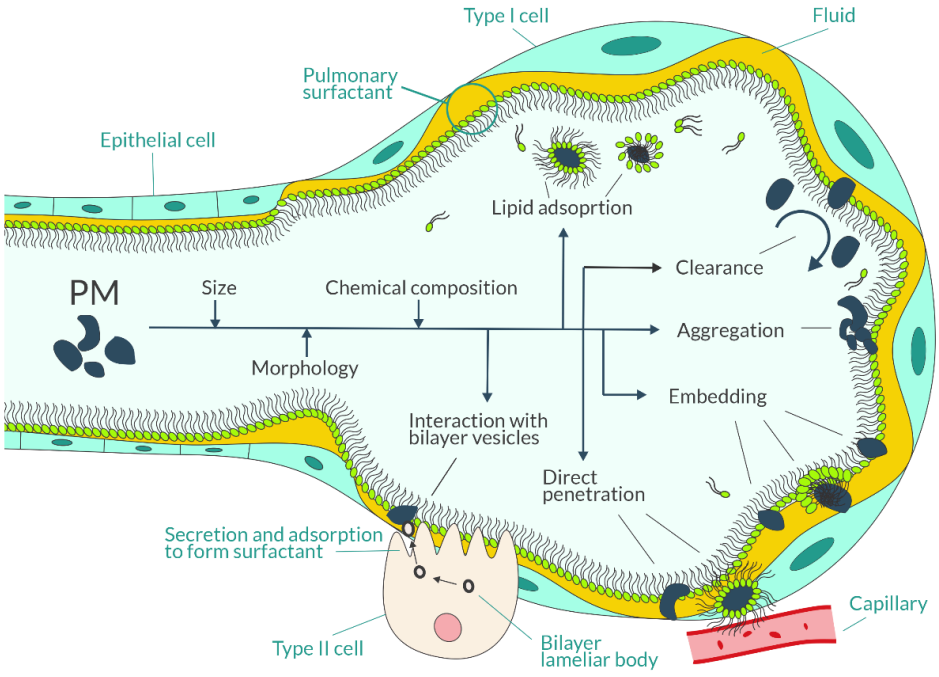

attributed to their higher length-to-diameter **Figure 2.3**: The internal structure of alveolar Type II cells. The primary function of Type II cells is the synthesis of protein and lipid molecules for pulmonary surfactant, with DPPC being the major phospholipid. The interaction

between lung surfactant and PM particles is influenced by the physical and chemical attributes of the particles, including their morphology, size, and chemical composition. PM can infiltrate alveoli either as singular particles or in aggregated form, leading to the disruption of cellular structure through direct penetration or the formation of a particle–bilayer vesicle complex. Following penetration, PM may further invade capillaries (Adapted from Wang et al., 2020).

ratio. Moreover, capillary force is proposed as a determinant of particle dynamics and disruption to pulmonary surfactant. Morphological features, such as sharp edges, surface defects, and fractures, enhance capillary force, influencing particle reactivity and potential toxicity (Fubini et al., 2007). Cylindrical or cubical particles, with their pinned air–water interface line at the edges, tend to exert higher capillary force (Chatterjee et al., 2013). Particulate-induced mechanical action contributes to mitochondrial damage, initiating cellular pathways that disrupt metabolic activity and inhibit ATP synthesis. Irregularly shaped particles further compromise cellular structure by damaging membranes and organelles (Wu et al., 2020). Particle accumulation disrupts pulmonary clearance, potentially causing indirect toxicity through prolonged contact with PM's toxic components and the subsequent cellular response.

2.1.3 Elemental composition as a factor influencing PM toxicity

The cytotoxic potential of PM fractions is associated not only with size and morphological characteristics but also with the chemical composition of particulates.

2.1.3.1 Potentially toxic elements (PTEs)

It has been proposed that PM exposure leads to cellular inflammation mediated by PTEs (Li et al., 2018; Niu et al., 2019; Vargas Buonfiglio & Comellas, 2020). PTEs penetrate cell membranes through mechanisms such as facilitated diffusion and transport, inducing an inflammatory response characterized by elevated

pro-inflammatory markers such as Interleukin-6 (IL-6), Interleukin1β (IL-1β), TNF-α, and Interleukin 8 (CXCL8) (Feng et al., 2020; Michael et al., 2013; Niu et al., 2019; Ren et al., 2020). Metal-induced oxidative stress is indicated by decreased antioxidant capacity, including superoxide dismutases (SODs), catalase, and glutathione peroxidase (Gpx) (Chan et al., 2019; Michael et al., 2013; Pardo et al., 2020).

Several studies report a negative correlation between cell viability and metal(-loid)s. For example, Pb disrupts cell function by mimicking Ca, inhibiting enzyme activity, and showing a significant positive correlation with increased nitric oxide radical ($NO^{\cdot}$) that triggers cell toxicity (Könczöl et al., 2012; Feng et al., 2020; Pardo et al., 2020; Niu et al., 2019). Ni toxicity is attributed to its higher binding capacity in enzymes and proteins, impairment of mitochondrial function, and induction of cell apoptotic mechanisms (Jan et al., 2020). Cu in $PM_{2.5}$ increases the expression of pro-inflammatory cytokine genes, indicating a cellular response to ROS accumulation (Figliuzzi et al., 2020), and Ni and Cu are linked to the accumulation of HO-1 (Heme oxygenase 1) (Li et al., 2018). Fe-containing particles exhibit cytotoxic and genotoxic effects by disrupting DNA and mitochondrial function, producing NO and OH radicals in lung epithelial cells (Jan et al., 2020; Ma et al., 2015). V, Cr, Mn, Cd, and Sb are reported to damage DNA plasmids (Michael et al., 2013; Xiao et al., 2014), while As and Zn are associated with the production of IL-8, indicating a pro-inflammatory response (Michael et al., 2013). Disruption in Zn homeostasis is proposed to contribute to endosomal membrane destabilization and cell apoptosis (Könczöl et al., 2012).

2.1.3.2 Toxic organic compounds in airborne particles

Organic compounds (e.g., PAHs, phenols, and atmospheric humic-like substances) constitute a substantial portion of PM (Pardo et al., 2020). PAHs, along with their atmospheric oxidation products (NPAHs and OPAHs), are recognized for their carcinogenic and mutagenic properties (Kitanovski et al., 2020; R. Li et al., 2015; Michael et al., 2013; Pehnec et al., 2020). The U.S. EPA designates 16 priority PAHs, including naphthalene (NAP), acenaphthylene (ACY), acenaphthene (ACE), fluorene (FLU), phenanthrene (PHEN), anthracene (ANTH), fluoranthene (FLTH), pyrene (PYR), benzo[a]anthracene (B[a]A), chrysene (CHRY), benzo[b]fluoranthene (B[b]F), benzo[k]fluoranthene (B[k]F), benzo[a]pyrene (B[a]P), benzo[g,h,i]perylene (B[ghi]P), indeno[1,2,3-*c,d*]pyrene (IND), and dibenz[a,h]anthracene (D[ah]A) (Akhbarizadeh et al., 2021; R. Roy et al., 2019). Benzo[a]pyrene (B[a]P), in particular, exhibits potent mutagenic activity (Michael et al., 2013; D. Wu et al., 2018). PAHs originate from both natural (e.g., volcanic eruption, biomass burning) and anthropogenic sources (e.g., vehicle exhaust, industrial activity, oil manufacturing, domestic heating, waste incineration, coal burning, etc.) (Pehnec et al., 2020). Low-temperature processes like biomass burning emit low molecular weight PAHs, while high-temperature anthropogenic activities, including thermal power plants and fuel combustion, generate high molecular weight PAHs (Ari et al., 2020; Pehnec et al., 2020).

The toxicity of PAHs is associated with the reduction of mitochondrial membrane potential, disruption of cellular metabolic processes, genotoxic potential, and induction of oxidative stress through ROS generation (R. Li et al., 2015). Due to their lipophilic nature, PAHs can permeate the cell membrane, undergoing metabolism into quinones

and subsequently semiquinones as part of the cellular defense mechanism. Redox cycling, wherein semiquinones are reduced back into quinones, leads to increased accumulation of ROS. PAH exposure induces the buildup of pro-inflammatory markers, including Interleukin-6 (IL-6), Interleukin1β (IL-1β), TNF-α, and HO-1. Furthermore, PAH-induced activation of Nrf2 suggests oxidative stress. In vivo studies also report increased proliferation of proinflammatory T cells and dendritic cells (Pardo et al., 2020).

Chromatography-based techniques are commonly employed for PAH quantification (Akhbarizadeh et al., 2021; R. Roy et al., 2019), while Nuclear Magnetic Resonance spectroscopy (NMR) and Fourier-transform infrared spectroscopy (FTIR) spectroscopy are applied for composition analysis. However, these techniques require large sample amounts and offer limited time and size resolution. A combined approach involving gas/liquid chromatography and mass spectrometry is recommended for comprehensive PAH characterization (Maceira et al., 2020).

2.2 Source analysis of PTEs in PM

Source apportionment (SA) are technique applied to determine the contribution of a particular pollution source to the level of ambient air pollution (Belis et al., 2014). It is a valuable quantitative method that enables the implementation of air quality management strategies. According to Hopke et al. (2020), major source types for PM include secondary inorganic species, natural soil and desert dust, sea salt, traffic emissions, industry, biomass burning, fossil fuel, coal, and oil combustion, and others. Mathematical modeling techniques for the identification of specific sources of airborne pollutants have been thoroughly used in numerous studies (Jan et al., 2020; Landis et al.,

2017; Ramírez et al., 2020; Sharma & Mandal, 2017). The most commonly applied modeling equations include enrichment factor (EF_c), principal component analysis (PCA), positive matrix factorization (PMF), and chemical mass balance (CMB) (Popoola et al., 2018).

Identifying enriched PTEs in PM may assist in providing a more accurate risk assessment for human exposure. The EF_c method identifies potential anthropogenic impact from contaminants by comparing the atmospheric concentration of a specific pollutant with its expected background proportions (Bern et al., 2019).EF_c>1.5 can be an indication of anthropogenic influence (Barbieri, 2016). Multivariate models that allow the estimation of the number of sources, the composition profile, and source contribution estimations of measured PM are commonly referred to as factor analysis. These include PCA and the more recent method of PMF (Mircea M et al., 2020). PCA identifies principal components or the direction of maximal data variation. This mathematical algorithm gives a visual representation of the samples and allows group categorization based on their similarities and differences (Ringnér, 2008). PMF is a receptor model that identifies the contribution of a particular source to the measured ambient pollutant concentration. Source profile and estimates of source contribution are determined by the elemental concentration of the sample and associated uncertainties (Hopke et al., 2006). Equations for PMF calculations are provided in various literature (Almeida et al., 2020; Alves et al., 2020; Landis et al., 2017). Finally, the CMB is a multiple regression model that estimates the individual contribution of a source to the total mass of a particular contaminant and total pollutant load by inputting individual pollutant concentration and source profiles (Coulter, 2004).

The source apportionment of PTEs is a complicated task due to various reasons. This is because the identification of anthropogenic influence for an individual pollutant is hindered by various combinations of contaminants from the same source. It is possible to track to an extent the sources of the majority of the PTEs:

- Zn, Pb, and Ni-dominated PM are suggested to be attributed to vehicle emissions. Moreover, Cu, Ba, Sb, Mn, Br, and Mo are also commonly established markers of vehicle exhaust (Almeida et al., 2020; Landis et al., 2017; Ramírez et al., 2020; Sharma & Mandal, 2017). Vehicle emissions are also the contributor to the high elemental concentration of As, Cd, Si, and Sb in the coarse and fine PM (de Miranda et al., 2018; Jaiprakash & Habib, 2017; Pant & Harrison, 2013; Soleimani et al., 2018; Zhang et al., 2018).

- Tracers of the road dust resuspension include Zn, Mn, and Cu (Ramírez et al., 2020; Soleimanian et al., 2019). Moreover, Al, Si, K, Ca, Ti, Mn, Ba, Cr, and Fe have been denoted as the chemical tracers of road salt emissions (de Miranda et al., 2018; Ramírez et al., 2020; Zannoni et al., 2016).

- Chemical elements that originate from industrial activity include As, Ni, Cr, Se, Pb, Cu, Ni (de Miranda et al., 2018; Popoola et al., 2018; Sharma & Mandal, 2017; Soleimani et al., 2018; Soleimanian et al., 2019). Zn is also considered one of the major tracer elements from industrial emissions (e.g., steel production, zinc smelting industry) (Jan et al., 2020; Ramírez et al., 2020).

- Contamination from tire wear and brake abrasion is commonly associated with Cu and Zn (Čabanová et al., 2019; Jan et al., 2020; Landis et al., 2017; Ye et al., 2017). Cu is used as a component of tire wear, and zinc oxide is used in the tire

vulcanization process (Alves et al., 2020; Esmaeilirad et al., 2020). Moreover, elements including Fe, Pb, Mo, Sb can also originate from tire wear contamination (de Miranda et al., 2018; Jan et al., 2020; Ramírez et al., 2020; Sharma & Mandal, 2017).

- Elements associated with soil emission and mineral dust include Al, Ti, Li, Fe, Si, Ca, Na, Mg (Sharma & Mandal, 2017; Soleimanian et al., 2019).

- Coal and oil combustion is one of the major sources of ambient pollution. It is mainly dominated by Zn, Ni, Co, and As (Jan et al., 2020; Ramírez et al., 2020). V has also been suggested as a byproduct of the oil combustion process in numerous studies (Almeida et al., 2020; Landis et al., 2019; K. Zhang et al., 2018).

- Combustion of fossil fuels is also associated with a high concentration of V (Hao et al., 2018; Landis et al., 2019; Ramírez et al., 2020). Moreover, Pb, Fe, Zn, Cr, Ba, Sb are found in PM coming from fossil fuel combustion sources (de Miranda et al., 2018; X. Liu et al., 2019; Peltier et. al., 2011; Pulles et al., 2012).

- Ni and V are elements associated with power plant emissions (Arhami et al., 2017; Esmaeilirad et al., 2020; Soleimani et al., 2018). Moreover, Cd, Pb, Cr are suggested markers of coal-heated power plants (K. Zhang et al., 2018).

2.3 Analytical techniques for PM characterization

Throughout the years of research on air pollution, numerous laboratory methods have been developed to investigate the elemental composition and morphological characteristics of atmospheric PM. These laboratory methods are typically categorized as either destructive or non-destructive, depending on whether they destroy/consume the material during the analysis. This section concentrates on off-line (laboratory) analytical

methods commonly utilized for PM characterization and addresses the following issues: (1) the type of data provided by these methods (e.g., images, spectra, composition, etc.); (2) specific technical features; (3) strengths and weaknesses; and (4) the procedure for sample preparation.

2.3.1 Destructive techniques for PM analysis

2.3.1.1 Inductively coupled plasma analysis (ICP)

ICP is an analytical technique commonly used in environmental research for trace element analysis. ICP is considered a hard ionization method, leading to the complete atomization of the majority of analyzed sample molecules. This process involves introducing the sample into the ICP instrument through a nebulizer and spray chamber, transforming it into a fine aerosol. The ICP system also consists of an ICP torch and an argon plasma-generating radiofrequency (RF) coil (ion source). The argon plasma, which contains positively charged ions and unbound electrons, ionizes the analyte (Wilschefski & Baxter, 2019). Ions in the sample are quantified according to their mass-charge (m/z) ratio (Thomas, 2019).

Two major types of ICP instruments include inductively coupled plasma-atomic emission spectroscopy (ICP-AES or sometimes named as optical emission spectroscopy due to multiple emissions from atoms, ions, and molecules (ICP-OES)) and inductively coupled plasma mass spectrometry (ICP-MS). Selection between the two depends on the sample matrix and regulatory limits. ICP-MS excels in precision for samples with low regulatory limits, resulting in lower detection limits (DL) (U.S. EPA, 2014). Moreover, the ICP-MS instrument coupled with collision cell technology can also reduce

polyatomic spectral interference. Regulatory methods for trace element determination in PM by ICP-MS include EPA 6020 and Method IO-3.5.

In contrast, ICP-OES is more robust for samples with higher regulatory limits and applicable for the analysis of soil, solid waste, groundwater, and wastewater. It is a more cost-effective option when low DLs are not essential but is less suitable for identifying elements with low regulatory limits (e.g., As, Hg). Regulatory methods for metal identification in PM by ICP-MS include EPA 6010 and Method IO-3.4 (U.S. EPA, 1999a, 2014). Internal standards employed for ICP analysis include ^{6}Li, ^{45}Sc, ^{89}Y, ^{103}Rh, ^{115}In, ^{159}Tb, ^{165}Ho, and ^{209}Bi. Certain elements should be avoided in cases where the sample matrix contains a high concentration of the recommended standard, as this would lead to bias in the internal standard recovery bias (U.S. EPA, 2014).

The primary advantage of the ICP instrument lies in its capability to conduct a multi-element analysis with low detection limits (DL). This enables the determination of elemental concentrations in the sub-µg/L range for a wide set of elements, all in a single run. However, the cost of the ICP instrument may be suitable for low-volume laboratories, prompting to consider more cost-effective alternatives (e.g., flame atomic absorption instruments).

In air pollution studies prior to ICP analysis samples are collected on filters (e.g., PTFE or quartz fiber filters). A critical consideration is the extraction of samples from the filter since ICP instruments analyze liquid samples. Various extraction methods, such as methanol or ultra-sonication in organic solvents, present certain challenges. Dissolving PM in aqueous solvents can alter its properties and should be carried out with caution. Some studies propose cutting the filter using a ceramic blade for ICP

analysis, assuming homogeneous PM deposition. Alternatively, solid samples can be analyzed without extraction using ICP instruments equipped with electrothermal vaporization or laser ablation. When neither is feasible, sample digestion with concentrated acids (e.g., nitric (HNO_3), hydrochloric (HCl), hydrofluoric acid (HF), and perchloric acid ($HClO_4$)) is a well-established sample preparation method, despite the associated toxicity risks (U.S. EPA, 2014).

Analyzing aerosols collected on filters poses challenges due to low analyte concentrations and limited sample mass (Kumar et al., 2020). Proper selection and combination of digestion acids are crucial to minimize interference and achieve low DL. *Aqua regia* (HNO_3 and HCl, 1:3 molar ratio) is commonly used for environmental analysis, but specific elements may require specific acid mixtures, such as HF for aluminosilicate matrices or HCl for platinum group elements (PGE). Employing a closed vessel system for wet digestion is preferred to reduce sample loss and prevent airborne contamination (Odman, 2004). Matusiewicz (2003) provides comprehensive information on wet digestion methods.

2.3.1.2 Ion chromatography (IC)

Ion chromatography (IC) is an analytical technique employed for assessing the atmospheric concentration of gaseous pollutants, and anionic/cationic species (Paull, 2005). The principle of separation in the IC lies in the electrostatic interactions between the ions with an opposite or similar charge. The separation column that contains negatively charged functional groups attracts positively charged cations. Similarly, anions are separated by competitive ionic binding to positively charged functional groups (Bhattacharyya, 2012). Ions that can be identified by the IC include SO_4^{2-} , NO_3^-,

NH_4^+, Ca^{2+}, Cl^-, Mg^{2+}, Na^+, K^+, and F^-. IC allows the identification of several ions simultaneously in a short period of time. In addition, IC allows for the identification of different oxidation states of an element (Michalski, 2016). The water-soluble fractions of PM, containing ionic species, are crucial for understanding the potential health effects linked to PM. Furthermore, it includes water-soluble variations of PTEs that can easily pass through the air-lung fluid interface (Kogianni et al., 2020).

Therefore, IC is a valuable tool to characterize the toxicity of PM exposure. Moreover, IC is used in source apportionment studies. Ionic concertation and statistical analysis allow the identification of potential pollution sources. Oxidation of SO_2 to form secondary SO_4^{2-}, is the indicator of contribution from coal or biomass burning (Guo et al., 2020). Agricultural activity produces a high concentration of NH_4^+ that results from the reaction between NH_3 and acidic species (Yiyun Wu et al., 2016). SO_4^{2-} and NH_4^+ also can originate from vehicle exhaust (W. Wang et al., 2018). A high Ca^{2+} to Mg^{2+} ratio suggests that ions come from the soil dust (Guo et al., 2020; Jusino-Atresino et al., 2016). Ions such as Cl^- and K^+ can originate from biomass burning, coal combustion, and sea salt (Agarwal et al., 2020).

For IC analysis, it is necessary to dissolve ambient samples collected on the filter in deionized water and subject them to ultrasonication. This process facilitates the extraction of water-soluble inorganic species. Subsequently, the leachate is filtered through a chosen filter medium, such as PTFE or nylon (Chithra & Shiva Nagendra, 2013; Choung et al., 2016; Murari et al., 2016; W. Wang et al., 2018; S. Zhou et al., 2014).

2.3.2 Non-destructive techniques for PM analysis

2.3.2.1 Scanning electron microscopy (SEM)

Electron microscopy-based techniques can be used for the analysis of a single particle to investigate the physicochemical and morphological features of individual particles. Scanning Electron Microscopy (SEM) and Transmission Electron Microscopy (TEM) are among the most widely utilized instruments in this category. The application of SEM and TEM for the characterization of PM has been well documented (Elmes & Gasparon, 2017; Laskin et al., 2019; Sielicki et al., 2011).

In SEM, a raster scan pattern directs high-energy electron beams onto the particle's position. These beams capture signals that provide information about the particle's surface topography, electrical conductivity, and other characteristics (Elmes & Gasparon, 2017). Figure 2.4 illustrates an example of a SEM micrograph of atmospheric particles.

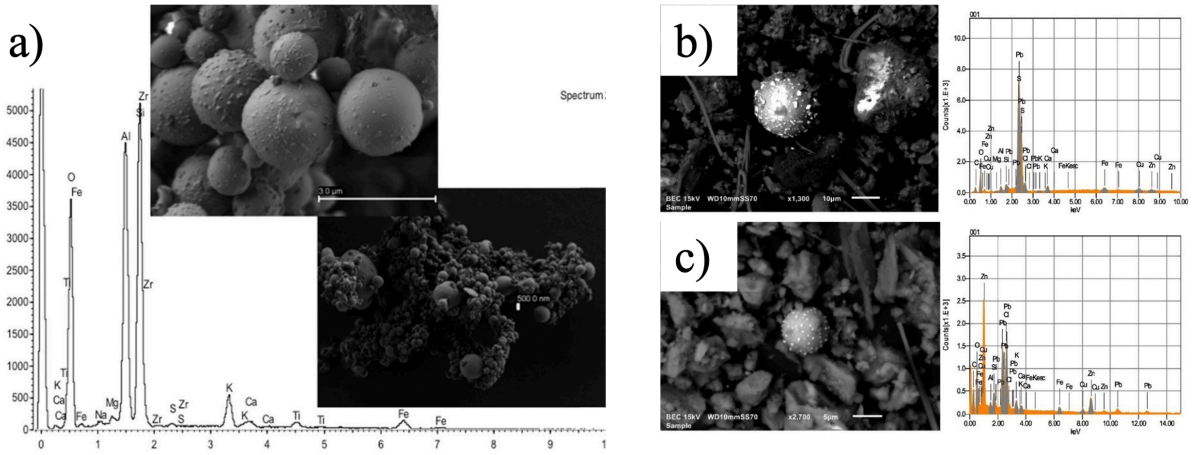

Figure 2.4: Examples of SEM micrographs and EDS spectra of (a) single particle and particle agglomerates of coal fly ash, (b) particles associated with CHPPs emission, and (c) PbO

particles (Reproduced from Oliveira et al. (2017) with permission of Environmental Research; Gonzalez et al. (2017) with permission of Atmospheric Research).

Various SEM instruments and their diverse operation modes offer an advanced approach to characterize PM particles. One example is the computer-controlled SEM (CC-SEM), which conducts quantitative analysis, yielding statistically significant data for sampled particles (Laskin et al., 2019; Y. Li et al., 2020). In this operational mode, approximately 50-100 images per substrate are captured at random locations across the sample at fixed magnifications followed by using software to categorize and quantify particles based on their morphology and elemental composition (Y. Li et al., 2020).

While automated SEM proves effective in rapidly examining particle surface data (~10,000 particles/hour), its application is limited when characterizing PM particles smaller than 0.1 μm (Laskin et al., 2019; Y. Li et al., 2020). Additionally, SEM provides only two-dimensional images of particle surfaces, making it inadequate for investigating internal structures or determining particle volume and, consequently, particle mass (Elmes & Gasparon, 2017). The use of a high-energy electron beam for higher magnification imaging can alter or damage the analyzed particles (Laskin et al., 2019; Wagner et al., 2019), as well as the substrate. Furthermore, SEM analysis under vacuum conditions hinders the reliable analysis of volatile components (Laskin et al., 2019).

Before conducting SEM analysis, it is essential to coat non-conductive samples with a thin layer (around 15-20 nm) (Li et al., 2020) of a conductive material, such as Au (Agarwal et al., 2020; Y. Li et al., 2020), C (RTI protocol), or Pt (Silva et al., 2020). However, this practice poses challenges if the samples are intended for subsequent analyses. Nevertheless, SEM analysis of PM collected on non-conductive and non-coated substrates like Teflon has been reported (Wagner et al., 2019). Despite these

drawbacks, SEM coupled with EDS remains the most widely utilized technique for single-particle characterization and is highly recommended for routine PM monitoring procedures as a rapid and straightforward tool to investigate the morphological features of PM.

2.3.2.2 Transmission electron microscopy (TEM)

Transmission electron microscopy (TEM) is a useful technique for toxicity assessment of airborne particulates as it provides insights on particle morphological structures, size distribution, and mixing state on a nano-sized scale (Figure 2.5) (Brostrøm et al., 2019; Salem et al., 2015; W. Zhou et al., 2016). TEM equipped with EDS can also provide information on the chemical composition of individual particles (Zhai et al., 2012).

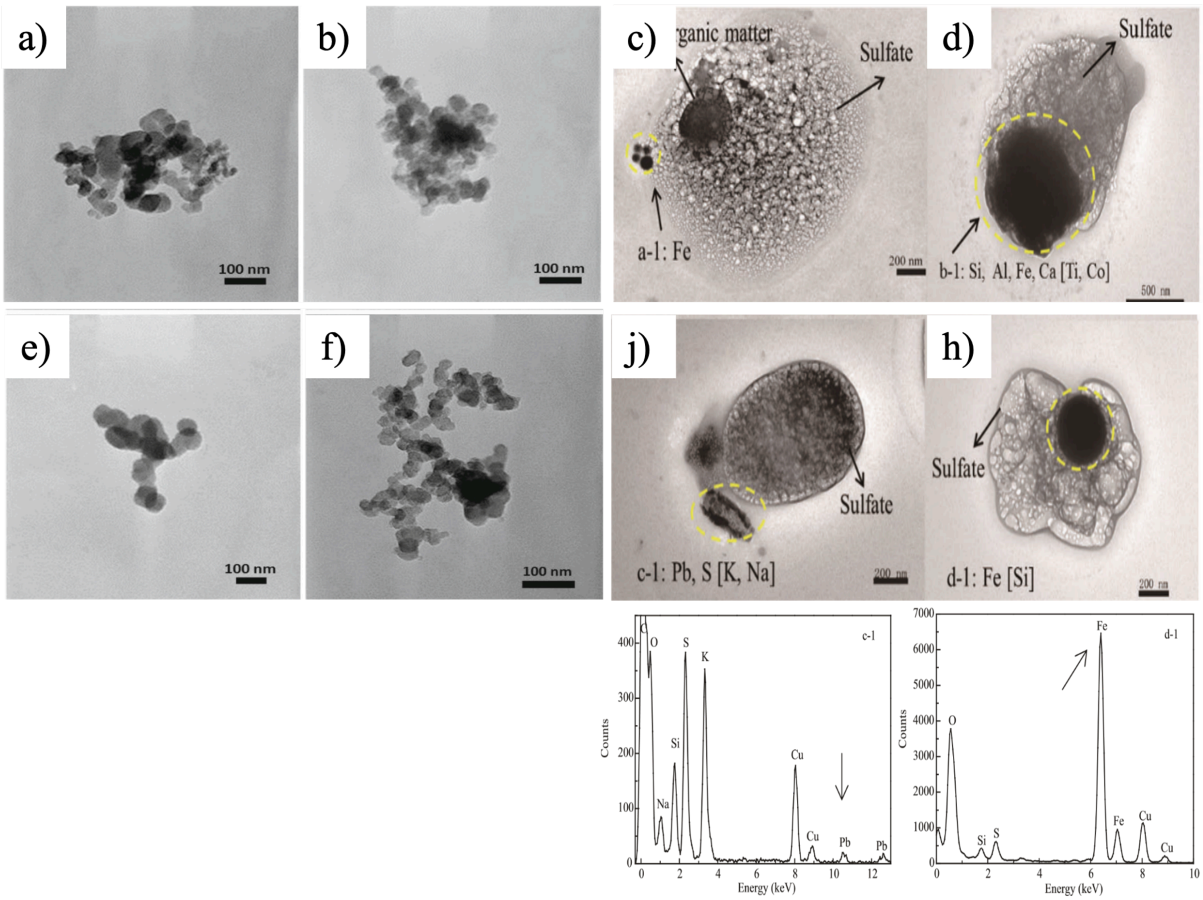

Figure 2.5: Examples of TEM micrographs coupled with EDS spectra of PM particles containing (a), (b) amorphous sulfate and silicate, (c), (h) Fe, (e), (f) crystalline silicate, (d) minerals, and (j) Pb (reproduced from Salem et al., 2015, with the permission from *Air Quality, Atmosphere, and Health* and Zhou et al., 2014, with the permission from *Journal of Environmental Science)*.

The main concept of TEM is based on the wave-like nature of electrons as they traverse the sample, generating a high-resolution image. An electron gun produces a high-voltage electron beam that passes through the TEM column, which is equipped with parallel electromagnetic lenses to focus the electrons.

The sample thickness should be limited to around 100 nm to enable electron passage. Characteristics including sample density may hinder the transmission of

electrons, particularly in high-density materials. TEM functions in a high vacuum environment (ranging from $<10^{-6}$-10^{6} Torr in conventional and environmental TEM instruments, respectively) due to electrons being incapable of traversing air molecules (C. Y. Tang & Yang, 2017). However, this condition can result in the evaporation of volatile PM components (Freedman et al., 2010). Additionally, the voltage should be kept under 400 kV to prevent sample damage (Kamšek & Kamšek, 2020).

While TEM analysis offers high magnification capabilities, reaching up to 1,000,000X (Mahmoud & Tan, 2017), obtaining statistically robust data on particle morphology and size distribution in air samples can be time-consuming. A resolution in the range of a few tens of nanometers is generally sufficient for airborne sample characterization. Despite being a comprehensive method for visualizing the internal structures of individual particles, TEM is limited by its high magnification, allowing only a partial view of the sample (Kamšek & Kamšek, 2020). Additionally, detecting secondary aerosol species and distinguishing species within homogeneous particles present certain challenges (W. Li et al., 2016).

A major drawback of TEM analysis lies in sample preparation. The sample preparation process may also include drying, freezing, or the application of conductive coating (Brostrøm et al., 2019). However, individual aerosol particles can be directly collected on carbon-coated TEM grids to avoid the effects of sample preparation (W. Li et al., 2016; Salem et al., 2015; W. Wang et al., 2018). It should be noted that aerosol particles collected on a grid may not be uniformly distributed (W. Li et al., 2016). Additionally, careful consideration of sampling time is crucial; longer sampling times may result in particle agglomerates rather than individual particles, while shorter

sampling times may not yield statistically significant data (Brostrøm et al., 2019). Given the specific limitations of TEM analysis, it is advisable to use it as a supplementary technique for PM characterization.

2.3.2.3 Energy-Dispersive X-ray Spectroscopy (EDS)

EDS is an instrument utilized to examine the bulk elemental composition of particles with an atomic mass equal to or greater than that of carbon. Its preference lies in its simplicity, convenience, and duration (30 seconds - 2 minutes analysis). Moreover, the tool often comes with pre-installed software for instant peak identification, and in many cases, electron microscopy equipment is equipped with an EDS device, allowing for the simultaneous investigation of particle morphology and chemistry (Sielicki et al., 2011). This simultaneous examination allows to establish correlations between the morphological characteristics of a specific group of particles and their chemical composition.

However, when investigating small or lower-density particles, EDS may provide the chemical composition of the substrate or background. Notably, background interferences, especially for elements such as C, O, and F originating from Teflon/PTFE filters (Wagner et al., 2019), hinder the quantification of elemental data from EDS analysis, resulting in relative abundance reports. Additionally, the inhomogeneity of particles at a certain point can sometimes lead to false spectra, as the chemistry at a specific location may not accurately represent the bulk chemistry. Enhancing accuracy involves studying a larger number of particles from the sampled aerosol and subjecting the acquired results to statistical analysis (Sielicki et al., 2011). While the outcomes are typically presented as elemental spectra for individual particles, one can also generate

elemental maps of the scanned region for major constituents. Comparing these maps helps to identify correlations between certain elements, suggesting the presence of specific compounds or common pollution sources (Hamdan et al., 2018).

2.3.2.4 X-ray-based techniques

X-ray Diffraction (XRD) is vital for determining the chemical speciation of mineral PM in air quality research (Kumar et al., 2020). It identifies major compounds based on peak characteristics and offers insights into both natural and anthropogenic sources (Hamdan et al., 2018). Qualitative and semi-quantitative analyses compare diffractogram peak values against mineral databases and employ the reference intensity ratio method, respectively (Jeong, 2008; Ahmady-Birgani et al., 2015; Engelbrecht et al., 2017; González et al., 2016; Satsangi & Yadav, 2014; Song & Yang, 2011). A quantitative XRD involves determining the weight proportions of minerals, however, is considered a complicated procedure (Jeong, 2008; Lu et al., 2007; De Berardis et al., 2007).

Two main sample handling approaches are the following: transferring material to a supporting surface or direct analysis of loaded substrates. The former minimizes issues related to sample placement and background interference (Jeong, 2008; De Berardis et al., 2007; González et al., 2016). However, direct analysis of sampled filters simplifies handling and prevents sample losses during transfer (Ahmady-Birgani et al., 2015; Smith, 1997).

XRD's accuracy is influenced by crystallinity, relative abundance, sample mass, and particle size. Crystallinity impacts peak visibility, affecting the detectability of partially crystalline and amorphous materials (Engelbrecht et al., 2017; Neupane et al.,

2020). XRD is recommended as a complementary tool due to limitations, and in cases of small particles, micro-XRD or two-dimensional XRD may be preferred (Bontempi et al., 2008; Kumar et al., 2020).

X-ray fluorescence (XRF) is a rapid and non-destructive technique for quantifying the elemental composition of PM, offering comparable results to more resource-intensive methods such as ICP-MS (Hamdan et al., 2018; Kumar et al., 2020). Its flexibility allows the simultaneous targeting of specific elements, trace elements, and PTEs (Atzei et al., 2019; Mazzei et al., 2008; Mazzei & Prati, 2009). XRF provides a quick analysis of PM composition due to its simplicity and speed (Canepari et al., 2009).

Quantitative XRF output, expressed in elemental concentrations (ng/m^3), is derived through sensitivity factor calculations using standard reference materials (SRMs), mass concentration (mass/area), filter area, and sampling volume rate (Do Nascimento et al., 2011; Dourado et al., 2020; Espinosa et al., 2019; Gunchin et al., 2019; Hamdan et al., 2018; Kchih et al., 2015; Lanzaco et al., 2019; Mazzei & Prati, 2009; Orogade et al., 2016; Owoade et al., 2016; Sara et al., 2013; Song & Yang, 2011). Uncertainties typically range from 5-15% for most elements (Mazzei et al., 2008; Ogundele et al., 2017; Owoade et al., 2016).

Crucial steps in quantitative XRF include instrument calibration and routine checks via SRMs (Atzei et al., 2019; Cuccia et al., 2013; Cuccia et al., 2010; Espinosa et al., 2019; Gunchin et al., 2019; Hamdan et al., 2018; Mazzei et al., 2008; Federico Mazzei & Prati, 2009;). Various XRF types, including energy dispersive XRF (ED-XRF), wavelength dispersive XRF (WD-XRF), and synchrotron radiation XRF (SR-XRF), have been applied in PM chemical characterization (Atzei et al., 2019;

Canepari et al., 2009; Cuccia et al., 2013; Cuccia et al., 2010; Kchih et al., 2015; Liang et al., 2018; Mazzei et al., 2008; Mazzei & Prati, 2009; Ogundele et al., 2017; Orogade et al., 2016; Owoade et al., 2016; Sara et al., 2013; Song & Yang, 2011; Do Nascimento et al., 2011; Franzin et al., 2020; Malandrino et al., 2013; Dourado et al., 2020; Lanzaco et al., 2019). XRF's advantage lies in minimal or no sample preparation, enabling analysis of atmospheric particulates in their original state, and allowing samples to be stored for re-analysis or measured using other techniques (Dourado et al., 2020; Kumar et al., 2020; Malandrino et al., 2013). Teflon filters are recommended substrates for XRF analysis, particularly in official standard operating procedures (SOPs) (IAEA, 1997; Sielicki et al., 2011; Research Triangle Institute International, 2009; U.S. EPA, 1999b).

X-ray spectrometry (XPS) is a valuable tool for the surface characterization of atmospheric particulates, providing chemical composition within a small particle area (detection depth <10 nm) (Elmes & Gasparon, 2017; Song & Peng, 2009; Zhang et al., 2018). Unlike bulk chemistry, surface composition is vital from a toxicological perspective, as these components interact first with body fluids after inhalation exposure (D. Atzei et al., 2019).

XPS generates energy spectra revealing intensity versus binding energy, offering semi-quantitative data on both elemental and chemical state composition with up to 0.1% accuracy (Cheng et al., 2013; Elmes & Gasparon, 2017; Xu et al., 2015). Its high sensitivity allows detection and quantification of elements including low-Z elements such as C, N, and O, at concentrations as low as 0.1% (González et al., 2017; Jilani et al., 2018; Xu et al., 2015). The method enables the study of functional groups of carbon at the particle's surface, though precautions are needed to avoid background interference

when using collection substrates containing carbon (Cheng et al., 2013; Guascito et al., 2015).

XPS does not require extensive sample preparation, and direct examination of samples is possible (Davide Atzei et al., 2014; Elmes & Gasparon, 2017; Jilani et al., 2018). However, it operates under high or ultrahigh vacuum conditions, leading to the evaporation of semi-volatile organic compounds (Atzei et al., 2019; González et al., 2017; Jilani et al., 2018; Rella & Malitesta, 2015). Therefore, XPS serves as a complementary technique, providing speciation capabilities, and is recommended for use with bulk chemistry analysis methods, such as XRF, to achieve comprehensive chemical characterization (Atzei et al., 2014). The flowchart for selecting the most suitable analytical methods and methods' classification are presented in Figures 2.6 and 2.7.

2.3.3 Determination of Intracellular and Mitochondrial ROS Production

Various techniques and assays are employed to assess the cytotoxic effects of PM exposure, with the choice depending on the toxicity mechanism. The most widely used method involves detecting cellular ROS levels using Dichlorodihydrofluorescein diacetate (DCFH-DA), a cell-permeable ester (Cáceres et al., 2020; Jan et al., 2020; Niu et al., 2019; Vattanasit et al., 2014; Wu et al., 2018; Yang et al., 2018). DCFH-DA is hydrolyzed by esterases within the cell, forming a stable fluorescent product (DFC) in the presence of ROS (Könczöl et al., 2012). While widely used and cost-effective, DCFH-DA has limitations, such as potential interference from increased superoxide radical formation and susceptibility to oxidation by other oxidizing species (Dikalov & Harrison, 2014).

An alternative method for mitochondrial ROS detection involves the use of the dihydroethidium fluorescent probe, which exhibits strong red fluorescence upon oxidation and is highly sensitive to superoxide (Dikalov & Harrison, 2014). Combining dihydroethidium with its derivative MitoSOX Red is suggested to enhance specific mitochondrial localization and indicate both cytosolic and mitochondrial superoxide levels (C. Yang et al., 2014). Flow cytometry is commonly employed to cell culture models, particularly the human lung adenocarcinoma cell line A549, serve as effective tools to investigate the mechanisms of particle-cell interaction following PM inhalation exposure (Figliuzzi et al., 2020; Jan et al., 2020; Lenz et al., 2013; Mitkus et al., 2013; Niu et al., 2019; Vattanasit et al., 2014). A549 cells, resembling alveolar type II cells responsible for surfactant production, offer insights into PM's cellular impact. Additionally, other cell models, such as the murine macrophage cell line RAW 264.7 and human bronchial epithelial cell lines (HBE and BEAS-2B), are used to study PM exposure effects (Cáceres et al., 2020; N. Li et al., 2018; Künzi et al., 2015).

2.3.4 Assessment of PTE Bioavailability via Bioaccessibility Testing

PM has a strong potential for the adsorption of PTEs (Niu et al., 2019; Vargas Buonfiglio & Comellas, 2020). Conventionally, the evaluation of the health impact of PM exposure is conducted by estimating the total concentrations of PTEs, which often leads to an overestimation of the potential health risk (Guney et al., 2017; Liu et al., 2019). To accurately assess the risk to human health, it is imperative to estimate not only the total amount of a contaminant but also the amount accessible for absorption. In this regard,

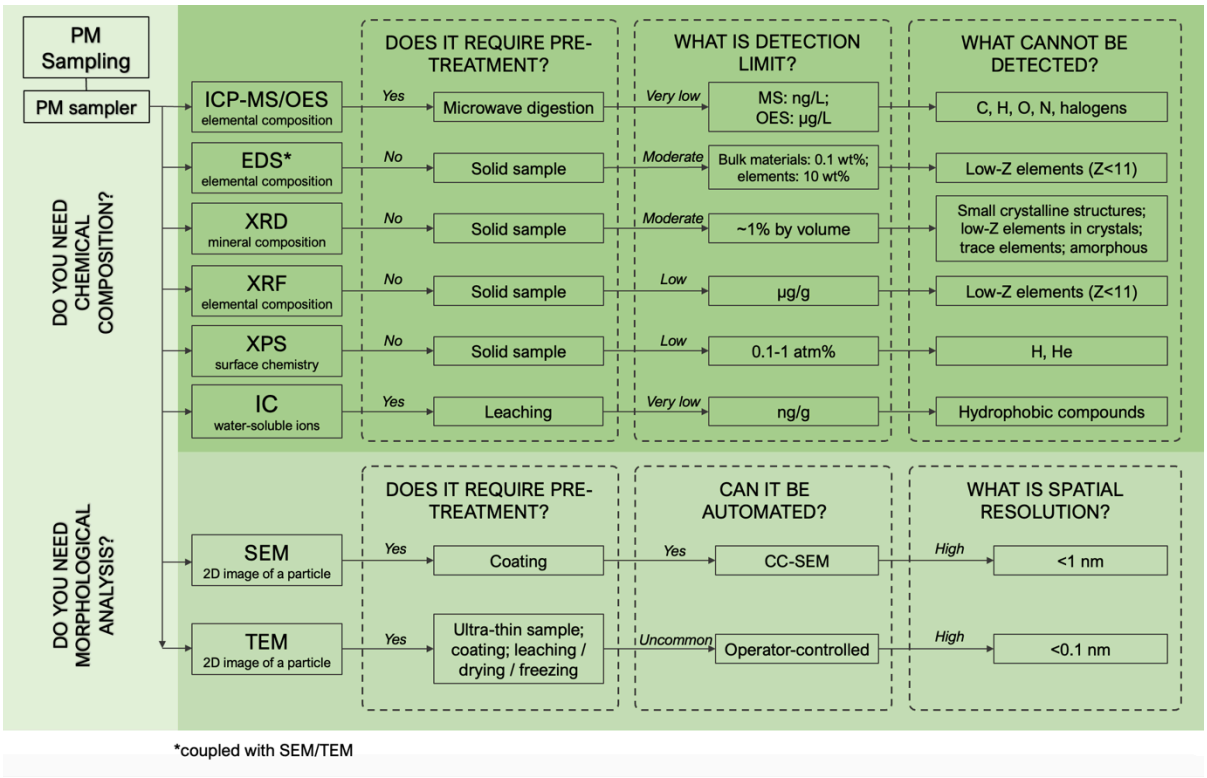

Figure 2.6: Flowchart for selecting the most appropriate PM characterization technique

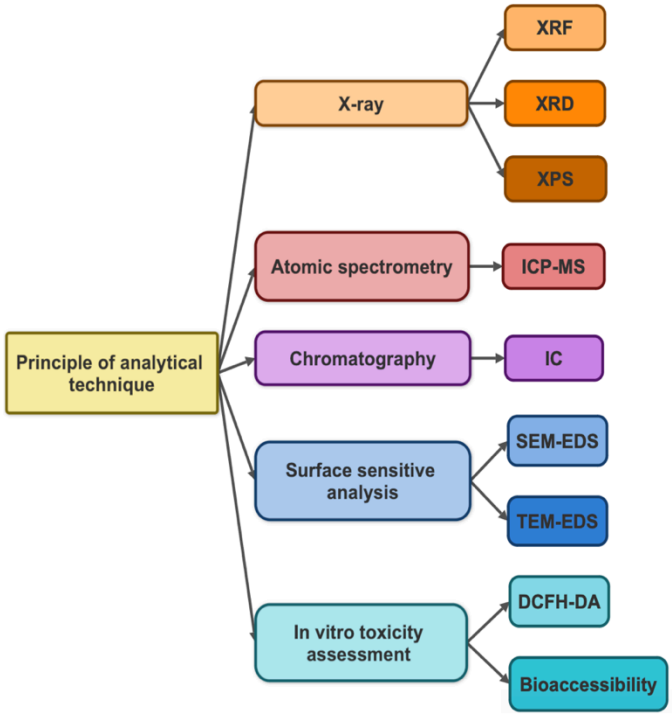

Figure 2.7: Classification of selected analytical methods for PM characterization

researchers have developed an *in vitro* method to estimate the fraction of metal readily available for absorption in human physiological fluids (e.g., gastrointestinal, lung fluid, synthetic sweat). This concept is referred to as *in vitro* bioaccessibility (Guney et al., 2016).

In earlier studies, *in vitro* lung bioaccessibility that simulates inhalation exposure was based on extraction techniques with simple chemical solutions (e.g., water, sodium chloride, ammonium acetate, ammonium citrate solutions) (Ren et al., 2020). However, the development of physiologically based techniques for lung bioaccessibility allowed maintaining the conditions as close as possible to those in the human body by using simulated lung fluids (SLFs). A variety of SLFs have been used during the development of *in vitro* bioaccessibility experiments (e.g., Gamble's solution (GS), Artificial Lysosomal Fluid (ALF), Hatch solution, and Simulated Epithelial Lung Fluid (SELF)). The most commonly used SLFs include GS (pH=7.4) and ALF (pH=4.5) which represent the interstitial fluid in the deep lung (GS) and lysosomal fluid in the alveolar macrophage (ALF) (Ren et al., 2020).

The current challenge in bioaccessibility research is the lack of a unified protocol creating a disparity in the result comparison. Moreover, external and internal factors (e.g., the composition of SLFs, solid–to–liquid ratio (S/L ratio), extraction time, agitation type/speed, particle size, and sample type) can affect the release bioaccessibility of pollutants in SLFs. The physiological parameters used in recent studies are presented in Table 2.1.

The original GS contains cations (e.g., Mg^{2+}, Na^{+}, Ca^{2+}, K^{+}) and anions (e.g., HCO_3^{-}, SO_4^{2-}, Cl^{-}, $H_2PO_4^{-}$), proteins, amino acids, and glucose. However, numerous

studies have established that modifying the original composition of GS can considerably affect the release of certain PTEs. The modification with amino acids (e.g., glycine, L–cysteine), and proteins (e.g., bovine serum albumin, mucin), as well as the addition of lung surfactant, have been attempted in various bioaccessibility studies (Boisa et al., 2014; Ren et al., 2020). Modification of GS with a lung surfactant is a relatively new concept suggested in prior literature (Julien et al., 2011; Boisa et al., 2014; Coufalík et al., 2016; Pelfrêne et al., 2017; Deary et al., 2021). A pulmonary surfactant contains protein and lipid components secreted by alveolar epithelial type II cells (Bernhard, 2016). DPPC is the major phospholipid (~40–80% by composition) present in the lung surfactant (Davies & Feddah, 2003). Several studies suggested different concentrations of DPPC for *in vitro* bioaccessibility experiments: 200 mg/L (Boisa et al., 2014); 100 mg/L (Coufalík et al., 2016; Pelfrêne et al., 2017); 0.02 wt% (Mbengue et al., 2015; Deary et al., 2021). Ren et al., (2020) argue that DPPC also acts as a weak chelating agent, significantly affecting the contaminant release (both metal (–loid) and organic) from atmospheric particles. Similarly, cholesterol is an essential component of lung surfactant (~10% by composition) that is critical to normal lung physiology (Gowdy & Fessler, 2013).

Few studies have attempted to investigate the effect of physiological parameters on the bioaccessibility of PTEs in PM (Julien et al., 2011; Boisa et al., 2014; Guney et al., 2017; Pelfrêne et al., 2017; Expósito et al., 2021; Tomašek et al., 2021). However, the available data on the bioaccessibility values of PTEs in Standard Reference Materials (SRMs) are very scarce. The present research, as well as existing literature (Boisa et al., 2014; Wiseman, 2015; Guney et al., 2016; Ren et al., 2020; Mishra et al.,

2021) emphasize the need to establish a standardized *in vitro* lung bioaccessibility protocol to further

Table 2.1: Experimental conditions used in recent bioaccessibility studies.

Reference	Sample type	Particle size	Contaminants analyzed	Lung solution	S/L ratio	Agitation method/ Speed	Extraction time
Haque et al. (2022)	Residential dust	1.1-2.7 µm	Pb	ALF, GS, SELF	1:1000	N/A	1 h, 4 h, 1 d, 1 w
Jia et al. (2022)	APM[(1)]	$PM_{2.5}$ $PM_{2.5-10}$	As, Cd, Co, Cr, Mn, Ni, Pb, V	SELF	N/A	100 rpm (a thermostatic oscillator)	24 h
Sun et al. (2022)	APM	$PM_{2.5}$	Cd, Pb	ALF, GS, Modified GS (with DPPC)	N/A	100 rpm	24 h
Zhou et al. (2022)	APM	$PM_{2.5}$	PAHs	SELF, SELF modified with DPPC (200 and 400 mg/L), BSA[2] (520 and 1040 mg/L), and HA[3] (200 and 400 µg/L)	1:1000-1:3000	100 rpm	24 h
Levesque et al. (2021)	Urban dust	<1.8 µm 1.8–10 µm	Al, B, Ba, Co, Cr, Fe, La, Mn, Mb, Sb, Sr, Ti, V, Zn	GS	1:3000	40 rpm (orbital shaker)	24 h
Schiavo et al. (2021)	School dust	<20 µm	Mn	ALF	1:1000	40 rpm (orbital shaker)	24 h
Gosselin & Zagury (2020)	Chromated copper arsenate (CCA)-contaminated soils	PM_{20}	As, Cr, Cu, Fe, Mn, Ni, Pb, Zn	ALF, GS	1:100	100 rpm (an incubator)	24 h
Y. Li et al. (2020)	Pb–contaminated alkaline urban soil	50–250 µm, 5–50 µm, 1–5 µm, <1 µm	As, Ba, Co, Cr, Cu, Ni, Mn, Pb, Zn	ALF, GS	1:5	N/A	4 h, 24 h, 100 h
Morais et al. (2019)	Fine surface dust Surface dust	≤10 µm ≤250 µm	As	GS	1:20	33 rpm (an incubator)	24 h
Luo et al. (2019)	APM	$PM_{2.5}$	Cd, Ni, Mn, Pb,	GS	Not specified	200 rpm	24 h

1 Atmospheric Particular Matter

2 Bovine Serum Albumin

3 Hyaluronic acid

elaborate on the PM toxicity in human cells. The flowchart for selecting the most appropriate PM toxicity method is presented in Figure 2.8.

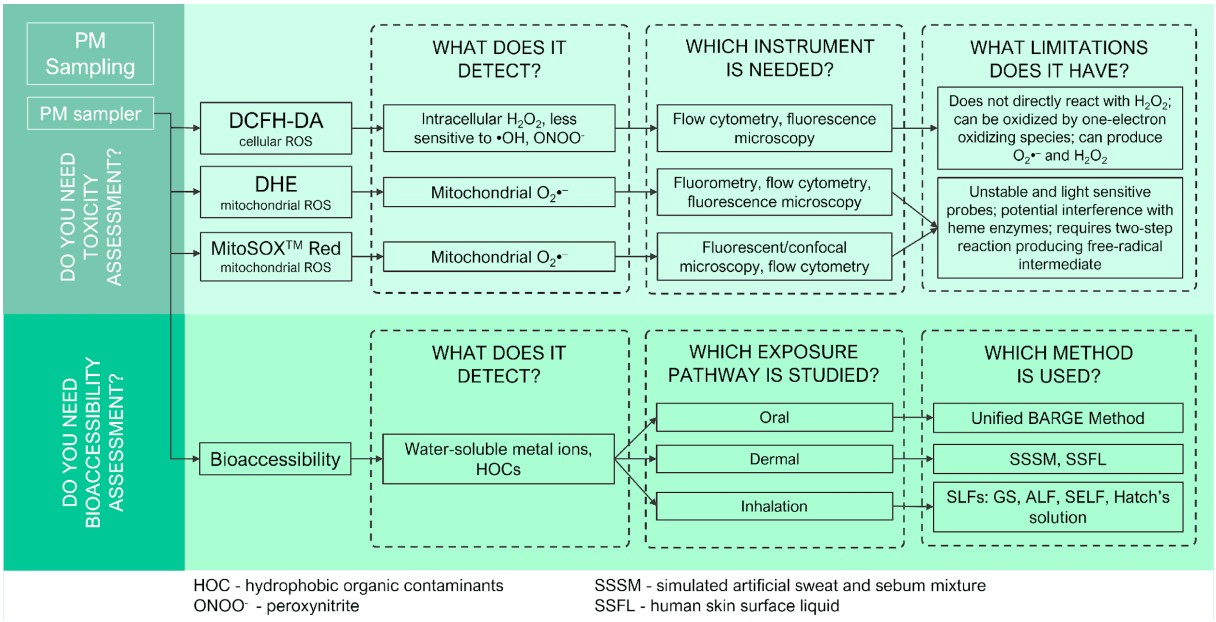

Figure 2.8: Flowchart for selecting the most appropriate PM toxicity assessment

2.4 Risk assessment as a tool to characterize human health risks

HHRA is a valuable strategy to identify hazardous substances, understand inhalation exposure, and propose effective management plans to mitigate health risks (Ren et al., 2020). The accurate estimation of risks associated with different levels of inhalable substances is crucial. The U.S. EPA has developed a tool to assess inhalation exposure and associated health risks, offering a framework that can be adopted directly or with modifications for assessing both carcinogenic and non-carcinogenic effects of contaminants (EPA & Risk Assessment, 2009). The detailed information on the HRA framework is outlined in Manual Part F: Supplemental Guidance for Inhalation Risk Assessment and Guidelines for Exposure Assessment EPA/600/Z-92/001. This approach involves risk estimation based on hazard identification, dose-response assessment,

exposure assessment, and risk characterization. Exposure assessment entails numerical estimation of exposure/dose, considering factors such as magnitude, duration, and frequency of exposure. The final step, risk characterization, utilizes cumulative hazard information obtained from previous stages to inform policy implementation (U.S. EPA, 2019).

The average daily dose (ADD) of the contaminant following inhalation exposure is estimated using the following equations:

$$ADD_{inh} = \frac{(C \times IR \times ED \times EF)}{AT \times BW,} \quad (2.1)$$

Where C is contaminant concentration in the air (mg/kg), IR is Inhalation rate (m^3/hour), EF is exposure frequency (day/annual), ED is exposure duration (annual), AT is the average time (lifetime in years×365 day/annual× 24 hour/day) and BW is body weight (kg) (U.S. EPA, 1992).

Non-carcinogenic and carcinogenic risks are estimated via hazard quotient (HQ), hazard index (HI), and lifetime cancer risk (LCR) using the following equations:

$$HQ = \frac{ADD_{inh}}{RfC}, \quad (2.2)$$

where ADD_{inh} is an average daily dose (mg/kg/day), and RfC is the US EPA reference dose for non-carcinogenic pollutants (mg/kg/day). HQ≥1 suggests a non-carcinogenic health effect on the exposed population (Fallahzadeh et al., 2018).

$$HI = \sum_{i=1}^{n} HQ, \quad (2.3)$$

where HQ is Hazard Quotient (no units) (Liu et al., 2019).

$$LCR = ADD_{inh} \times CFS_{inh}, \quad (2.4)$$

where ADD_{inh} is an average daily dose (mg/kg/day), and CFS is the cancer slope factor (mg/kg-bw/day).

The U.S. EPA typically aims for a risk range of one-in-a-million (10^{-6} risk) or one-in-ten-thousand risk (10^{-4} risk) for individuals exposed to airborne pollutants (U.S. EPA, 1992). Most studies assessing health risks associated with airborne pollutants primarily rely on estimating the potential dose or the quantity of inhaled chemicals, assuming that the potential dose equals the applied dose reaching target organs. This approach may lead to overestimation because the absorbed and bioavailable contaminant may only represent part of the potential dose. Thus, incorporating bioaccessibility, which considers the contaminant's bioavailability, can enhance the risk assessment framework (U.S. EPA, 2019).

While the toxicity of many contaminants is linked to solubility and the ability to cross cell boundaries, recent research suggests that even insoluble fractions, particularly redox-active metals such as Cu and Fe in PM, can induce oxidative stress and toxicity (Tacu et al., 2021). Insoluble PM fractions contribute to cell membrane disruption by forming particle agglomerates and generating phagocytic vesicles (Zou et al., 2016). Investigating the toxicity profiles of both soluble and insoluble PM fractions is crucial for a comprehensive understanding of health risks. Additionally, physical characteristics such as particle size, shape, and deposition mechanisms are often overlooked in estimating inhalation risks (Ren et al., 2020), highlighting the need for extensive research to comprehend the mechanisms underlying PM toxicity for better risk prediction.

The traditional deterministic method used in the described framework involves selecting a single-point value for each variable, disregarding uncertainties in contaminant concentrations and exposure parameters. On the other hand, probabilistic risk assessment estimates the likelihood and extent of adverse health outcomes due to inhalation exposure, incorporating uncertainties. Sensitivity analysis identifies variables with the most impact on risk assessment outcomes, while Monte Carlo simulation (MCS), a computational technique, performs random sampling and statistical modeling to simulate population behavior. MCS, typically running 10,000 or more trials, presents risk factors with uncertainties as a probability distribution, commonly setting the benchmark for health risk at the 95^{th} percentile (Harrison, 2009; Fakhri et al., 2018; Ganyaglo et al., 2019; Kaur et al., 2020; Verdonck et al., 2002).

2.5 Chapter summary

The chapter focuses on the determinants of particulate matter PM-induced cytotoxic effects and presents analytical techniques for studying the physicochemical toxicity of airborne particles. Notable findings highlight the influence of PM characteristics, such as size, morphology, and elemental composition, on associated health outcomes. The efficient and resource-friendly nature of SEM, especially when combined with EDS is emphasized, making it a strong recommendation for routine PM monitoring. Complementary techniques such as TEM and X-ray-based methods are suggested for more detailed analysis. This chapter emphasizes the need to incorporate bioaccessibility data and physicochemical characteristics into health risk assessments, stressing the importance of a comprehensive analytical approach for a comprehensive understanding of PM-related health risks.

CHAPTER 3: METHODOLOGY

This extensive research focuses on comprehensive air quality analysis covering the period from 2018 to 2023, and utilizing primary data collected between 2021 and 2023, along with air pollution monitoring data provided by relevant agencies. The thesis comprises six major components (Figure 3.1): first, modification of the *in vitro* lung bioaccessibility method; second, the chemical analysis of PM toxicity (PM samples collected in Astana, Kazakhstan) via PM bioaccessible concentration and health risk assessment, third, the characterization of PM morphology, with samples collected in Astana, Kazakhstan; forth, characterization of precipitation chemistry and its role in air quality; fifth, source identification utilizing both morphology data and secondary data on PM and gaseous pollutants concentrations; sixth, a population survey targeting adult urban residents of Astana to assess their knowledge and perception of air quality and the perceived air pollution situation in the region.

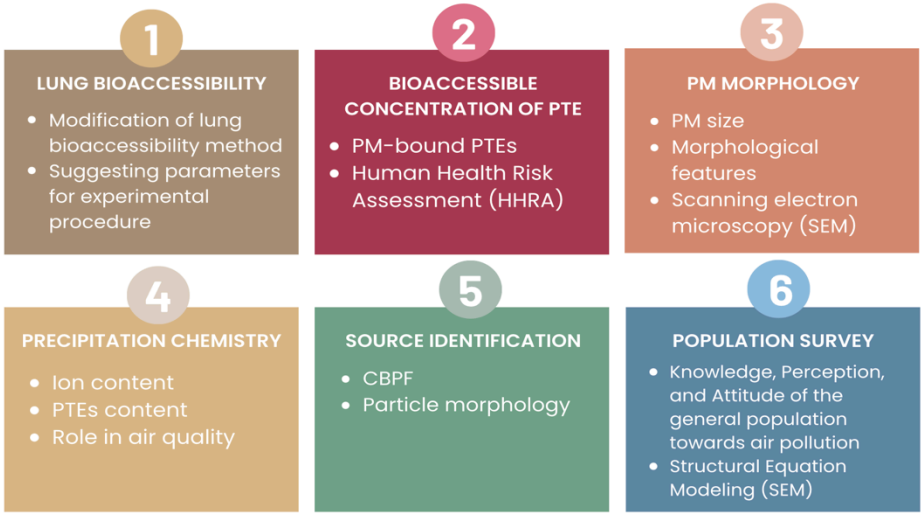

Figure 3.1: The major component of applied methodology

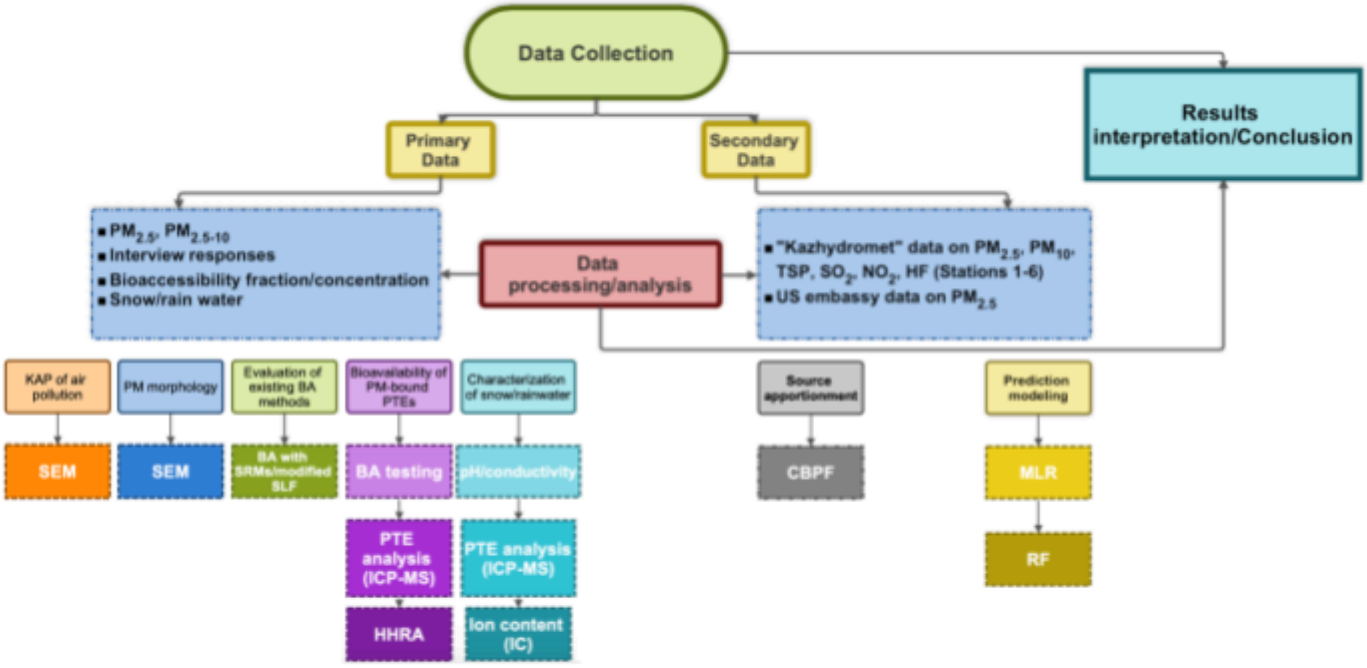

Figure 3.2: The methodology flowchart

The methodology for this thesis project includes the following (Figure 3.2):

1) **Data collection:**

Primary data contains (a) mass concentrations of $PM_{2.5}$ and $PM_{2.5-10}$ collected in Astana, Kazakhstan; (b) bioaccessible concentration of major PTEs in $PM_{2.5}$ and $PM_{2.5-10}$ samples; (c) data on PTEs and ionic concentrations in snow/rainwater samples collected in Astana, Kazakhstan; (d) survey responses on knowledge, perception, and attitude towards air quality among adult urban residents in Astana, Kazakhstan (Figure 3.2).

Secondary data contains (a) data on $PM_{2.5}$, PM_{10}, TSP, SO_2, NO_2, and HF concentrations provided by the National Air Quality Monitoring Network (NAQMN) of the National Hydrometeorological Service of Kazakhstan, "Kazhydromet" (Air pollution monitoring stations 1-6), and (b) $PM_{2.5}$ concentration data provided by US Embassy

2) **Data processing and analysis:**

This step involved (a) evaluation of existing lung bioaccessibility methods, which was later applied for (b) lung bioaccessibility of $PM_{2.5}$-bound PTEs; (c) characterization of PM morphological features via SEM; (d) characterization of snow/rainwater via ICP-MS and IC; and (e) SEqM analysis to determine major factors influencing public perception and attitude towards air pollution.

Secondary data on PM and gaseous was used for (a) source identification via CBPF and (b) construction of the PM prediction model.

3) Result interpretation and conclusions.

3.1 Study area

Astana (51°10'N latitude, 71°26' E longitude) is the capital city of Kazakhstan, located on a flat dry steppe zone with an area of 722 km^2 and 347 m above sea level (Figure 3.3). Astana belongs to a humid continental climate according to the Köppen climate classification system with long cold winters and warm dry summers and an average annual temperature of 4.2 ºC. The prevailing wind directions are south and southwest with an average wind speed of 3.9 m/sec. The average annual rainfall is 295 mm (Climate Data, 2023).

The city's population was estimated at 1,239,744 people at the start of 2022, with 594,742 male and 645,002 female residents, respectively. The average age of Astana residents was 30.1 years in 2021. At the beginning of 2022, 795,969 adults (≥20 years) were registered in Astana

(National Bureau of Statistics, 2022). The population of Astana has experienced continuous and rapid growth since 2001 e.g., an 11.2% increase in 2021 compared to 2020 (National Bureau of Statistics, 2022).

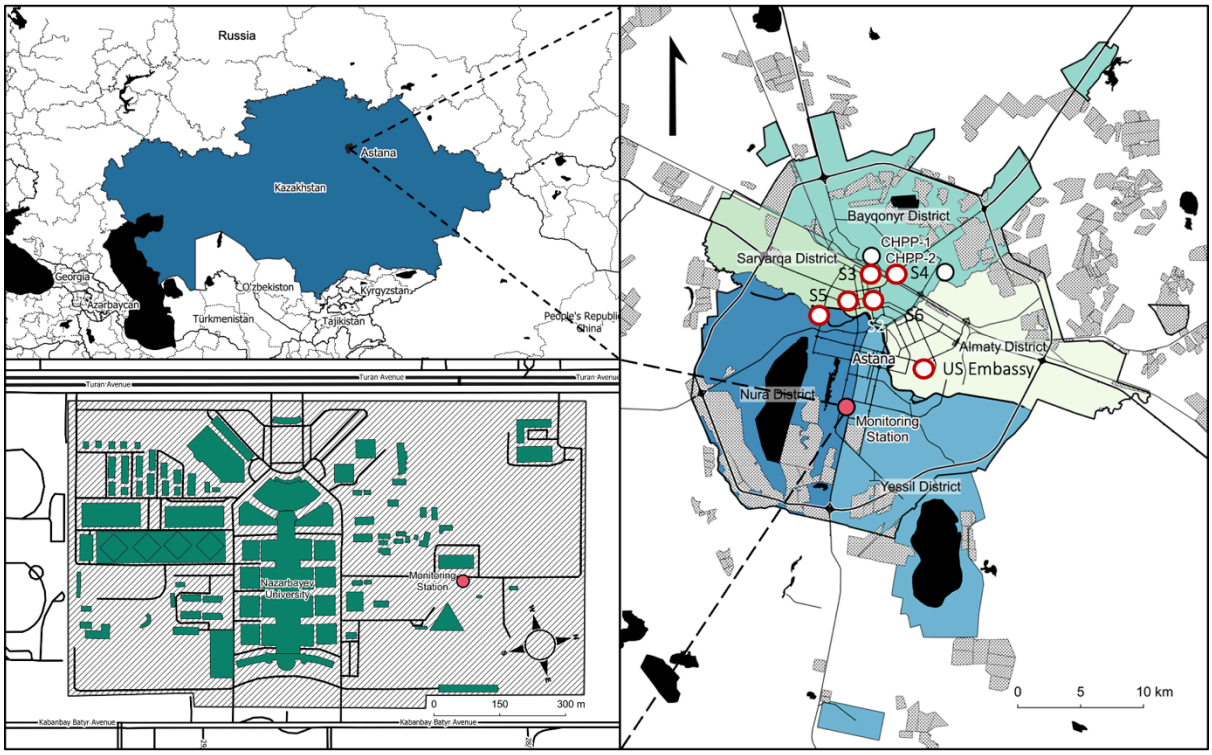

Figure 3.3: Locations of the study area, coal-heated power plants (CHPP-1 and CHPP-2), and air pollution monitoring stations (S1-S6), US embassy, Monitoring Station (Nazarbayev University).

3.2 Data collection

3.2.1 Primary data

3.2.1.1 $PM_{2.5}$ and $PM_{2.5-10}$ sampling

Seasonal $PM_{2.5}$ and $PM_{2.5-10}$ samples were collected in the urban area of Nazarbayev University Campus (51°5'N latitude, 71°23' E longitude) (Figure 3.3). The details of the sampling periods are presented in Table 3.1. The $PM_{2.5}$ and $PM_{2.5-10}$ samples were collected via Partisol 2025*i*-D Dichotomous Sequential Air Sampler

(ThermoFisher Scientific Inc.) that simultaneously collects two types of PM. The sampler installation was performed according to U.S. EPA 40 CFR Part 58, Appendices D and E siting criteria. The virtual impactor of the air sampler separates the airflow to maintain 15.0 L/min and 1.67 L/min for $PM_{2.5}$ and $PM_{2.5\text{-}10}$, respectively. The PM samples were collected for 24 h over 16 days on 47 mm diameter, 2 μm pore size PTFE filters. This resulted in 171 samples of $PM_{2.5}$ and 171 samples of $PM_{2.5\text{-}10}$. Each filter was pre-conditioned before and after collection in the equilibration room for at least 24 h at 30-40% humidity and 20°C-23°C. The gravimetric analysis of particle mass was performed via analytical balance (RadWag, XA 220.3Y.A) The particle mass concentration was calculated in $\mu g/m^3$. The filters were stored in a Petri dish at 4°C before use.

Table 3.1: Overview of $PM_{2.5}$ and $PM_{2.5\text{-}10}$ sampling periods.

Season	Sampling period	Number of samples	
		$PM_{2.5}$	$PM_{2.5\text{-}10}$
Winter	February 2, 2022, to February 16, 2022, December 9, 2022, to December 23, 2022, January 1, 2023, to February 2, 2023	41	41
Spring	March 3, 2022, to March 17, 2022, April 8, 2022, to April 21, 2022, May 22, 2023, to May 31, 2023, March 3, 2023, to March 4, 2023	47	47
Summer	June 1, 2022, to June 3, 2022, June 21, 2022, to June 28, 2022, July 16, 2022, to July 29, 2022, August 24, 2022, to August 31, 2022, May 31, 2023, to June 13, 2023	46	46
Fall	October 15, 2021, to October 21, 2021, October 24, 2021, to November 5, 2021, November 11, 2021, to November 11, 2021, September 9, 2022, to September 9, 2022	37	37

3.2.1.2 *Precipitation sampling*

The sampling site was located at Nazarbayev University Campus (51°5'N latitude, 71°23' E longitude). The sampling campaign was carried out from March 2022 to March 2023. The Palmex RS-2i rain sampler (Palmex Itd, Croatia) equipped with a 3 L

polyethylene bucket was set on the sampling site. The sampling bucket was cleaned with deionized water (DI) and dried each time before use. The sampling occurred after the precipitation event. The sampling bucket was taken out from the sampler, closed by the plastic cover to void contamination, and carried to the laboratory for further analysis. If several precipitation events happened in one day, the sample was taken on the next day. In total, 30 snow/rainwater samples were collected. The details of the sampling period are provided in Table 3.2. Rainwater samples were filtered with a 20 mL syringe and 0.45 μm PVDF filter.

Table 3.2: Overview of snow/rainwater sampling periods.

Season	Sampling period	Number of samples
Winter	December 13, 2022; December 22, 2022; January 4, 2023; January 20, 2023; January 23, 2023; February 10, 2023, February 24, 2023	7
Spring	March 18, 2022; March 24, 2022; April 6, 2022; April 19, 2022; April 21, 2022; April 22, 2022; May 22, 2022; May 31, 2022; March 10, 2023; March 14, 2023; March 15, 2023	12
Summer	June 1, 2022; June 5, 2022; June 13, 2022; June 25, 2022; July 5, 2022; August 11, 2022	6
Fall	September 11, 2022; September 27, 2022; October 9, 2022; October 22, 2022; November 15, 2022	5

3.2.1.3 KAP of air pollution among adult residents of Astana

The survey responses were collected during May and June of 2022. Two rounds of pre-testing with 20 respondents were conducted to ascertain the correct and rational interpretation of the survey questions. The link to the anonymous survey was distributed through social media platforms and the university's mail services. A total of 870 responses were collected. Incomplete, "straight-line", and inconsistent survey responses were excluded from further analysis, leading to a total of 782 responses being included

in the final analysis. The present research received prior approval from the International Research Ethics Committee of Nazarbayev University (NU IREC).

3.2.2 Secondary data

The secondary data were obtained from the NAQMN of the National Hydrometeorological Service of Kazakhstan, "Kazhydromet" and the US embassy air pollution monitoring station. The 4-hour (S1), and 3-hour measurements (S2-S4) of TSP, SO_2, CO, NO_2, and HF (October 2018-September 2020) (Sampler aspirator OP-824TTs), hourly $PM_{2.5}$ concentrations (the US embassy) (GAIA A12 Air Quality Sensor), and average daily concentrations of PM_{10}, SO_2, CO, NO_2, and NO (S5 and S6) (2019) have been utilized (Figure 3.3). The meteorological parameters used for the analysis include temperature (T), atmospheric pressure (P), relative humidity (RH), wind direction (WD), and wind speed (WS). Data for the analysis were divided into heating (October–April) and non-heating (May–September) periods.

3.3 Data processing and analysis

3.3.1 Evaluation of existing bioaccessibility testing methods

3.3.1.1 Standard reference materials (SRM)

In the present research, lung bioaccessibility was carried out with two SRMs: BGS 102, ironstone soil (particle size < 40 μm), collected from naturally contaminated soil in North Lincolnshire, UK; SRM 2691, coal fly ash (particle size < 45 μm), collected from a coal-heated power plant (Iatan Power Station, Iatan, MO, by Kansas City Power and Light Co., Kansas City, MO). These SRMs were selected for the experimental procedure to replicate the exposure to atmospheric particles from geogenic and industrial emission sources.

3.3.1.2 Modification of in vitro bioaccessibility method

To simulate human physiological conditions and examine the impact of various chemical compositions of lung fluids on the PTEs release, we formulated eight distinct lung solutions: original GS (adapted from Colombo et al., 2008); GS/2% DPPC (pH 7.4±0.1), GS/5% DPPC (pH 7.4±0.1), GS/0.25% cholesterol (pH 7.4±0.1), GS/0.5% cholesterol (pH 7.4±0.1), GS/2% DPPC+0.25% cholesterol) (pH 7.4±0.1), GS/5% DPPC+0.5% cholesterol) (pH 7.4±0.1) (pH 7.4±0.1), and ALF (pH 4.5±0.1) (chemical composition of the SLFs given in Table 3.3). The pH of the simulated lung fluids was adjusted to requirements when needed with $NaHCO_3$ and HCl.

About 0.2 g of SRMs were carefully weighted (4 digits) and added to 20 mL (37°C) of SLF in a 50 mL–PP centrifuge tube (Teflon with PTFE caps), representing a 1/100 S/L. Samples with lung fluid were placed horizontally in a laboratory orbital shaker incubator (IKA KS 4000 i Control) previously set to 37 °C and then were agitated at 100 rpm. A procedure blank was included in each batch. Briefly, 15 mL (37°C) of GS or ALF were carefully added into a 50 mL-PP centrifuge tube. The procedure for blanks was replicated as for SRM-containing samples. After the incubation period, blanks were carefully poured into a 20 mL syringe, and filtered with a 0.45 μm pore size hydrophilic PVDF membrane filter into a 50 mL tube. Blank samples were digested with 3:1 HNO_3/HCl mixture following microwave digestion in TFM^{TM} PTFE pressure vessels. and stored at 4°C until analyses.

The collection of samples was initially performed after 2 h, after which the tubes were centrifuged at 3,250 g for 10 min. The supernatant was carefully poured into a 20 mL syringe and then filtered with a 0.45 μm pore size hydrophilic PVDF membrane

filter into a 50 mL tube. 1 mL 70% HNO_3 was added to each tube for sample preservation. All samples were kept at 4°C until analyses. Experiments were also conducted at longer time intervals (1 d (24 h), 1 w (168 h), 4 w (336 h)), at lower agitation (20 rpm), and with lower S/L (1/500, corresponding to 0.04 g of SRMs).

Table 3.3: Chemical composition of SLF (adapted from Colombo et al., 2008).

Chemicals (g) in 1 L of solution		**GS**	**ALF**
Magnesium chloride hexahydrate ($MgCl_2.6H_2O$)		0.203	0.107
Sodium chloride (NaCl)		6.019	3.210
Potassium chloride (KCl)		0.298	—
Disodium hydrogen phosphate (Na_2HPO_4)		0.126	0.071
Sodium sulfate (Na_2SO_4)		0.063	0.039
Calcium chloride dehydrate ($CaCl_2.2H_2O$)		0.368	0.128
Sodium acetate ($C_2H_3O_2Na$)		0.574	—
Sodium hydrogen carbonate ($NaHCO_3$)		2.604	—
Sodium citrate dihydrate ($C_6H_5Na_3O_7.2H_2O$)		0.097	0.077
Sodium hydroxide (NaOH)		—	6.000
Citric acid ($C_6H_8O_7$)		—	20.80
Glycine (H_2NCH_2COOH)		—	0.059
Sodium tartrate dihydrate ($C_4H_4O_6Na_2.2H_2O$)		—	0.090
Sodium lactate ($C_3H_5NaO_3$)		—	0.085
Sodium pyruvate ($C_3H_3O_3Na$)		—	0.086
1,2-dipalmitoyl-sn-glycero-3-phosphocholine (DPPC) ($C_{37}H_{74}NO_8P$)	*5%:*	0.517	—
	2%:	0.207	—
Cholesterol ($C_{27}H_{46}O$)	*0.5%:*	0.052	—
	0.25%:	0.026	—

3.3.1.3 Elemental analysis

Samples were analyzed using ICP–MS (Thermo Fisher Scientific®, The iCAP™ RQ) to determine the bioaccessible concentration of Cd, Co, Cr, Cu, Mn, Ni, Pb, Sb, V, and Zn (detection limits [DL] in GS (ppm): 0.0005, 0.0023, 0.0140, 0.0485, 0.0122, 0.0211, 0.0019, 0.0063, 0.0317, 0.0253 respectively; DL in ALF: 0.0002, 0.0052, 0.0283, 0.5056, 0.0049, 0.0344, 0.0146, 0.0293, 0.0914, 0.2818, respectively). Prior to ICP analysis samples were digested in 3:1 HNO_3/HCl mixture following microwave digestion in TFM™ PTFE pressure vessels. A procedure blank was included in each digestion batch. Digestion was performed by adding 3 mL of HNO_3 and 1 mL of HCl to

the digestion vessel. Digested samples were carefully poured into a 20 mL syringe, filtered (0.45 μm PVDF filter) into a 50 mL tube, and made to a 25 mL volume with deionized water. The samples were stored at 4°C until the analyses.

The bioaccessible fraction ($\%_{bio}$) was calculated for each contaminant using the following formula (Guney et al., 2017):

$$\%_{bio} = \frac{C_{bio} \times V}{C_{total} \times m} \times 100, \quad (3.1)$$

where C_{total} is the concentration of a contaminant in SRM (mg/kg); m is the mass of the sample (g), C_{bio} is the bioaccessible concentration of a contaminant (mg/L) and V is the volume of a lung fluid (mL).

3.3.1.4 QA/QC

Procedure blanks were included in each experimental batch. For most of the *in vitro* bioaccessibility experiments, the results for the procedure blank were close to the instrumental detection limit. An internal standard (^{103}Rh) was used for all calibration standards, samples, and blanks. The variability between duplicates for *in vitro* bioaccessibility experiments was estimated by the relative standard deviation (RSD). To assess the effectiveness of the analytical procedure and calculate metal recovery, a bioaccessibility experiment was performed with ALF with and without SRM samples and with a spiking solution containing 1 mg/L of Co, Ni, Pb, and Zn (Table 3.4). Briefly, 15 mL of ALF was added into a 50 mL-PP centrifuge tube. 1 ml of a multi-element IV-ICPMS-71A solution (10 μg/ml) was used for spiking. For samples containing SRM, 0.2 g of SRM 2691 was added to five 50 mL-PP centrifuge tubes. Spiking was done at 2 h, 1 d, 3 d, 1 w, and 2 w test duration. Spiking samples were digested with a 3:1

HNO_3/HCl mixture following microwave digestion in TFM™ PTFE pressure vessels and analyzed via ICP-MS.

Table 3.4: Recovery % of Co, Ni, Pb, and Zn in ALF.

	Recovery (%)			
	Co	Ni	Pb	Zn
Spike (no sample) –2 h	82	89	80	77
Spike – 1 d	87	88	77	74
Spike – 3 d	93	46	115	83
Spike – 1 w	91	95	83	83
Spike – 2 w	91	97	80	82
Spike (SRM 2691) – 2 h	69	55	60	5
Spike – 1 d	74	66	54	19
Spike – 3 d	57	50	25	–2
Spike – 1 w	74	72	21	24
Spike – 2 w	79	77	21	30

3.3.2 Bioavailability of PM-bound PTEs

3.3.2.1 In vitro lung bioaccessibility of PM-bound PTEs

The ALF was employed to estimate the bioaccessible concentration of PTEs in $PM_{2.5}$. The composition of lung fluid is specified in Table 3.3. Briefly, 41 PTFE filters were put into 15 mL–PP centrifuge tubes (Teflon with PTFE caps) and mixed with 10 mL of ALF (37 °C). The $PM_{2.5}$ samples with ALF were placed horizontally in a laboratory orbital shaker incubator (IKA KS 4000 i Control) set to 37 °C and 100 rpm agitation for 1 week. The extracted lung fluid was carefully poured into a 20 mL syringe following the filtration with a 0.45 μm pore size hydrophilic PVDF membrane filter. For the sample preservation, 0.5 mL of 70% HNO_3 was added to each tube. All samples were kept at 4°C (maximum duration is ten weeks) until the analysis. For the elemental analysis samples were digested in a microwave digestor (speedwave® ENTRY, BERGHOF) in TFM™ PTFE pressure vessels using a 3:1 HNO_3/HCl mixture. A

procedure blank was included in each digestion batch. A mixture of 1.5 mL of HNO_3 and 0.5 mL of HCl was added to each digestion vessel. All digested samples were filtered with a 20 mL syringe and 0.45 µm PVDF filter into a 50 mL tube and stored at 4°C until elemental analysis.

Samples were analyzed using ICP–MS (Thermo Fisher Scientific®, The iCAP™ RQ) to estimate the bioaccessible concentration (mg/kg) of Cd, Co, Cr, Cu, Fe, Mn, Ni, Pb, Sb, V, and Zn (detection limits [DL] in ALF (ppm): 0.0002, 0.0052, 0.0283, 0.5056, 0.0049, 0.0344, 0.0146, 0.0293, 0.0914, 0.2818).

The bioaccessible concentration for each PTE was calculated using the following formula:

$$C_{bio} = m_{bio} \times 1000/m, \quad (3.2)$$

where C_{bio} is the bioaccessible concentration of a contaminant (mg/kg) and m_{bio} is bioaccessible mass (mg).

3.3.3 Inhalation HHRA via bioaccessible concentration of PTE

HHRA was conducted using the Inhalation Dosimetry Methodology outlined by the U.S. EPA (U.S. EPA, 2009). This methodology incorporates the assessment of exposed populations, exposure conditions, and the quantification of potential doses or chemical intake. Based on these considerations, evaluation of environmental exposure to adults and children was performed in the present research. Exposure concentration (EC, µg/m^3), carcinogenic risk (CR), and hazard index (HI) were calculated for HHRA of PTEs in $PM_{2.5}$.

EC for chronic exposure for each PTE was calculated using the following formula (U.S. EPA, 2009):

$$EC = \frac{C_{bio} \times ET \times EF \times ED}{AT}, \quad (3.3)$$

where C_{bio} is the bioaccessible concentration of each PTEs (μg/m^3), ET is the exposure time (hours/day) (ET = 24 hours/day for adults and children), EF is exposure frequency (days/year) (ET = 350 days/year for adults and children), ED is exposure duration (years) (ED = 20 years for non-carcinogenic risk, and ED = 70 years for carcinogenic risk), and AT is averaging time (ED in years 365 day/year 24 hours/day) (AT = ED × 365 × 24 h for non-carcinogenic PTEs and AT = 70 × 365 × 24 h for carcinogenic PTEs) (Sánchez-Piñero, et al., 2021; Novo-Quiza et al., 2023).

CR was estimated using the following formula (U.S. EPA, 2009):

$CR_i = IUR_i \times EC$, (3.4)

where IUR_i is inhalation unit risk (μg/m^3)$^{-1}$.

$$HQ_i = \frac{EC}{RfC_i \times 1000}, \quad (3.5)$$

where RfC_i is is the reference concentration of chronic inhalation exposure (mg/m^3).

IUR_i of each PTE (1.8×10^{-3}, 8.4×10^{-2}, 9.0×10^{-3}, and 2.6×10^{-4} for Cd, Cr (VI), Co, and Ni, respectively) (U.S. EPA 2009); and RfC_i is the reference concentration of chronic inhalation exposure (mg m^{-3}) of each PTE (1.0×10^{-5}, 1.0×10^{-4}, 6.0×10^{-6}, 5.0×10^{-5}, 1.4×10^{-5}, 2.0×10^{-4}, and 1.0×10^{-4} for Cd, Cr (VI), Co, Mn, Ni, Sb, and V, respectively) (U.S. EPA 2019a,b).

HI_c and HI_{nc} were calculated as follows (U.S. EPA, 2009):

$HI_c = \Sigma CR_i$, (3.6)

$HI_{nc} = \Sigma HQ_i$, (3.7).

3.3.3 Investigation of PM morphology

Ten $PM_{2.5}$ and $PM_{2.5-10}$ sample filters collected during the summer (July) and winter (January) seasons were selected for source identification based on morphological features. Each filter paper was cut into 1 mm^2 sized squares, mounted on carbon tape, and coated with a 15 nm Au layer using a sputter coater (Q150T) to improve sample conductivity. Samples were analyzed via Field-Emission SEM (FE-SEM) (ZEISS Crossbeam 540) operated using ORS Dragonfly Pro software. PM samples were analyzed under high-vacuum conditions (10^{-5} mbar sample chamber pressure), at a working distance of 3.6 mm with an accelerating voltage of 5 kV, scan speed 3, and 117 pA probe current. Specified instrumental settings enabled the successful identification of PM particles with a geometric diameter <100 nm. The percent distribution for particle types was estimated manually, by calculating a number of particles of a specific type (based on morphological characteristics) relative to a total number of particles on the SEM image.

3.3.4 Characterization of snow and rainwater

Snow and rainwater samples were filtered using 20 mL syringes and 0.45 µm pore size PVDF filters. Some samples (n = 5) were filtered twice to remove solid particles. The pH of precipitation samples was measured using a pH meter (METTLER TOLEDO™ SevenCompact™). Three standard buffer solutions at pH 10.01, 7.00, and 4.01 were used before measurement for calibration. The electric conductivity of the samples was measured via a conductivity meter (WTW inoLab® Multi 9310 IDS). Samples were then preserved at 4°C.

The ICP-MS (Thermo Fisher Scientific®, The iCAP™ RQ) was used to estimate the concentration (µg/L) of Cd, Co, Cr, Cu, Fe, Mn, Ni, Pb, Sb, V, and Zn. Prior to

elemental analysis samples were digested with 3 mL HNO_3 and 1 mL of HCl in a microwave digestor (speedwave® ENTRY, BERGHOF) and filtered with 0.45 μm pore size PVDF filters. Digested samples were stored at 4 °C before the analysis.

The soluble fractions of samples were analyzed for seven major anions (F^-, Cl^-, NO_2^-, SO_4^{2-}, Br^-, NO_3^-, PO_4^{3-}) and six major cations (Li^+, Na^+, NH_4^+, K^+, Ca^{2+}, Mg^{2+}) by using Ion Chromatography (IC, Dionex™ ICS-6000 Ion Chromatography System). The instrument had a built-in eluent generator (ultrapure water mixed with KOH for anions and methane sulfonic acid for cations) and was operated using Chromeleon™ Chromatography Data System (version 7.2.9) software. The injection volume and flow rate during instrument operation were set at 2.5 μL and 0.38 mL/min, respectively. The ultrapure water used during cleaning, blank preparation, and calibration was produced using a Milli-Q® Direct Water Purification System (15.0 MΩ/cm resistivity).

The IC instrument was calibrated prior to analysis using separate anion and cation standard solutions with six concentration values ranging from 0.05 to 10 mg/L. The standard solutions were prepared using Sigma-Aldrich TraceCERT® Certified Reference Materials (Multi Anion Standard 2 for IC (Product No. 53798), Multi Anion Standard 3 for IC (55698), Nitrite Standard for IC (67276), and Multi Cation Standard 2 for IC (93159)). The detection limit (DL) for ionic concentrations was calculated as the sum of the average and three standard deviations of the blank values.

3.3.5 Source apportionment via CBPF

The identification of air pollutant sources was achieved through the application of CBF and CBPF modeling, incorporating mathematical calculations based on (Eq. 3.8):

$$CBF\ \Delta\theta\ = \frac{m_{\Delta\theta | C \geq x}}{n_{\Delta\theta}}, \quad (3.8)$$

where $m_{\Delta\theta}$ is the number of samples within the wind sector Δθ with concentration C ≥ x, and $n_{\Delta\theta}$ is the total number of ambient samples in the wind sector Δθ, X is a threshold for the episodes of ambient pollutant concentrations (e.g., the 75th or 90th percentiles) (Uria-Tellaetxe & Carslaw, 2014).

CBPF is based on ambient pollutant concentrations exceeding a specific threshold for a particular wind speed and direction sector. This enables a comparison of directional information about major pollution sources with a spatial map to assess consistency with pollution levels from significant emission sources at monitoring stations. Unlike CBF, CBPF relies on probability calculation employing wind speed, defined as (Eq. 3.9):

$$CBPF\,\Delta\theta,\ \Delta u = \frac{m\Delta\theta, \Delta u | C \geq x}{n\Delta\theta, \Delta u}, \quad (3.9)$$

where $m\Delta\theta$ is the number of samples in the wind sector Δθ and wind speed interval Δu with the concentration C ≥ threshold x; $n\Delta\theta,\ \Delta u$ is the total number of ambient samples in the wind sector Δθ and wind speed interval Δu (Jeričević et al., 2019; Sooktawee et al., 2020).

Bivariate polar plots use wind speed (r) and wind direction (θ) to display statistical information (e.g., mean pollutant concentrations). The data are segmented into bins based on wind conditions, and a Generalized Additive Model (Eq. 3.10) is applied for surface fitting to capture non-linear relationships and variable interactions in air pollution studies (Sooktawee et al., 2020).

$$\sqrt{C_i} = \beta_0 + s\left(u_i, \vee_i\right) + \varepsilon_i, \quad (3.10)$$

where C_i is pollutant concentration (μg/m^3), β_0 is the overall mean of response, $s\left(u_i, \vee_i\right)$ is isotropic smooth function of the *i*th value of wind covariates $u_i\ and\ \vee_i$ (

$u = \overline{u}.\sin sin\,(2\pi/\theta)$ and $v = \overline{u}.\cos cos\,(2\pi/\theta))$, $\overline{u}$ is mean with speed (m/sec), and ε_i is the *i*th residual (Uria-Tellaetxe & Carslaw, 2014).

CBPF can incorporate not only individual pollutant concentration points exceeding a specified threshold but also an interval of pollutant concentrations, defined as:

$$CBPF\ \Delta\theta, \Delta u(i) = \frac{m\Delta\theta,\Delta u|y\geq C\geq x}{n\Delta\theta,\Delta u}, \quad (3.11)$$

where $m\Delta\theta,\ \Delta u$ is the number of samples in the wind sector $\Delta\theta$ at the wind speed interval Δu (that have a concentration C between threshold interval y and x), and $n\Delta\theta, \Delta u$ is the total number of ambient samples at that particular wind direction and wind speed interval.

Unlike the bivariate CBF model, CBPF considers concentration intervals in addition to individual values above a threshold, offering more detailed insights into both prominent and 'hidden' pollution sources (Sooktawee et al., 2020). The CBF and CBPF analysis was performed with 'R' programming language with the Openair package (Carslaw and Beevers, 2012) (Carslaw, 2012).

3.3.6 $PM_{2.5}$ concentration prediction modeling

3.3.7.1 Statistical analysis

The Spearman's correlation test was applied to non-normally distributed datasets to determine the correlation coefficient (r) between $PM_{2.5}$ concentration and independent variables (i.e., PM_{10}, SO_2, CO, NO_2, NO, T, P, RH, WD, and WS). MLR was then executed to assess the relationship between the dependent variable ($PM_{2.5}$) and independent variables, with pre-regression assumptions verified. Model validation

employed statistical methods such as VIF, RMSE, MAE, NME, IA, PA, and R^2 (Thongthammachart & Wanida, 2019). Stata 14.2 software by StataCorp® was used for statistical analysis.

3.3.7.2 Machine Learning (ML) approach

The RF algorithm was employed for an ML model to predict $PM_{2.5}$ concentrations. The MLR dataset was divided into training (80%) and testing data (20%) due to the substantial number of predictor variables (10) and the dataset size (n = 7,912 for S5, n = 6,931 for S6). Python was utilized for RF model development and performance evaluation, using the same indices employed for MLR model validation. Furthermore, 10-fold cross-validation (CV) was conducted to assess training set performance, involving ten iterations of dividing it into training and validation subsets, followed by model performance analysis (Park et al., 2020; Kulkarni et al., 2022).

3.3.7.3 HHRA

The AIRQ+ software was used to estimate the impact of air pollution and associated health burdens for specific pollutants. The "Life Table Evaluation module" was utilized for HHRA to quantify DALY, a combination of YLL and YLD associated with $PM_{2.5}$ inhalation exposure in Astana (Eq. 3.12).

DALY = YLL + YLD, (3.12)

where YLL is Years of Life Lost due to premature death and YLD is Years of Life Lost due to Disability.

Data on respiratory and cardiovascular mortality and morbidity were used for YLD calculation, while YLL data were obtained from the national socio-economic

status database of the Republic of Kazakhstan. The RR was calculated using the mean $PM_{2.5}$ concentration and β from previous studies. AIRQ+ then employs RR to determine YLL for different age groups (Eq. 3.13).

$$RR = e^{\beta \times \Delta x}, \quad (3.13)$$

where Δx denotes the difference between the observed $PM_{2.5}$ concentrations and the threshold $PM_{2.5}$ concentration assumed to cause adverse health effects.

YLD values were calculated based on mortality cases, disability weights, and PAF for each disease or disability group. PAF accounts for the fraction of the population exposed to elevated $PM_{2.5}$ concentrations (Eq. 3.14).

$$YLD = \sum(\text{Mortality cases} \times \text{Disability weight} \times \text{PAF}), \quad (3.14)$$

where, Disability weight is the specific disability level for each disease or disability group and $PAF_{i,g}$ is the population attributable fraction of disease or disability group i for a population group g, which is calculated as (Jung et al., 2019; Yang et al., 2019):

$$PAF = \frac{Population\ proportion_g \times (RR_{i,g} - 1)}{Population\ proportion_g \times (RR_{i,g} - 1) + 1}, \quad (3.15)$$

where Population proportion g is the fraction of the population exposed to elevated $PM_{2.5}$ concentrations in a population group g (Jung et al., 2019; Yang et al., 2019).

3.3.7 KAP of air pollution among residents of Astana

3.3.8.1 Instrumentation

The framework of the survey instrument was adapted from Chin et al. (2019). The 32-item questionnaire was created via an online research software, Qualtrics (Qualtrics LLC, UT, US), in the form of a self-administered questionnaire. The snowballing sampling technique has been used. The online questionnaire was designed in three

languages: English, Kazakh, and Russian, to guarantee that respondents could comfortably respond to questions in their preferred language. A sample of the survey in English is provided in Appendix A. The survey response collection was approved by the institutional research ethics committee (Nazarbayev University Institutional Research Ethics Committee (NU IREC)) (NU IREC approval number: 564/28042022).

The survey questionnaire was divided into three sections. The first part contained seven questions on the sociodemographic parameters of the studied population (age, gender, education, employment status, work environment, average household income, and chronic health conditions). The second part contained three questions to assess the awareness of the studied population about air pollution. This section had three multiple-choice questions to understand the perception of the general public on air quality in the region, knowledge about potential sources of air pollution, and the sources of information regarding air pollution-related topics. The second part also contained six true/false questions further evaluating participants' knowledge of air pollution monitoring systems, sources of gaseous pollutants, air pollution-related indicators (e.g., API), and health effects related to air pollution. The third part evaluated the participants' attitudes toward environmental protection and was composed of sixteen statements on a 5-point Likert scale. Statements covered the attitude of the studied population toward economic cost and governmental pollution management prices as well as Willingness-to-pay (WTP for environmental protection.

3.3.8.2 Statistical analysis

With regard to the assessment of knowledge of potential sources of air pollution in Section 2a of the questionnaire, each correct answer was given 1 point, leading to a total

of 8 maximum points. In Section 2b, 1 point was given for a correct answer, -0.2 for an incorrect response, and 0 points when answered 'I don't know' (leading to a total of 6 points). In Section 3 of the questionnaire, a higher score on a 5-point Likert scale indicated more positive attitudes in Statements 17, 19, 21, 25, 27, 28, 29, 31, and 32; whereas statements 20, 22, 23, 26, and 30 were scored in reverse i.e., a higher score indicating a negative attitude toward environmental protection.

Four statements (#17, 23, 26, and 30) represent the affective component of the attitude scale whereas five statements (#18, 25, 27, 28, and 32) denote the cognitive element. The conative component of the attitude scale is reflected in the five statements related to WTP for environmental protection (statements #19, 21, 24, 29, and 31).

The statistical analyses including descriptive analysis, t-tests, and chi-square association tests have been conducted via Stata 14.2 by StataCorp. 2015 (TX, US) to assess the relationships between knowledge about air pollution, concerns about air quality, attitudes towards environmental protection, and demographic characteristics.

3.3.8.3 Structural Equation Modeling (SEqM) and Model Validity

The SEqM tool was used to evaluate the proposed model's reliability and validity and to test the hypotheses set. SEqM allows multivariate analysis of the relationships between the variables (Hair et al., 2018). Table 3.5 and Figure 3.4 represent the SEqM's latent, observable variables, related questions, and the model itself. First, the partial-least squares technique was used to identify the path loadings. Each latent variable was described through a minimum of two observable variables. Then, to check the hypothesis, bootstrapping was used to derive heterotrait-heteromethod correlation statistics, thus, calculating the standard error, which helps to identify the bootstrap

confidence interval (95% limit). The model validity was then checked through statistical values such as outer loadings, Cronbach's Alpha, average variance extracted, Dillon-Goldstein's rho, and composite reliability. The acceptance criteria were the following: outer loadings > 0.7, Cronbach's Alpha > 0.7, Average variance extracted > 0.5, Dillon-Goldstein's rho (rho_A) > 0.7, and composite reliability > 0.7.

Table 3.5: Latent, observable variables and their corresponding questions.

Latent variable	Observable variable	Question
Environmental Attitude	EA1	Educating the younger generation about the knowledge of environmental protection is important.
	EA2	Taking care of the environment is something I really care about.
	EA3	Air pollution caused by cars is extremely dangerous to health.
	EA4	To protect the environment, Kazakhstan needs economic growth.
	EA5	I do not mind paying more money to use better-quality gasoline, which leads to less pollution.
	EA6	Protecting the environment should be given priority, even if it causes slower economic growth.
Perception of national air pollution and economy	P1	Air pollution is a fair price to pay for economic development.
	P2	The economic growth of Kazakhstan is currently more important than environmental protection.
	P3	There is no point in doing what I can for the environment unless everyone does the same.
	P4	Kazakhstani worry too much about industrial development polluting the atmosphere and degrading human health.
	P5	Nothing can be done by me or my family/friends to improve the current atmospheric situation.
	P6	The air quality in Kazakhstan is getting better because of modern science and technology.
	P7	Kazakhstan's government has to reduce atmospheric pollution, but it should not cost me any money.
WTP	WP1	I do not mind an increase in taxes if the extra money is used to prevent further atmospheric pollution.
	WP2	I am willing to accept cuts in my standards of living to protect the environment.
	WP3	I would contribute part of my income if I were certain that the money would be used to prevent atmospheric pollution.
Institutional knowledge	KoI1	Sulfur dioxide (SO_2), which is a serious air pollutant, mainly comes from coal-heated power plants and residential heating.
	KoI2	Air pollution is a fair price to pay for economic development.
Knowledge of local air quality	KoLAQ1	The air quality in Kazakhstan is getting better because of modern science and technology.

KoLAQ2	Kazakhstani worry too much about industrial development polluting the atmosphere and degrading human health.

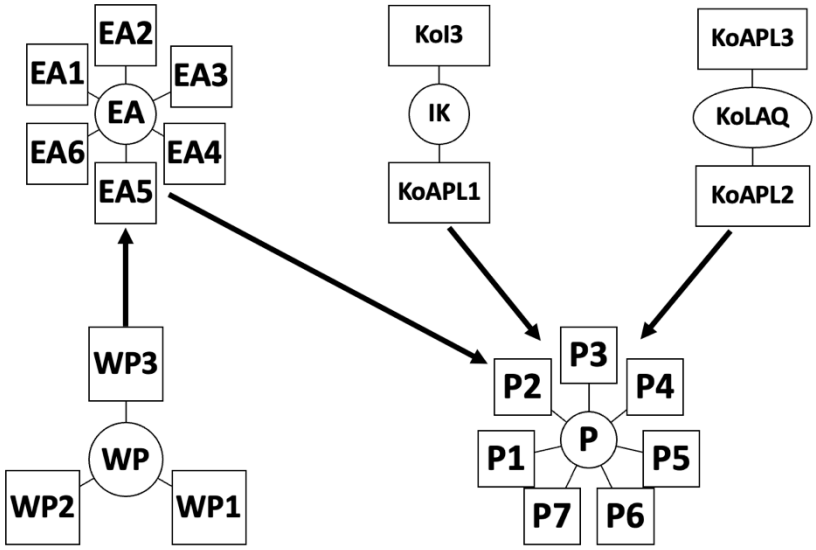

Figure 3.4: Proposed SEqM model.

3.4 Chapter summary

This chapter describes the methodological framework utilized in the current research. A comprehensive air quality analysis using air pollution data from 2018 to 2023 as well as research findings from experimental procedures were employed for (1) morphological characterization of PM particles collected in Astana; (2) identification of major local emission sources; (3) characterization of PM toxicity via *in vitro* lung bioaccessibility and health risk assessment; (4) investigation of precipitation chemistry; (5) modeling of PM concentration and (6) assessment of knowledge, perception, and attitude of the local population about air pollution.

CHAPTER 4: RESULTS AND DISCUSSION

4.1 Effect of SLF composition on lung bioaccessibility

4.1.1 Bioaccessibility of PTEs in GS and ALF

Overall, higher bioaccessibility (%) in ALF than in GS was present for all PTEs after testing for 1 w (Table 4.1). The bioaccessibility in ALF was the highest for Ni (SRM 2691) and Cd (BGS 102) (61.9% and 91.0%, respectively). Only for selected PTEs (e.g., Cr, Cu, V in SRM 2691 and Cu, Mn, V in BGS 102) the bioaccessible concentration was above the DL when using GS. Vanadium in SRM 2691 showed the highest bioaccessible concentration (50.1 $mg \cdot kg^{-1}$) in GS. For BGS 102, dissolved in GS, the highest bioaccessibility fraction of 43.9% was observed for Cu.

Table 4.1: Bioaccessible concentrations ($C_{bio\text{-}cumul}$, $mg \cdot kg^{-1}$ ± RSD (relative standard deviation in %)) and fractions ($\%_{bio}$) of Cd, Co, Cr, Cu, Mn, Ni, Pb, Sb, V, and Zn for a 1 w extraction in GS and ALF and an S/L ratio of 1/100 (n = 4) for selected PTEs in SRM 2691 and BGS 102.

	SRM 2691				**BGS 102**			
PTEs	GS		ALF		GS		ALF	
	$C_{bio\text{-}cumul}$	$\%_{bio}$	$C_{bio\text{-}cumul}$	$\%_{bio}$	$C_{bio\text{-}cumul}$	$\%_{bio}$	$C_{bio\text{-}cumul}$	$\%_{bio}$
Cd	<0.06 ± —*	—**	1.02 ± 8.42	—	<0.06± —	<22.0 ± —	0.25 ± 14.3	91.0 ± 14.3
Co	$<3\times10^{-4}$ ± —	<1.11 ± —	0.01 ± 7.23	54.6 ± 7.23	<0.29 ± —	<0.72 ± —	18.7 ± 4.11	46.9 ± 4.11
Cr	18.6 ± 19.6	27.3 ± 19.6	41.7 ± 1.86	61.4 ± 1.86	<1.74 ± —	<0.78 ± —	26.5 ± 0.18	11.8 ± 0.18
Cu	9.86 ± 11.7	—	94.1 ± 1.00	—	11.4 ±3.71	43.9 ± 3.71	<63.2 ± —	—
Mn	<1.52 ± —	<0.76 ± —	108 ±6.07	54.1 ± 6.07	12.6 ± 21.0	0.17 ± 21.0	4.51 ± 1.03	61.5 ± 1.03
Ni	<2.64 ± —	<4.98 ± —	32.8 ± 3.40	61.9 ± 3.40	<2.64 ± —	<3.30 ± —	0.02 ± 1.17	24.1 ± 1.17
Pb	<0.23± —	<0.80 ± —	13.0 ± 1.11	44.9 ± 1.11	<0.23 ± —	<0.29 ± —	0.03 ± 1.18	36.5 ± 1.18
Sb	<0.79 ± —	—	<3.66 ± —	—	<0.79 ± —	—	10.5 ± 4.15	—
V	50.1 ± 19.0	—	172 ± 6.13	—	10.2 ± 2.93	2.87 ± 2.93	0.03 ± 1.81	7.57 ± 1.91
Zn	<3.16 ± —	<2.64 ± —	61.0 ± 0.74	50.8 ± 0.74	<3.16 ± —	<1.65 ± —	0.05 ± 3.31	25.8 ± 3.31

* RSD not present

** Bioaccessibility value (%) not present

The difference in pH of GS and ALF is the major parameter affecting the PTEs release resulting in different bioaccessibility measurements as PTEs mobility is generally inversely proportional to pH constituents (McLean & Bledsoe, 1992). Moreover, the presence of citrate in ALF accelerates the metal release by forming metallic complexes, increasing the chelating capability of ALF (Hedberg et al., 2010; Hillwalker & Anderson, 2014). This overall outcome is also in line with literature suggesting that PTEs tend to be more bioaccessible in the acidic environment of ALF (Julien et al., 2011; Guney et al., 2016; Pelfrêne et al., 2017; Verougstraete et al., 2022).

4.1.2 Bioaccessibility of PTEs in GS modified with DPPC and cholesterol

For the one-week extraction period, the presence of DPPC and cholesterol had a bidirectional effect, increasing and decreasing the bioaccessibility of certain PTEs i.e., the ones with concentrations above DLs (e.g., Cu, Mn, and V in BGS 102, and Cr, Cu, and V in SRM 2691) (Table 4.2).

For BGS 102, the bioaccessibility of Cu and Mn in BGS 102 remained similar when testing in modified GS. However, a formulation with a combination of 5% DPPC+0.5% cholesterol resulted in an increase in Cu bioaccessibility from 43.5% to 51.5%. When 5% DPPC only was present, the bioaccessibility of V in BGS 102 increased from 2.87% to 8.35%.

For SRM 2691, the bioaccessible fraction of Cr increased with individual incorporation of 0.25% cholesterol or 5% DPPC, rising from 27.3% to 31.5% and 33.2%, respectively. In contrast, the formulations containing DPPC + cholesterol in the two tested concentrations resulted in a decrease in Cr bioaccessibility: to 22.4% in the

2% DPPC + 0.25% cholesterol, which further decreased to 16.7% in the 5% DPPC + 0.5% cholesterol. Moreover, the individual addition of 0.5% cholesterol slightly decreased Cr bioaccessibility from 27.3% to 22.0%. The bioaccessible concentration of V (original: 50.1 $mg \cdot kg^{-1}$) in modified GS also increased, with a higher bioaccessible concentration in the formulation with 0.25% cholesterol (61.2 $mg \cdot kg^{-1}$) and 5% DPPC (57.5 $mg \cdot kg^{-1}$) concentration. Similarly, the bioaccessible concentration of V slightly decreased when tested in GS modified with DPPC + cholesterol (e.g., 41.8 $mg \cdot kg^{-1}$ in 2% DPPC + 0.25% cholesterol and 33.1 2% $mg \cdot kg^{-1}$ in 5% DPPC + 0.5% cholesterol). The bioaccessible concentration of Cu in SRM 2691 showed a slight increase in all modifications employed. The 5% DPPC + 0.5% cholesterol resulted in the highest bioaccessible concentration of Cu (original: 9.86 $mg \cdot kg^{-1}$ and modified: 12.4 $mg \cdot kg^{-1}$).

The combination of DPPC and cholesterol in the solution can promote the formation of hydrophobic lipid bilayers or micelles favoring the solubilization of hydrophobic compounds. Moreover, they can act as the stabilizing ligand, interacting with metal ions (e.g., Cu^{2+}) and preventing the formation of metal aggregates. The findings indicate that the effect of SLF modification is highly sample and element-specific. The results also suggest that for a more effective *in vitro* dissolution of V, it is recommended to use GS with DPPC in higher concentrations. Moreover, for Cu-containing samples, it is feasible to employ a combination of DPPC and cholesterol in higher concentrations when testing with GS. However, the findings also suggested that using a higher concentration of cholesterol in GS can lead to the formation of lipid-rich complexes or aggregates that can act as salting–out agents, decreasing the solubility of metal ions (e.g., Cr).

Table 4.2: Bioaccessible concentrations ($C_{bio\text{-}cumul}$, $mg \cdot kg^{-1}$ ± RSD (relative standard deviation in %)) and fractions ($\%_{bio}$ ± RSD (relative standard deviation in %)) of selected PTEs in SRM 2691 and BGS 102 for a 1 w extraction and an S/L ratio of 1/100 in modified GS (n = 12).

SRM 2691

PTEs	Not modified		Low Cholesterol		High Cholesterol		Low DPPC		High DPPC		Low Cholesterol/Low DPPC		High Cholesterol/ High DPPC	
	$C_{bio\text{-}cumul}$	$\%_{bio}$	$C_{bio\text{-}cumul}$	$\%_{bio}$	$C_{bio\text{-}cumul}$	$\%_{bio}$	$C_{bio\text{-}cumul}$	$\%_{bio}$	$C_{bio\text{-}cumul}$	$\%_{bio}$	$C_{bio\text{-}cumul}$	$\%_{bio}$	$C_{bio\text{-}cumul}$	$\%_{bio}$
Cd	<0.06 ± —*	—**	<0.06± —	—	<0.06 ± —	—	<0.06 ± —	—	<0.06 ± —	—	<0.06 ± —	—	<0.06 ± —	—
Co	$<3\times10^{-4}$ ± —	<1.11 ± —	$<3\times10^{-4}$ ± —	<1.11 ± —	$<3\times10^{-4}$ ± —	<1.11 ± —	$<3\times10^{-4}$ ± —	<1.11 ± —	$<3\times10^{-4}$ ± —	<1.11 ± —	$<3\times10^{-4}$ ± —	<1.11 ± —	$<3\times10^{-4}$ ± —	<1.11 ± —
Mn	<1.52 ± —	<0.76 ± —	<1.52 ± —	<0.76 ± —	<1.52 ± —	<0.76 ± —	15.7 ± 6.61	7.83 ± 6.61	<1.52 ± —	<0.76 ± —	<1.52 ± —	<0.76 ± —	<1.52 ± —	<0.76 ± —
Ni	<2.64 ± —	<4.98 ± —	<2.64 ± —	<4.98 ± —	<2.63 ± —	<4.97 ± —	<2.63 ± —	<4.97 ± —	<2.64 ± —	<4.98 ± —	<2.64 ± —	<4.98 ± —	<2.64 ± —	<4.97 ± —
Pb	<0.23± —	<0.80 ± —	<0.23± —	<0.80 ± —	<0.23± —	<0.80 ± —	<0.23± —	<0.80 ± —	<0.23± —	<0.80 ± —	<0.23± —	<0.80 ± —	<0.23± —	<0.80 ± —
Sb	<0.79 ± —	—	≤0.81± —	—	<0.79 ± —	—	<0.79 ± —	—	≤0.86 ± —	—	<0.79 ± —	—	<0.79 ± —	—
Zn	<3.16 ± —	<2.64 ± —	<3.16 ± —	<2.64 ± —	≤3.92 ± —	<3.26 ± —	<3.16 ± —	<2.64 ± —	<3.16 ± —	<2.64 ± —	≤26.5 ± —	≤22.1 ± —	<3.16 ± —	<2.64 ± —

BGS 102

PTEs	Not modified		Low Cholesterol		High Cholesterol		Low DPPC		High DPPC		Low Cholesterol/Low DPPC		High Cholesterol/ High DPPC	
	$C_{bio\text{-}cumul}$	$\%_{bio}$	$C_{bio\text{-}cumul}$	$\%_{bio}$	$C_{bio\text{-}cumul}$	$\%_{bio}$	$C_{bio\text{-}cumul}$	$\%_{bio}$	$C_{bio\text{-}cumul}$	$\%_{bio}$	$C_{bio\text{-}cumul}$	$\%_{bio}$	$C_{bio\text{-}cumul}$	$\%_{bio}$
Cd	<0.06± —	<22.0 ± —	<0.06± —	<22.0 ± —	<0.06± —	<22.0 ± —	<0.07± —	<26.6 ± —	<0.06± —	<22.0 ± —	<0.06± —	<21.9 ± —	<0.06± —	<21.9 ± —
Co	<0.29 ± —	<0.72 ± —	<0.29 ± —	<0.72 ± —	<0.29 ± —	<0.72 ± —	<0.29 ± —	<0.72 ± —	<0.29 ± —	<0.72 ± —	<0.29 ± —	<0.72 ± —	<0.29 ± —	<0.72 ± —
Cr	<1.74 ± —	<0.78 ± —	<1.74 ± —	<0.78 ± —	<1.74 ± —	<0.78 ± —	11.8± 20.0	5.26 ± 20.0	<1.74 ± —	<0.78 ± —	<1.74 ± —	<0.77 ± —	<1.74 ± —	<0.77 ± —
Ni	<2.64 ± —	<3.30 ± —	<2.64 ± —	<3.30 ± —	<2.64 ± —	<3.30 ± —	<2.64 ± —	<3.29 ± —	<2.64 ± —	<3.30 ± —	<2.63 ± —	<3.29 ± —	<2.63 ± —	<3.29 ± —
Pb	<0.23 ± —	<0.29 ± —	≤0.30 ± —	<0.38 ± —	<0.23 ± —	<0.30 ± —	<0.23 ± —	<0.29 ± —	<0.23 ± —	<0.29 ± —	<0.23 ± —	<0.29 ± —	<0.23 ± —	<0.29 ± —
Sb	<0.79 ± —	—	<0.79 ± —	—	<0.79 ± —	—	<0.79 ± —	—	<0.79 ± —	—	<0.79 ± —	—	<0.79 ± —	—
Zn	<3.16 ± —	<1.65 ± —	<3.16 ± —	<1.66 ± —	<3.16 ± —	<1.66 ± —	<13.2 ± —	<6.89 ± —	<3.72 ± —	<1.95 ± —	<3.16 ± —	<1.65 ± —	<3.16 ± —	<1.65 ± —

* RSD not present.

** Bioaccessibility value (%) not present.

To formulate a solution that closely emulates the composition of fluids naturally present in human lungs, it may be viable to substitute a lung surfactant with DPPC or cholesterol. DPPC plays a critical role in facilitating the release of contaminants from particulates, serving as a mild chelating agent, thereby enhancing the wettability of hydrophobic particles, and preventing particle agglomeration. Recent studies have investigated the impact of DPPC on metal release. Pelfrêne et al. (2017) demonstrated that the incorporation of DPPC did not exert a substantial impact on the bioaccessibility of most PTEs they examined. However, they suggested that a concentration of approximately 100 mg/L of DPPC should be employed in SLFs. W. Li et al. (2016) reported a 5.6–18% reduction in Pb bioaccessibility in GS upon the exclusion of DPPC, as investigated across various environmental settings. This further underscores the importance of lung surfactants in the *in vitro* dissolution of selected PTEs.

4.2 Effect of S/L ratio on lung bioaccessibility

Lower particle load resulted in a higher bioaccessibility in ALF for Co, Ni, Pb, V, and Sb (BGS 102) and Co, Cr, Mn, Ni, and Pb (SRM 2691) (Figure 4.1). The average bioaccessibility values for lower S/L ratio (BGS 102) decreased in the following order: Pb (94.8%) > Co (90.8%) > Ni (59.8%) >Sb (20.5%) >V (19.5%). In a higher S/L ratio (BGS 102), however, Co was the most bioaccessible metal (46.9%), followed by Pb (36.5%), Ni (24.1%), Sb (10.5%), and V (7.57%). In SRM 2691, Cr showed the highest solubility in ALF in both S/L ratio values (61.9% and 86.0% in 1/100 and 1/500 S/L ratio, respectively). In a 1/100 particle loading, Pb was the least bioaccessible element in ALF (44.8%), while in a 1/500 S/L ratio, Mn was the least soluble (54.1 %). The

extraction in GS showed a similar trend, but lower bioaccessibility values. In BGS 102, the bioaccessibility of V was 5 times higher in a lower S/L ratio (2.87% and 14.5%, respectively). In SRM 2691 the bioaccessibility value of Cu increased from 9.9% to 58.0% for a lower S/L ratio value in GS.

Several studies examined the effect of different S/L ratios on the bioaccessibility of PTEs in SLFs ranging from 1/20,000 to 1/2 (Pelfrêne et al., 2017). A study by Julien et al. (2011) suggested that metal release in SLFs decreases with the increase in particle loading. The same author argues that the S/L ratio of >1/500 increases the probability of solution saturation and competition between soluble PTEs. Similarly, a study by Tomašek et al. (2021) compared S/L ratios of 1:10, 1:20, 1:100, 1:500, and 1:1000 for volcanic ash samples and found that a lower S/L ratio resulted in higher *in vitro* lung bioaccessibility for Al, Co, Cr, Cu, Fe, Mn and V. However, a study by Pelfrêne et al. (2017) suggested that the bioaccessibility of Ba, Cd, Co, Cr, Cu, Mn, Ni, Pb, Sr, and Zn in three SRMs (BCR-723, NIST 2710a, and NIST 1648a) remains consistent regardless of the S/L ratio (i.e., range of 1:1,000 to 1:10,000) in ALF.

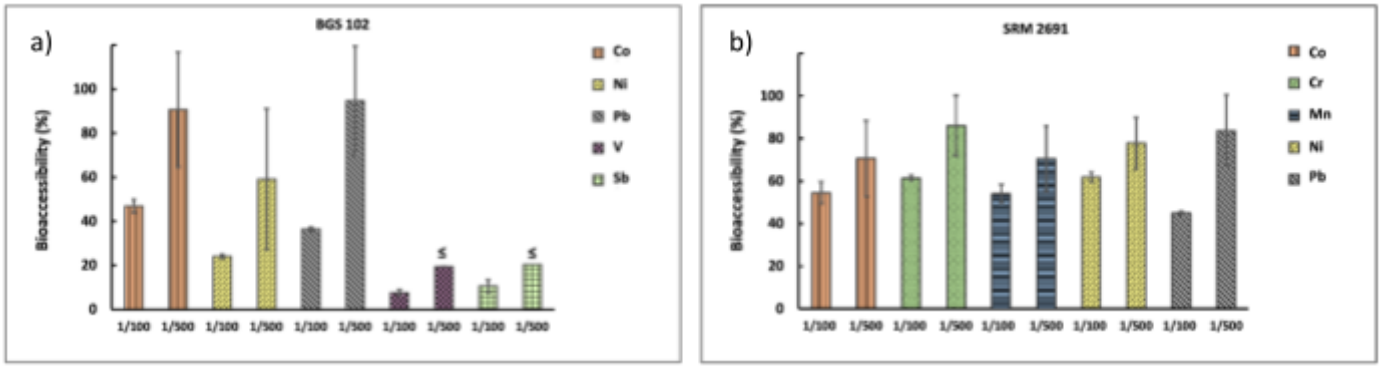

≤One of the replicate values is less than DL.

Figure 4.1: The comparison of solid–to–liquid ratio (1/100; 1/500) and bioaccessibility of selected PTEs in (a) BGS 102 and (b) SRM 2691 in ALF extraction for 1w.

Although an S/L ratio of 1/100 is the most employed for *in vitro* bioaccessibility experiments (Kastury et al., 2017), it can result in particle agglomeration and chelator saturation which disrupts the dissolution of PTEs in SLF (Kastury et al., 2018). However, a higher particle load can provide a more accurate simulation of human PM exposure that ranges from 20 μg/m^3 to 500 μg/m^3 relative to 5–20 mL of lung fluid (Julien et al., 2011). The effect of the S/L ratio on bioaccessibility is also sample and metal-specific, which was supported by the findings of the present research. Moreover, other physiological parameters used for *in vitro* experiments can impact as well (Gosselin & Zagury, 2020). The number of particle loads should also be practical for researchers to handle, while still accurately reflecting the conditions of the system being studied (Julien et al., 2011).

4.3 Effect of extraction time on lung bioaccessibility

The solubility rate of Co, Cr, Mn, Ni, and Pb (BGS 102) in ALF showed a consistent increase up to 4 w (672 h) (Figure 4.2). As a result, for Co, Cr, Mn, Ni, and Pb, the cumulative bioaccessible fraction (%) was the highest at 4 w (52.2%, 16.6%, 62.4%, 35.2%, and 41.1%, respectively).

The effect of extraction time on PTEs bioaccessibility in ALF was highly element-specific for SRM 2691. The bioaccessibility of Mn and Cr in SRM 2691 exhibited a similar pattern to that observed in BGS 102 when tested in ALF. At a 4 w (672-hour) extraction period, both PTEs showed the highest bioaccessibility, reaching 58.6% and 73.4%, respectively. However, Pb and Zn were soluble in ALF at the highest rate at the beginning of the experiment (2h) (73.3% and 76.3%, respectively), followed by a sharp decline and gradual growth over time. For Co (SRM 2691), specifically, the

solubilization rate decreased within 1d (24 h) extraction and increased with longer test durations.

Selected PTEs (e.g., Cu, Cr, and V) in both SRMs generally showed poor solubility in GS and no apparent dependency on test duration. However, for Cu and V in BGS 102, the highest bioaccessibility value in GS was reached at 1 d (24 h) (51.7% and 3.23%, respectively), followed by a subtle drop and increase at 4 w (672 h) extraction. The solubility of Cr and V in SRM 2691, similar to the extraction in ALF, showed a gradual solubility growth with longer test times.

The extraction times used in bioaccessibility studies range from several minutes to 360 d in the literature (Twining et al., 2005; Ren et al., 2020). However, no consensus has been reached on the optimal extraction time for lung bioaccessibility testing, and the selection of test duration was based on the specific research question and the material being tested. Lima et al. (2013) investigated the effect of rapid and slow dissolution rates (10 min–360 days) on bioaccessibility

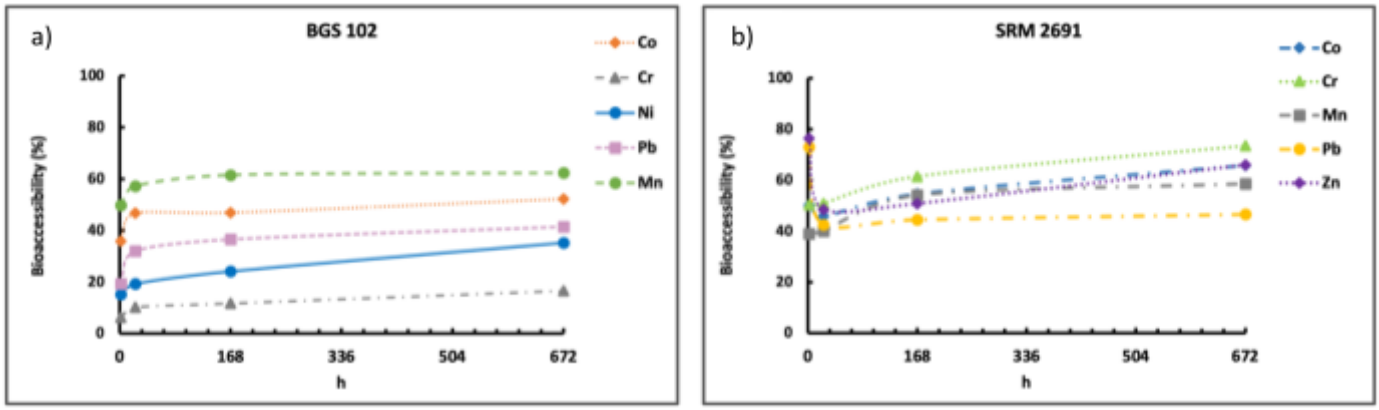

Figure 4.2: The comparison of cumulative bioaccessibility (%) of selected PTEs in (a) BGS 102 and (b) SRM 2691 in ALF vs time (h) (1/100 S/L ratio, 100 rpm).

measurements of Ni, Cd, and Zn compounds in GS. Rapid dissolution of these PTEs is proposed to be highly affected by the presence of soluble sulfur compounds (Lima et al., 2013). Zereini et al. (2012) explain that a steady solubility decrease following the highest dissolution time of selected PTEs is most likely caused by either the reabsorption of dissolved PTEs onto the surfaces of the atmospheric particles or sticking onto the surface of the centrifuge tube after a certain period. A study by Tang et al. (2019) investigated the bioaccessibility of As, Cr, Ni, Cu, Zn, Pb, Cd, Co, and V in airborne PM after 8 h, 24 h, 48 h, and 72 h extraction with solubility equilibrium reached after 24 h-72 h. According to Julien et al. (2011), the optimal time to estimate the bioaccessibility of PTEs in SRMs at the upper limit is 24 h. However, the findings of the present research do not support these recommendations suggesting longer test duration (> 4 w) for particles of geological origin and coal ash samples.

4.4 Effect of agitation on lung bioaccessibility

Agitation is a mechanical step commonly applied for experimental procedure on *in vitro* lung bioaccessibility (Ren et al., 2020). Agitation represents a mechanical force that occurs in the lungs during normal breathing. A spontaneous particle agglomeration in SLFs, when no agitation is employed, can reduce the available surface area affecting the interaction between contaminants and chelators (Ansoborlo et al., 1990), decreasing elemental solubility. In the present work, the solubility of most PTEs in ALF (e.g., Cd, Co, Cr, Mn, Ni, Pb, Sb, and Zn in BGS 102 and Co, Cr, and Ni in SRM 2691) increased with a higher agitation speed (Figure 4.3). However, bioaccessibility of Pb and Zn (SRM 2691) in ALF showed a slightly higher value when 20 rpm agitation was employed (45.0 % vs 46.1%, and 61.0% vs 63.7%, respectively). In ALF, Ni (SRM

2691) and Cd (BGS 102) were the most bioaccessible element at 100 rpm, with 61.9% and 91.0% solubility, respectively (compared to 54.6% and 79.7% at 20 rpm, respectively). Increasing agitation speed yielded a 25% increase in the bioaccessibility of Mn (BGS 102) in ALF. The solubility of selected PTEs (e.g., Cu and Mn in BGS 102, and Cr, Cu, and V in SRM 102) followed a similar pattern in GS with higher bioaccessibility values at 100 rpm.

Lower agitation speed can increase the probability of particle clogging reducing the bioaccessibility of PTEs, however, it might more accurately represent lung physiology. Although a higher agitation speed (e.g., 100 rpm) yielded higher bioaccessibility values for selected PTEs, we are hesitant to recommend it for a routine bioaccessibility procedure, unless supported by *in vivo* validation. Future research can dive more into understanding the effect of different agitation methods (e.g., end–over–end rotation, orbital shaking, magnetic stirring, occasional stirring) on bioaccessibility measurements.

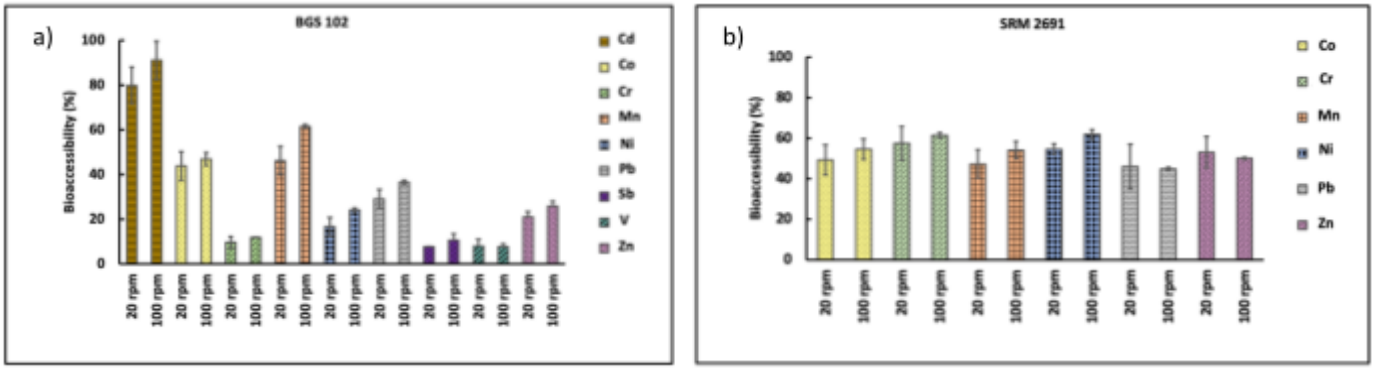

Figure 4.3: Effect of agitation on bioaccessibility of selected PTEs in (a) BGS 102 and (b) SRM 2691 in ALF (1 w, 1:100 S/L ratio).

4.5 Reproducibility, uncertainty, and limitations of the lung bioaccessibility method

The optimization of parameters for the *in vitro* lung bioaccessibility experiments was followed by the estimation of reproducibility and uncertainty regarded the studied SRMs and PTEs. The average bioaccessibility values and RSD were obtained for the two SRMs in 36 replicates. The RSD values of the selected PTEs in the SRMs were, on average, less than 20%, indicating good reproducibility in assessing metal bioaccessibility. The RSD values of > 20% are primarily associated with possible contamination.

For the present dissertation, the estimation of the metal recovery was carried out by the addition of a spiking solution containing Co, Ni, Pb, and Zn into the ALF with and without SRM 2691 (Table 3.4). The recovery percentage for Co, Ni, Pb, and Zn in ALF without samples was somewhat satisfactory. The sorption for spiked metals in SRM 2691 decreased in order: Co > Ni > Zn > Pb. For *in vitro* tests containing SRM 2691 the recovery percentage for Pb and Zn were, in general, lower than for other spiking metals. Moreover, after 2h the percent recovery of Zn was 5%, reaching the highest value of 30% after 2 w extraction. A low percent recovery of certain spiking metals can be attributed to several factors including the matrix effect, analyte loss, instrumental sensitivity, and contamination during sample handling and analysis. It is crucial to account for the sample losses for the result interpretation step. One approach is to correct for low recovery by averaging the recovery observed when analyzing spiked samples. Alternatively, calibrators should consider the same pre-treatment process as the samples to address this issue (Mateos et al., 2020).

4.6 Total PM mass concentration

The average concentration of collected $PM_{2.5}$ samples was 28.7 μg/m^3 (range: 0 - 543 μg/m^3) which exceeds the WHO annual air quality guidelines by 5.75 times (5 μg/m^3). It should be noted that dust incursions were not considered for the calculation of mean PM values. In terms of the mean concentration of $PM_{2.5}$, fall was the most polluted season (mean: 38.5 μg/m^3), followed by winter (mean: 34.3 μg/m^3), summer (mean: 23.5 μg/m^3), and spring (mean: 21.6 μg/m^3) (Figure 4.4a). The highest 24-h $PM_{2.5}$ concentration of 543 μg/m^3 was observed in November and was 36.2 times higher than WHO's 24-h air quality guideline level (15 μg/m^3). The second-highest concentration was detected in February (531 μg/m^3) (Figure 4.5a). The AQI for $PM_{2.5}$ ranged from good to hazardous throughout the sampling period, mostly falling within a good or moderate category (Figure 4.6a). However, the number of days that are classified in terms of AQI as unhealthy for sensitive individuals, unhealthy, and hazardous out of the whole sampling period were 9, 10, and 3, respectively.

Similarly, the average $PM_{2.5-10}$ concentration of 226 μg/m^3 (range: 0 - 1,564 μg/m^3) exceeds WHO's annual permissible level by 15.1 times (15 μg/m^3). The highest 24-h $PM_{2.5-10}$ concentration was observed in June (1,564 μg/m^3) which exceeds WHO's 24-h standards by 34.8 times (Figure 4.4b). In the present work, the concentration of $PM_{2.5-10}$ across four seasons was the highest in summer (mean: 272 μg/m^3), followed by spring (mean: 268 μg/m^3), fall (mean: 158 μg/m^3), and winter (mean: 135 μg/m^3) (Figure 4.5b). The $PM_{2.5-10}$ concentration concerning AQI varied substantially throughout the sampling period. Out of 171 sampling days, 17 and 13 days fell within the hazardous and very unhealthy categories, respectively (Figure 4.6b).

The evaluation of air pollution levels in Astana from 2017 to 2021, based on API (Air Pollution Index) and calculation of GR (greatest repeatability) criteria, points out a

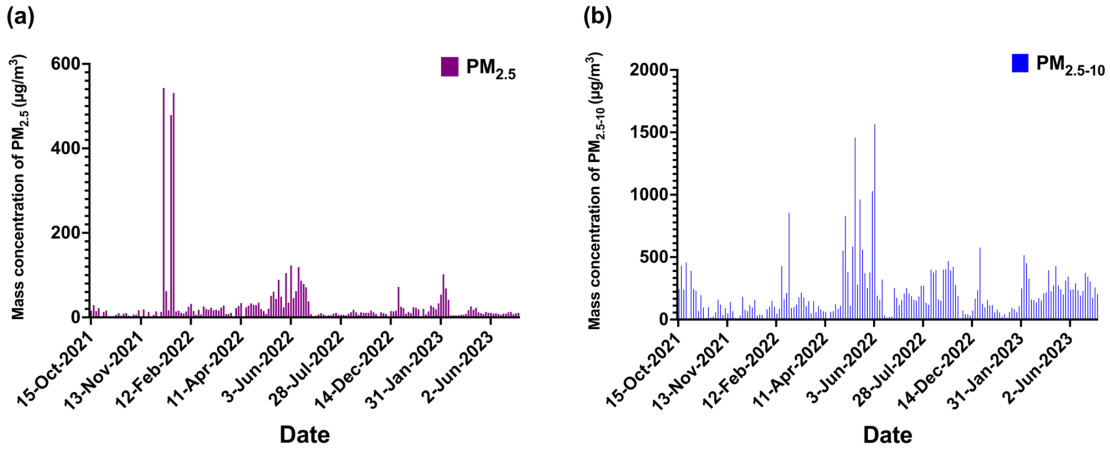

Figure 4.4: Total mass concentration (µg/m^3) (24 h) of (a) $PM_{2.5}$ and (b) $PM_{2.5\text{-}10}$

consistent classification of Astana's air quality level as the 3^d degree, indicating a high level of air pollution. Furthermore, according to Beisenova et al. (2023), the annual average concentration of $PM_{2.5}$ exceeded the WHO maximum permissible level of 5 µg/m^3 for the years 2017-2021, with recorded values of 0.70 mg/m^3, 0.88 mg/m^3, 1.27 mg/m^3, 3.17 mg/m^3, and 1.39 mg/m^3, respectively, indicating a substantial deviation from the recommended air quality standards. This is predominantly attributed to the emissions of pollutants from various sources such as CHPPs, transportation, and the

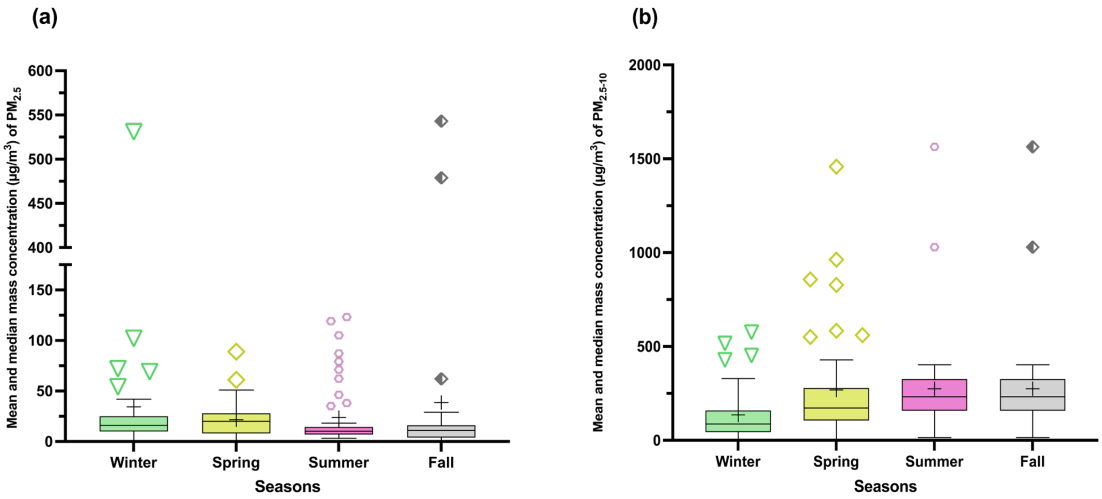

private sector

Figure 4.5: Mean and median mass concentration (μg/m^3) of (a) $PM_{2.5}$ and (b) $PM_{2.5-10}$ in four seasons.

Figure 4.6: The mass concentration (μg/m^3) of (a) $PM_{2.5}$ and (b) $PM_{2.5-10}$ with respect to AQI category

(Beisenova et al., 2023). Moreover, fossil fuel combustion remains the primary contributor to air pollution in Kazakhstan accounting for 66% of electricity and heat production through coal burning. In the household sector, the coal consumption is

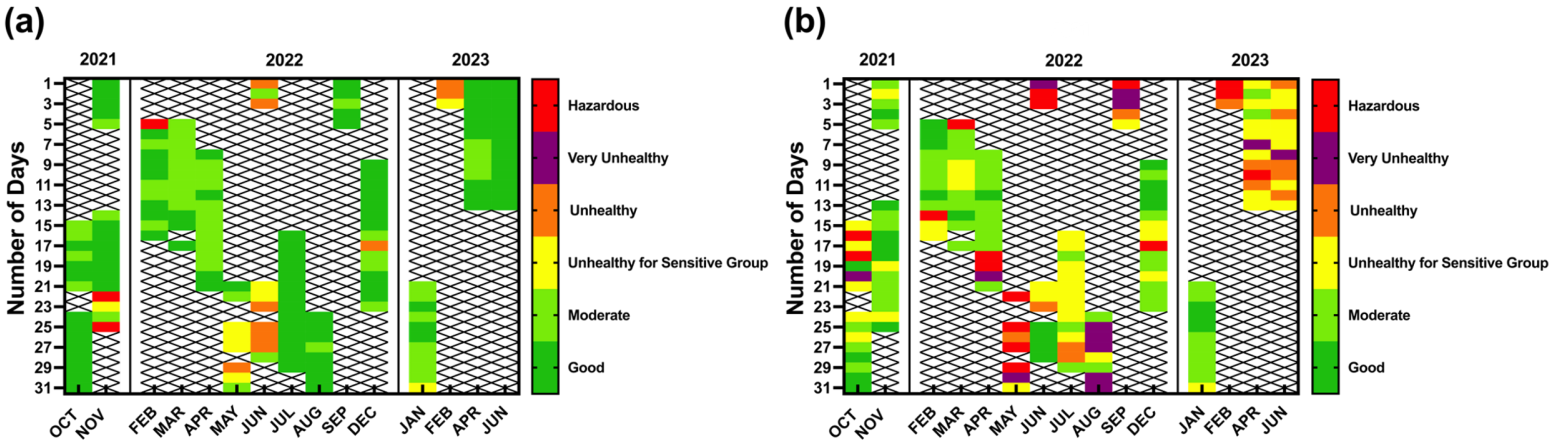

estimated at 157 kg per person, which is the second highest coal consumption per capita, globally.

4.7 *In vitro* lung bioaccessibility of PM-bound PTEs

Inhalation bioaccessible concentrations (mg/kg) of selected PTEs (i.e., Cd, Co, Cr, Cu, Fe, Mn, Ni, Pb, V, and Zn) are presented in Figure 4.7. A considerable variation in bioaccessible concentrations of PTEs was observed, which suggests the chemical **Figure**

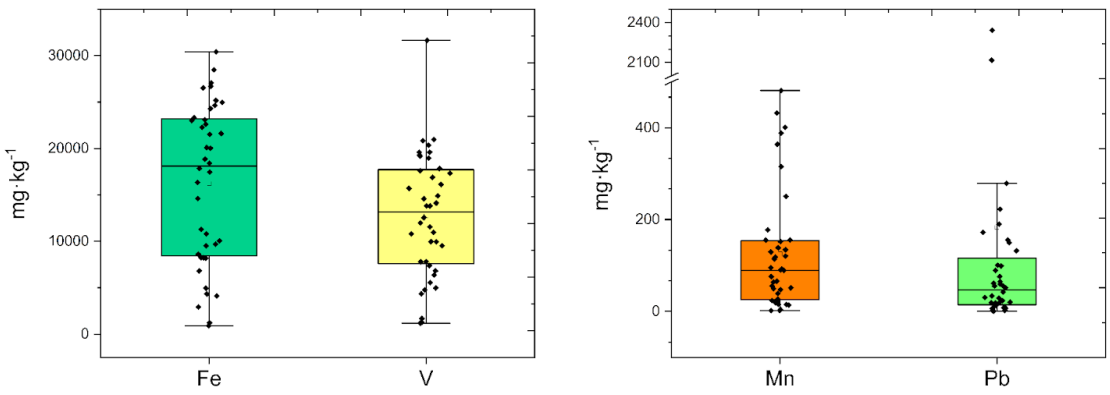

4.7: Bioaccessible concentration (mg/kg) of PTEs (Cd, Co, Cr, Cu, Fe, Mn, Ni, Pb, V, and Zn) in $PM_{2.5}$ in ALF

heterogeneity of atmospheric particles (Sánchez-Piñero et al., 2021). The mean bioaccessible concentration of PTEs increased in the following order: Co <Cd< Mn < Pb < Zn < Ni < Cr < Cu < V < Fe. Cumulative bioaccessibility (mg/kg) was high for most PTEs (e.g., Cr, Cu, Fe, Mn, Ni, Pb, V, and Zn), which indicates the high potential of those PTEs to be solubilized in phagocytes once inhaled (Guney et al., 2017).

Especially, for Fe (mean: 16,229 mg/kg, range: (906 - 30,419 mg/kg) and V (mean: 10,725 mg/kg, range: (687-27,092 mg/kg) the bioaccessible concentrations were the highest in $PM_{2.5}$ samples, which indicates the contribution from soil emission, combustion of fossil fuels (Peltier et al., 2011; Pulled et al., 2012; Sharma et al., 2017), and power plant emissions (Geiger & Cooper, 2010; Landis et al., 2017; Sharma et al., 2017; Soleimani et al., 2017; Arhami et al., 2017; Esmaeilirad et al., 2020). Among studied PTEs, Cd, Cr, and Ni are classified as human carcinogens, and exposure to those metals is linked to lung and nasal cancer (U.S. EPA, IRIS, 2023). In the present research, the mean bioaccessible concentrations of Cd, Cr, and Ni were 10, 736, and 724 mg/kg, respectively. The elevated bioaccessible concentration of Cr (mean: 736, range: (46.0-1,546) mg/kg), Cu (mean: 781, range: (42.0-1,326) mg/kg), Ni (mean: 724, range: (52.0-3,039) mg/kg), and Zn (mean: 665, range: (32.9-1,788) mg/kg) can indicate that collected $PM_{2.5}$ originates from coal-heated power plants activity and vehicle emission (Geiger & Cooper, 2010; Sharma et al., 2017). Although not classified as a human carcinogen, animal studies revealed that exposure to high concentrations of Cu can induce DNA damage (U.S. EPA, IRIS, 1988). Exposure to Zn and its compounds is

reported to induce metal fume fever in humans, however, the exposure level is not available (U.S. EPA, IRIS 2005).

4.8 Inhalation risk assessment using the bioaccessible concentration of PTEs

The bioaccessible concentration of PTEs is widely applied for the calculation of carcinogenic and non-carcinogenic health risks instead of total contaminant concentration in prior literature (Sánchez-Piñero, et al., 2021; Novo-Quiza et al., 2023; Liu et al., 2019; Wang et al., 2021). In the present dissertation, the carcinogenic and non-carcinogenic risks were evaluated for $PM_{2.5}$-associated PTEs (Table 4.3). The U.S. EPA suggests threshold lifetime cancer risk of 1.0×10^{-6} and 1.0×10^{-4} for risks associated with single and multiple carcinogens, respectively (U.S. EPA, 2019b).

Table 4.3: Mean and maximum (Max) HQ, CR for selected PTEs (Cd, Cr, Co, Mn, Ni, V) and Hazard Index (HI_{nc} and HI_c) estimated for adults and children.

PTE	Adults				Children			
	HQ		CR		HQ		CR	
	Mean	Max	Mean	Max	Mean	Max	Mean	Max
Cd	2.96×10^{-5}	1.95×10^{-4}	1.52×10^{-10}	1.01×10^{-9}	8.87×10^{-6}	5.86×10^{-5}	4.56×10^{-11}	3.02×10^{-10}
Cr	2.20×10^{-4}	4.56×10^{-4}	5.21×10^{-7}	1.09×10^{-6}	6.51×10^{-5}	1.37×10^{-4}	1.56×10^{-7}	3.28×10^{-7}
Co	3.30×10^{-5}	7.23×10^{-5}	5.09×10^{-10}	1.12×10^{-9}	9.90×10^{-6}	2.17×10^{-5}	1.53×10^{-10}	3.35×10^{-10}
Mn	7.39×10^{-5}	2.84×10^{-4}	N/A	N/A	2.12×10^{-5}	8.52×10^{-5}	N/A	N/A
Ni	1.52×10^{-3}	6.40×10^{-3}	1.59×10^{-9}	6.66×10^{-9}	4.57×10^{-4}	1.92×10^{-3}	4.76×10^{-10}	2.00×10^{-9}
V	3.16×10^{-3}	7.99×10^{-3}	N/A	N/A	9.49×10^{-4}	2.30×10^{-3}	N/A	N/A

HI_c	N/A	N/A	5.23×10^{-7}	1.10×10^{-6}	N/A	N/A	1.57×10^{-7}	3.31×10^{-7}
HI_{nc}	5.04×10^{-3}	1.54×10^{-2}	N/A	N/A	1.51×10^{-3}	4.62×10^{-3}	N/A	N/A

In the present investigation, all mean CRs estimated for adult and children exposure are below the proposed U.S. EPA threshold of 1.0×10^{-6}. Both mean HI_c estimated for adults and children (5.23×10^{-7} and 1.57×10^{-7}, respectively) do not exceed the cumulative cancer risk of 1.0×10^{-4}. However, the maximum CR for adults of 1.10×10^{-6} was slightly above the suggested U.S. EPA threshold. Moreover, in the sample collected in January, the individual cancer risk for Cr (1.09×10^{-6}) also exceeded a risk value of 1.0×10^{-4}.Regarding the non-carcinogenic health risk, HQ values for Cd, Cr, Co, Mn, Ni, and V, as well as mean and maximum HI for both adult and children exposure (5.04×10^{-3}, 1.54×10^{-2} for adults, 1.51×10^{-3}, 4.62×10^{-3} for children) were within U.S. EPA acceptable threshold value (HQ < 1), suggesting no non-carcinogenic risk via inhalation exposure.

The HHRA in the present research, however, does not consider mechanisms other than PTEs dissolution in the lung fluid, such as PM deposition and clearance rates and absorption of PTEs in the alveolar barrier. Moreover, carcinogenic and non-carcinogenic risk values for Cr were estimated using total Cr concentration (Cr(III) + Cr(VI)) and RfC ad IUR values for Cr(VI), which can lead to the overestimation of the risk.

4.9 Morphological characterization of PM particles from different emission sources

During the analysis of SEM images, several distinct groups of PM were observed including bioaerosols, coal fly ash (CFA), dust (classified as either natural or

construction), and soot particles. $PM_{2.5}$ and $PM_{2.5-10}$ collected in the summer and winter seasons were used for SEM analysis. The distribution of PM particles during the summer was as follows: 48.2% of particles were identified as natural dust (ND), 32.5% construction dust PM, 14.5% CFA, 1.8% vehicular traffic generated PM, and 3% PM of biological origin. In winter construction dust, CFA, ND, and road dust exhaust particles accounted for 32.5%, 31.6%, 31.1%, and 4.9% of all observed particles, respectively. Spring and summer, characterized by minimal snow coverage, facilitate strong winds that lift ND, increasing coarse PM concentrations. Additionally, the ongoing heating period in spring leads to elevated fine PM levels compared to summer. The blossoming flora in spring may also generate unique pollen-related particles, distinctly observed in SEM micrographs during this season. The findings illustrate expected seasonal distribution patterns with elevated concentrations of $PM_{2.5}$ (e.g., CFA) observed during the winter and fall periods, coupled with lower $PM_{2.5-10}$ (e.g., ND) concentrations from the start of the heating season and subsequent increases in CHPP output.

Moreover, the occurrence of rainfall in September-October immediately followed by snowfall can affect overall concentrations of coarse PM, particularly ND. Construction activities are rarely affected by seasons, thus having close to zero change in year-round concentrations.

4.9.1 Bioaerosols

Bioaerosols (e.g., pollen, bacteria, viruses, and spores) are airborne solid particles of biological origins that are the crucial component of the biosphere-atmosphere interaction and climate (Kolpakova, 2017). Bioaerosols, specifically fungi spores, are closely linked to respiratory diseases such as allergic

rhinitis, and allergic asthma (Priyamvada et al., 2017). In the present research work, SEM images of PM samples collected in the summer season revealed distinctive bioaerosol particles, particularly spores (e.g., Chaldosporium fungi spore), characterized by an irregular, heavily textured surface with an elongated, disk-like morphology (Figure 4.8e). The fungus spores, specifically the Chaldosporium species, of cosmopolitan distribution are regularly observed on all kinds of plants, animals, soils, and all other organic matter (Bensch et al., 2012). In the present work, bioaerosols account for a small fraction (~3%) of PM particles.

4.9.2 CFA

CFA is another example of a common pollutant observed in the present research. CFA is a byproduct of coal combustion often containing heavy metals, such as As, Pb, and Hg (Chen et al., 2004). CFA is closely associated with adverse health outcomes (e.g., aggravation of respiratory conditions, neurodevelopmental disorders, sleep problems) (Zierold et al., 2020). In general, CFA particles are spherical or irregularly shaped with smooth surfaces and a high surface area-to-volume ratio (Chen et al., 2004). The typical size range of inhalable CFA fraction varies between 1.98 μm to 5.64 μm (Brown et al., 2011). However, the morphology of CFA can vary depending on the type of coal combusted (Chen et al., 2004). The CFA particles are more typical for the winter and fall seasons. Most CFA particles observed in January were spherically shaped and < 2.5 μm in size (Figure 4.8a-d). Moreover, some particles exhibited irregular morphology (e.g., dents and cracks) (Figure 4.8d).

The physical attributes of CFA (e.g., particle, size, shape, internal microstructures, stiffness, surface area) govern cellular entry mechanisms and

subsequent interaction and, hence, determine their biological toxicity (Kisku et al., 2018). Larger CFA particles (> 10 μm) may adhere to the nasal mucosa or nasopharynx and can be expelled from respiratory system via clearance mechanisms (e.g., sneezing), while smaller particles (< 5 μm) can directly infiltrate the bronchi, potentially causing lung damage (e.g., chronic lung tissue fibrosis) (Xie et al., 2021). Moreover, CFA particles can enter the bloodstream through skin contact or oral intake. In the bloodstream, CFA micro particles can be phagocytized across various tissues (especially spherical CFA particles) causing cellular damage (Chen et al., 2024).

4.9.3 Dust particles

Dust particles are byproducts of soil erosion and mineral crushing (Sairanen et al., 2019; Katra, 2020). Depending on the emission source, the morphology ranges from highly angular to moderately angular with rounded corners. Typically, mineral dust particles are irregularly shaped (e.g., of anthropogenic origin or mineral crushing), ranging in size between several microns to hundreds of microns (Adamiec et al., 2016). Particles originating from minerals are bigger compared to other dust particles and tend to form large aggregates. In the present research, single particle or particle agglomerates originating from mineral crushing were observed in January (Figure 4.8a-b). Potential emission sources include construction activity and degradation of pavement (Adamiec et al., 2016).

ND comprises smaller, angular PM compared to clustered crushed mineral particles. Although both types are classified as coarse, ND particles are notably smaller. Wind and water erosion produce Si and Ca-rich airborne particles and mid-air collisions break them into smaller, angular PM (Iordandis et al., 2007). ND particles do not

typically form large aggregates. In the present research, July samples contained ND particles (Figure 4.9c-d) with sharp edges, and a small amount of surface debris, possibly due to mid-air collisions.

Road dust PM is a collection of particles generated by vehicular traffic, comprising emissions from car exhaust, tire abrasion, road surface deterioration, and metal brake dust. Among these, brake wear-derived particles are highly prevalent. They exhibit complex morphologies and size variations (Figure 6c), which makes identification challenging.

4.9.4 Soot particles

Soot is formed from the incomplete combustion of biomass, organic matter, and especially fossil fuels. It consists of tiny particles of carbon and other chemicals that are

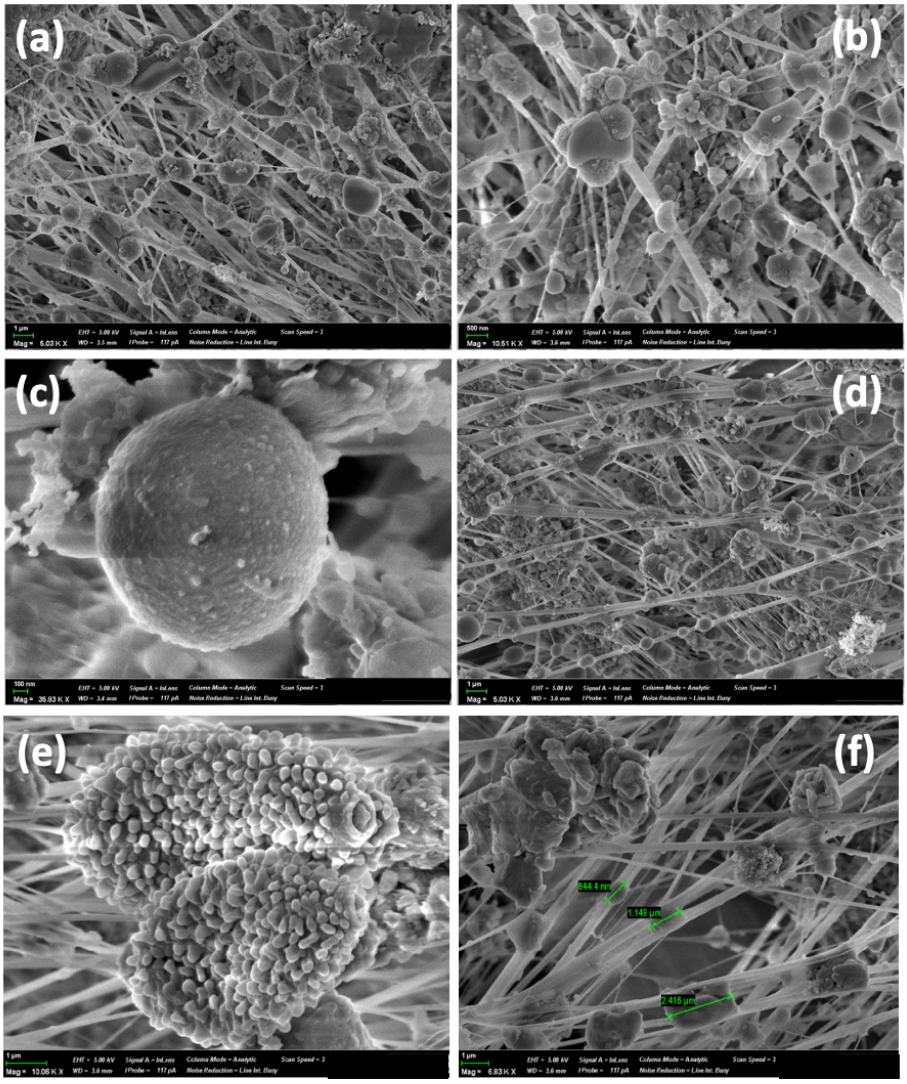

clustered **Figure 4.8**: SEM images of PTFE filters with $PM_{2.5}$ collected in (a, b) winter (January) and (c, d) summer (July) in Astana, (e) Chladosporium spores, ~7µm size, observed in the summer period, and (f) soot particles observed in winter (January)

together in complex shapes. Soot particles can penetrate deep into the lungs due to their extremely irregular and complex shapes. Continuous exposure of the respiratory epithelia to soot particles can lead to disruptions in lung functions increasing the cancer risk. The biological toxicity includes direct contact-mediated dysfunctions (e.g., ROS production, cell hyperplasia, lung cell apoptosis). Additionally, clinical and animal studies revealed the systemic immune response to soot exposure that contributes to

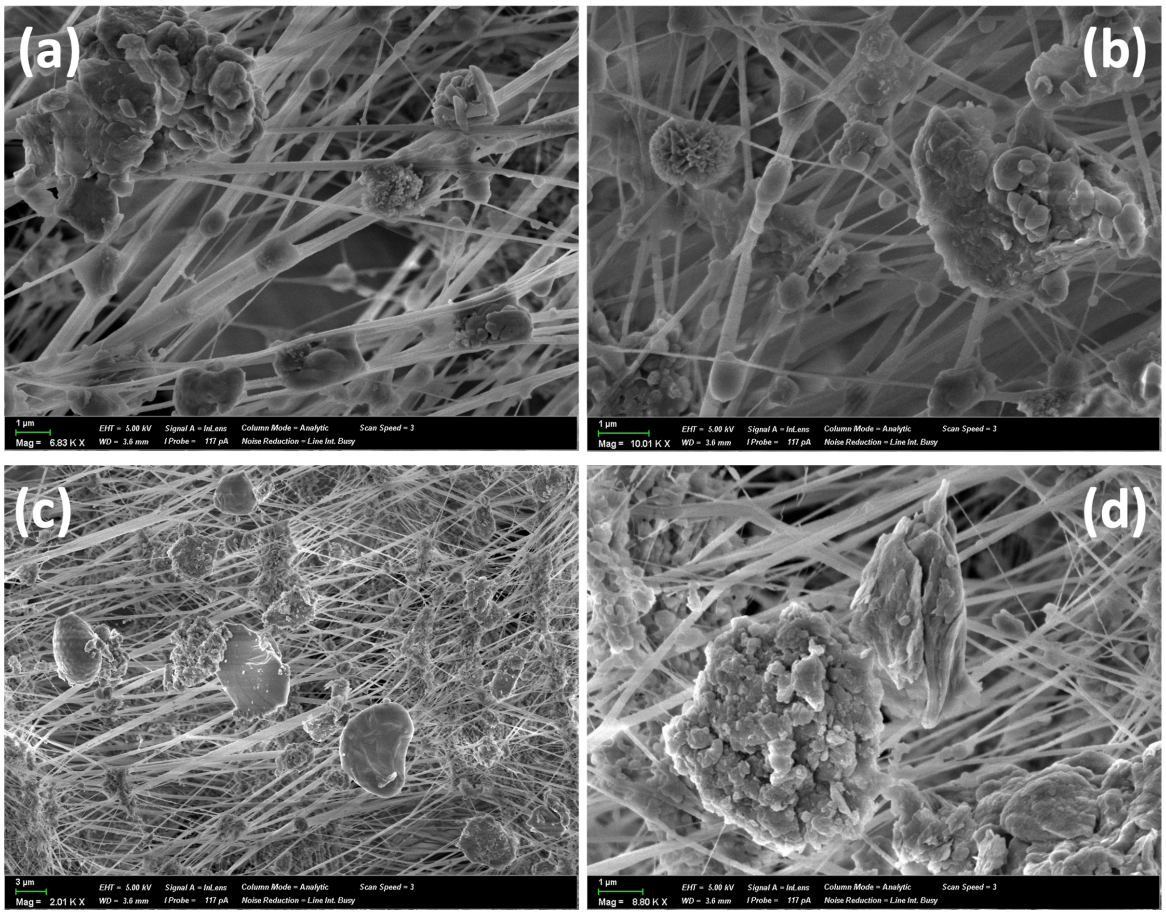

tissue remodeling and

Figure 4.9: SEM images of PTFE filters with $PM_{2.5-10}$ collected in (a, b) winter (January) and (c, d) summer (July) in Astana

fibrosis, leading to breathing difficulties (Niranjian & Thakur, 2017). Soot particles can also contribute to climate change by absorbing sunlight and warming the atmosphere. Soot is a major component of air pollution in metropolitan areas, particularly in regions with heavy traffic (China et al., 2014). Soot particles include a wide range of sizes and shapes, however, overall, most particles share similar patterns of complex structure (Figure 4.8a and Figure 4.9d). The size of observed soot particles ranged from ~4 μm to ~8.5 μm.

4.10 Characterization of snow and rainwater

The interaction between precipitation and PM leading to changes in their physico-chemical properties has piqued the interest of multiple researchers (e.g., Han et al. 2020, Gonzalez and Aristizabal, 2012, Zeng et al. 2021). This interaction is characterized by PM removal from the atmosphere, i.e. wet deposition or "scavenging", which happens when PM becomes nuclei for condensation and subsequent cloud formation or when particles are caught during rainfall (Gonzalez and Aristizabal, 2012). Precipitation episodes were confirmed to significantly lower SO_4^{2-} levels in PM_{10}, with a positive correlation between scavenging ratio and rainfall intensity as well as particle diameter due to high water solubility of sulfates (Gonzalez & Aristizabal, 2012). Moreover, concentrations of metallic cations in rainwater such as Ca^{2+} and Mg^{2+} were linked to $PM_{2.5}$ and PM_{10}, which contribute to acid buffering (Zeng et al., 2021). Han et al. (2019) further underline the significance of airborne particles in rainwater alkalinization, hinting at possible exacerbation of acid rain issues if air pollution mitigation strategies target only PM levels without considering rainwater chemistry.

3.10.1 pH and conductivity of snow and rainwater

The variation in pH of snow and rainwater samples as well as precipitation (mm) are presented in Figure 4.10. The highest pH value of 8.51 was detected in February 2023, whereas the lowest pH of 6.47 was recorded in May 2022. The average pH value was 7.11 which can be attributed to the higher alkaline content of snow and rainwater samples. A typical rainwater pH value is close to 5.60 due to the acidic characteristics of the CO_2 that dissolves in the atmosphere (Payus et al., 2020). The pH level of rainwater observed in Kazakhstan is primarily influenced by the high concentration of PM in the atmosphere rich in $CaCO_3$ and $Ca(HCO_3)_2$, leading to buffering acidity of rainwater.

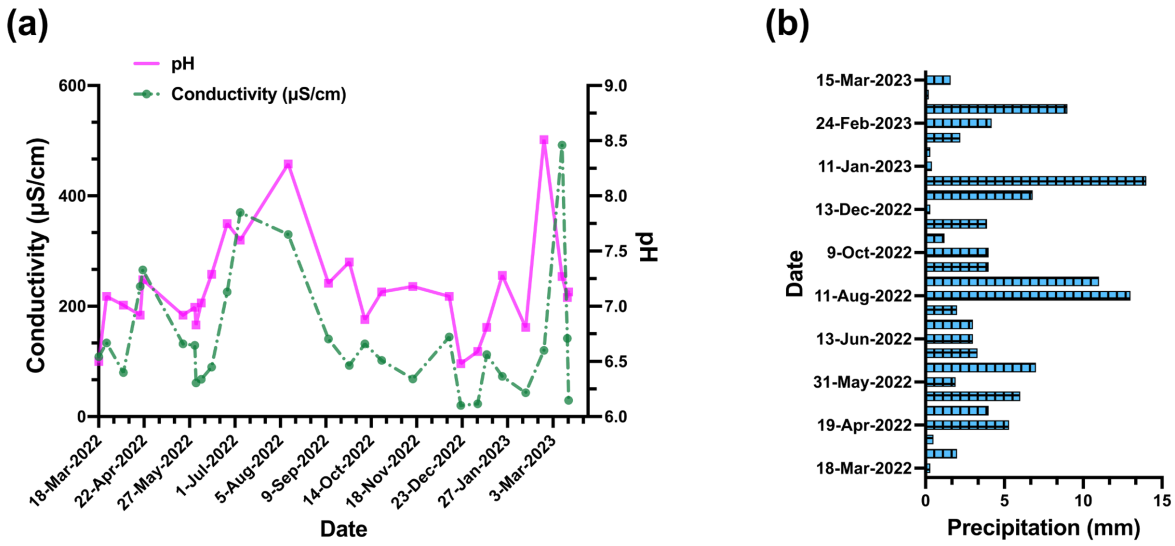

Figure 4.10: (a) Physical parameters (conductivity (µS/cm) and pH) and (b) precipitation (mm)

The average ion conductivity of snow and rainwater samples was 224.2 µS/cm (Figure 4.10a). Peaks in conductivity are prominent in mid-summer and early spring, suggesting elevated air pollution levels, as reflected by the high ionic conductivity. Prior studies have also demonstrated the association of higher conductivity with the increased total ion concentrations (Zhong et al., 2022). The increase in conductivity during

summer can be attributed to the intensified use of fertilizers and pesticides for agricultural purposes, as it mainly arises from salt particle dissolution in rainwater. Furthermore, high wind activity in Astana city during spring and summer elevates suspended dust particles, influencing salt content and increasing conductivity values (Omogbehin and Oluwatimilehin, 2022).

4.10.2 PTEs content

The present research analyzed the PTE content in snow and rainwater samples (Table 4.4). The PTEs (e.g., Cr and Cd) can dissolve in both terrestrial and aquatic surroundings followed by adverse environmental impact (Majumdar et al., 2020). The average concentration of most PTEs (e.g., Cd, Co, Cr, Cu, Mn, and Pb) was below the WHO's maximum permissible concentration of heavy metals in drinking water. The lowest average concentration of 0.15 µg/L (range: 0.04 - 0.36 µg/L) was observed for Cd, whereas the V showed the highest average concentration (108 µg/L, range: 63.1-159 µg/L) in precipitation samples during all seasons (Figure 4.11). Emissions from non-ferrous and ferrous metallurgy, as well as fuel combustion, are related to Cd emissions (Pacyna et al., 2009). A potential source of V in the snow and rainwater samples is vehicular traffic, notably emissions from diesel-powered vehicles. Diesel fuel exhibits a higher V content relative to other fuels, and as diesel engines undergo combustion, V may be released into the atmosphere (Li et al., 2020).

The average concentration of Ni (84.0 µg/L, range: 5.20 - 612 µg/L) exceeded WHO permissible level (70 µg/L). The use of coal and liquid fuels is among the main sources of atmospheric Ni, however, the highest proportion of Ni was observed during

non-heating seasons (e.g., summer and fall seasons) (Figure 4.11). In addition, the production of glass, bricks, non-ferrous metals, and cement also contributes to the release of Ni into the atmosphere (Tian et al., 2012). The Cr concentration of 77.4 µg/L observed in one sample collected in spring was also higher than the WHO drinking water threshold of 30 µg/L. The presence of Co is directly linked to coal combustion, industrial emissions, traffic, and mining processes (Mihajlidi-Zelić et al., 2006).

Table 4.4: Range (Max-Min), mean, standard deviation (SD), and median for PTEs (Cd, Co, Cr, Cu, Fe, Mn, Ni, Pb, and V) in snow and rainwater samples and recommended threshold values (µg/L).

PTEs	Range (Min-Max)	Mean	SD	Median	WHO limits[1]	AA-EQS Inland Surface Water limits[2]	MAC-EQS Inland Surface Water limits[3]
Cd	(0.04-0.36)	0.15	0.07	0.13	3.00	≤0.08 (Class 1)	≤0.45 (Class 1)
Co	(0.10-6.90)	1.70	1.65	1.20	N/A	N/A	N/A
Cr	(4.20-77.4)	16.7	14.1	13.8	30.0	N/A	N/A
Cu	(2.57-41.3)	10.2	9.06	7.17	2,000	N/A	N/A
Mn	(0.50-212)	63.2	57.1	55.9	80.0	N/A	N/A
Ni	(5.20-612)	84.0	134	30.2	70.0	20	N/A
Pb	(0.10-14.1)	2.39	3.72	0.62	9.00	7.2	N/A
Sb	(0.38-3.00)	1.39	0.99	1.86	20.0	N/A	N/A
V	(63.1-159)	108	24.6	106	N/A	N/A	N/A

1. WHO guidelines for drinking water quality
2. Annual average for Inland surface water limits according to EU Directive 2008/105/EC
3. Maximum allowable concentration for Inland surface water limits according to EU Directive 2008/105/EC

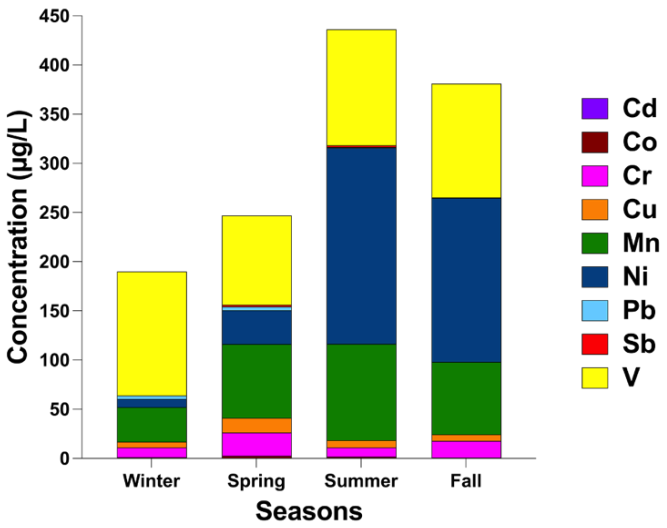

Figure 4.11: Average concentration of PTEs (µg/L) (Cd, Co, Cr, Cu, Mn, Ni, Pb, Sb, and V) in precipitation in four seasons

4.10.3 Ion content

The temporal variation of major ions in precipitation is shown in Table 4.5. Overall, the mean concentration of major ions did not exceed the available permissible levels for groundwater, drinking, and surface waters. However, the highest concentration of F^- (1.82 mg/L) observed in April, exceeded the WHO limit for drinking water (1.5 mg/L). The highest mean ion concentration was recorded for SO_4^{2-} (17.8 mg/L, range: 0.02 - 77.5 mg/L).

Table 4.5: pH, electric conductivity (EC) (µS/cm), precipitation (mm), major ion concentration (mg/L), and total anion and total cation concentrations (meq/L) from the soluble fraction of snow and rainwaters

	Range (Min-Max)	Mean	SD	Median	WHO limits[1]	EU environmental guidelines[2]
pH	(6.48-8.51)	7.15	0.46	7.09	no health-based guidelines; optimal range for treatment and distribution: 6.5-8.5	N/A
EC	(20.1-492)	142	110	116	N/A	N/A
Precipitation	(0.20-14.0)	4.09	3.80	3.15	N/A	N/A
F^-	(0.01-1.82)	0.31	0.39	0.14	1.5	N/A
Cl^-	(0.01-55.5)	14.3	12.8	8.15	no health-based guidelines; taste: 200-300 for NaCl, KCl, $CaCl_2$	N/A
NO_2^-	(0.02-3.97)	1.47	1.02	1.23	3.0	N/A
NO_3^-	(0.01-32.6)	6.01	8.30	3.61	50	groundwater: 50
SO_4^{2-}	(0.02-77.5)	17.8	20.6	10.1	no health-based guidelines; taste: 250	N/A
PO_4^{3-}	(0.03-1.27)	0.39	0.41	0.27	N/A	N/A
Br^-	<DL	<DL	<DL	<DL	N/A	N/A
Li^+	<DL	<DL	<DL	<DL	N/A	N/A
K^+	(0.01-45.6)	11.9	11.1	8.16	N/A	N/A
Na^+	(0.01-16.3)	3.46	4.86	1.97	no health-based guidelines; taste: 200	N/A
NH_4^+	(0.0-16.4)	3.46	4.68	1.55	no health-based guidelines; odor: 1.5; taste: 35	N/A
Ca^{2+}	(0.02-50.8)	14.9	13.8	10.3	N/A	N/A
Mg^{2+}	(0.00-3.87)	0.84	0.89	0.52	N/A	N/A
∑anions	(0.06-3.36)	1.10	0.97	0.80	N/A	N/A

∑cations	(0.00-4.49)	1.43	1.24	0.96	N/A	N/A

1. WHO guidelines for drinking water
2. EU environmental guidelines for groundwater and surface water

The mean concentration for major ions increased in the following order: $F^- > PO_4^{3-} > Mg^{2+} > NO_2^- > Na^+ = NH_4^+ > NO_3^- > K^+ > Cl^- > Ca^{2+} > SO_4^{2-}$. Three major peaks for ion concentrations were observed in April (F^-, Cl^-, NO_3^-, SO_4^{2-}, K^+, Na^+, NH_4^+, Ca^{2+}, Mg^{2+}), July (F^-, Cl^-, NO_2^-, NO_3^- , SO_4^{2-} , K^+, Na^+, NH_4^+, Ca^{2+}, Mg^{2+}), and December (F^-, Cl^-, NO_2^-, K^+, Na^+, NH_4^+) (Figure 4.12).

The high concentrations of alkaline substances (e.g., Na^+, K^+, Mg^{2+}, Ca^{2+}, NH_4^+, NH_3, and $CaCO_3$) in areas with significant emissions of SO_2 and NO_x can result in the

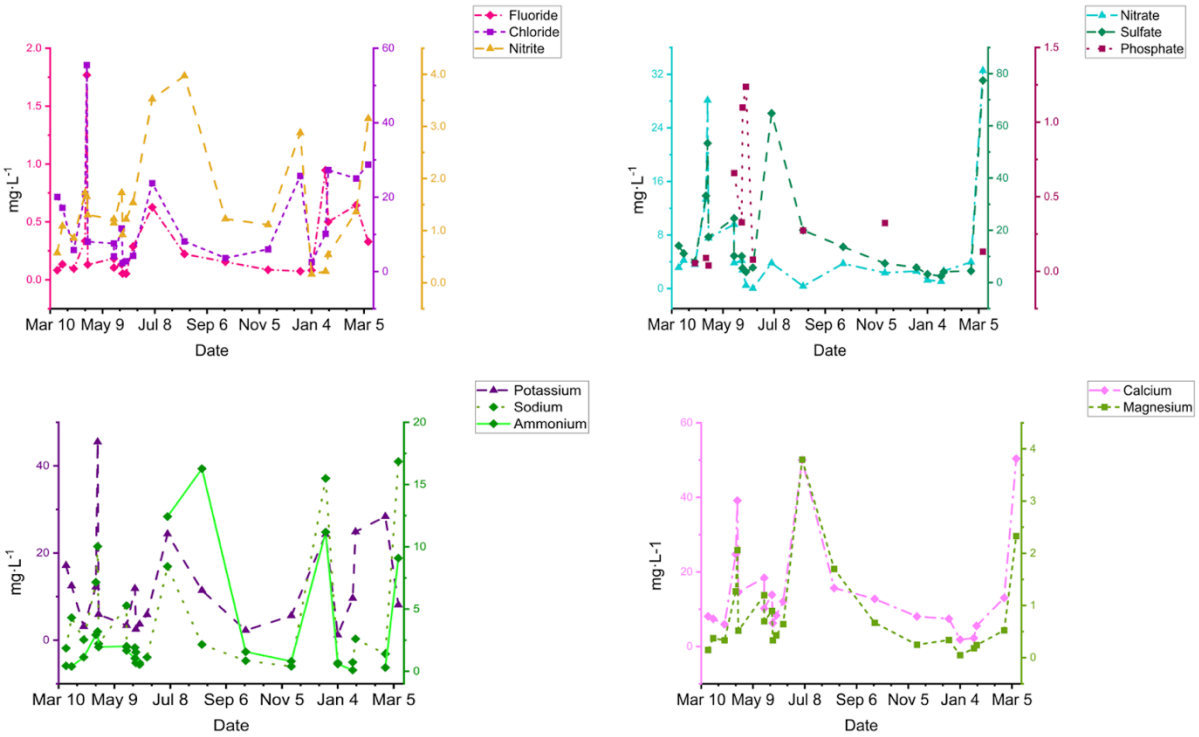

neutralization of rainwater (Mihajlidi-Zelić et al., 2006). Moreover, high correlation coefficients between SO_4^{2-}, NO_2^-, and NO_3^- (0.61 and 0.8, respectively) (Figure 4.13) suggest a common source. Ca is a prevalent constituent of the Earth's crust and is consequently abundant in soil bases, as well as being disseminated through agricultural

activities. A high correlation coefficient between Ca^{2+} and Mg^{2+} (0.93) indicates the possible contribution of material of crustal origin (Colon-Santos et al., 2016). The rainwater samples collected in spring are influenced by intensive application of ammonium-based fertilizers for agricultural purposes. This practice further underscores the impact of $CaCO_3$ on the acidity of rainwater (Güllü et al., 2005; Koçak et al., 2009). Moreover, NH_4^+, SO_4^{2-}, and NO_2^- showed a moderate and high correlation (0.53 and 0.93, respectively), suggesting a common anthropogenic source or/and emphasizing the significance of HNO_3 and H_2SO_4 neutralization by NH_3 to form NH_4^+ salts in aerosols and cloud water (Colon-Santos et al., 2016). Additionally, NH_3 and $CaCO_3$ may be introduced into rainwater through the deposition of aerosols. Aerosols can also contribute to the generation of SO_4^{2-} in the atmosphere, although primary sources of these ions are combustion activities and the transformation of gas particles in reactions involving H_2SO_4 and NH_3 or other alkaline compounds.

Figure 4.12: Concentrations of water-soluble ions (mg/L) (F^-, Cl^-, NO_2^-, NO_3^-, SO_4^{2-}, PO_4^{3-}, K^+, Na^+, NH_4^+, Ca^{2+}, Mg^{2+}) in snow and rainwater samples by date collected in Astana from March 2022 to March 2023

Figure 4.13: Pearson correlation matrix of measured concentrations of soluble fractions as well as total sums of all anions (including HCO_3^-) and cations (including H^+)

4.11 Source apportionment via CBPF

4.11.1 Pollution profile of $PM_{2.5}$

The annual (2018-2019 and 2019-2020) and seasonal (heating and non-heating periods) variations in $PM_{2.5}$ concentrations in Astana are presented in Table 4.6. The annual average $PM_{2.5}$ concentrations notably decreased in 2019-2020 (16.5 μg/m^3) compared to 2018-2019 (29.7 μg/m^3), both exceeding WHO standards of 5 μg/m^3

(annual mean). Elevated fine PM concentrations were observed during heating periods (44.8 μg/m^3 in 2018-2019 and 20.8 μg/m^3 in 2019-2020), while non-heating period concentrations were similar (13.0 μg/m^3 and 12.0 μg/m^3, respectively) in two study cycles. A notable 54% reduction in $PM_{2.5}$ during the 2019-2020 heating period, possibly linked to COVID-19 lockdowns, aligns with findings in Almaty, reporting a 34% reduction during the same period (Kerimray et al., 2020). Prior literature also highlights different air pollution patterns during lockdowns, with Tudu et al., 2022 reporting reductions in PM_{10}, NO_2, and SO_2 in Kolkata, India, and Briz-Redón et al., 2021 reporting decreased NO_2 concentrations in eleven Spanish cities.

The diurnal and monthly variations in $PM_{2.5}$ concentrations are depicted in Figure 4.14(a, b). Notably, recurrent peaks are observed on Thursday (Figure 4.14(a) and Monday (Figure 4.14b)), indicating pollutant accumulation during working days, possibly linked to increased energy consumption early in the week. However, in the 2019-2020 cycle, $PM_{2.5}$ concentrations increased toward the end of the week, potentially due to heightened traffic (Ji et al., 2019). Throughout the day, $PM_{2.5}$ concentrations decrease until 18:00, attributed to reduced heating needs and increased atmospheric dispersion during daylight. A peak around 23:00 indicates nighttime pollutant accumulation, possibly influenced by temperature drop and inversion conditions (Bathmanabhan et al., 2010). The elevated concentration could also be affected by foggy conditions and icing through particle trapping, secondary PM formation, and surface deposition. December (Figure 4.14(a) and March (Figure 4.14b)) mark the periods with the highest $PM_{2.5}$ concentrations.

Table 4.6: Periodic variations in the hourly concentration of $PM_{2.5}$ (µg/m^3) (S5) in 2018-2019 and 2019-2020.

	2018-2019			2019-2020	
	Annual	**Heating**	**Non-heating**	**Annual**	**Heating**
Mean	29.7	44.8	13.0	16.5	20.8
Standard Deviation	50.0	64.2	12.7	29.2	34.6
Range (25th-95th)	8.8-87.1	19.0-136	5.80-38.4	5.70-51.1	6.20-66.4
Missing data (%)	3.8	6.2	1.6	7.1	6.2

Wind and pollution rose diagrams for $PM_{2.5}$ show the relationship between meteorological parameters and $PM_{2.5}$ concentrations at the receptor (Figure 4.15a, b). The predominant wind direction was generally from west to south, with higher wind speeds recorded in the south-south-west and south-west directions (Figure 4.15a)). The prevailing direction of elevated concentrations of $PM_{2.5}$ (Figure 4.15b)) was also evident, with episodes of very high $PM_{2.5}$ (> 300 µg/m3) concentrations observed in the east and east-north-east directions. These findings indicate that the wind profile aligns with the city's ventilation characteristics, suggesting that $PM_{2.5}$ sources are primarily situated in the downwind direction.

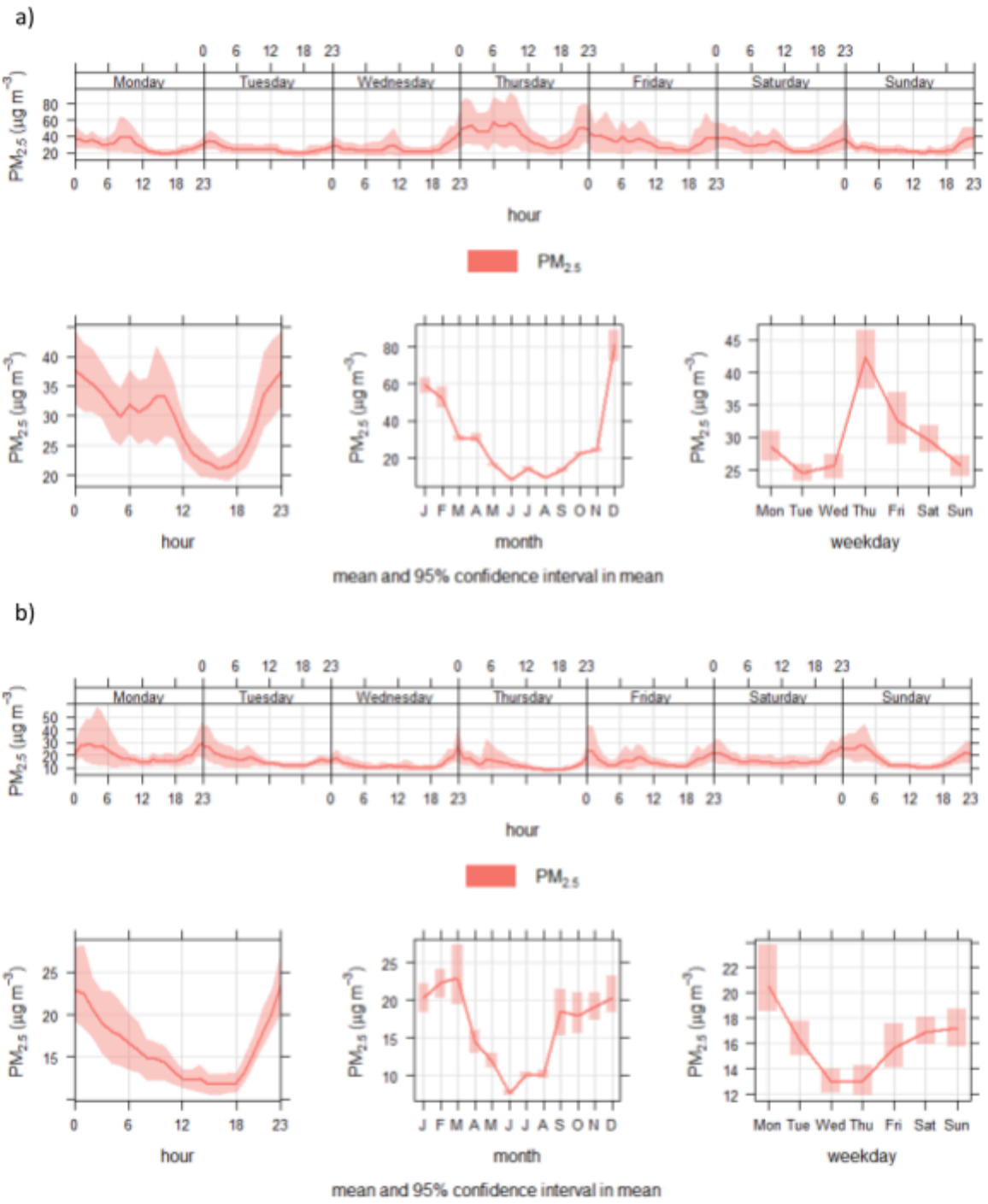

Figure 4.14: Diurnal and monthly variations of $PM_{2.5}$ concentrations for 2018-2019 (a) and 2019-2020 (b).

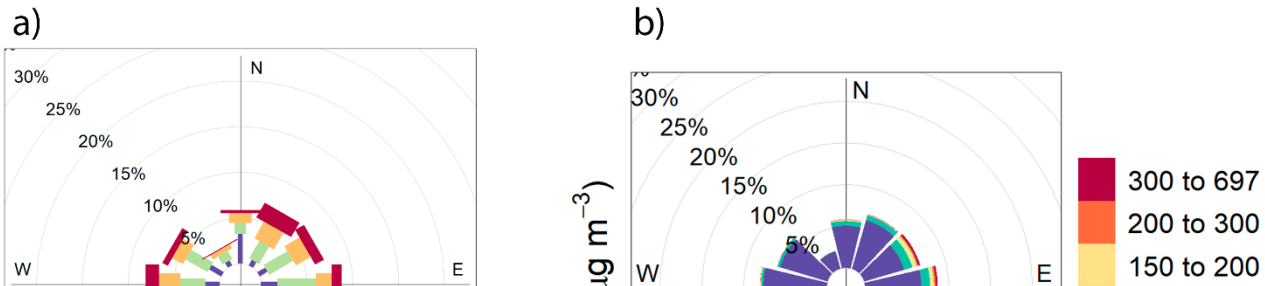

Figure 4.15: Diagrams of wind rose (a) and of pollution rose for $PM_{2.5}$ (b).

4.11.2 Pollution profile of TSP, SO_2, CO, NO_2, HF

An analysis of the annual (study cycles 2018-2019 and 2019-2020) and periodic variations (heating (October to April) and non-heating periods (May to September)) of TSP and gaseous pollutants was conducted to evaluate the meteorological factors influencing the increase in pollutant concentrations in Astana, utilizing data from air pollution monitoring stations S1, S2, S3, and S4 (Table 4.7 and Table 4.8). The prevailing wind direction at most monitoring stations (S1, S3, and S4) was influenced by southern winds, while station S2 experienced a prevailing wind from the west-north-west direction (Figure 4.16a-d).

4.11.3 Study cycle: 2018-2019

In the study cycle of 2018-2019, monitoring station S4, located in the city's busiest traffic area, recorded the highest annual average concentration of pollutants (excluding

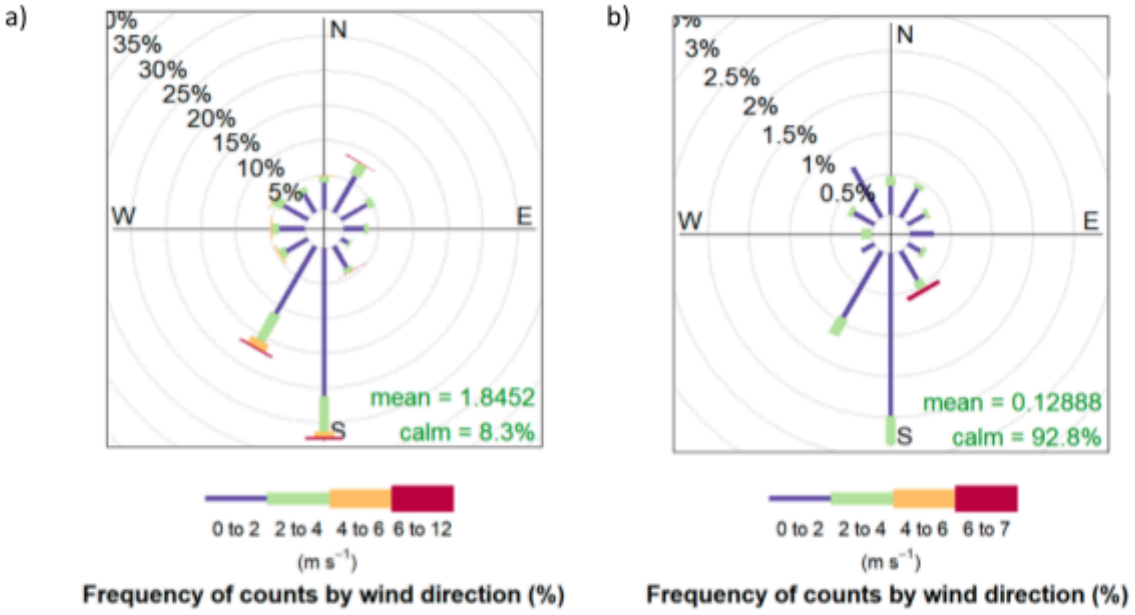

Figure 4.16: Wind rose diagrams for S1 (a), S2 (b), S3 (c), and S4 (d).

TSP) (Table 4.7). This site showed notably elevated levels of TSP and CO compared to other measured pollutants, suggesting a significant contribution from exhaust emissions. Despite larger TSP particles having limited respiratory tract penetration, prolonged exposure to high concentrations may lead to cytotoxic effects due to PTEs (e.g., Cu, Pb, As, Cd), increasing the risk of airway inflammation (Shim et al., 2021).

The S3, also influenced by traffic, recorded the highest TSP levels, with readings peaking at 1,500 $\mu g/m^3$ and with an average concentration of 347 $\mu g/m^3$, exceeding the nationally accepted maximum allowable TSP concentration of 150 $\mu g/m^3$ (Assanov et al., 2021). In comparison to data from 2016 (Kerimray et al., 2018), the average annual TSP concentration during 2018-2019 showed a slight decrease across all four stations (400 $\mu g/m^3$ in 2016). However, the study cycle of 2018-2019 recorded a maximum TSP concentration of 1,700 $\mu g/m^3$, exceeding the maximum of 1,614 $\mu g/m^3$ in 2016.

The concentrations of CO fluctuated from 600 to 2,800 $\mu g/m^3$, with a high mean value of 1,157 $\mu g/m^3$, drastically exceeding the daily maximum allowable concentration of 60 $\mu g/m^3$ according to Kazakhstani standards (Kazhydromet, 2021). When inhaled, CO transforms into carboxyhemoglobin (COHb) in the bloodstream, impeding cellular oxygen uptake (American Lung Society, 2020). Specific social groups consistently exposed to high CO levels, including public transportation workers, traffic wardens, and garage/tunnel personnel, face potential health risks (WHO, 2000). A study among autoworkers documented elevated COHb concentrations in their blood serum (Bol et al., 2018). Chronic CO exposure can lead to various health conditions, from acute coronary syndrome, such as myocardial infarction, to noticeable brain damage (Lee et al., 2015).

Elevated levels of NO_2 were observed during this study cycle, primarily associated with vehicular emissions, highlighting it as a key indicator of traffic-related pollution (Atkinson et al., 2018). Prolonged exposure to NO_2 has been linked to increased mortality from respiratory and cardiovascular diseases (Atkinson et al., 2018; Huang et al., 2021). NO_2 concentrations varied from 16.6 $\mu g/m^3$ (S2) to 211 $\mu g/m^3$ (S4). Importantly, S4 exceeded the WHO air quality guideline value of 40 $\mu g/m^3$ for NO_2 (WHO, 2006), possibly due to higher traffic volumes in that area. The annual average NO_2 concentration at S4 (211 $\mu g/m^3$) drastically exceeded the reported average in 2016 (80 $\mu g/m^3$) (Kerimray et al., 2019), emphasizing the localized impact of traffic on NO_2 levels.

Anthropogenic sources (e.g., CHPPs and industrial facilities such as aluminum production and phosphate fertilizer plants) contribute to the ambient HF emissions level. Occupational exposure to HF can occur through inhalation or skin contact. Chronic inhalation exposure to HF can lead to nose, throat, and lung irritation, skeletal fibrosis, liver, and kidney damage (US EPA, 2016).

In 2018-2019, the concentrations of selected pollutants (TSP, SO_2, CO, NO_2, HF) doubled, on average, during the heating season compared to the non-heating period (Figure 4.17). This pattern, similar to $PM_{2.5}$ trends, is attributed to increased fuel consumption in colder weather coupled with adverse meteorological conditions. Notably, during the heating season, TSP concentrations peaked at 416 μg/m3 (S1), and CO reached 1,321 μg/m3 (S4). In the non-heating period, S4 recorded the highest mean concentrations of CO and TSP at 291 $\mu g/m^3$ and 914 $\mu g/m^3$, respectively. Interestingly, NO_2 levels in S4 were notably higher during the non-heating period (257 $\mu g/m^3$) than

the heating period (179 µg/m^3), highlighting the pronounced impact of traffic-related emissions in S4 during warmer months.

4.11.4. Study cycle: 2019-2020

During the 2019-2020 study cycle, there was a noticeable decrease in the concentrations of various ambient pollutants compared to the 2018-2019 period (Figure 4.18). Notably, CO and TSP were marked by the highest average annual concentrations among the studied pollutants. TSP concentrations showed minimal variation across stations, reaching 150 µg/m^3 at S1, which is the upper limit of national air quality standards.

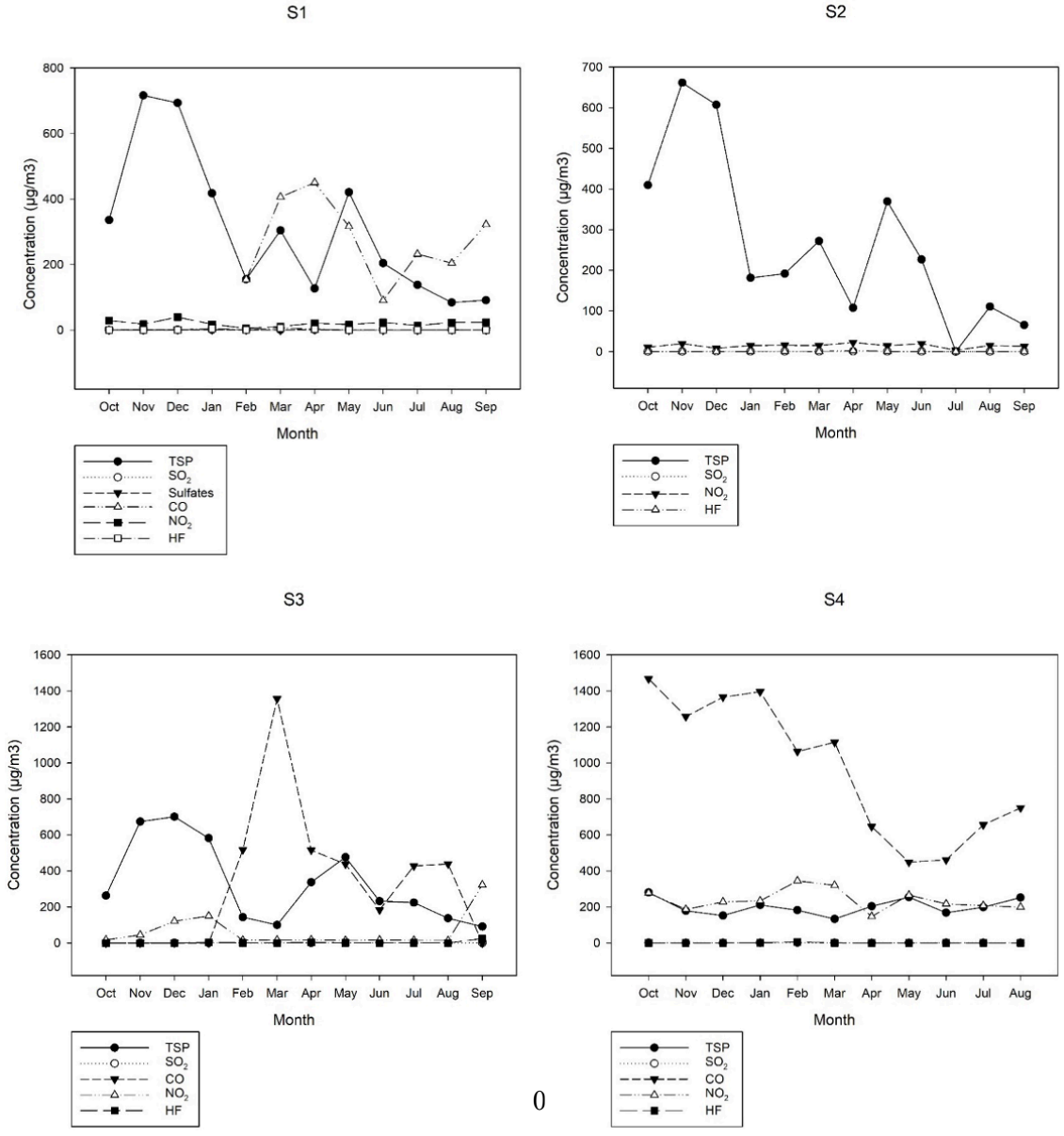

Considering the residential location of S1, domestic heating emissions could be a significant contributor. S4 recorded the highest average annual CO concentration at 963 $\mu g/m^3$ (range: 570 to **Figure 4.17**: Average monthly concentrations ($\mu g/m^3$) of TSP, SO_2, sulfates, CO, NO_2, and HF (S1, S2, S3, S4) in 2018-2019.

2,030 µg/m^3), suggesting a potential influence from traffic-related sources. In

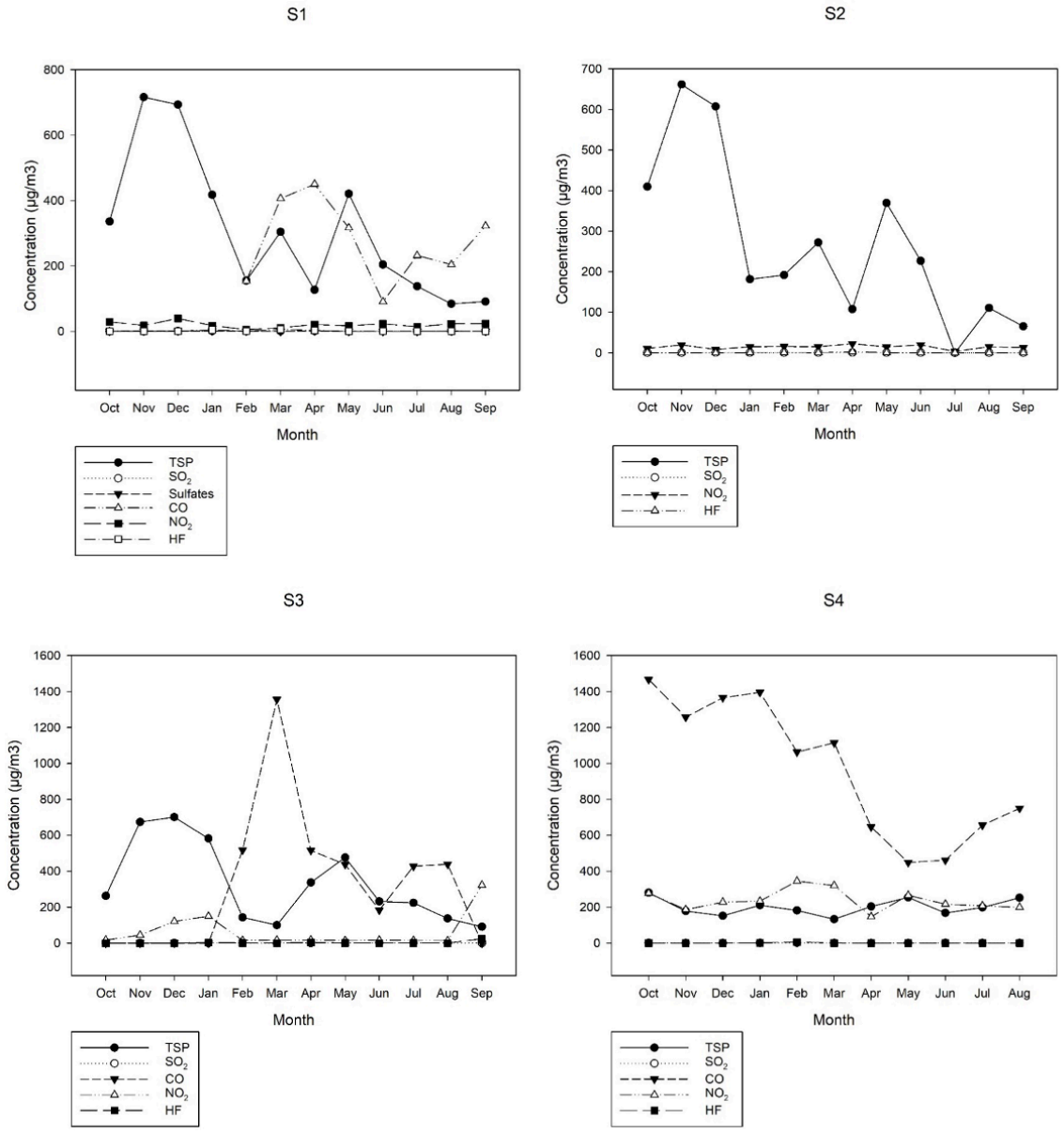

2019-2020, **Figure 4.18**: Average monthly concentrations (µg/m^3) of TSP, SO_2, sulfates, CO, NO_2, and HF (S1, S2, S3, S4) in 2019-2020.

S4 also registered the highest NO_2 concentration (237 µg/m^3), exceeding WHO guideline values (WHO, 2006). Similar to the 2018-2019 study cycle, these findings highlight the exposure of the general population to elevated concentrations of ambient pollutants, potentially associated with adverse health effects.

Pollutant concentrations increased by 35% during the heating period compared to the non-heating season. The S4 recorded mean concentrations of 1,232 μg/m^3 for CO and 191 μg/m^3 for TSP during the heating period. Conversely, in the non-heating period, S4 exhibited a mean CO concentration of 585 μg/m^3 (range: 440 - 871 μg/m^3) and TSP peaked at 217 μg/m^3 (range: 100 - 400 μg/m^3). This consistent trend of higher concentrations during the heating period is most likely due to slower air movement, increased air density, trapping ambient air pollutants, and increased residential heating activities (Manisalidis et al., 2020).

4.11.5 Pollution profile of SO_2

The concentration of SO_2 during the two study periods, in general, did not exceed WHO air quality guidelines. Results also revealed that the SO_2 concentration was higher during the heating period compared to the non-heating period. Moreover, the difference between the two periods was small (Figure 4.17 and Figure 4.18). The highest mean annual concentration was recorded in 2019-2020 (S1) (1.45 μg/m^3) (Table 4.8). Episodes of SO_2 concentrations exceeding 100 μg/m^3 were observed in S1 during November 2019 and February 2020 (Figure 4.18). The peak monthly mean concentrations were predominantly recorded in February for S1, S2, and S3 across both study periods. In contrast, S4 exhibited its highest monthly mean concentration in March (Figure 4.18).

The diurnal patterns of SO_2 concentration indicated peak concentration on specific workdays: Monday (S1), Saturday (S2), Sunday (S3), and Tuesday (S4) (Figure 4.19). The second highest SO_2 concentration was noted on Thursday (S1, S3, S4). Notably,

elevated concentrations were observed in the evening (19:00) for S1 and S4, in the morning (7:00) for S2, and in the afternoon (13:00) for S4.

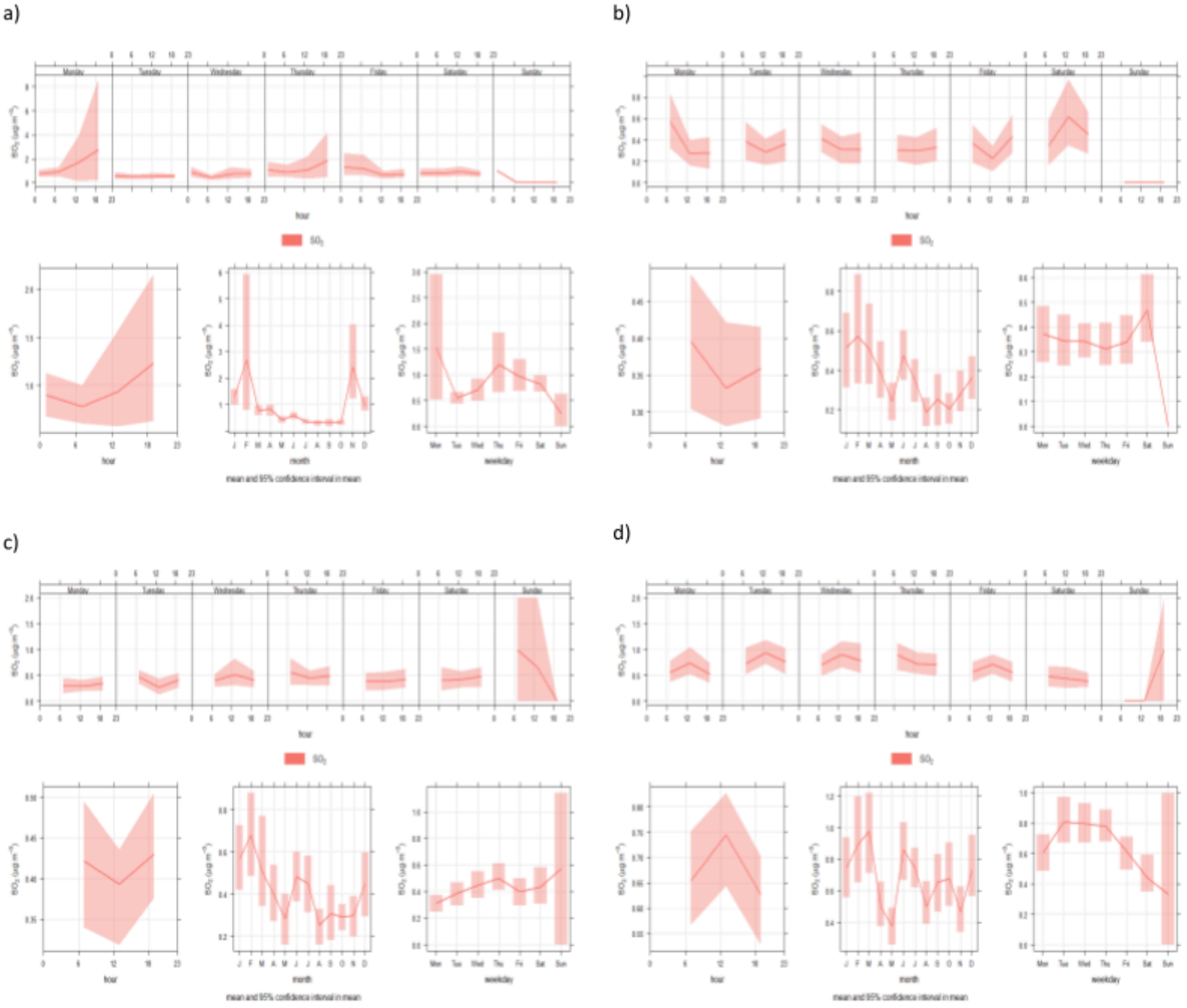

Figure 4.19: Diurnal and monthly variations of SO_2. (a): S1, (b): S2, (c): S3, and (d): S4 concentrations for 2018-2020.

Table 4.7: Periodic variations of ambient pollutant concentrations (μg/m^3) (S1, S2, S3, S4) in 2018-2019.

S1

Pollutant	Annual				Heating				Non-heating			
	Mean	St. Dev	Range (25th-95th)	Missing data (%)	Mean	St. Dev	Range (25th-95th)	Missing data (%)	Mean	St. Dev	Range (25th-95th)	Missing data (%)
TSP	305	579	0.00-1400	18.4	416	719	0.00-1900	19.4	178	315	0.00-800	17.2
SO_2	0.51	1.05	0.00-2.00	18.4	0.61	1.21	0.00-3.00	19.4	0.39	0.82	0.00-2.00	17.2
CO	271	419	108-650	18.4	348	640	95.0-803	19.4	238	275	110-517	17.2
NO_2	20.3	28.6	0.00-70.0	18.4	20.8	30.7	0.00-60.0	19.4	19.7	26.0	0.00-70.0	17.2
HF	1.35	8.28	0.00-5.00	18.4	2.28	11.2	0.00-14.5	19.4	0.30	1.52	0.00-1.00	17.2

S2

Pollutant	Annual				Heating				Non-heating			
	Mean	St. Dev	Range (25th-95th)	Missing data (%)	Mean	St. Dev	Range (25th-95th)	Missing data (%)	Mean	St. Dev	Range (25th-95th)	Missing data (%)
TSP	66.7	557	0.00-1400	18.4	398	704	0.00-1935	19.4	175	255	0.00-700	17.2
SO_2	0.38	0.76	0.00-2.00	18.4	0.42	0.85	0.00-2.00	19.4	0.33	0.65	0.00-2.00	17.2
CO	n/a	n/a	n/a	18.4	n/a	n/a	n/a	19.4	n/a	n/a	n/a	17.2
NO_2	16.5	38.1	0.00-60.0	18.4	16.4	45.6	0.00-73.5	19.4	16.5	27.3	0.00-50.1	17.2
HF	1.23	7.45	0.00-4.00	18.4	1.89	8.81	0.00-8.00	19.4	0.49	5.45	0.00-2.00	17.2

S3

Pollutant	Annual				Heating				Non-heating			
	Mean	St. Dev	Range (25th-95th)	Missing data (%)	Mean	St. Dev	Range (25th-95th)	Missing data (%)	Mean	St. Dev	Range (25th-95th)	Missing data (%)
TSP	347	605	0.00-1500	18.8	142	711.15	0.00-1700	20.8	232	351	0.00-895	17.2

SO_2	0.42	0.87	0.00-2.00	18.3	0.43	0.86	0.00-2.00	20.8	0.41	0.90	0.00-2.00	17.2
CO	286	377	0.00-920	18.3	236.00	390	0.00-1000	20.8	364	341	158-900	17.2
NO_2	37.7	37.7	0.00-170	18.3	51.53	70.2	0.00-190	20.8	16.1	25.7	0.00-70.0	17.2
HF	0.96	6.32	0.00-2.50	18.3	1.40	7.97	0.00-5.00	20.8	0.28	1.51	0.00-0.00	17.2

S4

	Annual				**Heating**				**Non-heating**			
Pollutant	Mean	St. Dev	Range (25^{th}-95^{th})	Missing data (%)	Mean	St. Dev	Range (25^{th}-95^{th})	Missing data (%)	Mean	St. Dev	Range (25^{th}-95^{th})	Missing data (%)
TSP	329	568	0.00-1400	18.5	365	681	0.00-1600	19.3	291	331	0.00-800	17.7
SO_2	0.57	1.05	0.00-2.00	18.4	0.54	1.05	0.00-2.00	19.3	0.61	1.06	0.00-2.00	17.3
CO	1157	856	600-2800	18.4	1321	996	658-3400	19.3	914	508	560-1759	17.3
NO_2	211	211	40.0-544	18.4	179	164	20.0-470	19.3	257	208	110-600	17.3
HF	2.53	21.8	0.00-4.00	18.4	4.02	28.2	0.00-10.5	19.3	0.34	2.41	0.00-1.00	17.3

Table 4.8: Periodic variations of ambient pollutant concentrations (µg/m^3) (S1, S2, S3, S4) in 2019-2020.

S1

Pollutant	**Annual**				**Heating**				**Non-heating**			
	Mean	St. Dev	Range (25^{th}-95^{th})	Missing data (%)	Mean	St. Dev	Range (25^{th}-95^{th})	Missing data (%)	Mean	St. Dev	Range (25^{th}-95^{th})	Missing data (%)
TSP	150	126	0.00-400	18.8	132	141	0.00-400	19.3	117	0.78	0.00-2.00	18.0
SO_2	1.45	9.00	0.00-4.00	18.8	2.17	11.7	0.00-6.00	19.3	0.45	0.78	0.00-2.00	18.0
CO	469	324	260-960	18.8	433	382	227-1098	19.3	519	519	360-855	18.0
NO_2	12.8	12.8	0.00-40.0	18.8	15.6	24.5	0.00-50.0	19.3	8.92	8.92	0.00-30.0	18.0
HF	0.27	2.33	0.00-0.00	18.8	0.47	3.03	0.00-1.00	19.3	0.00	0.00	0.00-0.00	18.0

S2

Pollutant	Annual				Heating				Non-heating			
	Mean	St. Dev	Range (25^{th}-95^{th})	Missing data (%)	Mean	St. Dev	Range (25^{th}-95^{th})	Missing data (%)	Mean	St. Dev	Range (25^{th}-95^{th})	Missing data (%)
TSP	122	114	0.00-300	18.8	102	124	0.00-400	19.3	152	90.8	100-300	18.1
SO_2	0.35	1.00	0.00-2.00	18.8	0.39	1.19	0.00-2.00	19.3	0.30	0.63	0.00-2.00	18.1
NO_2	12.2	15.6	0.00-40.0	18.8	11.7	16.0	0.00-40.0	19.3	13.0	15.1	0.00-30.0	18.1
HF	0.23	1.75	0.00-0.00	18.8	0.39	2.27	0.00-0.00	19.3	0.00	0.00	0.00-0.00	18.1

S3

Pollutant	Annual				Heating				Non-heating			
	Mean	St. Dev	Range (25^{th}-95^{th})	Missing data (%)	Mean	St. Dev	Range (25^{th}-95^{th})	Missing data (%)	Mean	St. Dev	Range (25^{th}-95^{th})	Missing data (%)
TSP	146	131	0.00-400	18.8	133	150	0.00-400	19.8	164	95.8	100-300	16.7
SO_2	0.41	0.95	0.00-2.00	18.8	0.47	1.07	0.00-2.00	19.8	0.34	0.74	0.00-2.00	16.7
CO	727	534	400-1500	18.8	896	621	500-1920	19.8	490	216	300-800	16.7
NO_2	10.4	10.4	0.00-30.0	18.8	11.59	16.7	0.00-40.0	19.8	8.67	10.8	0.00-30.0	16.7
HF	0.39	2.50	0.00-0.00	18.8	0.67	3.24	0.00-2.20	19.8	0.00	0.00	0.00-0.00	16.7

S4

Pollutant	Annual				Heating				Non-heating			
	Mean	Std	Range (25^{th}-95^{th})	Missing data (%)	Mean	Std	Range (25^{th}-95^{th})	Missing data (%)	Mean	Std	Range (25^{th}-95^{th})	Missing data (%)
TSP	203	161	100-400	18.8	191	190	0.00-600	19.2	217	170	100-400	18.1
SO_2	0.79	1.28	0.00-3.00	18.8	0.90	1.48	0.00-4.00	19.2	0.64	0.90	0.00-2.00	18.1
CO	963	720	570-2030	18.9	1232	828	780-2478	22.3	585	194	440-871	18.1
NO_2	237	237	160-533	18.8	254	178	210-622	19.2	213	85.7	230-410	18.1
HF	0.60	5.21	0.00-0.00	18.8	1.02	6.78	0.00-1.00	19.2	0.00	0.00	0.00-0.00	18.1

The pollution roses (Figure 4.20) indicate that elevated SO_2 concentrations at S1 originated from potential sources in the north, northeast, west-south-west, and south

directions. For S2, a significant SO2 source was identified in the south-south-eastern part of Astana. Similarly, for S3, high SO2 concentrations were observed in the south, north-north-east, east, and east-south-east directions. Furthermore, at S4, directions with notable SO2 concentrations included south-south-east, south, east-south-east, east, and west.

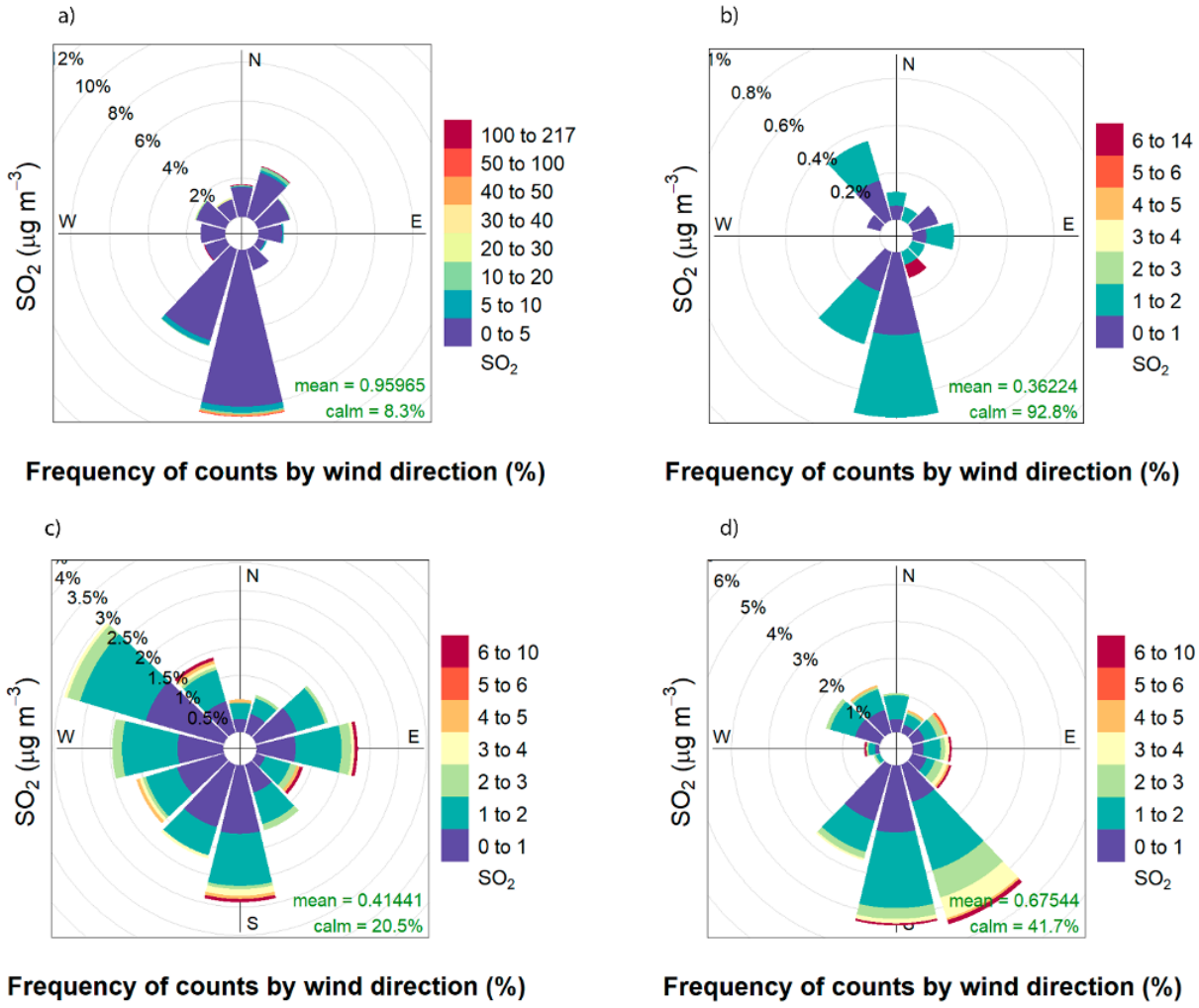

Figure 4.20: Pollution rose diagrams of SO_2 concentrations for S1 (a), S2 (b), S3 (c), and S4 (d).

4.11.6 Potential emission sources of $PM_{2.5}$

The bivariate polar plots (Figure 4.21) depicting monthly $PM_{2.5}$ concentrations and meteorological data offer insights for pollutant source identification. The elevated $PM_{2.5}$ levels (red color) were observed at S5 during the winter season (December, January, and

February) in the north and east-north-east directions. Although potential $PM_{2.5}$ sources

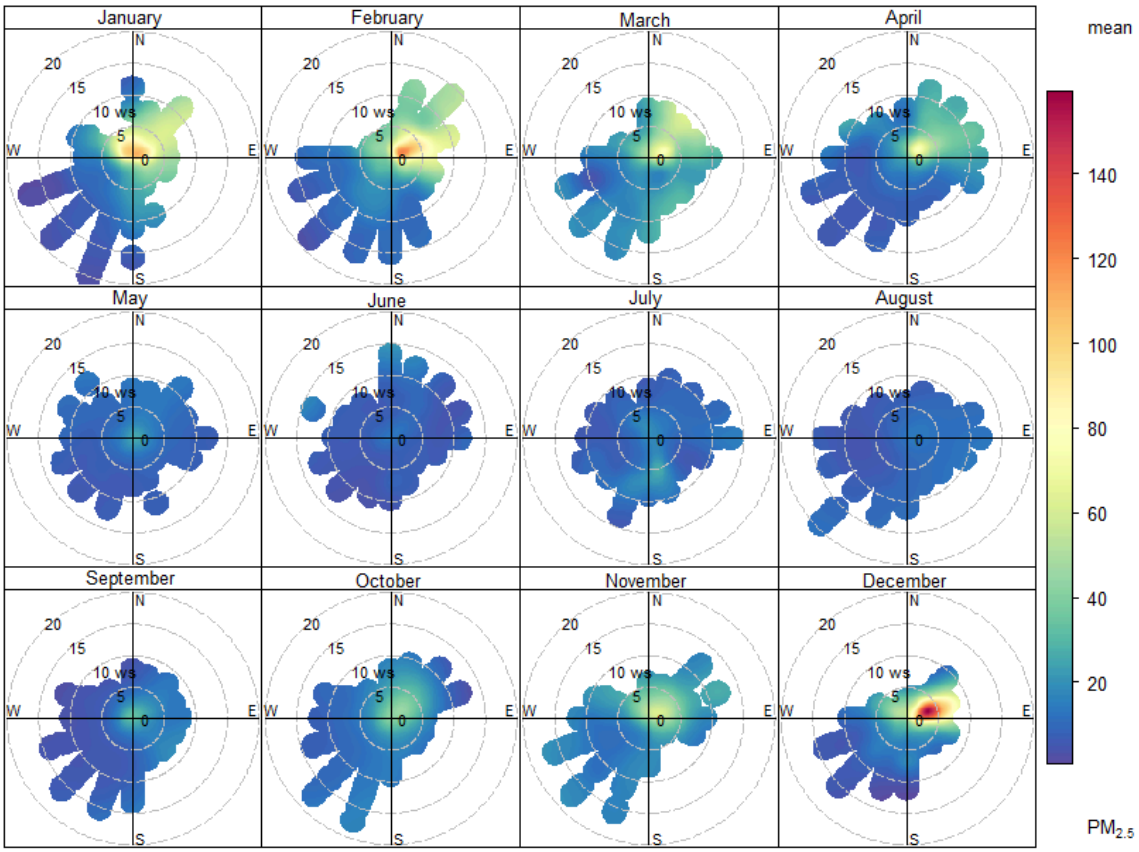

are **Figure 4.21**: Bivariate polar plots of monthly mean $PM_{2.5}$ concentrations.

distant from the monitoring station, the positioning aligns with coal-heated power plants (CHPP-1 and CHPP-2) and residential coal combustion in that direction. The heightened $PM_{2.5}$ concentrations during colder months also suggests power plant emissions contribute to the observed increase.

The CBPF plots showing $PM_{2.5}$ concentrations for the 75th (Figure 4.22a) and 95th percentiles (Figure 4.22b) were generated to assess the likelihood of elevated $PM_{2.5}$ concentrations relative to specific wind speed and direction sectors. Figure 5(a) highlights the influence of CHPP-2 on $PM_{2.5}$ emissions in the northeastern region of

Astana. Additionally, the highest concentration of fine particles (95th percentile) is centered in the polar coordinate (Figure 4.22b), which supports that, during periods of low wind speed, the pollutants tend to accumulate or persist at the monitoring stations rather than dispersing or being transported by the wind (Sooktawee et al., 2020). Potential sources may include vehicular exhaust (Askariyeh et al., 2020), possibly linked to heavy traffic in this city area.

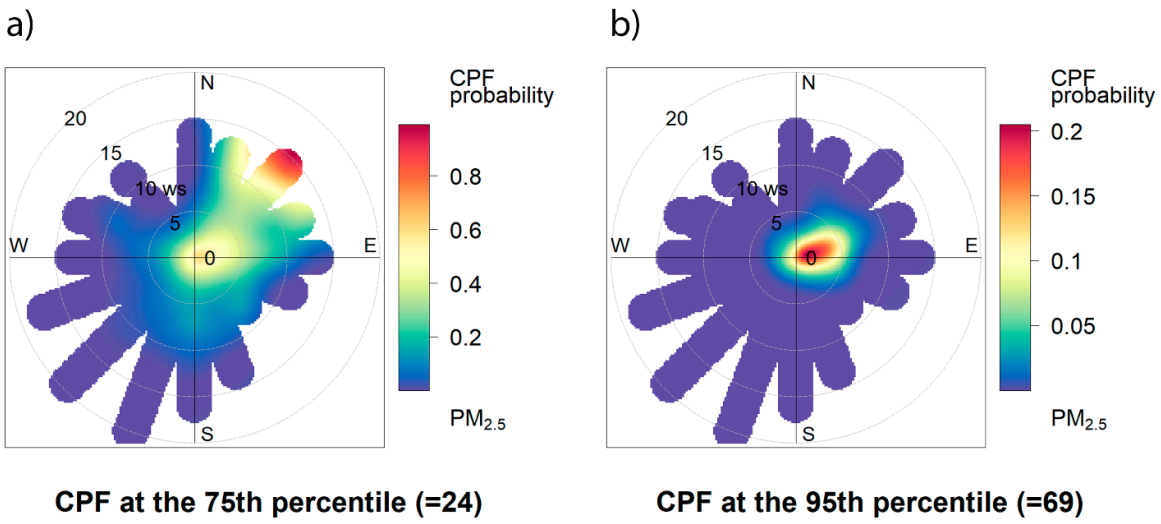

Figure 4.22: CBPF plots of $PM_{2.5}$ concentrations for 75th percentile (a) and 95th percentile (b).

While CBPF plots offer insights into the spatial distribution of $PM_{2.5}$, they lack information on its temporal variation. To address this, hourly CBPF plots were generated to examine the diurnal changes in $PM_{2.5}$ concentrations (Figure 4.23). The probabilities of

95th percentile $PM_{2.5}$ concentrations were noted at 8:00, 22:00, and 23:00. Higher $PM_{2.5}$ concentration during nocturnal periods can be attributed to stable atmospheric

conditions and a reduced boundary layer, limiting the vertical dispersion of pollutants

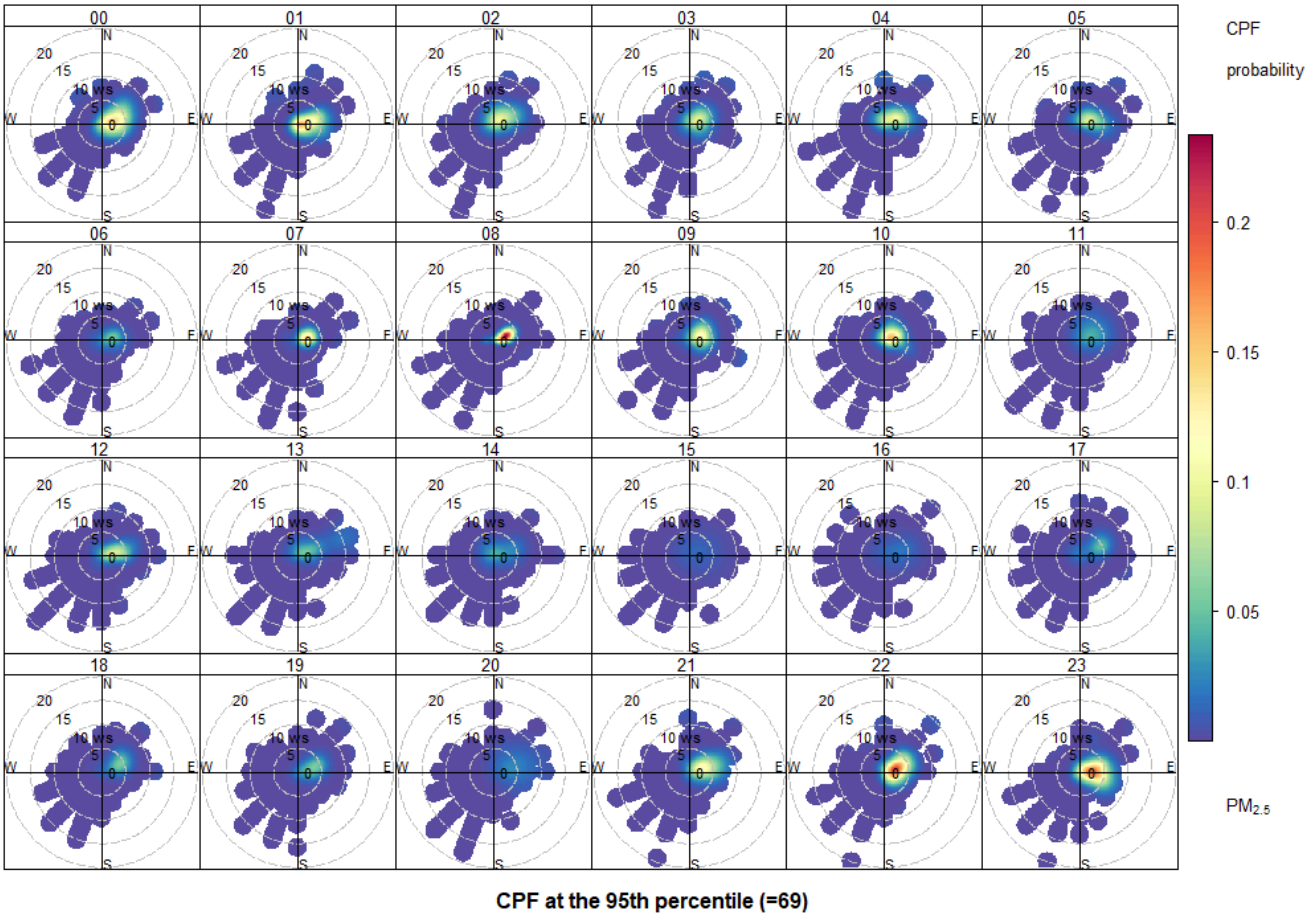

(Sooktawee et al., 2020).

Figure 4.23: CBPF plots of $PM_{2.5}$ concentrations for the 95th percentile (hourly).

4.11.7 Potential sources of SO_2

In Astana, both CHPP-1 and CHPP-2 surpassed the permissible SO_2 emissions level in 2019, amplified by the absence of a functional dry desulfurization system in certain boiler units, such as the No. 7 power boiler (Azhigaliyev, 2019). This led to inconsistent SO_2 concentration patterns, with the highest annual mean concentrations recorded in 2014 (31 µg/m^3) and 2016 (40 µg/m^3). Although these readings complied with Kazakhstani standards for maximum permissible concentration, they exceeded the

WHO annual limit of 20 µg/m3 (WHO, 2006). Maximum concentrations reached 1,653 µg/m^3 in 2014 and 1,614 µg/m^3 in 2016 (Kerimray et al., 2018).

CBPF plots were employed to pinpoint the potential source of SO_2 emissions (Figure 4.24). The CBPF analysis indicates a probability (> 20%) of SO_2 concentrations exceeding the 75th percentile (> 1 µg/m^3) in the eastern, east-southeastern, and southeastern regions of Astana (S3 and S4) (Figure 4.24). Potential sources may include a residential district to the south-southeast or the concrete plant. Surprisingly, peak SO_2 concentrations are also observed in the southwestern direction, suggesting an unidentified emission source (Figure 4.24a). Given the absence of residential or industrial facilities nearby, the potential source could be sulfur-polluted water bodies in that area. Additionally, S1, located in a heavy traffic network, contributes to the local air quality.

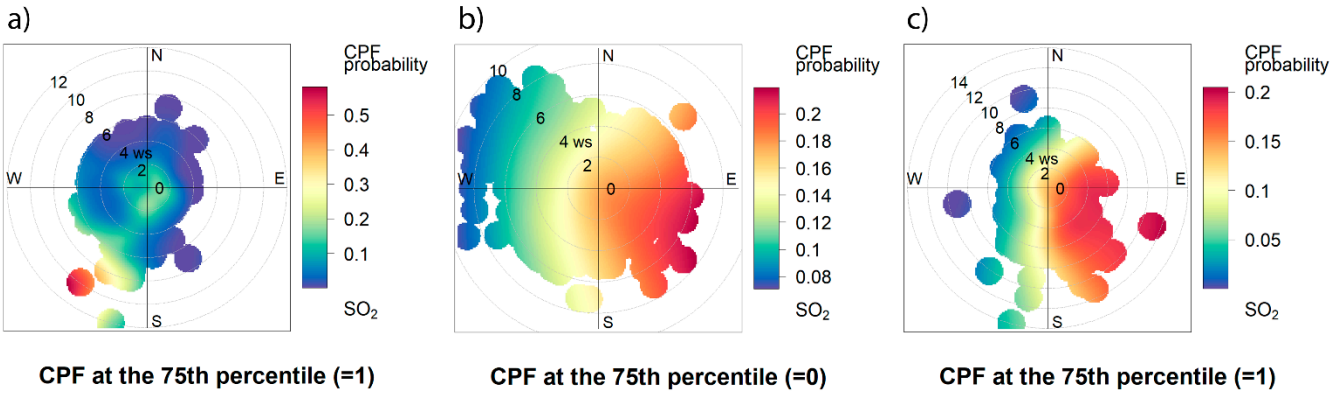

Figure 4.24: CBPF plots of SO_2 concentration for 75th percentile at S1 (a), S3 (b), and S4 (c).

For S3 and S4, elevated SO_2 concentrations are linked to CHPP-2 activity in the northeastern area and coal heating in private districts to the east, east-southeast, and southeast of Astana.

4.12 $PM_{2.5}$ concentration modeling via MLR and ML

4.12.1 $PM_{2.5}$ pollution profile

In 2019, $PM_{2.5}$ concentrations (Table 4.9) exhibited both annual and seasonal variations (during heating, October–April, and non-heating periods, May–September). The S6 recorded a higher annual average $PM_{2.5}$ concentration (58.0 μg/m^3) compared to S5 (14.5 μg/m3). This discrepancy may be attributed to the proximity of S6 to CHPPs and areas with heavy traffic. Notably, both S5 and S6 exceeded the WHO's permissible annual mean concentration of 5 μg/m^3 (WHO, 2020).

Table 4.9: Annual and seasonal variations in the concentration of $PM_{2.5}$ (μg/m^3) in 2019.

	S5			S6		
	Annual	**Heating**	**Non-Heating**	**Annual**	**Heating**	**Non-Heating**
Mean	14.5	18.1	10.4	58.0	77.2	38.7
SD	26.1	33.7	11.1	75.1	93.6	41.8
Range (25th-95th)	(5.60–43.6)	(5.90–54.2)	(5.30–29.5)	(21.8-186)	(26.6-242)	(19.7–107)
Min	0	0	0	5.7	5.7	7.1
Max	824	824	126	1086	1086	985

During the heating period, the average concentrations of $PM_{2.5}$ at both monitoring stations exceeded those observed during the non-heating period. The peak concentration of $PM_{2.5}$ was observed in January, reaching 1,086 μg/m^3 at S6 (Figure 4.25b). At each monitoring station, a two-fold increase in average $PM_{2.5}$ concentrations was noted during the heating period. This elevation is most likely attributed to increased emissions from residential heating, higher rates of particulate resuspension, and atmospheric reactions leading to $PM_{2.5}$ formations (Cichowicz, 2017).

The $PM_{2.5}$ levels exhibited weekly variations at S5 and S6, reaching peaks of 70 μg/m^3 on Saturday (S5) and 20 μg/m^3 on Thursday (S6). Similar patterns have been

observed in previous studies (Meng et al., 2020; Kerimray et al., 2018; Assanov et al., 2021). Examining hourly concentrations, both stations showed a characteristic trend with peaks around midnight, followed by a gradual decrease until approximately 16:00 (Figure 4.25c). The midnight peak could be attributed to a temperature decrease, potentially coupled with inversion conditions, leading to pollutant accumulation (Bathmanabhan et al., 2010). This hourly pattern, resembling a "W-shape," has been documented in other studies (Chen et al., 2015; Yao et al., 2015; Huan et al., 2018), indicating a potential link with atmospheric stability during nighttime hours (Yao et al., 2015).

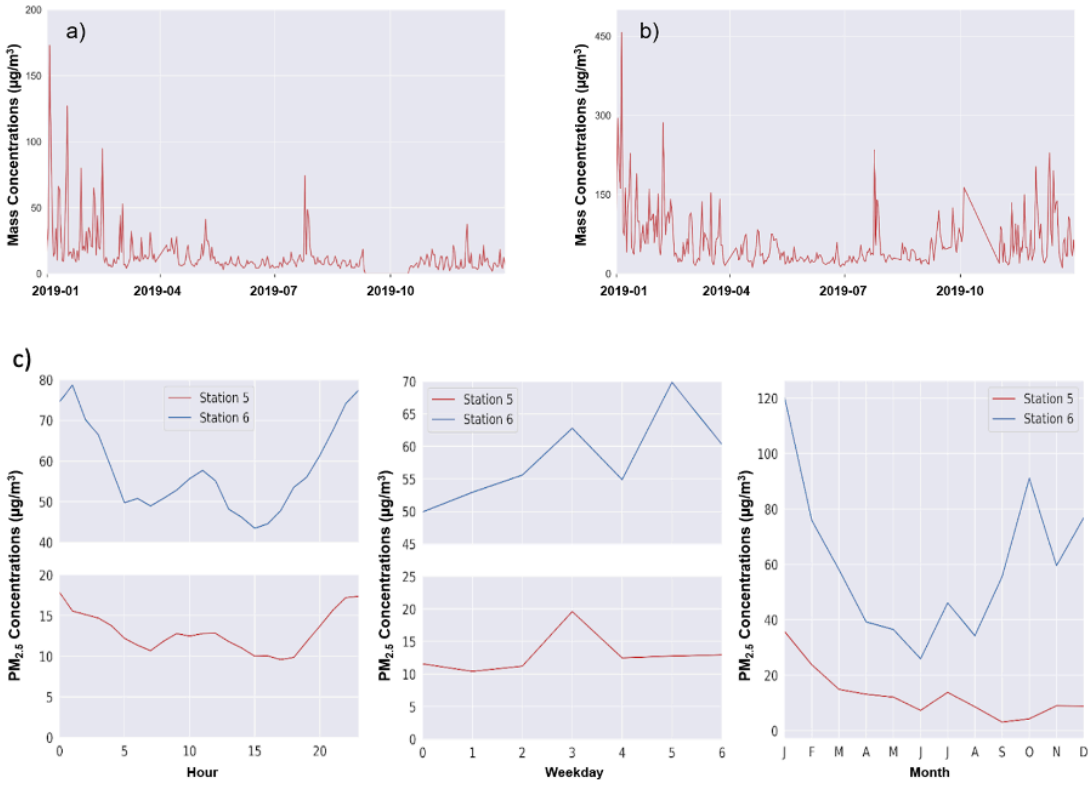

Figure 4.25: Time series plot of $PM_{2.5}$ concentrations for S5 (a) and S6 (b), and diurnal (c), weekly, and monthly variations of $PM_{2.5}$ for S5 and S6 in 2019.

4.12.2 Pollution Profiles of PM_{10}, CO, NO, NO_2, and SO_2

In the study year, the annual mean PM_{10} concentration at S5 complied with the WHO annual limit of 15 μg/m^3, while S6 exceeded this threshold (Table 4.10). S6 exhibited a twofold increase in average PM_{10} concentrations during the heating season compared to the non-heating period (79.1 μg/m^3 vs. 41.4 μg/m^3). High PM_{10} levels are an environmental concern due to their association with increased cardiorespiratory hospital admissions among the elderly and the aggravation of chronic bronchitis (Kelly & Fussel, 2012; Kerimray et al., 2018). In 2019, at both S5 and S6, the annual mean NO concentration remained below the EU maximum permissible limit for NO_x of 30 μg/m^3.

Additionally, the average annual NO_2 concentrations at both stations did not exceed WHO air quality guidelines (40 μg/m^3). During the heating period at S6, the highest average NO_2 concentration was recorded at 40.7 μg/m^3 (range: 20.6-77.6 μg/m^3). Nevertheless, the annual average SO_2 concentration at S6 exceeded the maximum permissible limit for residential areas established by the National Air Quality Standards (60 μg/m^3) (NAAQS, 2018), with a mean of 125 μg/m^3 and a range of 2.90 to 949 μg/m^3. During the heating period, a high SO_2 concentration was observed at S6, with a mean of 239 μg/m^3 and a range of 7.70 μg/m^3 to 1114 μg/m^3. The S6 recorded an increase in SO_2 levels in November and December, reaching concentrations up to 1000 μg/m^3. These findings raise concerns as SO_2, being highly soluble, can be readily absorbed in the respiratory tract, leading to airway inflammation and associated health risks for vulnerable populations such as the asthmatic group (WHO, 2006; WHO 2000).

The S6 recorded the highest annual mean CO concentration, reaching 630 μg/m^3 (range: 323 μg/m^3 - 1,553 μg/m^3) (Table 4.10). Meanwhile, S5 exhibited a lower annual

average CO concentration, ranging from 35 to 931 μg/m^3, with a mean of 338 μg/m^3. The mean at both S5 and S6 drastically exceeded the daily maximum permissible CO level according to Kazakhstani standards (annual average of 60 μg/m3) (Kazhydromet, 2021).

Table 4.10: Periodic variations in ambient pollutant concentrations (μg/m^3) in 2019.

S5									
	Annual			Heating			Non-Heating		
Air Pollutant	**Mean**	**SD**	**Range (25th–95th)**	**Mean**	**SD**	**Range (25th–95th)**	**Mean**	**SD**	**Range (25th–95th)**
PM_{10}	3.12	3.8	(1.5–7.3)	2.73	2.23	(1.4–5.7)	3.80	3.82	(1.9–9.5)
CO	485	3,006	(34.1–931)	250	549	(35.2–1,011)	745	4,330	(33.2–838)
NO	29.9	33.8	(2.4–88.2)	25.3	32.0	(1–83.9)	35.1	35	(12.5–94.7)
NO_2	25.8	25.8	(1.2–32.4)	10.3	26.7	(1.2–37.1)	9.60	24.7	(1.6–23.5)
SO_2	19.7	18.6	(7.9–58.1)	20.9	20.7	(8.00–63.7)	18.3	15.8	(7.8–45)
S6									
	Annual			Heating			Non-Heating		
Air Pollutant	**Mean**	**SD**	**Range (25th–95th)**	**Mean**	**SD**	**Range (25th–95th)**	**Mean**	**SD**	**Range (25th–95th)**
PM_{10}	60.3	75.9	(23.4–190)	79.1	94.5	(27.9–244)	41.4	43.4	(21.3–114)
CO	630	495	(323–1,553)	742	540	(405–1726)	518	416	(269–1245)
NO	9.01	21.0	(1.10–41.1)	9.17	18.9	(1.10–42.5)	8.86	22.8	(1.10–37.1)
NO_2	39.7	27.1	(17.2–81.0)	40.7	23.9	(20.6–77.6)	38.7	30.0	(15.1–88.5)
SO_2	125	320	(2.90–949)	239	422	(7.70–1114)	10.3	10.9	(2.90–28.0)

Notably, S6 recorded episodes of extremely high CO concentrations in September, peaking at 30,000 μg/m^3. Chronic CO poisoning can lead to adverse neurological symptoms, including cognitive impairments, movement disorders, speech impairment, and mood disturbances. This poses a particular risk to population groups employed in the transportation sector, traffic wardens, and garage/tunnel workers (WHO, 2000).

4.12.3 Correlation between $PM_{2.5}$, conventional atmospheric pollutants, and meteorological parameters

Table 4.11 shows a correlation between $PM_{2.5}$ and various atmospheric pollutants and meteorological parameters, revealing positive correlations with PM_{10}, SO_2, CO, NO_2, NO, P, and RH, along with negative correlations with WS and T. At S6, a robust

correlation (r = 0.99) between $PM_{2.5}$ and PM_{10} was evident during both heating and non-heating periods, while S5 displayed a similar strong correlation (r = 0.76) only during the non-heating period. Additionally, a high correlation (r = 0.87 for S5 and S6) between $PM_{2.5}$ and CO was noted, along with a moderate correlation ($0.30 < r < 0.80$) between $PM_{2.5}$ and nitrogen gases during the heating period at both stations. Furthermore, moderate negative correlations with $PM_{2.5}$ were observed for T, WS, and WD during the heating period. These outcomes suggest potential common origins for PM and other air pollutants, aligning with expectations that more severe air pollution events may coincide with lower temperatures (indicating increased heating activity) and weaker wind dispersion. This pattern is consistent with prior research reporting similar correlation coefficients between PM ($PM_{2.5}$ and PM_{10}), gaseous pollutants (e.g., CO, NO2, and SO2), and meteorological parameters such as atmospheric and dew point temperatures and WD (e.g., Thongthammachart et al., 2019; Dutta et al., 2021).

Table 4.11: Correlation coefficients (r) between $PM_{2.5}$, selected atmospheric pollutants, and meteorological parameters.

		S5						S6					
		Heating			Non-Heating			Heating			Non-Heating		
Parameters correlated with $PM_{2.5}$		**r**	**Significance**	**Sample Size**	**r**	**Significance**	**Sample Size**	**r**	**Significance**	**Sample Size**	**r**	**Significance**	**Sample Size**
Pollutant concentration	PM_{10}	0.12	0.096	188	0.76	<0.001	165	0.99	<0.001	160	0.99	<0.001	157
	SO_2	0.03	0.716	188	0.23	0.003	165	−0.09	0.239	160	−0.02	0.758	157
	CO	0.87	<0.001	188	−0.17	0.025	165	0.87	<0.001	160	0.62	<0.001	157
	NO_2	0.48	<0.001	188	0.17	0.031	165	0.55	<0.001	160	0.18	0.023	157
	NO	0.49	<0.001	188	0.47	<0.001	165	0.48	<0.001	160	0.28	<0.001	157
Meteriological parameters	T	−0.45	<0.001	188	0.23	0.003	165	−0.47	<0.001	160	0.01	0.868	157
	P	0.23	0.002	188	0.05	0.528	165	0.36	<0.001	160	0.24	0.003	157
	RH	0.10	0.161	188	−0.16	0.037	165	0.03	0.697	160	0.01	0.869	157
	WD	−0.35	<0.001	188	−0.16	0.044	165	−0.61	<0.001	160	−0.39	<0.001	157
	WS	−0.38	<0.001	188	−0.17	0.028	165	−0.15	0.069	160	0.13	0.119	157

4.12.4 MLR predictive models

The development of four predictive models for $PM_{2.5}$ concentrations at S5 and S6 during heating and non-heating periods involved the use of the MLR equation. Notably, these models demonstrated a robust fit to the data, as evidenced by high R^2 values (0.84 for heating, 0.68 for non-heating, and 0.99 combined). Analysis of the VIF indicated the absence of multicollinearity (VIF < 5) among predictor variables for both periods in S5 and S6.

Examining the impact of independent variables across predictive models, PM_{10} and CO concentration are the most influential factors based on the Shapley–Owen value. Specifically, in S5 (heating), S5 (non-heating), and S6 (non-heating), PM_{10} contributed 52.3%, 73.4%, and 78.8%, respectively, to the variation in $PM_{2.5}$ concentrations. Moreover, CO explained 80.2% of the variation in S5 (heating). The predictive models underscored a positive correlation between PM_{10} and $PM_{2.5}$ concentrations. Additionally, in S5 (non-heating), positive influences of CO, NO, and NO_2 were observed, revealing a contrasting impact on other stations, where the overall influence was negative.

Table 4.12: MLR equation for $PM_{2.5}$ predictions for air pollution monitoring data (S5 and S6) (2019).

	Model	**VIF**
	S5	
Heating	$PM_{2.5}$ (μg/m^3) = (−5.75) + 0.29(PM_{10}) (μg/m^3) + 1.00(CO)(μg/m^3) − 0.13(NO_2) (μg/m^3)	(1.04–1.63)
Non-heating	$PM_{2.5}$ (μg/m^3) = (−2.72) + 0.68(PM_{10}) (μg/m^3) + 0.14(SO_2) (μg/m^3) − 0.13(NO_2) (μg/m^3) + 0.32(NO) (μg/m^3)	(1.09–1.89)
	S6	
Heating	$PM_{2.5}$ (μg/m^3) = (−5.32) + 0.98(PM_{10}) (μg/m^3) + 0.04(CO)(μg/m^3) − 0.02(NO) (μg/m^3) + 0.01(WS)(m/sec)	(1.37–4.43)
Non-heating	$PM_{2.5}$ (μg/m^3) = 74.24 + 1.02(PM_{10}) (μg/m^3) − 0.02(NO_2) (μg/m^3) − 0.02(CO)(μg/m^3) − 0.02(P)(mmHg)	(1.08–1.99)

Common sources, such as fossil fuel combustion, biomass burning, and wildfires, contribute to urban $PM_{2.5}$ and PM_{10}. The positive correlation coefficients between $PM_{2.5}$, PM_{10}, and NO (Table 4.11) indicate a common origin, with gaseous pollutants such as NO_x primarily originating from vehicular exhaust and stationary fossil fuel combustion. Figures 4.26 depict how the expected values of $PM_{2.5}$ concentrations correspond to the observed data from S5 and S6 in 2019 for both study periods, revealing a consistent trend. The predictive models exhibited a strong fit in estimating $PM_{2.5}$ concentrations, supported by various validation techniques (Table 4.12). Error metrics, such as MAE and NME, indicated reliable model performance. MAE values, ranging from 0.49 to 6.37, reflected minimal error between observed and expected $PM_{2.5}$ concentrations. However, RMSE values (2.33–8.48) suggested potential differences between observed and predicted values (Table 4.13).

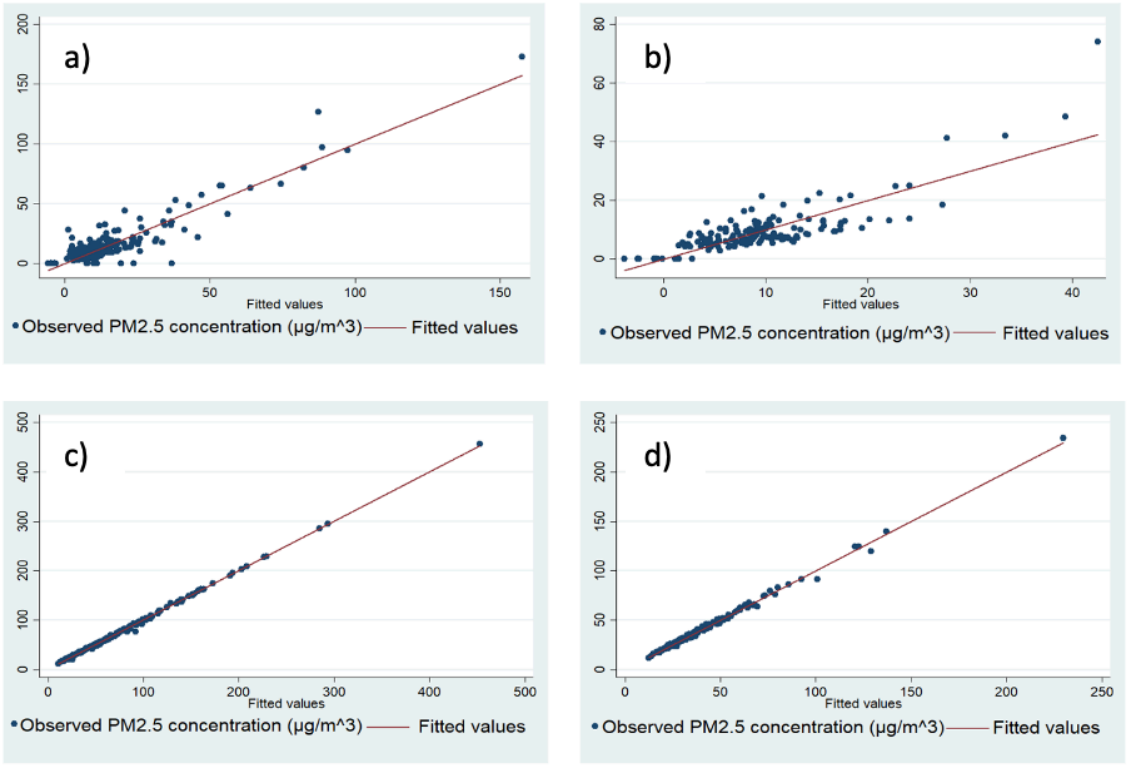

Figure 4.26: Predicted vs. observed $PM_{2.5}$ concentration (S5, S6) during heating (a, c) and (non-heating (b, d) periods.

Table 4.13: Performance indicators for model validation (S5 and S6).

	S5		S6	
	Heating	**Non-Heating**	**Heating**	**Non-Heating**
Mean absolute error (MAE)	6.37	3.57	1.55	1.47
Root-mean-square error (RMSE)	8.48	5.29	2.42	2.15
Normalized absolute error (NMAE)	0.39	0.37	0.02	0.04
Coefficient of determination (R^2)	0.84	0.68	0.99	0.99
Index of Agreement (IA)	0.95	0.90	0.99	0.99
Prediction accuracy (PA)	0.84	0.69	0.99	1.01
Observed mean (O_i)	16.4	9.29	77.4	38.8
Predicted mean (P_i)	16.3	9.29	77.3	38.8
Observed standard deviation (O_{std})	21.3	9.28	61.8	26.9
Predicted standard deviation (P_{std})	19.6	7.07	61.7	27.9

4.12.5 RF prediction models

The RF-based prediction models outperformed the MLR models for $PM_{2.5}$ concentration based on expected vs. observed concentrations of $PM_{2.5}$ (Figure 4.27), higher R^2 values

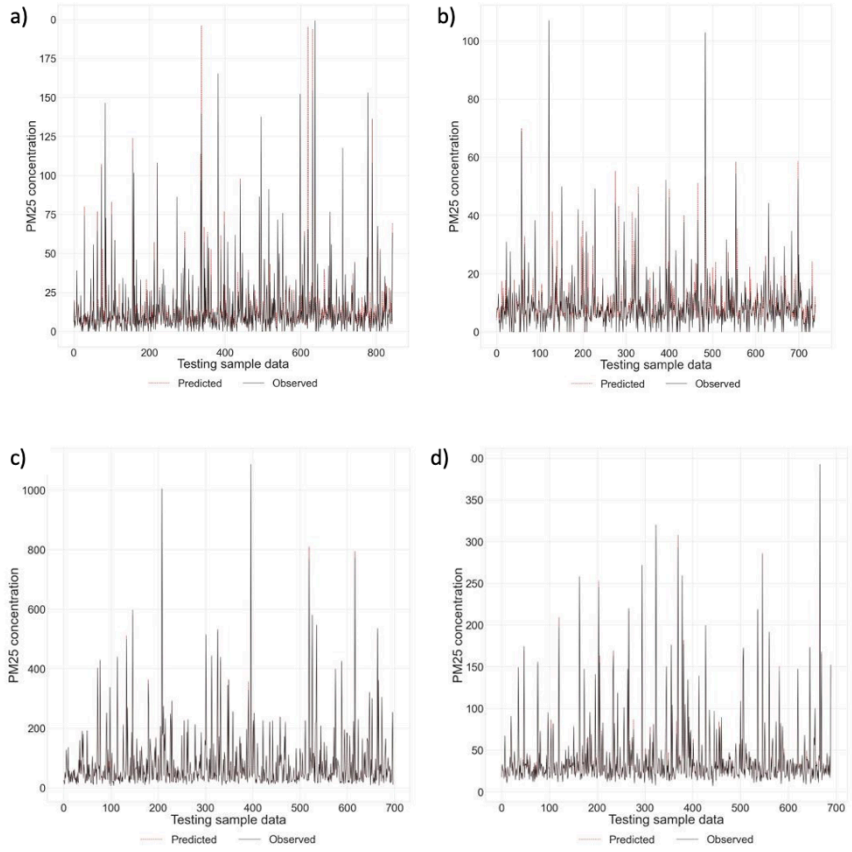

Figure 4.27: Expected and observed concentrations of $PM_{2.5}$ (S5, S6) for heating (a, c) and non-heating (b, d) periods.

values (ranging from 0.79 to 0.98) (Figures 4.28), and residuals (Figures 4.29).

The statistical metrics assessing model accuracy, including MAE, RMSE, and 10-fold cross-validation, consistently suggest the better performance of RF-based models over MLR models (Table 4.14). These findings are consistent with recent studies employing both MLR and diverse machine learning algorithms for PM concentration prediction. Notably, lower MAE, RMSE, and CV-MSE (Cross-validation of MSE) values during the non-heating period suggest potential influences from seasonal variations and specific factors affecting $PM_{2.5}$ formation mechanisms, such as industrial activity, coal-burning in municipal areas, variations in secondary pollutant

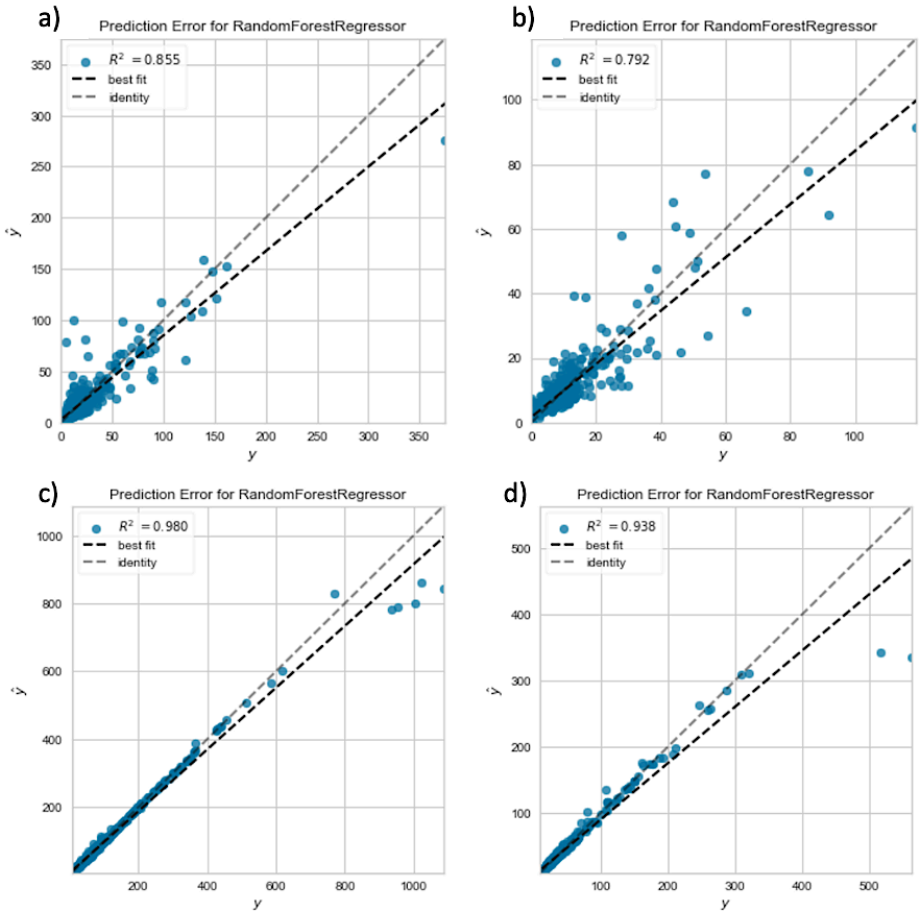

concentrations, or changes

Figure 4.28: Scatterplot for $PM_{2.5}$ concentrations (S5, S6) during the (a,c) heating and (b,d) non-heating periods

in diffusion rates.

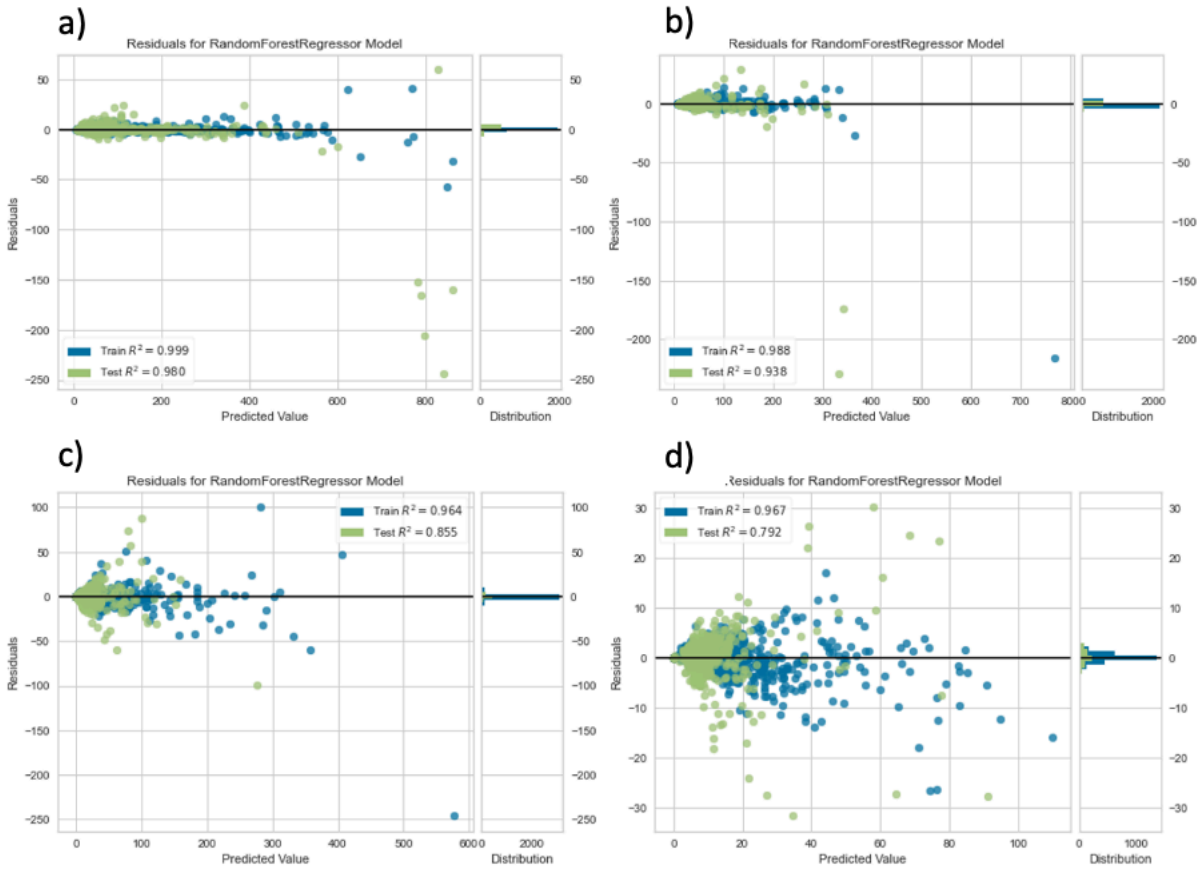

Figure 4.29: Residuals distribution (S5, S6) for the heating (a, c) and non-heating (b, d) periods.

Table 4.14: Model performance evaluation for the RF-based $PM_{2.5}$ concentration prediction model.

Model Performance Indicator	MAE (µg/m^3)	RMSE (µg/m^3)	CV-MSE (µg/m^3)
S5 Heating	3.95	8.70	175
S5 Non-heating	2.30	4.38	30.2
S6 Heating	3.07	16.5	141
S6 Non-heating	0.63	4.29	75.3

During the non-heating period at S5, PM_{10} (63%) and NO (14%) concentrations were identified as the primary predictors of $PM_{2.5}$ concentrations, while CO (69%) and

PM_{10} (15%) concentrations were the major predictors for the heating period forecasts. The correlation coefficients for S6 reflected similar patterns, with PM_{10} being the dominant contributor (> 95%).

As revealed by RF, the strong correlation between $PM_{2.5}$ and PM_{10} concentrations at S6 explains the discrepancy in predictive accuracy between S5 and S6 concentration forecasts. This can be attributed to the substantial contribution of PM_{10} content to the composition of $PM_{2.5}$. Further investigation into the relationship between PM_{10} and $PM_{2.5}$ concentrations at S6 would require advanced laboratory tools, such as elemental analysis.

The meteorological parameters demonstrated a comparatively lower overall contribution to $PM_{2.5}$ concentrations (e.g., < 0.87% for S6) when compared to other pollutants. However, during the heating period (S5), temperature was the third most influential factor for $PM_{2.5}$ concentrations (4.55%). This connection may be associated with increased rates of coal burning and industrial activities for local residential heating, a phenomenon documented in the literature (Shaziayani et al., 2022; Joharestani et al., 2019; Enebish et al., 2020). Notably, wind speed (S5, S6) contributed only 1.51% to $PM_{2.5}$ variations, as opposed to prior studies (Shaziayani et al., 2022; Joharestani et al., 2019; Enebish et al., 2020). This difference could be explained by the unique climate features of Astana, characterized by the free flow of both cold Arctic air and warm air masses, a distinction not present in previously studied regions (Shaziayani et al., 2022; Joharestani et al., 2019; Enebish et al., 2020; Ly et al., 2020). The area's high-speed and frequent winds might lead to a weak or non-existent correlation between $PM_{2.5}$

concentrations and wind speed, while seasonal variations in wind directions could remain crucial in influencing variations in $PM_{2.5}$ concentrations.

4.12.6 Comparison between prediction methods

The RF-based models perform better, in general, due to their robust capability for nonlinear fitting (Ren et al., 2021). This is particularly beneficial in air quality modeling, where accuracy is influenced by variations in meteorological parameters, industrial production, urban coal-burning rates, and vehicle exhaust across different seasons (Shaziayani et al., 2022; Meng et al., 2020; Kerimray et al., 2018; Ren et al., 2021; Enebish et al., 2020). Notably, the ML approach, unlike MLR modeling, eliminates the need for data adjustment, such as normalizing the distribution of dependent and independent variable data (Khan et al., 2022; Joharestani et al., 2019).

The RF-based model is less effective when predicting high $PM_{2.5}$ concentration values (Figure 4.27 and Figure 4.28), overestimating predicted values. In contrast, MLR predictions are more conservative. While RF is feasible for environmental studies, exploring other machine learning techniques, such as XGBoost, artificial neural networks (ANN), or ARIMA, is advisable to address this limitation and assess if they demonstrate similar trends (Park et al., 2018; Ejohwomu et al., 2022; Bekkar et al., 2021; Zheng et al., 2021).

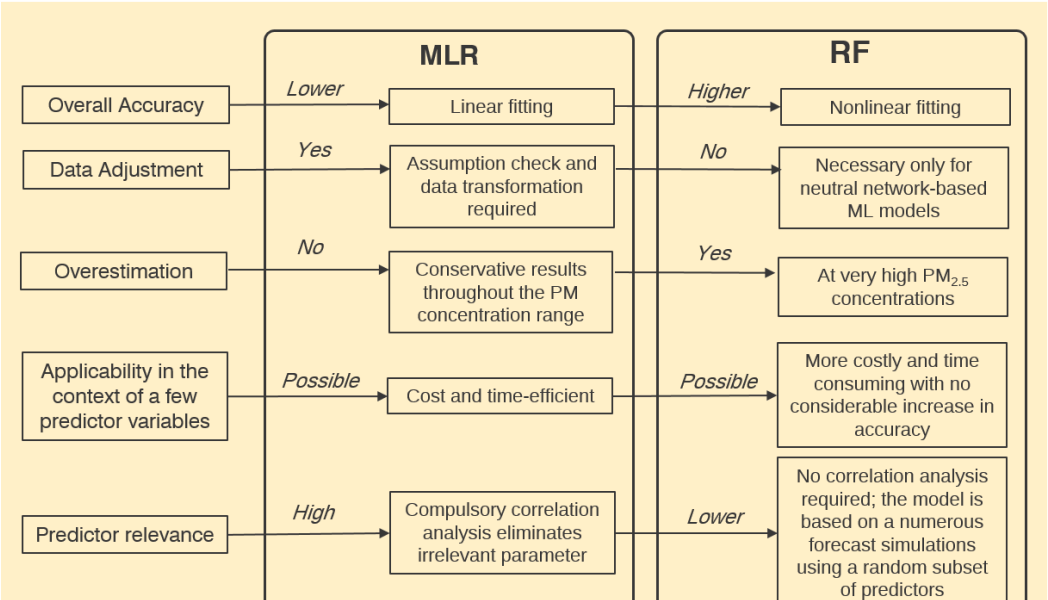

Figure 4.30: Comparison between MLR and RF approaches for PM prediction modeling.

Despite statistical models (e.g., MLR, Generalized Additive Model, and Linear Mixed-Effects Model) having an overall lower accuracy compared to the RF-based approach, they may prove more effective in scenarios with a limited number of predictor variables, as seen in locations with limited air pollution and meteorological data such as Astana (Kulkarni et al., 2022). The RF algorithm, relying on the average results of numerous decision trees with random predictor variables, can lead to significant deviations between predicted and observed pollutant concentrations due to irrelevant parameters (Park et al., 2022; Ren et al., 2021). Therefore, a statistical model with a thorough correlation analysis, eliminating accuracy-disrupting variables, could be a viable alternative to RF, especially in contexts with data limitations and high computational requirements of other ML approaches such as ANN or XGBoost. A comparison between the two approaches is presented in Figure 4.30.

4.12.7 HHRA

An assessment of health risks was conducted via the AIRQ+ software to estimate the potential impacts of $PM_{2.5}$ exposures on mortality from respiratory and cardiovascular diseases. Data for four distinct age groups (0–1, 2–14, 15–64, and 65–120 years old) in Astana were obtained from government statistical databases (Table 4.15).

Table 4.15: The demographic distribution and recorded mortality cases in Astana for 2019 across various age groups.

Age Group	Population	Mortality Cases
0–1	28,736	171
2–14	286,368	87
15–64	712,275	1878
65–120	51,005	2193

Table 4.16 displays YLL for the observed year with a $PM_{2.5}$ threshold at 10 μg/m^3. The annual YLL, considering all natural causes of mortality based on mean $PM_{2.5}$ concentrations from S5 and S6, yielded values of 12.7 years (0.00, 25.3; 95% CI) and 130.6 years (0.00, 253; 95% CI) for all age groups in 2019. Specifically, individuals aged 30 to 120 had YLL values of 3.82 years (0.00, 7.59; 95% CI) and 39.3 years (0.00, 75.9; 95% CI) for mean concentrations detected on S5 and S6. Per 100,000 individuals, the YLL values reached a peak of 1.18 years (0.00, 2.34; 95% CI) and 12.1 years (0.00, 23.4; 95% CI) for S5 and S6, respectively.

Table 4.16: YLL values estimated by AirQ+.

	S5		S6	
Parameters	**Mean**	**95% CI**	**Mean**	**95% CI**
YLL per total population (all ages)	12.7	(0.00–25.3)	131	(0.00–253)
YLL per total population (age 30–64)	3.82	(0.00–7.59)	39.3	(0.00–75.9)
YLL per 100,000 people (all ages)	1.18	(0.00–2.34)	12.1	(0.00–23.4)
YLL per 100,000 people (age 30–64)	0.35	(0.00–0.70)	3.64	(0.00–7.04)

The disease burden for Astana's population in 2019 was determined through the PAF methodology. Given the assumption of universal exposure to elevated $PM_{2.5}$ levels in Astana, the employed value of PP was equal to 1. However, due to the absence of comprehensive medical records, calculating YLD for the population based solely on AIRQ+ data proved to be impractical.

To address this, YLD was estimated by incorporating mortality causes for respiratory and cardiovascular diseases from AIRQ+, data sourced from the Kazakhstan Statistical Agency, and relevant parameters derived from prior literature on β and disability weights, as outlined in Table 4.17 (Bureau of National Statistics, 2021; Jung et al., 2019; Yin et al., 2017).

Table 4.17**:** Exposure-response coefficients, morbidity cases, and disability weights for respiratory and cardiovascular diseases in Astana.

$B_{respiratory}$	Morbidity $Cases_{respiratory}$	Disability $Weight_{respiratory}$	$\beta_{cardiovascular}$	Morbidity $Cases_{cardiovascular}$	Disability $Weight_{cardiovascular}$
0.0079	250,666	0.703	0.00068	30,318	0.787

The YLD and DALY results for each observed disease are presented in Table 4.18. In 2019, the YLD for the total population, considering mean $PM_{2.5}$ concentrations from S5, were 1,912 years for respiratory disease and 235 years for cardiovascular disease. At S6, the YLD for the entire population was 6,477 and 923 years for respiratory disease and cardiovascular disease, respectively. The YLD per 100,000 population in 2019, based on the mean $PM_{2.5}$ concentration from S5, was 177 years for respiratory diseases and 21.8 years for cardiovascular diseases. For S6, using the mean $PM_{2.5}$ concentration, the YLD per 100,000 individuals was 601 years for respiratory disease and 85.6 years for cardiovascular disease. The substantial variation in YLD for different diseases may be attributed to differences in exposure-response coefficient values (Yin et al., 2017).

Table 4.18: YLD estimated for respiratory and cardiovascular morbidity and DALY values.

Parameter		S5	S6
Respiratory disease	YLD per total population	1,912	6,477
	YLD per 100,000 individuals	177	601
Cardiovascular disease	YLD per total population	235	923
	YLD per 100,000 individuals	21.8	85.6
DALY per total population		2,160	7,531
DALY per 100,000 individuals		200	698

The DALY for respiratory and cardiovascular conditions attributed to $PM_{2.5}$ concentrations from S5 was estimated at 2,160 years for the overall population. Additionally, for the S5, the DALY per 100,000 population was equal to 200 years. Based on mean $PM_{2.5}$ concentrations detected at S6, the DALY for the entire population was 7,531 years, with a corresponding DALY per 100,000 individuals of 698 years.

These findings align with DALY values reported in other case studies. For example, the DALY attributable to air pollution in Spain was 286 years per 100,000 individuals, with a 97.5% confidence level ranging from 53 to 469 years per 100,000 individuals in 2012 (WHO, 2016c). The elevated DALY values identified for data from S6 can be attributed to the high $PM_{2.5}$ concentrations recorded in the monitoring station.

4.13 KAP of air pollution among Astana residents

4.13.1 Sociodemographic characteristics of the studied population

The general demographic characteristics of the participants (Table 4.19) show that out of the total 782 respondents, 46.7% (n = 365) were male, and 43.1% (n = 425) were female. The most prevalent age group of the participants was 25–34 years old (29.2%, n = 228). Half of the respondents had at least a bachelor's degree (49.9%, n=390). More than a third of the study population (41.7%, n = 326) identified as unemployed, while 30.3% (n = 237) were self-employed. The majority (54.0%, n = 422) of the participants described the environment they spend most of their time in as an environment where air quality is not a concern whereas 10.1% (n = 79) and 11.0% (n = 86) of the studied population were engaged in industrial and urban sectors, respectively. One-third of the respondents (36.1%, n = 282) had an average monthly household income of less than 100,000 KZT, while 37.2% (n = 291) of the participants reached the average wage of the Kazakhstani population (263,905 KZT in 2022) (Bureau of National Statistics, 2022).

4.13.2 Relationship between air quality perception and sociodemographics

The public perception of air quality in Astana (Table 4.20) was affected by participants' age, gender, education, employment status, the environment in which the

respondent spent most of their time, average monthly household income ($p < 0.001$), and health status (HBP ($p<.001$) and COPD ($p = 0.005$)).

Almost half of the respondents (42.1%, n = 329) classified the air quality as moderately polluted and causing no harm. Among the respondents in the 35–44 age

Table 4.19: General demographic characteristics of the respondents (n=782).

Demographic Characteristics	n	%	Demographic Characteristics	n	%
Age category			**Average monthly household income**		
18-24	59	7.60	<100,000 KZT	282	36.1
25-34	228	29.2	100,000-250,000 KZT	291	37.2
35-44	184	23.6	250,001-500,000 KZT	98	12.5
45-54	147	18.8	500,001-1,000,000 KZT	51	6.5
55-64	76	9.70	>1,000,000 KZT	60	7.7
65+	87	11.1	**Health status**		
Gender			High Blood Pressure		
Male	365	46.7	Yes	190	24.3
Female	415	53.1	No	591	75.7
Undefined	2	0.3	Cardiovascular conditions		
Education			Yes	21	2.7
Secondary school degree	8	1.0	No	760	97.3
High school degree	72	9.2	Diabetes		
Specialized secondary education	233	29.8	Yes	8	1.00
Bachelor's degree	390	49.9	No	773	99.0
Master's degree or above	79	10.1	Asthma		
Employment status			Yes	11	1.40
Full-time employment	106	13.6	No	770	98.6
Part-time employment	69	8.8	COPD		
Self-employed	237	30.3	Yes	12	1.50
Unemployed	326	41.7	No	769	98.5
Student	40	5.1			
Retired	4	0.5			
Environment					
Not a concern	422	54.0			
Industrial environment/concern	79	10.1			
Urban environment/concern	86	11.0			
Another environment/concern	22	2.8			
Not working	52	6.7			
Home environment	121	15.5			

category, half (52.7%, n = 97) considered the air quality in Astana moderately polluted, causing no detrimental effect to the general population. However, one-third of the respondents in the 45–54 and 55–64 age groups (34.3% (n = 50), and 30.3% (n = 23), respectively) classified the air quality as highly polluted.

Half of the female population (50.7%, n = 210) described the region as moderately polluted with no significant effect, while one-third (32.6%, n = 119) of male respondents shared a similar perception. Respondents with graduate degrees and full-time employment were more likely to consider the air quality level as moderately dangerous to human health (55.7%, n = 44; 49.5%, n = 52, respectively). The majority (69.6%, n = 55) of participants working in an industrial environment noted a high level of air pollution.

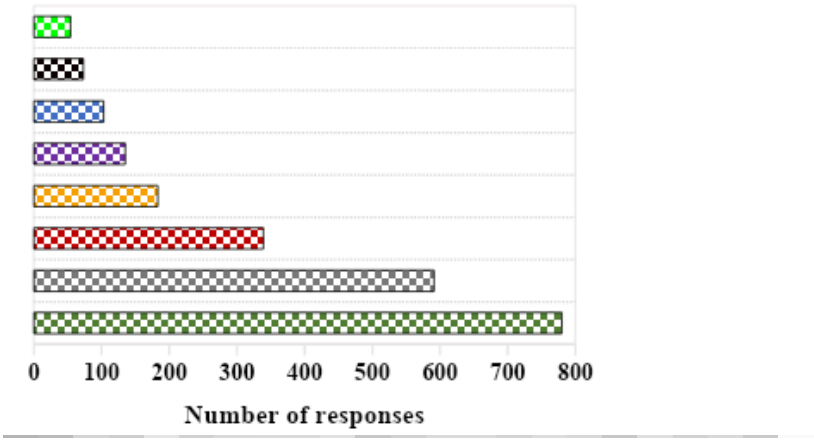

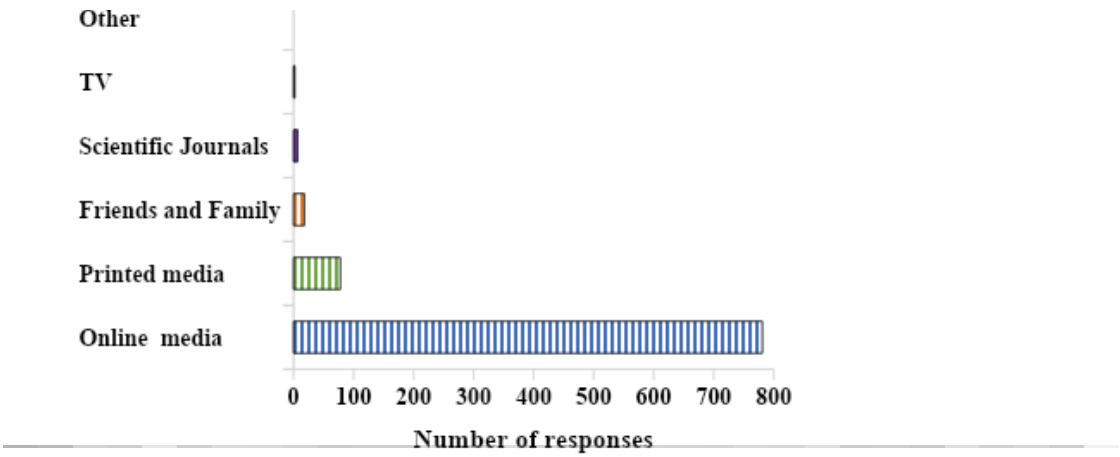

Table 4.20: Perception of air quality among respondents.

Demographic Characteristics	Highly polluted		Moderately polluted/cause harm		Moderately polluted/cause no harm		Not polluted at all		χ^2	p
	n	%	n	%	n	%	n	%		
Age category									73.5	< 0.001
18-24	10	17.0	22	37.3	21	35.6	6	10.2		
25-34	29	12.7	46	20.2	109	47.8	44	19.3		
35-44	39	21.2	27	14.7	97	52.7	21	11.4		
45-54	50	34.3	36	24.7	48	32.9	12	8.2		
55-64	23	30.3	16	21.1	29	38.2	8	10.5		
65+	13	14.9	36	41.4	25	28.7	13	14.9		
Gender									48.2	< 0.001
Male	105	28.9	100	27.4	119	32.6	41	11.2		
Female	59	14.3	82	19.81	210	50.7	63	15.2		
Undefined	0	0.00	2	100	0	0.00	0	0.00		
Education									219	< 0.001
Secondary school degree	1	12.5	1	12.5	5	62.5	1	12.5		
High school degree	7	9.72	4	5.56	19	26.4	42	58.3		
Specialized secondary education	69	29.7	39	16.8	86	37.1	38	16.4		
Bachelor's degree	74	19.0	96	24.6	199	51.0	21	5.38		
Master's degree or above	13	16.5	44	55.7	20	25.3	2	2.53		
Employment status									236	< 0.001
Full-time employment	15	14.3	52	49.5	31	29.5	7	6.67		
Part-time employment	8	11.6	4	5.80	16	23.2	41	59.4		
Self-employed	70	29.5	38	16.0	92	38.8	37	15.6		
Unemployed	65	19.9	67	20.6	177	54.3	17	5.21		
Student	4	10.0	21	52.5	13	32.5	2	5.00		
Retired	2	50.0	2	50.0	0	0.00	0	0.00		
Environment									191	< 0.001
Not a concern	66	15.6	75	17.8	201	47.6	80	19.0		
Industrial environment/concern	55	69.6	6	7.6	15	19.0	3	3.08		
Urban environment/concern	8	9.41	30	35.3	33	38.8	14	16.5		
Another environment/concern	4	18.2	11	50.0	5	22.7	2	9.09		

Not working	14	26.9	13	25.0	22	42.3	3	5.77		
Home environment	17	14.1	49	40.5	53	43.8	2	1.65		
Average monthly household income									68.1	< 0.001
<100,000 KZT	60	21.3	49	17.4	123	43.6	50	17.7		
100,000-250,000 KZT	62	21.3	57	19.6	139	47.8	33	11.3		
250,001-500,000 KZT	16	16.3	33	33.7	45	45.9	4	4.08		
500,001-1,000,000 KZT	16	31.4	14	27.5	9	17.6	12	23.5		
>1,000,000 KZT	10	17.0	31	52.5	13	22.0	5	8.47		
Health status										
High blood pressure									54.9	< 0.001
Yes	71	37.4	42	22.1	45	23.7	32	16.8		
No	93	15.7	142	24.0	284	48.1	72	12.2		
Cardiovascular conditions									0.63	0.89
Yes	5	23.8	6	28.56	8	38.1	2	9.52		
No	159	20.9	178	23.4	321	42.2	102	13.4		
Diabetes									2.16	0.54
Yes	1	12.5	2	25.0	5	62.5	0	0.00		
No	163	21.1	182	23.5	324	41.9	104	13.5		
Asthma									6.87	0.08
Yes	1	9.09	6	54.6	4	36.4	0	0.00		
No	163	21.2	178	23.1	325	42.2	104	13.5		
COPD									7.98	0.05
Yes	0	0.00	6	50.0	6	50.0	0	0.00		
No	164	21.3	178	23.2	323	42.0	104	13.5		
Total	164	21.0	184	23.6	329	42.1	104	13.3		

4.13.3 Respondents' knowledge of air pollution-related topics

Table 4.21 summarizes the relationship between participants' knowledge of air pollution-related topics (maximum score: 14.0) and demographics. Most participants consider industrial emissions, vehicle exhaust, and coal burning as the major sources of air pollution

(Figure 4.31). Furthermore, almost all respondents (99.9%) use online resources for air pollution-related information (Figure 4.32). The knowledge score was considerably low and varied significantly ($p < 0.001$) by age category, education, employment status, environment where respondents spend most of their time, and average monthly household income, it also varied by health status (asthma ($p = 0.002$), and COPD ($p = 0.05$)). A higher level of knowledge was noted among participants in the 18–24 age category (mean =6.75 ± 3.14, $p < 0.001$). Overall, participants who obtained a graduate degree demonstrated a higher level of knowledge of air pollution-related topics (mean = 6.44 ± 2.84, $p < 0.001$).

The students, participants who worked in urban environments, and those with higher economic status (i.e., average monthly household income > 1,000,000 KZT) showed a higher level of knowledge compared to the rest of the population (Table 4.21). Notably, participants diagnosed with asthma had the highest average knowledge score (mean = 7.20 ± 3.84, $p = 0.002$).

Table 4.21: Level of knowledge of air pollution among respondents.

Demographic Characteristics	**Level of knowledge of air pollution**	
	Mean	
Age category		
18-24	6.75±3.14	
25-34	4.32±2.93	*df*=5
35-44	3.84±2.80	p<0.001
45-54	4.31±2.73	
55-64	4.79±2.87	
65+	4.67±2.20	
Gender		
Male	4.70±2.78	*df*=2
Female	4.27±2.97	p=0.119
Undefined	4.70±1.27	

Education		
Secondary school degree	4.93±3.44	
High school degree	5.77±2.82	*df*=4
Specialized secondary education	4.31±2.53	p<0.001
Bachelor's degree	3.92±2.85	
Master's degree or above	6.44±2.84	
Employment status		
Full-time employment	6.07±2.78	
Part-time employment	5.52±2.71	*df*=5
Self-employed	4.32±2.54	p<0.001
Unemployed	3.48±2.67	
Student	7.31±2.88	
Retired	6.35±2.00	
Environment		
Not a concern	4.07±2.80	
Industrial environment/concern	4.21±2.56	*df*=5
Urban environment/concern	6.33±3.13	p<0.001
Another environment/concern	6.24±3.13	
Not working	4.37±3.01	
Home environment	4.49±2.52	
Average monthly household income		
<100,000 KZT	3.58±2.23	
100,000-250,000 KZT	4.34±3.03	*df*=4
250,001-500,000 KZT	5.30±2.98	p<0.001
500,001-1,000,000 KZT	6.16±2.77	
>1,000,000 KZT	6.54±2.84	
Health status		
High blood pressure		
Yes	4.19±2.72	*df*=1
No	4.56±2.92	p<0.128
Cardiovascular conditions		
Yes	4.33±2.01	*df*=1
No	4.48±2.90	p=0.234
Diabetes		
Yes	3.53±2.59	*df*=1

	No	4.48±2.88	p=0.351
Asthma			
	Yes	7.20±3.84	*df*=1
	No	4.43±2.85	p=0.002
COPD			
	Yes	6.10±3.45	*df*=1
	No	4.45±2.87	p=0.05

The bivariate analysis further supported the impact of participants' knowledge on their environmental attitudes and perceptions. Similar to the present study, Hou et al. (2021) found a moderate level of ambient air pollution health literacy among the respondents, and they observed an association between literacy level and specific covariates such as education, living arrangement, marital status, and area of residence. However, Odonkor and Mahami. (2020), which assessed knowledge, attitudes, and perception of air pollution in Accra, Ghana, revealed that a low level of education and elderly age were associated with lower literacy regarding air pollution and related health effects. The highest level of environmental knowledge was evident for participants with a graduate degree, which suggests that formal education is a leading factor in promoting environmental awareness. However, within the context of Kazakhstan, despite 51.7% of the employed population having a bachelor's degree (Bureau of National Statistics, 2022), the prevailing majority still demonstrates a low level of environmental literacy.

Interestingly, some countries (e.g., Germany, Sweden) (Grund & Brock, 2022) with reported lower percentages of bachelor graduates show higher levels of public awareness of environmental issues. Moreover, in China, for instance, where tertiary education is acquired by only 10% of the population between the ages of 25 and 64 (OECD, 2023), environmental education is a requirement for elementary and secondary school levels (Wu, 2012). Moreover, a study by Clayton et al., 2018 which assessed the level of knowledge and environmental attitude

among 1,433 Chinese students and adults, revealed a moderate level of knowledge (14.3 and 15.1 points out of 22 for adults and university students, respectively) and high intention for pro-environmental behavior. This implies the existence of additional confounding variables influencing environmental literacy, in addition to institutional knowledge.

4.13.4. Attitude toward environmental protection and Willingness to Pay (WTP)

Most participants were largely in agreement with the statements regarding environmental protection, (mean score > 3.00 (neutral response)) (Figure 4.33). Almost 30% of the respondents prioritized environmental protection over economic growth. The strongest agreement was noted for statements about the importance of environmental literacy (mean = 3.34) ("Educating younger generations about the knowledge of environmental protection is important.") and general attitude towards environmental protection (mean = 3.30) ("Taking care of the environment is something I really care about.").

Opinions against environmental protection were mostly neutral or supportive (mean > 3.20). Almost 42% of the study population supported the statement "The economic growth of Kazakhstan is currently more important than environmental protection." Almost half of the respondents (43.2%) were skeptical about the individual actions that can be taken to improve air quality ("Nothing can be done by me or my family or friends to improve the atmospheric situation."). Moreover, one-third of the participants expressed a lack of motivation towards individual actions unless the initiative is supported in the community ("There is no point in doing what I can for the environment unless everyone does the same.").

Most respondents either demonstrated a WTP for environmental protection or remained neutral in their WTP statements (Figure 4.33). Half of the respondents (51.4%) supported the idea of governmental intervention for environmental protection without self-involvement (mean

= 3.4) (“Kazakhstan’s government has to reduce atmospheric pollution, but it should not incur any costs to me.”), only 32.0% of the surveyed population expressed their WTP extra taxes for enhancing air quality (mean = 2.96) (“I do not object to a tax increase if the additional funds are utilized to prevent further atmospheric pollution.”). Furthermore, 36.0% of participants expressed their preparedness to accept a reduction in their standard of living to protect the environment.

A low level of environmental knowledge can explain the current perception of air quality among Astana residents. In general, the respondents do not consider the current local air quality as a threat to public health. It should be noted that Astana and Almaty (the second major city in the country) were ranked as the most polluted cities in Kazakhstan according to API, with substantial regional variation in airborne pollutants concentration (Kerimray et al., 2018). A collaborative effort between the World Bank and the Ministry of Environment and Water

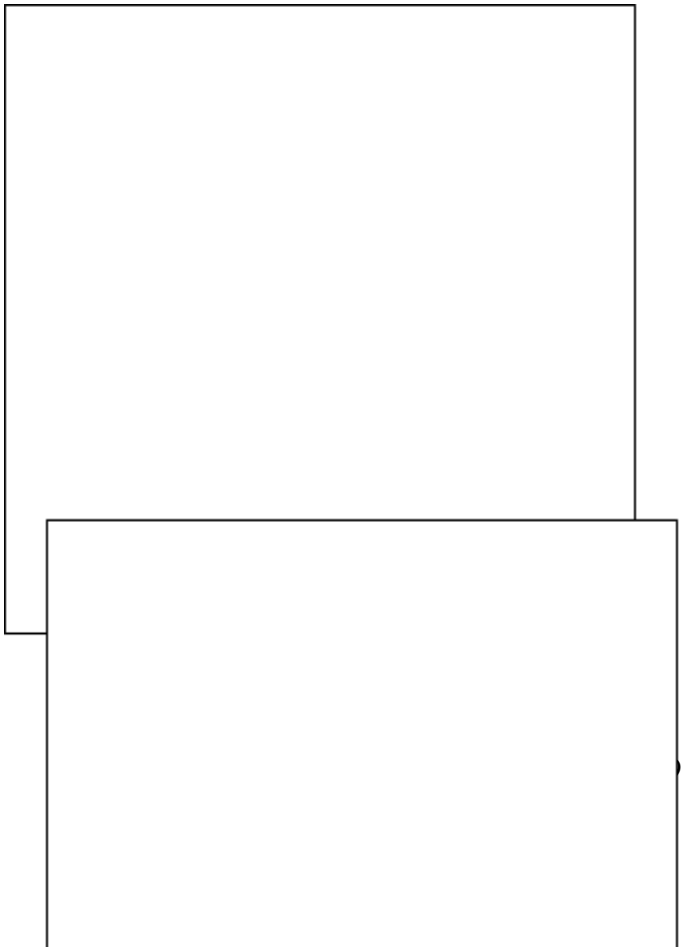

Resources of Kazakhstan also states concentrations of airborne pollutants such as PM_{10}, NO_2, and SO_2 exceeding the European Union air quality guidelines in ten Kazakhstani cities (The World Bank, 2021).

The increased activity of CHPPs and domestic coal combustion during winter months substantially contribute to serious degradation of air quality due to the increased demand for heating during extreme cold episodes. The annual coal consumption of CHPPs in Astana is estimated at 3.2 million tons. On top of this, according to data from a 2018 household survey, two-thirds of Kazakhstani households still use solid fuels such as coal, biomass, and wood for heating (The World Bank, 2021).

4.13.5 SEqM validity check

The hypothetical model was first subjected to a validity check using partial least squares analysis, after which the hypotheses set could be confirmed/rejected via bootstrapping. Starting with a convergent validity check (Table 4.22) and outer loadings checks, most values exceed the acceptable limit of 0.7 including WP2 whereas several others were smaller than that value (P5, P3, P7, and KoAPI1). This states that KoAPI1 is weak in representing the "Knowledge" construct. Values for P5, P3, and P7 were within the acceptable limits (between 0.4 and 0.7) and their removal does not increase composite reliability (Hair et al., 2018). The values at the lower range could be attributed to the question wording and to the understanding of the respondents which may be subjective.

Table 4.23 represents the reliability and validity checks of the constructs. The institutional knowledge construct is the least reliable (Cronbach's alpha, Dillon-Goldstein's rho, and composite reliability are lower than the acceptable limit), which may be attributed to the limited number of questions.

Table 4.24 demonstrates the values for discriminant validity which indicates the differences between the constructs. All the values are distinct and discriminant. Table 4.25

Table 4.22: Convergent validity.

Variable	Outer loading	Variable	Outer loading
P1	0.447	EA4	0.726
P2	0.462	P4	0.622
WP1	0.872	P5	0.675
WP2	0.772	EA5	0.824
P3	0.468	EA6	0.752
EA1	0.769	P6	0.544
WP3	0.683	P7	0.707
KoI1	0.134	KoI2	0.996
EA2	0.791	KoLAQ 2	0.765
AM3	0.836	KoLAQ 1	0.807

Table 4.23: Construct reliability and validity.

	Cronbach's Alpha	rho_ A	Composite Reliability	Average Variance Extracted (AVE)
Environmental attitude	0.875	0.878	0.905	0.615
Institutional knowledge	0.090	0.534	0.563	0.505
Knowledge of local air quality	0.381	0.383	0.763	0.618
Perception of national air pollution and economy	0.670	0.693	0.765	0.324
WTP	0.684	0.750	0.822	0.608

represents the hypothesis test check using bootstrapping, showing that all four hypotheses are supported.

Table 4.24: Discriminant validity of constructs.

	Environmental attitude	Institutional knowledge	Knowledge of national air pollution	Perception of national air pollution and economy	WTP
Environmental attitude	0.78				
Institutional knowledge	-0.02	0.71			
Knowledge of national air pollution	0.27	0.35	0.79		
Perception of national air pollution and economy	0.22	0.71	0.82	0.57	
WTP	0.53	0.03	0.26	0.23	0.78

Table 4.25: Hypothesis test results.

	Original Sample (O)	Sample Mean (M)	Standard Deviation (STDEV)	t statistics (|O/STDEV|)	p-value
Environmental attitude □ Perception of national air pollution and economy	0.06	0.06	0.02	3.85	<0.001
Institutional knowledge □ Perception of national air pollution and economy	0.49	0.49	0.03	19.76	<0.001
Knowledge of local air quality □ Perception of national air pollution and economy	0.63	0.63	0.03	25.46	<0.001
WTP □ Environmental attitude	0.53	0.54	0.03	18.92	<0.001

Table 4.26 shows that the effect of *Knowledge of local air quality* on the *perception of national air pollution and the economy* is the strongest (i.e., with the largest path value: 0.626). The effects of *Institutional knowledge* on the *Perception of national air pollution and economy* and

Table 4.26: Path coefficient values.

Path	Coefficient
Environmental attitude □ perception of national air pollution and economy	0.063
Institutional knowledge □ Perception of national air pollution and economy	0.492
Knowledge of local air quality □ perception of national air pollution and economy	0.626
WTP □ Environmental attitude	0.533

WTP on *Environmental attitude* are also strong (0.492 and 0.533, respectively). Interestingly, the effect of Environmental attitude on the perception of national air pollution and the economy is minimal.

The results of the SEM analysis further highlight the significance of local air quality knowledge and its effect on the public perception of national air pollution and the economy. This resonates with other studies where knowledge and education are prime factors in improving environmental attitudes (Sudarmadi et al., 2001; Meinhold & Malkus, 2005). It suggests that increasing environmental literacy among the general public should be considered a priority to promote pro-environmental behavior. In addition, since almost all respondents use online resources for air pollution-related information, it is crucial to disseminate knowledge of air pollution and related health effects through easily accessible means to benefit a population with varying socioeconomic backgrounds (Finn & Fallon, 2017). One possible way to spread environmental knowledge is through online platforms (e.g., social media) that have expanded in recent years. Yang & Wu (2019) investigated the effect of using social media for health-related information and its correlation with protective behavior during episodes of high air pollution in China. Results revealed that using social media for health-related information predicted the users' attitude towards protective behavior (e.g., wearing dust masks during haze episodes).

Pro-environmental behavior can also be effectively promoted by considering individual intentions (Bamberg & Möser, 2007). The intention for individual actions is associated with personal self-consciousness and self-identity (Huang et al., 2020). Studies also indicate that individuals who perceive themselves as environmentalists are more likely to act (Tabernero et al., 2015; Carfora et al., 2017). Moreover, a perceived lack of control over environmental issues

affects the willingness to take individual actions and pay for environmental protection, in a form of environmental taxes and prices for higher-quality gasoline (Vicente et al., 2021).

There is a common belief that developing countries are less concerned with environmental protection because their focus is driven by survival and material concerns. However, emerging evidence also suggests no association between national income and WTP for environmental protection. Some studies indeed speculate that due to presumably higher pollution levels, environmental protection is a greater concern for developing countries (Dunlap & York, 2016; Shao et al., 2018). In the present research, SEM analysis revealed a relationship between WTP for environmental protection and environmental attitude, indicating that respondents' readiness to spend money on environmental protection shapes their attitude toward environmental issues and gives them a sense of control over their own actions. These findings support the importance of a perceived lack of control over environmental issues and its association with behavior intentions and attitudes toward pro-environmental behavior. In the bivariate analysis, the majority of the respondents expressed either WTP for environmental protection or remained neutral in their WTP statements, which further supports the results of the SEM analysis.

One form of payment for environmental preservation is environmental taxation. New environmental regulations introduced penalties and fees to minimize noncompliance with emission standards in Kazakhstan. However, the emission limit values (ELVs) established for industrial plants in Kazakhstan are higher than those recommended by international guidelines (e.g., the EU Industrial Emissions Directive) (Assanov et al., 2021). Moreover, environmental sanctions are more directed toward government budget revenue rather than toward environmental protection (Abakhanov, 2020). However, in 2021, Kazakhstan adopted its Environmental Code that established the payment for negative environmental impact (NEI),

which is subjected to a gradual increase every three years for large corporations. The estimation of NEI for stationary sources is set based on the emission concentrations. The base pollution tax for the emissions within ELVs also depends on the monthly calculation index (MCI) and tax coefficient per ton of pollutant. Stationary sources with emissions higher than ELVs are subjected to administrative penalties and environmental damage payments (The World Bank, 2021). Almost 40% of the respondents support paying more for higher quality fuel if it improves air quality ("I do not mind paying more money to use better quality gasoline, which leads to less pollution."). For mobile sources (e.g., passenger vehicles), the pollution tax is based on the engine size and type of fuel (e.g., unleaded gasoline, diesel fuels, compressed gas) with different rates for summer (June-October) and winter (November-May) periods (The World Bank, 2021).

4.14 Chapter summary

This chapter presents the major findings of the current dissertation. The first part focuses on the effects of method modification for *in vitro* lung bioaccessibility. The second part consists of the characterization of PM collected in Astana, Kazakhstan, including toxicity assessment of PM via *in vitro* lung bioaccessibility and inhalation risk assessment, PM morphology, and source identification. The third part of the current research describes precipitation chemistry and its role in air quality. The third part contains findings on source identification via CBPF. The fifth part compares MLR and RF approaches for $PM_{2.5}$ prediction modeling. Lastly, the sixth part focuses on the identification of major determinants of the perception and attitude of the general public on air pollution. The major findings of this chapter are the following:

- The modification of GS with 0.25% cholesterol and 5% DPPC and a combination of both in a higher concentration increases both bioaccessibility (e.g., Cr in SRM 2691 and V in BGS 102) and the bioaccessible concentration (e.g., Cu in SRM 269) of selected PTEs.
- A 1/500 S/L ratio yielded a higher elemental bioaccessibility of both reference materials in ALF (e.g., up to 94.8% for Pb in BGS 102), however, the use of a higher particle load (e.g., 1/100 S/L ratio) might be a more accurate simulation of inhalation exposure.
- The increase in solubility of selected PTEs after 4-week extraction indicates that a longer test duration may be necessary for routine measurement of metal dissolution in SLFs.
- A higher agitation speed, though resulted in higher bioaccessibility measurement, should be supported by *in vivo* validation.
- The mean $PM_{2.5}$ and $PM_{2.5\text{-}10}$ concentrations in PM samples were 28.7 $\mu g \cdot m^{-3}$ (max: 534 $\mu g \cdot m^{-3}$) and 226 $\mu g \cdot m^{-3}$ (maximum: 1,564 $\mu g \cdot m^{-3}$), respectively, drastically exceeding WHO guidelines.
- SEM analysis revealed several distinct PM groups (e.g., bioaerosols, CFA, natural and construction dust, and soot). The $PM_{2.5}$ and $PM_{2.5\text{-}10}$ collected in summer period composed of ND (48.2%), construction dust (32.5%), CFA (14.5%), vehicular PM (1.8%), and biological-origin PM (3%), while PM collected in winter contained construction dust, CFA, ND, and road dust/car exhaust particles at 32.5%, 31.6%, 31.1%, and 4.9%, respectively.
- The inhalation HRA via bioaccessible pollutant concentration revealed no carcinogenic/non-carcinogenic risk for the exposed population.
- Chemical analysis of PM and snow and rain samples revealed potential common sources including vehicular exhaust, coal, and liquid fuel combustion.

- The CBPF plots depicting $PM_{2.5}$ concentrations at the 75th (>29.3 μg/m3) and 95th percentile (>87.1 $\mu g/m^3$) indicated the influence of both coal-heated power plant activities (CHPP-2) and residential heating on city air pollution.
- The CBPF analysis for the 75th percentile (>1 μg/m3) of SO_2 concentration suggested an unidentified pollution source in the southwestern part of Astana and revealed a combined contribution from vehicular emissions and the influence of CHPPs.
- The RF-based $PM_{2.5}$ prediction model outperformed MLR, showing better adaptability to nonlinear data and higher sensitivity to seasonal variations.
- Both models identified PM_{10} and CO concentrations as crucial predictors for $PM_{2.5}$ concentrations.
- DALY for 2019 was high ranging from 2,160 to 7,531 years.
- SEqM suggests that knowledge is the key factor in enhancing awareness and perception of national air pollution levels.
- Respondents with low environmental literacy classified Astana as a moderately polluted region with no association with adverse health outcomes (i.e., perception underestimating the reality), while those engaged in industrial work considered it a highly polluted area associated with health hazards.
- A moderate agreement was observed among the population groups with the statements for environmental protection and WTP statements.

CHAPTER 5: CONCLUSIONS

This thesis offers a thorough examination of air quality in Astana, Kazakhstan, encompassing a detailed analysis of spatial and temporal variations in PM and gaseous pollutants. This chapter focuses on key findings, limitations, and recommendations for future research.

The analysis of pollutant concentrations in Astana, Kazakhstan (based on primary data and concentration data obtained from governmental agencies) revealed a high concentration of PM

(e.g., TSP, PM_{10}, $PM_{2.5-10}$, $PM_{2.5}$) and gaseous pollutants (e.g., SO_2, CO, NO_2, NO, and HF). The annual concentrations of ambient pollutants, in general, drastically exceeded annual and 24-hour WHO air quality guidelines as well as national air quality standards in 2018-2023. For example, the annual mean concentrations of $PM_{2.5}$ in the period of 2018-2019 and 2019-2020 were 29.7 $\mu g/m^3$ and 16.5 $\mu g/m^3$, respectively. In 2018-2020 the concentration of CO ranged from 600 to 2,800 $\mu g/m^3$, while in 2019-2020 the SO_2 concentration range was 7.70-1,114 $\mu g/m^3$. The mean 24-hour of $PM_{2.5}$ and $PM_{2.5-10}$ concentrations in PM samples collected in 2021-2023 were 28.7 $\mu g \cdot m^{-3}$ (max: 534 $\mu g \cdot m^{-3}$) and 226 $\mu g \cdot m^{-3}$ (maximum: 1,564 $\mu g \cdot m^{-3}$), respectively. This research work presented modifications for the *in vitro* lung bioaccessibility protocol of selected PTEs (Cd, Co, Cr, Cu, Mn, Ni, Pb, Sb, V, and Zn) suggesting seven distinct formulations of GS (containing DPPC and cholesterol in different proportions) and one ALF, as well as variations of physiological parameters such as S/L ratio, extraction time, and agitation. The modification of GS with 0.25% cholesterol and 5% DPPC can enhance the bioaccessibility and bioaccessible concentration of selected PTEs. The use of DPPC and cholesterol is recommended for evaluating pulmonary bioaccessibility. A lower S/L ratio. (e.g., 1/500) increased bioaccessibility in ALF, especially for Pb in BGS 102, but a higher particle load (1/100 S/L ratio) may better simulate inhalation exposure. Extended testing durations may be needed for routine metal dissolution measurements in SLFs, while higher agitation speeds increase bioaccessibility measurements. The application of the same parameters to inhalation bioaccessibility testing of selected PTEs (Cd, Co, Cr, Cu, Fe, Mn, Ni, Pb, V, and Zn) in $PM_{2.5}$ collected in Astana revealed, in general, high bioaccessible concentration of PTEs in ALF (e.g., for Fe (mean: 16,229 mg/kg, range: (906-30,419 mg/kg) and for V (mean: 10,725 mg/kg, range: (687-27,092 mg/kg)). However, HHRA suggested acceptable carcinogenic and non-carcinogenic risks. Morphological

characterization via SEM, CBPF analysis, and chemical speciation of PM and precipitation revealed cumulative contribution from coal combustion (CHPPs and residential heating), as well as vehicular emissions on the local air quality. Distinct particle groups observed during SEM analysis included bioaerosols, coal fly ash (CFA), dust (natural or construction), and soot particles. Physical features of PM particles (e.g., particle, size, shape, internal microstructures, stiffness, surface area) contribute to their biological toxicity, and therefore are one of the major factors determining the carcinogenic and non-carcinogenic risk due to PM exposure. Additionally, the DALY analysis revealed 2,160 to 7,531 years lost due to air pollution for the general population, which further underscores the PM-related adverse health impact. KAP analysis revealed the major issue of low awareness about air pollution-related topics among the general population that does not consider air quality in Astana of low quality.

To successfully implement air pollution mitigation interventions and provide continuous education to the local population regarding air quality and associated health effects, it is crucial to prioritize increasing public environmental literacy via online channels (e.g., social media) as online resources are among the most common sources of information. The current research work underscores the necessity for a more comprehensive and accessible air pollution monitoring system for an accurate assessment of air quality. Although immediate measures for air pollution mitigation are of utmost importance, their feasibility in the near future may be limited. The most effective strategy for the current time might be increasing environmental literacy among the residents of Astana, allowing public perception to influence governmental decisions regarding air pollution-related regulations. The comprehensive analysis of Astana air quality suggests that urban air quality exhibited significant deterioration in recent years, potentially contributing to elevated adverse health outcomes.

5.1 Limitations of the current research

Unlike other reference materials, such as NIST 1648a (urban atmospheric PM) and BCR 038 (coal fly ash), SRM 2691 and BGS 102 utilized in the present study are not commonly used in environmental studies for the routine quality control assessment of total metal concentrations. Moreover, the particle size fractions of SRM 2691 and BGS 102 used for *in vitro* bioaccessibility experiments are not typical size fractions used in environmental research.

Moreover, the lack of comparison of the bioaccessible concentration of PTEs in PM collected in Astana, Kazakhstan, with other SLFs (e.g., GS) is another limitation of the present research. Comparison of the solubility of PTEs in different physiological fluids is imperative when studying the bioavailability of PTEs in different parts of the respiratory system. However, due to the study's instrumental setup and the necessity to avoid cone contamination of ICP-MS, conducting experimental procedures using GS was not feasible. Thirdly, small amounts of accumulated PM as well as general inhomogeneity of PM deposition on filters dictated the need to consume entire filters by bioaccessibility analyses, making quantification of the total PTEs concentration and, subsequently, estimation of bioaccessible fraction (%) impossible.

The FE-SEM was not equipped with detectors for estimating particles' elemental composition, thus making it impossible to investigate particle chemistry, which may have improved PM classification. In addition, the use of PTFE filters is excellent for acid digestion but less practical for SEM compared to other options (e.g., glass or quartz filters), as the fibrous structure of the filter can affect the focus plane.

The accuracy of DALY calculation for HHRA in Kazakhstan is limited by a lack of specific population data, and incorporating recent Kazakhstani data would be essential for

calculation accuracy. The current HRA, however, focuses on chronic $PM_{2.5}$ exposures, lacking short-term effects evaluation, and not considering other pollutants such as O_3, NO_x, and other PM fractions, which would provide a more comprehensive understanding of health risks.

5.2 Recommendations for future work

Future air quality analysis should include data from a more diverse air pollution monitoring system that covers a more extensive study area. Moreover, the secondary data provided by governmental agencies and utilized for scientific investigation should be compared with data from other available organizations with monitoring stations in Astana (e.g., AirKaz). The public availability of air pollution data in Kazakhstan remains one of the major challenges of air quality research. Future research should also focus on the comparison of bioaccessible fractions and bioaccessible concentrations of PTEs in PM (collected in the study area) in various physiological fluids (not limited to ALF). Lack of data on total elemental concentration in PM also hindered studying the correlation between PM-bound PTEs and precipitation chemistry.

BIBLIOGRAPHY

Abakhanov, E. (2020). New Environmental Code of Kazakhstan: Expectations and Prospects. *Central Asian Bureau for Analytical Reporting*. https://cabar.asia/en/new-environmental-code-of-kazakhstan-expectations-and-prospects.

Adamiec, E., Jarosz-Krzemińska, E., & Wieszała, R. (2016). Heavy metals from non-exhaust vehicle emissions in urban and Motorway Road dust. *Environmental Monitoring and Assessment*, *188*(6). https://doi.org/10.1007/s10661-016-5377-1.

Agarwal, A., Satsangi, A., Lakhani, A., & Kumari, K. (2020). Seasonal and spatial variability of secondary inorganic aerosols in $PM_{2.5}$ at Agra: Source apportionment through receptor models. *Chemosphere*, *242*. https://doi.org/10.1016/j.chemosphere.2019.125132.

Agibayeva, A., Guney, M., Karaca, F., Kumisbek, A., Kim, J., & Avcu, E. (2022). Analytical Methods for Physicochemical Characterization and Toxicity Assessment of Atmospheric Particulate Matter: A Review. *Sustainability*, *14*, 13481. https://doi.org/10.3390/su142013481.

Ahmady-Birgani, H., Mirnejad, H., Feiznia, S., & McQueen, K. (2015). Mineralogy and geochemistry of atmospheric particulates in western Iran. *Atmospheric Environment*, *119*, 262–272. https://doi.org/10.1016/j.atmosenv.2015.08.021.

Akhbarizadeh, R., Dobaradaran, S., Amouei Torkmahalleh, M., Saeedi, R., Aibaghi, R., & Faraji Ghasemi, F. (2021). Suspended fine particulate matter ($PM_{2.5}$), microplastics (MPs), and polycyclic aromatic hydrocarbons (PAHs) in air: Their possible relationships and health implications. *Environmental Research*, *192*. https://doi.org/10.1016/j.envres.2020.110339.

Akhtar, U., Scott, J., Chu, A., & Evans, G. (2011). In vivo and in vitro assessment of particulate matter toxicology. *Environmental Science and Engineering (Subseries: Environmental Science)*, *9783642122774*, 427–449. https://doi.org/10.1007/978-3-642-12278-1_22.

Alves, D., Riegel, R., Klauck, C., Ceratti, A., Hansen, J., Cansi, L., Pozza, S., de Quevedo, D., & Osório, D. (2020). Source apportionment of metallic elements in urban atmospheric particulate matter and assessment of its water-soluble fraction toxicity. *Environmental Science and Pollution Research*, *27*(11), 12202–12214. https://doi.org/10.1007/s11356-020-07791-8.

American Lung Society. (2020). Carbon Monoxide. https://www.lung.org/clean-air/at-home/indoor-air-pollutants/carbon-monoxide.

Ansoborlo, E., Chalabreysse, J., Escallon, S., & Hengé-Napoli, M. (1990). *In vitro* solubility of uranium tetrafluoride with oxidizing medium compared with *in vivo* solubility in rats. *International Journal of Radiation Biology, 58*(4), 681–689. 10.1080/09553009014552031.

Arhami, M., Hosseini, V., Zare Shahne, M., Bigdeli, M., Lai, A., & Schauer, J. (2017). Seasonal trends, chemical speciation, and source apportionment of fine PM in Tehran. *Atmospheric Environment*, *153*, 70–82. https://doi.org/10.1016/j.atmosenv.2016.12.046.

Ari, P., Ari, A., Dumanoğlu, Y., Odabasi, M., & Gaga, E. (2020). Organic chemical characterization of size-segregated particulate matter samples collected from a thermal power plant area. *Environmental Pollution*, *262*. https://doi.org/10.1016/j.envpol.2020.114360.

Askariyeh, M., Zietsman, J., & Autenrieth, R. (2020). Traffic contribution to $PM_{2.5}$ increment in the near-road environment. *Atmospheric Environment*, *224*. https://doi.org/10.1016/j.atmosenv.2019.117113.

Assanov, D., Zapasnyi, V., & Kerimray, A. (2021). Air quality and industrial emissions in the cities of Kazakhstan. *Atmosphere*, *12*(3), 314. https://doi.org/10.3390/atmos12030314.

Atkinson, R.W., Butland B., Anderson R., & Maynard R. (2018). Long-term concentrations of nitrogen dioxide and mortality: a meta-analysis of cohort studies. *Epidemiology, 29*(4), 460–472. DOI: 10.1097/EDE.0000000000000847

Atzei, Davide, Fantauzzi, M., Rossi, A., Fermo, P., Piazzalunga, A., Valli, G., & Vecchi, R. (2014). Surface chemical characterization of PM_{10} samples by XPS. *Applied Surface Science*, *307*, 120–128. https://doi.org/10.1016/j.apsusc.2014.03.178

Ault, A., Peters, T., Sawvel, E., Casuccio, G., Willis, R., Norris, G., & Grassian, V. (2012). Single-particle SEM-EDX analysis of iron-containing coarse particulate matter in an urban environment: Sources and distribution of iron within Cleveland, Ohio. *Environmental Science and Technology*, *46*(8), 4331–4339. https://doi.org/10.1021/es204006k.

Azhigaliyev, M. (2019). *CHP was accused of the release of toxic substances in the capital*. Tengrinews. Retrieved September 24, 2021, from https://tengrinews.kz/kazakhstan_news/tets-obvinili-v-vyibrose-toksichnyih-veschestv-v-stolitse-377342/.

Aztatzi-Aguilar, O., Valdés-Arzate, A., Debray-García, Y., Calderón-Aranda, E., Uribe-Ramirez, M., Acosta-Saavedra, L., Gonsebatt, M., Maciel-Ruiz, J., Petrosyan, P., Mugica-Alvarez, V., Gutiérrez-Ruiz, M., Gómez-Quiroz, L., Osornio-Vargas, A., Froines, J., Kleinman, M., & De Vizcaya-Ruiz, A. (2018). Exposure to ambient particulate matter induces oxidative stress in lung and aorta in a size- and time-dependent manner in rats. *Toxicology Research and Application*, *2*, 239784731879485. https://doi.org/10.1177/2397847318794859.

Bakand, S., Hayes, A., & Dechsakulthorn, F. (2012). Nanoparticles: A review of particle toxicology following inhalation exposure. Inhal. Toxicol. 24, 125–135. DOI: 10.3109/08958378.2010.642021

Baimatova, N., Derbissalin, M., Kabulov, A., & Kenessov, B. (2016). Adsorption of benzene, toluene, ethylbenzene and O-xylene by carbon-based adsorbents. *Eurasian Chemico-Technological Journal*, *18*(2), 123. https://doi.org/10.18321/ectj433

Bamberg, S., & Möser, G. (2007). Twenty years after Hines, Hungerford, and Tomera: A new meta-analysis of Psycho-Social Determinants of pro-environmental behaviour. *Journal of Environmental Psychology*, *27*(1), 14–25. https://doi.org/10.1016/j.jenvp.2006.12.002.

Bathmanabhan, S., Nagendra, S., & Madanayak, S. (2010). Analysis and interpretation of particulate matter – PM_{10}, $PM_{2.5}$ and PM_1 emissions from the heterogeneous traffic near an urban roadway. *Atmospheric Pollution Research*, *1*(3), 184–194. https://doi.org/10.5094/apr.2010.024.

Beisenova, R., Zhumashev, B., Tazitdinova , R., Rakhymzhan , Z., Tulegenova, S., & Zhaznayeva , Z. (2023). Assessment and forecast of atmospheric air quality at the regional level. example of central Kazakhstan. *Journal of Environmental Management and Tourism*, *14*(7), 2904. https://doi.org/10.14505/jemt.v14.7(71).08 .

Bekkar, A., Hssina, B., Douzi, S., & Douzi, K. (2021). Air-pollution prediction in smart city, deep learning approach. *J. Big Data*, *8*, 161. https://doi.org/10.1186/s40537-021-00548-1.

Bensch, K., Braun, U., Groenewald, J., & Crous, P. (2012). The genus Cladosporium. *Studies in Mycology*, 72, 1–401. https://doi.org/10.3114/sim0003.

Bernhard, W. (2016). Lung surfactant: Function and composition in the context of development and respiratory physiology. *Annals of Anatomy, 208*, 146–150. https://doi.org/10.1016/j.aanat.2016.08.003.

Boisa, N., Elom, N., Dean, J., Deary, M., Bird, G., & Entwistle, J. (2014). Development and application of an inhalation bioaccessibility method (IBM) for lead in the PM_{10} size fraction of soil. *Environment International*, *70*, 132–142. https://doi.org/10.1016/j.envint.2014.05.021.

Bol, O., Koyuncu, S. & Günay, N. (2018). Prevalence of hidden carbon monoxide poisoning in auto service workers; a prospective cohort study. *Journal of Occupational Medical Toxicology, 13*(35). https://doi.org/10.1186/s12995-018-0214-9.

Bontempi, E., Benedetti, D., Zacco, A., Pantos, E., Boniotti, S., Saletti, C., Apostoli, P., & Depero, L. E. (2008). Analysis of crystalline phases in airborne particulate matter by two-dimensional X-ray diffraction (XRD2). Journal of Environmental Monitoring, 10, 82–88. DOI: 10.1039/B715517D

Briz-Redón, Á., Belenguer-Sapiña, C., & Serrano-Aroca, Á. (2021). Changes in air pollution during COVID-19 lockdown in Spain: A multi-city study. *Journal of Environmental Sciences*, *101*, 16–26. https://doi.org/10.1016/j.jes.2020.07.029.

Brown, P., Jones, T., & BéruBé, K. (2011). The internal microstructure and fibrous mineralogy of fly ash from coal-burning power stations. *Environmental Pollution*, *159*(12), 3324–3333. https://doi.org/10.1016/j.envpol.2011.08.041.

Bureau of National Statistics of the Agency for Strategic Planning and Reforms of the Republic of Kazakhstan. Yearbook on Demographics of the Republic of Kazakhstan. (2021). Available online: https://stat.gov.kz/ (accessed on 20 August 2022).

Cáceres, L., Paz, M.L., Garcés, M., Calabró, V., Magnani, N.D., Martinefski, M., Martino Adami, P.V., Caltana, L., Tasat, D., & Morelli, L., et al. (2020). NADPH oxidase and mitochondria are relevant sources of superoxide anion in the oxinflammatory response of macrophages exposed to airborne particulate matter. Ecotoxicol. Environ. Saf. 205, 111186. doi: 10.1016/j.ecoenv.2020.111186

Canepari, S., Perrino, C., Astolfi, M.L., Catrambone, M., & Perret, D. (2009). Determination of soluble ions and elements in ambient air suspended particulate matter: Inter-technique comparison of XRF, IC and ICP for sample-by-sample quality control. Talanta, 77, 1821–1829. https://doi.org/10.1016/j.talanta.2008.10.029

Carfora, V., Caso, D., Sparks, P., & Conner, M. (2017). Moderating effects of pro-environmental self-identity on pro-environmental intentions and behavior: A multi-behavior study. *Journal of Environmental Psychology*, *53*, 92–99. https://doi.org/10.1016/j.jenvp.2017.07.001.

Carlsen, L., Bruggemann, R., & Kenessov, B. (2018). Use of partial order in environmental pollution studies demonstrated by Urban BTEX air pollution in 20 major cities worldwide. *Science of The Total Environment*, *610–611*, 234–243. https://doi.org/10.1016/j.scitotenv.2017.08.029

Carslaw, D., & Beevers, S. (2013). Characterizing and understanding emission sources using bivariate polar plots and K-means clustering. *Environmental Modelling & Software*, *40*, 325–329. https://doi.org/10.1016/j.envsoft.2012.09.005.

Cassee, F., Héroux, M., Gerlofs-Nijland, M., & Kelly, F. (2013). Particulate matter beyond mass: Recent health evidence on the role of fractions, chemical constituents and sources of emission. *Inhalation Toxicology*, *25*(14), 802–812. https://doi.org/10.3109/08958378.2013.850127.

Chan, Y., Wang, B., Chen, H., Fai Ho, K., Cao, J., Hai, G., Herbert, C., Thomas, P.S., Saad, S., & Gregory George Oliver, B. (2019). www.physiology.org/journal/ajplung

Chatterjee, N., & Flury, M. (2013). Effect of particle shape on capillary forces acting on particles at the air–water interface. Langmuir, 29, 7903–7911. DOI: 10.1021/la4017504

Chen, W., Tang, H., & Zhao, H. (2015). Diurnal, weekly, and monthly spatial variations of air pollutants and air quality of Beijing. *Atmospheric Environment*, 119, 21–34. https://doi.org/10.1016/j.atmosenv.2015.08.040.

Chen, Y., Fan, Y., Huang, Y., Liao, X., Xu, W., & Zhang, T. (2024). A comprehensive review of toxicity of coal fly ash and its leachate in the ecosystem. *Ecotoxicology and Environmental Safety*, *269*, 115905. https://doi.org/10.1016/j.ecoenv.2023.115905.

Chen, Y., Shah, N., Huggins, F., Huffman, G., Linak, W., & Miller, C. (2004). Investigation of primary fine particulate matter from coal combustion by computer-controlled scanning electron microscopy. *Fuel Processing Technology*, *85*(6–7), 743–761. https://doi.org/10.1016/j.fuproc.2003.11.017.

Cheng, W., Weng, L.T., Li, Y., Lau, A., Chan, C.K., & Chan, C.M. (2013). Surface chemical composition of size-fractionated urban walkway aerosols determined by x-ray photoelectron spectroscopy. Aerosol Sci. Technol., 47, 1118–1124. DOI:10.1080/02786826.2013.824066

Cheng, Y., Ermolieva, T., Cao, G., & Zheng, X. (2018). Health impacts of exposure to gaseous pollutants and particulate matter in Beijing—A non-linear analysis based on the new evidence. *International Journal of Environmental Research and Public Health*, *15*(9). https://doi.org/10.3390/ijerph15091969.

Chin, Y., De Pretto, L., Thuppil, V., & Ashfold, M. (2019). Public awareness and support for environmental protection–A focus on air pollution in peninsular Malaysia. *PLoS ONE*, *14*(3). https://doi.org/10.1371/journal.pone.0212206.

China, S., Salvadori, N., & Mazzoleni, C. (2014). Effect of traffic and driving characteristics on morphology of atmospheric soot particles at freeway on-ramps. *Environmental Science & Technology*, *48*(6), 3128–3135. https://doi.org/10.1021/es405178n.

Chuang, K.J., Yan, Y.H., Chiu, S.Y., Cheng, T.J. (2011). Long-term air pollution exposure and risk factors for cardiovascular diseases among the elderly in Taiwan. Occup. Environ. Med. 68, 64–68. DOI: 10.1136/oem.2009.052704

Cichowicz, R., Wielgosiński, G., & Fetter, W. (2017). Dispersion of atmospheric air pollution in summer and winter season. Environmental Monitoring Assessment, 189, 605. https://doi.org/10.1007/s10661-017-6319-2.

Climate Data. (2023). Data and graphs for weather and climate in Astana. Astana climate: Weather Astana & temperature by month. https://en.climate-data.org/asia/kazakhstan/astana/astana-491/.

Colombo, C., Monhemius, A., & Plant, J. (2008). Platinum, palladium and rhodium release from vehicle exhaust catalysts and road dust exposed to simulated lung fluids. *Ecotoxicology and Environmental Safety*, *71*(3), 722–730. https://doi.org/10.1016/j.ecoenv.2007.11.011.

Cortese, A., Lova, L., Comoli, P., Volpe, E., Villa, S., Mallucci, G., La Salvia, S., Romani, A., Franciotta, D., & Bollati, V., et al. (2020). Air pollution as a contributor to the inflammatory activity of multiple sclerosis. J. Neuroinflamm., 17. DOI: 10.1186/s12974-020-01977-0

Coufalík, P., Mikuška, P., Matoušek, T., & Večeřa, Z. (2016). Determination of the bioaccessible fraction of metals in urban aerosol using simulated lung fluids. *Atmospheric Environment*, *140*, 469–475. https://doi.org/10.1016/j.atmosenv.2016.06.031.

Cuccia, E., Massabò, D., Ariola, V., Bove, M. C., Fermo, P., Piazzalunga, A., & Prati, P. (2013). Size-resolved comprehensive characterization of airborne particulate matter. Atmospheric Environment, 67, 14–26. https://doi.org/10.1016/j.atmosenv.2012.10.045

Darynova, Z., Torkmahalleh, M., Abdrakhmanov, T., Sabyrzhan, S., Sagynov, S., Hopke, P., & Kushta, J. (2020). SO_2 and HCHO over the major cities of Kazakhstan from 2005 to 2016: Influence of political, economic and industrial changes. Scientific Reports, 10, 12635. https://doi.org/10.1038/s41598-020-69344-w.

Davies, N., & Feddah, M. (2003). A novel method for assessing dissolution of aerosol inhaler products. *International Journal of Pharmaceutics*, *255*(1–2), 175–187. https://doi.org/10.1016/S0378-5173(03)00091-7.

de Kok, T., Driece, H., Hogervorst, J., & Briedé, J. (2006). Toxicological assessment of ambient and traffic-related particulate matter: A review of recent studies. *Mutation Research/Reviews in Mutation Research*, *613*(2–3), 103–122. https://doi.org/10.1016/j.mrrev.2006.07.001.

de Kok, T.M.C.M., Driece, H.A.L., Hogervorst, J.G.F., Briedé, J.J. (2006). Toxicological assessment of ambient and traffic-related particulate matter: A review of recent studies. Mutat. Res. Rev. Mutat. Res. 613, 103–122. DOI: 10.1016/j.mrrev.2006.07.001

de Miranda, R., de Fatima Andrade, M., Dutra Ribeiro, F., Mendonça Francisco, K., & Pérez-Martínez, P. (2018). Source apportionment of fine particulate matter by positive matrix factorization in the metropolitan area of São Paulo, Brazil. *Journal of Cleaner Production*, 202, 253–263. https://doi.org/10.1016/j.jclepro.2018.08.100.

Deary, M., Amaibi, P., Dean, J., & Entwistle, J. (2021). New insights into health risk assessments for inhalational exposure to metal(-loid)s: The application of aqueous chemistry modeling in understanding bioaccessibility from airborne particulate matter. *Geosciences (Switzerland)*, *11*(2), 1–16. https://doi.org/10.3390/geosciences11020047.

Do Nascimento, F. S., Losno, R., Colin, J. L., De Mello, W. Z., & Da Silva, H. E. (2011). Atmospheric total suspended particulate trace element identification by XRF at Ilha Grande, State of Rio de Janeiro, Brazil. Water, Air, & Soil Pollution, 214, 525–538. DOI:10.1007/s11270-010-0443-8

Dourado, T.A., Gemeiner, H., Gomes, A.C.F., Almeida, E., da Silva, A.C., Valadão, N., & Menegário, A.A. (2020). Elemental Composition of Particulate Matter in the Southeastern Brazilian Ceramic Pole by Synchrotron Radiation X-ray Fluorescence Technique (SR-XRF). J. Braz. Chem. Soc., 31, 1203–1215. https://doi.org/10.21577/0103-5053.20200006

Dunlap, R., & York, R. (2016). The globalization of environmental concern and the limits of the postmaterialist values explanation: Evidence from four multinational surveys. *The Sociological Quarterly*, *49*(3), 529–563. https://doi.org/10.1111/j.1533-8525.2008.00127.x.

Dutta, A., & Jinsart, W. (2021). Risks to health from ambient particulate matter (PM2.5 and PM10) to the residents of an Indian City: An analysis of prediction model. *Human and Ecological Risk Assessment: An International Journal, 27,* 1094–1111. https://doi.org/10.1080/10807039.2020.1807902.

Elmes, M., & Gasparon, M. (2017). Sampling and single particle analysis for the chemical characterisation of fine atmospheric particulates: A review. J. Environ. Manag. 202, 137–150.

Enebish, T., Chau, K., Jadamba, B., & Franklin, M. (2020). Predicting ambient $PM_{2.5}$ concentrations in Ulaanbaatar, Mongolia with machine learning approaches. *Journal of exposure science & environmental epidemiology, 31*, 699–708. https://doi.org/10.1038/s41370-020-0257-8.

Engelbrecht, J. P., Stenchikov, G., Jish Prakash, P., Lersch, T., Anisimov, A., & Shevchenko, I. (2017). Physical and chemical properties of deposited airborne particulates over the Arabian Red Sea coastal plain. Atmospheric Chemistry and Physics, 17, 11467–11490. https://doi.org/10.5194/acp-17-11467-2017

Esmaeilirad, S., Lai, A., Abbaszade, G., Schnelle-Kreis, J., Zimmermann, R., Uzu, G., Daellenbach, K., Canonaco, F., Hassankhany, H., Arhami, M., et al. (2020). Source apportionment of fine particulate matter in a Middle Eastern Metropolis, Tehran-Iran, using PMF with organic and inorganic markers. Sci. Total Environ., 705. DOI: 10.1016/j.scitotenv.2019.135330

Espinosa, A. A., Miranda, J., Hernández, E., Reyes, J., Alarcón, A. L., Torres, M. C., & Sosa, R. (2019). Temporal variation of suspended particles (TSP, PM10, and PM2.5) and chemical composition of PM10 in a site at the coast of the Gulf of Mexico. Air Quality, Atmosphere & Health, 12, 1267–1277. DOI:10.1007/s11869-019-00730-8

Expósito, A., Markiv, B., Ruiz-Azcona, L., Santibáñez, M., & Fernández-Olmo, I. (2021). Understanding how methodological aspects affect the release of trace metal(loid)s from urban dust in inhalation bioaccessibility tests. *Chemosphere*, *267*, 129181. https://doi.org/10.1016/j.chemosphere.2020.129181.

Fakhri, Y., Mousavi Khaneghah, A., Conti, G. O., Ferrante, M., Khezri, A., Darvishi, A., Ahmadi, M., Hasanzadeh, V., Rahimizadeh, A., Keramati, H., et al. (2018). Probabilistic risk assessment (Monte Carlo simulation method) of Pb and Cd in the onion bulb (Allium cepa) and soil of Iran. Environmental Science and Pollution Research, 25(31), 30894–30906. DOI: 10.1007/s11356-018-3081-0

Fallahzadeh, R. A., Khosravi, R., Dehdashti, B., Ghahramani, E., Omidi, F., Adli, A., & Miri, M. (2018). Spatial distribution variation and probabilistic risk assessment of exposure to chromium in ground water supplies; a case study in the east of Iran. Food and Chemical Toxicology, 115, 260–266. DOI: 10.1016/j.fct.2018.03.019

Farina, F., Sancini, G., Mantecca, P., Gallinotti, D., Camatini, M., & Palestini, P. (2011). The acute toxic effects of particulate matter in mouse lung are related to size and season of collection. *Toxicology Letters*, *202*(3), 209–217. doi: 10.1016/j.toxlet.2011.01.031.

Feng, X., Shao, L., Xi, C., Jones, T., Zhang, D., & Bérubé, K. (2020). Particle-induced oxidative damage by indoor size-segregated particulate matter from coal-burning homes in the Xuanwei lung cancer epidemic area, Yunnan Province, China. *Chemosphere*, *256*. https://doi.org/10.1016/j.chemosphere.2020.127058.

Figliuzzi, M., Tironi, M., Longaretti, L., Mancini, A., Teoldi, F., Sangalli, F., & Remuzzi, A. (2020). Copper-dependent biological effects of particulate matter produced by brake systems on lung alveolar cells. *Archives of Toxicology*, *94*(9), 2965–2979. https://doi.org/10.1007/s00204-020-02812-4.

Finn, S., & O'Fallon, L. (2017). The emergence of environmental health literacy–from its roots to its potential. *Environ Health Perspectives, 125*(4). https://doi.org/10.1289/ehp.1409337.

Franzin, B. T., Guizellini, F. C., de Babos, D. V., Hojo, O., Pastre, I. A., Marchi, M., Fertonani, F. L., Oliveira CM, R. R. (2020). Characterization of atmospheric aerosol (PM10 and PM2.5) from a medium sized city in São Paulo state, Brazil. Journal of Environmental Science, 89, 238–251. DOI: 10.1016/j.jes.2019.09.014

Freedman, M.A., Baustian, K.J., Wise, M.E., & Tolbert, M.A. (2010). Characterizing the morphology of organic aerosols at ambient temperature and pressure. Anal. Chem., 82, 7965–7972. https://doi.org/10.1021/ac101437w

Fubini, B., & Fenoglio, I. (2007). Toxic potential of mineral dusts. *Elements*, *3*(6), 407–414. DOI:10.2113/GSELEMENTS.3.6.407

Gamble, J. L. (1967). Chemical Anatomy, Physiology and Pathology of Extracellular Fluid: A Lecture Syllabus. Harvard University Press.

Ganyaglo, S. Y., Gibrilla, A., Teye, E. M., Owusu-Ansah, E. D. G. J., Tettey, S., Diabene, P. Y., & Asimah, S. (2019). Groundwater fluoride contamination and probabilistic health risk assessment in fluoride endemic areas of the Upper East Region, Ghana. Chemosphere, 233, 862–872. DOI: 10.1016/j.chemosphere.2019.05.276

Geiger, A. & Cooper, J. (2010) Overview of Airborne Metals Regulations, Exposure Limits, Health Effects, and Contemporary Research. Environmental Protection Agency, Portland, 1–56. https://www3.epa.gov/ttnemc01/prelim/otm31appC.pdf.

Ghadikolaei, M.A., Wei, L., Cheung, C.S., Yung, K.F., & Ning, Z. (2020). Particulate emission and physical properties of particulate matter emitted from a diesel engine fueled with ternary fuel (diesel-biodiesel-ethanol) in blended and fumigation modes. Fuel 263, 116665. https://doi.org/10.1016/j.fuel.2019.116665

González, L. T., Rodríguez, F. E. L., Sánchez-Domínguez, M., Leyva-Porras, C., Silva-Vidaurri, L. G., & Acuna-Askar, K. (2016). Chemical and morphological characterization of TSP and PM2.5 by SEM-EDS, XPS and XRD collected in the metropolitan area of Monterrey, Mexico. Atmospheric Environment, 143, 249–260. https://doi.org/10.1080/02786826.2019.1645292

Gosselin, M., & Zagury, G. (2020). Metal(-loid)s inhalation bioaccessibility and oxidative potential of particulate matter from chromated copper arsenate (CCA)-contaminated soils. *Chemosphere*, *238*. https://doi.org/10.1016/j.chemosphere.2019.124557.

Gowdy, K., & Fessler, M. (2013). Emerging roles for cholesterol and lipoproteins in lung disease. *Pulmonary Pharmacology and Therapeutics*, *26*(4), 430–437. https://doi.org/10.1016/j.pupt.2012.06.002.

Guascito, M.R., Cesari, D., Chirizzi, D., Genga, A., & Contini, D. (2015). XPS surface chemical characterization of atmospheric particles of different sizes. Atmos. Environ., 116, 146–154. https://doi.org/10.1016/j.atmosenv.2015.06.028

Gunchin, G., Manousakas, M., Osan, J., Karydas, A. G., Eleftheriadis, K., Lodoysamba, S., Shagjjamba, D., Migliori, A., Padilla-Alvarez, R., Streli, C., et al. (2019). Three-year long source apportionment study of airborne particles in Ulaanbaatar using X-ray fluorescence and positive matrix factorization. Aerosol and Air Quality Research, 19, 1056–1067. https://doi.org/10.4209/aaqr.2018.09.0351

Guney, M., Bourges, C., Chapuis, R., & Zagury, G. (2017). Lung bioaccessibility of As, Cu, Fe, Mn, Ni, Pb, and Zn in fine fraction (< 20 μm) from contaminated soils and mine tailings. *Science of the Total Environment*, *579*, 378–386. https://doi.org/10.1016/j.scitotenv.2016.11.086.

Guney, M., Chapuis, R., & Zagury, G. (2016). Lung bioaccessibility of contaminants in particulate matter of geological origin. *Environmental Science and Pollution Research*, *23*(24), 24422–24434. https://doi.org/10.1007/s11356-016-6623-3.

Guo, B., Zhang, D., Pei, L., Su, Y., Wang, X., Bian, Y., Zhang, D., Yao, W., Zhou, Z., & Guo, L. (2021). Estimating $PM_{2.5}$ concentrations via random forest method using satellite, auxiliary, and ground-level station dataset at multiple temporal scales across China. *Science of the Total Environment, 778*, 146288. https://doi.org/10.1016/j.scitotenv.2021.146288.

Hair, J., Hult, G., Ringle, C., & Sarstedt, M. (2018). *A primer on Partial Least Squares Structural Equation Modeling (PLS-SEM)*. SAGE Publications, Inc. https://www.pls-sem.net/pls-sem-books/advanced-issues-in-pls-sem/.

Hamdan, N. M., Alawadhi, H., Jisrawi, N., & Shameer, M. (2018). Characterization of fine particulate matter in Sharjah, United Arab Emirates using complementary experimental techniques. Sustainability, 10, 1088. https://doi.org/10.3390/su10041088

Han, D., Shen, H., Duan, W., & Chen, L. (2020). A review on Particulate Matter Removal Capacity by urban forests at different scales. *Urban Forestry and Urban Greening*, *48*, 126565. https://doi.org/10.1016/j.ufug.2019.126565.

Han, Y., Xu, H., Bi, X., Lin, F., Jiao, L., Zhang, Y., & Feng, Y. (2019). The effect of atmospheric particulates on the rainwater chemistry in the Yangtze River Delta, China. *Journal of the Air & Waste Management Association*, *69*(12), 1452–1466. https://doi.org/10.1080/10962247.2019.1674750.

Hao, J., Zhang, F., Chen, D., Liu, Y., Liao, L., Shen, C., Liu, T., Liao, J., & Ma, L.(2019). Association between ambient air pollution exposure and infants small for gestational age in Huangshi, China: A cross-sectional study. Environmental Science Pollution Research, 26, 32029–32039. https://doi.org/10.1007/s11356-019-06268-7.

Haque, E., Jing, X., Bostick, B., & Thorne, P. (2022). *In vitro* and in silico bioaccessibility of urban dusts contaminated by multiple legacy sources of lead (Pb). *Journal of Hazardous Materials Advances*, *8*, 100178. https://doi.org/10.1016/j.hazadv.2022.100178.

Hedberg, Y., Gustafsson, J., Karlsson, H., Möller, L., & Wallinder, I. (2010). Bioaccessibility, bioavailability and toxicity of commercially relevant iron-and chromium-based particles: *in vitro* studies with an inhalation perspective. *Particle and Fibre Toxicology*, *7*(23). http://www.particleandfibretoxicology.com/content/7/1/23.

Hillwalker, W., & Anderson, K. (2014). Bioaccessibility of metals in alloys: Evaluation of three surrogate biofluids. *Environmental Pollution*, *185*, 52–58. https://doi.org/10.1016/j.envpol.2013.10.006.

Hou, W., Huang, Y., Lu, C., Chen, I., Lee, P., Lin, M., Wang, Y., Sulistyorini, L., & Li, C. (2021). A national survey of ambient air pollution health literacy among adult residents of Taiwan. *BMC Public Health*, *21*, 1604. https://doi.org/10.1186/s12889-021-11658-z.

Huang, H., Jiang, Y., Xu, X., & Cao, X. (2018). *In vitro* bioaccessibility and health risk assessment of heavy metals in atmospheric particulate matter from three different functional areas of Shanghai, China. *Science of The Total Environment*, *610–611*, 546–554. https://doi.org/10.1016/j.scitotenv.2017.08.074.

Huang, L., Ou, J., & Gao, J. (2020). Nationwide response to air pollution: Environmental behavior model based on self-identity and social identity process. *The International Journal of Electrical Engineering & Education*, *0*(0). https://doi.org/10.1177/0020720920940604.

Huang, Y.C.T., Karoly, E.D., Dailey, L.A., Schmitt, M.T., Silbajoris, R., Graff, D.W., & Devlin, R. (2011). Comparison of gene expression profiles induced by coarse, fine, and ultrafine particulate matter. J. Toxicol. Environ. Health Part A Curr. Issues 74, 296–312. DOI: 10.1080/15287394.2010.516238

Iordanidis, A., Buckman, J., Triantafyllou, A., & Asvesta, A. (2007). Esem–EDX characterisation of airborne particles from an industrialised area of northern Greece. *Environmental Geochemistry and Health*, *30*(5), 391–405. https://doi.org/10.1007/s10653-007-9124-y.

IPCC. (2013). Climate Change 2013: The Physical Science Basis. Contribution of Working Group I to the Fifth Assessment; Report of the Intergovernmental Panel on Climate Change 2013; Cambridge University Press: Cambridge, UK; New York, NY, USA, 2013; p. 1535.

Jan, R., Roy, R., Bhor, R., Pai, K., & Satsangi, P. (2020). Toxicological screening of airborne particulate matter in atmosphere of Pune: Reactive oxygen species and cellular toxicity. *Environmental Pollution*, *261*. https://doi.org/10.1016/j.envpol.2019.113724.

Jan, R., Roy, R., Bhor, R., Pai, K., & Satsangi, P.G. (2020). Toxicological screening of airborne particulate matter in atmosphere of Pune: Reactive oxygen species and cellular toxicity. Environ. Pollut. 261, 113724. https://doi.org/10.1016/j.envpol.2019.113724

Janjua, S., Powell, P., Atkinson, R., Stovold, E., & Fortescue, R. (2019). Individual-level interventions to reduce personal exposure to outdoor air pollution and their effects on long-term respiratory conditions. *Cochrane Database of Systematic Reviews*, https://doi.org/10.1002/14651858.cd013441.

Jeong, G.Y. (2008). Bulk and single-particle mineralogy of Asian dust and a comparison with its sources oils. J. Geophys. Res. Atmos., 113. DOI:10.1029/2007JD008606

Jeričević, A., Gašparac, G., Mikulec, M., Kumar, P., & Prtenjak, M. (2019). Identification of diverse air pollution sources in a complex urban area of Croatia. *Journal of Environmental Management*, *243*, 67–77. https://doi.org/10.1016/j.jenvman.2019.04.024.

Ji, D., Gao, W., Maenhaut, W., He, J., Wang, Z., Li, J., Du, W., Wang, L., Sun, Y., Xin, J., Hu, B., & Wang, Y. (2019). Impact of air pollution control measures and regional transport on carbonaceous aerosols in fine particulate matter in urban Beijing, China: Insights gained from long-term measurement. *Atmospheric Chemistry and Physics*, *19*(13), 8569–8590. https://doi.org/10.5194/acp-19-8569-2019.

Jia, B., Tian, Y., Dai, Y., Chen, R., Zhao, P., Chu, J., Feng, X., & Feng, Y. (2022). Seasonal variation of dissolved bioaccessibility for potentially toxic elements in size-resolved PM: Impacts of bioaccessibility on inhalable risk and uncertainty. *Environmental Pollution*, *307*. https://doi.org/10.1016/j.envpol.2022.119551.

Jilani, A., Hussain, S.Z., Othman, M.H.D., Zulfiqar, U., Shakoor, M.B., Khan, I.U., & Al-Ghamdi, A.A. (2018). A comprehensive study on the surface chemistry of particulate matter collected from Jeddah, Saudi Arabia. J. Atmos. Chem., 75, 271–283. DOI:10.1007/s10874-018-9376-1

Joharestani, M., Cao, C., Ni, X., Bashir, B., & Talebiesfandarani, S. (2019). $PM_{2.5}$ Prediction Based on Random Forest, XGBoost, and Deep Learning Using Multisource Remote Sensing Data. *Atmosphere*, 10, 373. https://doi.org/10.3390/atmos10070373.

Julien, C., Esperanza, P., Bruno, M., & Alleman, L. (2011). Development of an *in vitro* method to estimate lung bioaccessibility of metals from atmospheric particles. *Journal of Environmental Monitoring*, *13*(3), 621–630. https://doi.org/10.1039/c0em00439a.

Jung, S., Kang, H., Sung, S., & Hong, T. (2019). Health risk assessment for occupants as a decision-making tool to quantify the environmental effects of particulate matter in construction projects. *Building and Environ*ment, 161, 106267. https://doi.org/10.1016/j.buildenv.2019.106267.

Kamšek, A.R. (2020). Transmission Electron Microscopy. Available online: http://matrika.fmf.uni-lj.si/letnik-7/stevilka-2/kamsek.pdf (accessed on 6 March 2022).

Kastury, F., Smith, E., & Juhasz, A. (2017). A critical review of approaches and limitations of inhalation bioavailability and bioaccessibility of metal(-loid)s from ambient particulate matter or dust. *Science of the Total Environment, 574*, 1054–1074. https://doi.org/10.1016/j.scitotenv.2016.09.056.

Katra, I. (2020). Soil erosion by wind and dust emission in semi-arid soils due to agricultural activities. *Agronomy*, *10*(1), 89. https://doi.org/10.3390/agronomy10010089.

Kaur, L., Rishi, M. S., & Siddiqui, A. U. (2020). Deterministic and probabilistic health risk assessment techniques to evaluate non-carcinogenic human health risk (NHHR) due to fluoride and nitrate in groundwater of Panipat, Haryana, India. Environmental Pollution, 259, 113711. DOI: 10.1016/j.envpol.2019.113711

Kazhydromet. (2021). *Monthly climate bulletin*. Retrieved February 20, 2022, from https://www.kazhydromet.kz/ru/ecology/ezhemesyachnyy-informacionnyy-byulleten-o-sostoyanii-okruzhayuschey-sredy.

Kchih, H., Perrino, C., & Cherif, S. (2015). Investigation of desert dust contribution to source apportionment of PM10 and PM2.5 from a southern Mediterranean coast. Aerosol and Air Quality Research, 15, 454–464. https://doi.org/10.4209/aaqr.2014.10.0255

Kelly, F., & Fussell, J. (2012). Size, source and chemical composition as determinants of toxicity attributable to ambient particulate matter. *Atmospheric Environment, 60*, 504–526. https://doi.org/10.1016/j.atmosenv.2012.06.039.

Kerimray, A., Assanov, D., Kenessov, B., & Karaca, F. (2020). Trends and health impacts of major urban air pollutants in Kazakhstan. *Journal of the Air and Waste Management Association*, *70*(11), 1148–1164. https://doi.org/10.1080/10962247.2020.1813837.

Kerimray, A., Baimatova, N., Ibragimova, O. P., Bukenov, B., Kenessov, B., & Plotitsyn, P. (2020). Assessing air quality changes in large cities during COVID-19 lockdowns: The impacts of traffic-free urban conditions in Almaty, Kazakhstan. *Science of The Total Environment*, 730, 139179. https://doi.org/10.1016/j.scitotenv.2020.139179.

Kerimray, A., Bakdolotov, A., Sarbassov, Y., Inglezakis, V., & Poulopoulos, S. (2018). Air pollution in Astana: analysis of recent trends and air quality monitoring system. *Materials Today: Proceedings*, *5*(11), 22749–22758. https://doi.org/10.1016/j.matpr.2018.07.086.

Khan, A., Sharma, S., Chowdhury, K., & Sharma, P. A novel seasonal index–based machine learning approach for air pollution forecasting. (2022). *Environmental Monitoring Assessment, 194*, 429. https://doi.org/10.1007/s10661-022-10092-x.

Kim, E., & Hopke, P. (2004). Comparison between conditional probability function and nonparametric regression for fine particle source directions. *Atmospheric Environment*, *38*(28), 4667–4673. https://doi.org/10.1016/j.atmosenv.2004.05.035.

Kim, K.H., Kabir, E., Kabir, S. (2015). A review on the human health impact of airborne particulate matter. Environ. Int. 74, 136–143. DOI: 10.1016/j.envint.2014.10.005

Kim, S., Kim, T. Y., Yi, S. M., & Heo, J. (2018). Source apportionment of $PM_{2.5}$ using positive matrix factorization (PMF) at a rural site in Korea. *Journal of Environmental Management*, *214*, 325–334. https://doi.org/10.1016/j.jenvman.2018.03.027.

Kim, Y., Kim, J.,& Lee, H. (2011). Burden of disease attributable to air pollutants from municipal solid waste incinerators in Seoul, Korea: A source-specific approach for environmental burden of disease. *Science of the Total Environment, 409*, 2019–2028. https://doi.org/10.1016/j.scitotenv.2011.02.032.

Kisku, G. C., Kumar, V., Sahu, P., Kumar, P., & Kumar, N. (2018). Characterization of coal fly ash and use of plants growing in ash pond for phytoremediation of metals from contaminated agricultural

land. *International Journal of Phytoremediation*, *20*(4), 330–337. https://doi.org/10.1080/15226514.2017.1381942.

Kitanovski, Z., Shahpoury, P., Samara, C., Voliotis, A., & Lammel, G. (2020). Composition and mass size distribution of nitrated and oxygenated aromatic compounds in ambient particulate matter from southern and central Europe-implications for the origin. Atmos. Chem. Phys., 20, 2471–2487.

Kogianni, E., Kouras, A., & Samara, C. (2021). Indoor concentrations of PM2.5 and associated water-soluble and labile heavy metal fractions in workplaces: Implications for inhalation health risk assessment. Environ. Sci. Pollut. Res., 28, 58983–58993. DOI: 10.1007/s11356-019-07584-8

Kolpakova, A., Hovorka, J., & Klán, M. (2017). Pollen characterization in size segregated atmospheric aerosol. IOP Conference Series: Earth and Environmental Science, 95(6), 062001. https://doi.org/10.1088/1755-1315/95/6/062001.

Könczöl, M., Ebeling, S., Goldenberg, E., Treude, F., Gminski, R., Gieré, R., Grobéty, B., Rothen-Rutishauser, B., Merfort, I., & Mersch-Sundermann, V. (2011). Cytotoxicity and genotoxicity of size-fractionated iron oxide (magnetite) in A549 human lung epithelial cells: Role of ROS, JNK, and NF-κB. Chem. Res. Toxicol. 24, 1460–1475.

Könczöl, M., Goldenberg, E., Ebeling, S., Schäfer, B., Garcia-Käufer, M., Gminski, R., Grobéty, B., Rothen-Rutishauser, B., Merfort, I., & Gieré, R., et al. (2012). Cellular uptake and toxic effects of fine and ultrafine metal-sulfate particles in human A549 lung epithelial cells. Chem. Res. Toxicol., 25, 2687–2703. DOI: 10.1021/tx200051s

Kulkarni, P., Sreekanth, V., Upadhya, A., & Gautam, H. (2022). Which model to choose? Performance comparison of statistical and machine learning models in predicting $PM_{2.5}$ from high-resolution satellite aerosol optical depth. *Atmospheric Environment, 282*, 119164. https://doi.org/10.1016/j.atmosenv.2022.119164.

Kumar, P., Kalaiarasan, G., Porter, A.E., Pinna, A., Kłosowski, M.M., Demokritou, P., Chung, K.F., Pain, C., Arvind, D.K., Arcucci, R., et al. (2020). An overview of methods of fine and ultrafine particle collection for physicochemical characterisation and toxicity assessments. Sci. Total Environ. 756, 143553.

Kumar, P., Kalaiarasan, G., Porter, A.E., Pinna, A., Kłosowski, M.M., Demokritou, P., Chung, K.F., Pain, C., Arvind, D.K., Arcucci, R., et al. (2020). An overview of methods of fine and ultrafine particle collection for physicochemical characterisation and toxicity assessments. Sci. Total Environ. 756, 143553. https://doi.org/10.1016/j.scitotenv.2020.143553

Kumar, P., Pirjola, L., Ketzel, M., & Harrison, R. (2013). Nanoparticle emissions from 11 non-vehicle exhaust sources – A review. *Atmospheric Environment*, *67*, 252–277. https://doi.org/10.1016/J.ATMOSENV.2012.11.011.

Landis, M., Patrick Pancras, J., Graney, J., White, E., Edgerton, & E., Legge, A. (2017). Source apportionment of ambient fine and coarse particulate matter at the Fort McKay community site, in the Athabasca Oil Sands Region, Alberta, Canada. *Science of the Total Environment*, *584–585*, 105–117. https://doi.org/10.1016/j.scitotenv.2017.01.110.

Lanzaco, B. L., López, M. L., Olcese, L. E., & Toselli, B. M. (2019). Elemental composition of PM0.25 collected in an urban site of Argentina: A first case study. Spectrochimica Acta Part B: Atomic Spectroscopy, 161, 105712. https://ri.conicet.gov.ar/handle/11336/125581

Laskin, A., Moffet, R.C., & Gilles, M.K. (2019). Chemical Imaging of Atmospheric Particles. Acc. Chem. Res., 52, 3419–3431.

Lee, Y., Lee, P., Choi, S., An, M., Jang, A. (2021). Effects of Air Pollutants on Airway Diseases. *International Journal of Environmental Research and Public Health, 18,* 9905. https://doi.org/10.3390/ijerph18189905. DOI: 10.1021/acs.accounts.9b00396

Levesque, C., Wiseman, C., Beauchemin, S., & Rasmussen, P. (2021). Thoracic fraction (PM_{10}) of resuspended urban dust: Geochemistry, particle size distribution and lung bioaccessibility. *Geosciences (Switzerland)*, *11*(2), 1–18. https://doi.org/10.3390/geosciences11020087.

Li, D., Xu, Y., Zhang, X., Yang, Z., Wang, S., He, Q., & Jia, Z. (2021). Water quality, natural chemical weathering and ecological risk assessment of the contaminated area of vanadium ore in Yinhua River, China: Evidence from major ions and trace elements. *Acta Geochimica*, *41*(1), 84–99. https://doi.org/10.1007/s11631-021-00509-8 .

Li, N., Champion, W., Imam, J., Sidhu, D., Salazar, J., Majestic, B., & Montoya, L. (2018). Evaluation of cellular effects of fine particulate matter from combustion of solid fuels used for indoor heating on the Navajo Nation using a stratified oxidative stress response model. *Atmospheric Environment*, *182*, 87–96. https://doi.org/10.1016/j.atmosenv.2018.03.031.

Li, R., Kou, X., Geng, H., Xie, J., Yang, Z., Zhang, Y., Cai, Z., & Dong, C. (2015). Effect of ambient PM2.5 on lung mitochondrial damage and fusion/fission gene expression in rats. Chem. Res. Toxicol., 28, 408–418.

Li, W., Sun, J., Xu, L., Shi, Z., Riemer, N., Sun, Y., Fu, P., Zhang, J., Lin, Y., Wang, X., Shao, L., Chen, J., Zhang, X., Wang, Z., & Wang, W. (2016). A conceptual framework for mixing structures in individual aerosol particles. *Journal of Geophysical Research*, *121*(22), 13,784–13,798. https://doi.org/10.1002/2016JD025252.

Li, Y., Shao, L., Wang, W., Zhang, M., Feng, X., Li, W., & Zhang, D. (2020). Airborne fiber particles: Types, size and concentration observed in Beijing. *Science of the Total Environment*, *705*, 135967. https://doi.org/10.1016/j.scitotenv.2019.135967.

Li, Z., & Hu, B. (2018). Perceived health risk, environmental knowledge, and contingent valuation for improving air quality: New evidence from the Jinchuan mining area in China. *Economics & Human Biology*, *31*, 54–68. https://doi.org/10.1016/j.ehb.2018.07.007.

Liang, L., Liu, N., Landis, M., Xu, X., Feng, X., Chen, Z., Shang, L., & Qiu, G. (2018). Chemical characterization and sources of $PM_{2.5}$ at 12-h resolution in Guiyang, China. *Acta Geochimica*, *37*(2), 334–345. https://doi.org/10.1007/s11631-017-0248-1.

Lima, R., Carneiro, L., Afonso, J., & Cunha, K. (2013). Evaluation of solubility in simulated lung fluid of metals present in the slag from a metallurgical industry to produce metallic zinc. *Journal of Environmental Science and Health, Part A*, *48*(5), 489–494. https://doi.org/10.1080/10934529.2013.730405.

Lin, C., Lin, R., Chen, P., Wang, P., & De Marcellis-Warin, N.(2018). A global perspective on sulfur oxide controls in coal-heated power plants and cardiovascular disease. Scientific Reports, 8(1). https://doi.org/10.1038/s41598-018-20404-2.

Liu, X., Ouyang, W., Shu, Y., Tian, Y., Feng, Y., Zhang, T., & Chen, W. (2019). Incorporating bioaccessibility into health risk assessment of heavy metals in particulate matter originated from different sources of atmospheric pollution. *Environmental Pollution*, *254*. https://doi.org/10.1016/j.envpol.2019.113113.

Loomis, D., Grosse, Y., Lauby-Secretan, B., El Ghissassi, F., Bouvard, V., Benbrahim-Tallaa, L., Guha, N., Baan, R., Mattock, H., Straif, K. (2013). The carcinogenicity of outdoor air pollution. Lancet Oncol. 14, 1262–1263. DOI: 10.1016/s1470-2045(13)70487-x

Lu, S., Luan, Q., Jiao, Z., Wu, M., Li, Z., Shao, L., & Wang, F. (2007). Mineralogy of inhalable particulate matter (PM10) in the atmosphere of Beijing, China. Water, Air, & Soil Pollution, 186, 129–137. DOI:10.1007/s11270-007-9470-5

Luo, X., Zhao, Z., Xie, J., Luo, J., Chen, Y., Li, H., & Jin, L. (2019). Pulmonary bioaccessibility of trace metals in $PM_{2.5}$ from different megacities simulated by lung fluid extraction and DGT method. *Chemosphere*, *218*, 915–921. https://doi.org/10.1016/j.chemosphere.2018.11.079.

Ly, B., Matsumi, Y., Vu, T., & Sekiguchi, K. (2020). The effects of meteorological conditions and long-range transport on PM2.5 levels in Hanoi revealed from multi-site measurement using compact sensors and machine learning approach. *Journal of Aerosol Science, 152,* 105716. https://doi.org/10.1016/j.jaerosci.2020.105716.

Lyu, M., Ibragimova, N., & Adambekov, D. (2018). Determination of the main indicators of atmospheric air pollution in different districts of Almaty City in connection with the incidence of pulmonary diseases. *Journal of Biotechnology*, *280*. https://doi.org/10.1016/j.jbiotec.2018.06.252

Ma, S., Ren, K., Liu, X., Chen, L., Li, M., Li, X., Yang, J., Huang, B., Zheng, M., & Xu, Z. (2015). Production of hydroxyl radicals from Fe-containing fine particles in Guangzhou, China. Atmos. Environ., 123, 72–78. DOI:10.1016/j.atmosenv.2015.10.057

Maceira, A., Marcé, R.M., & Borrull, F. (2020). Analytical methods for determining organic compounds present in the particulate matter from outdoor air. TrAC Trends Anal. Chem. 122, 115707. DOI:10.1016/j.trac.2019.115707

Mahmoud, M. E., & Tan, J. C. (2017). Metal-organic framework based composites. In Comprehensive Composite Materials II, 525–553. Elsevier: Amsterdam, The Netherlands.

Majumdar, A., Satpathy, J., Kayee, J., & Das, R. (2020). Trace metal composition of rainwater and aerosol from Kolkata, a megacity in eastern India. *SN Applied Sciences*, *2*(12). https://doi.org/10.1007/s42452-020-03933-2.

Malandrino, M., Di Martino, M., Giacomino, A., Geobaldo, F., Berto, S., Grosa, M.M., & Abollino, O. (2013). Temporal trends of elements in Turin (Italy) atmospheric particulate matter from 1976 to 2001. Chemosphere, 90, 2578–2588. DOI: 10.1016/j.chemosphere.2012.10.102

Manisalidis, I., Stavropoulou, E., Stavropoulos, A., & Bezirtzoglou, E. (2020). Environmental and Health Impacts of Air Pollution: A Review. *Frontiers in public health*, *8*, 14. https://doi.org/10.3389/fpubh.2020.00014.

Mateos, R., Oliveira, C. M., Díez-Pascual, A. M., Vera-López, S., San Andrés, M. P., & da Silva, R. J. N. (2020). Impact of recovery correction or subjecting calibrators to sample preparation on

measurement uncertainty: PAH determinations in waters. *Talanta*, *207*, 120274. https://doi.org/10.1016/j.talanta.2019.120274

Mazzei, F., D'Alessandro, A., Lucarelli, F., Nava, S., Prati, P., Valli, G., & Vecchi, R. (2008). Characterization of particulate matter sources in an urban environment. Sci. Total Environ., 401, 81–89. https://doi.org/10.1016/j.scitotenv.2008.03.008

Mbengue, S., Alleman, L., & Flament, P. (2015). Bioaccessibility of trace elements in fine and ultrafine atmospheric particles in an industrial environment. *Environmental Geochemistry and Health*, *37*(5), 875–889. https://doi.org/10.1007/s10653-015-9756-2.

McLean, J., & Bledsoe, B. (1992). Behavior of metals in soils. Report: EPA/540/S-92/018.

Meinhold, J., & Malkus, A. (2005). Adolescent environmental behaviors. *Environment and Behavior*, *37*(4), 511–532. https://doi.org/10.1177/0013916504269665.

Meng, F.; Wang, J.; Li, T.; Fang, C. Pollution Characteristics, Transport Pathways, and Potential Source Regions of PM2.5 and PM10 in Changchun City in 2018. (2020). *Int. J. Environ. Res. Public Health, 17*, 6585. https://doi.org/10.3390/ijerph17186585.

Michael, S., Montag, M., & Dott, W. (2013). Pro-inflammatory effects and oxidative stress in lung macrophages and epithelial cells induced by ambient particulate matter. *Environmental Pollution*, *183*, 19–29. https://doi.org/10.1016/j.envpol.2013.01.026.

Michalski, R. (2016). Principles and Applications of Ion Chromatography. In Application of IC-MS and IC-ICP-MS in Environmental Research; Wiley: Hoboken, NJ, USA. ISBN: 978-1-119-08547-8

Mihajlidi-Zelić, A., Deršek-Timotić, I., Relić, D., Popović, A., & Đorđević, D. (2006). Contribution of marine and continental aerosols to the content of major ions in the precipitation of the Central Mediterranean. *Science of The Total Environment*, *370*(2-3), 441–451. https://doi.org/10.1016/j.scitotenv.2006.07.017.

Miller, S., Anderson, M., Daly, E., & Milford, J. (2002). Source apportionment of exposures to volatile organic compounds. I. Evaluation of receptor models using simulated exposure data. *Atmospheric Environment*, *36*(22), 3629–3641. https://doi.org/10.1016/S1352-2310(02)00279-0.

Mishra, A., Pervez, S., Candeias, C., Verma, M., Bano, S., Dugga, P., Verma, S., Tamrakar, A., Shafi, S., Pervez, Y., & Gupta, V. (2021). Bioaccessibility features of particulate bound toxic elements: Review of extraction approaches, concentrations and Health Risks. *Journal of the Indian Chemical Society*, *98*(11), 100212. https://doi.org/10.1016/j.jics.2021.100212.

Morais, M., Gasparon, M., Delbem, I., Caldeira, C., Freitas, E., Ng, J., & Ciminelli, V. (2019). Gastric/lung bioaccessibility and identification of arsenic-bearing phases and sources of fine surface dust in a gold mining district. *Science of the Total Environment*, *689*, 1244–1254. https://doi.org/10.1016/j.scitotenv.2019.06.394.

Morawska, L., Thai, P., Liu, X., Asumadu-Sakyi, A., Ayoko, G., Bartonova, A., Bedini, A., Chai, F., Christensen, B., & Dunbabin, M. Applications of low-cost sensing technologies for air quality monitoring and exposure assessment: How far have they gone?. (2018). *Environment International, 116,* 286–299. https://doi.org/10.1016/j.envint.2018.04.018.

NAAQS. Ambient Air Quality Standards for SO_2. 2018. Available online: https://www.epa.gov/so2-pollution/primary-national-ambient-air-quality-standard-naaqs-sulfur-dioxide (accessed 20 April 2022).

National Bureau of Statistics and agency for strategic planning and reforms of the Republic of Kazakhstan. (2022). *Demographic Statistics*. The Agency for strategic planning and reforms of the Republic of Kazakhstan. https://taldau.stat.gov.kz/ru/NewIndex/GetIndex/703831?keyword=.

Nazhmetdinova, A., Sarmanbetova, G., & Magai, A. (2018). The characteristics of pollution in the big industrial cities of Kazakhstan by the example of Almaty. *Journal of Environmental Health Science and Engineering*, *16*(1), 81–88. https://doi.org/10.1007/s40201-018-0299-1

Neupane, B. B., Sharma, A., Giri, B., & Joshi, M. K. (2020). Characterization of airborne dust samples collected from core areas of Kathmandu Valley. Heliyon, 6, e03791. https://doi.org/10.1016/j.heliyon.2020.e03791

Nguyen, T., Vuong, Q., Lee, S., Xiao, H., & Choi, S. (2022). Identification of source areas of polycyclic aromatic hydrocarbons in Ulsan, South Korea, using hybrid receptor models and the conditional bivariate probability function. *Environmental Science: Processes and Impacts*, *24*(1), 140–151. https://doi.org/10.1039/d1em00320h.

Niranjan, R., & Thakur, A. K. (2017). The toxicological mechanisms of environmental soot (black carbon) and carbon black: Focus on oxidative stress and inflammatory pathways. *Frontiers in Immunology*, *8*. https://doi.org/10.3389/fimmu.2017.00763.

Niu, X., Ho, K., Hu, T., Sun, J., Duan, J., Huang, Y., Lui, K., & Cao, J. (2019). Characterization of chemical components and cytotoxicity effects of indoor and outdoor fine particulate matter ($PM_{2.5}$) in Xi'an, China. *Environmental Science and Pollution Research*, *26*(31), 31913–31923. https://doi.org/10.1007/s11356-019-06323-3.

Novo-Quiza, N., Sanromán-Hermida, S., Sánchez-Piñero, J., Moreda-Piñeiro, J., Muniategui-Lorenzo, S., & López-Mahía, P. (2023). In-vitro inhalation bioavailability estimation of metal(oid)s in atmospheric particulate matter ($PM_{2.5}$) using simulated alveolar lysosomal fluid: A dialyzability approach. *Environmental Pollution*, *317*, 120761. https://doi.org/10.1016/j.envpol.2022.120761.

Odonkor, S., & Mahami, T. (2020). Knowledge, Attitudes, and Perceptions of Air Pollution in Accra, Ghana: A Critical Survey. *Journal of Environmental and Public Health, 2020*. https://doi.org/10.1155/2020/3657161.

Ogundele, L. T., Owoade, O. K., Hopke, P. K., Olise, F. S. (2017). Heavy metals in industrially emitted particulate matter in Ile-Ife, Nigeria. Environmental Research, 156, 320–325. DOI: 10.1016/j.envres.2017.03.051

Omogbehin, M., & Oluwatimilehin, I. (2022). Changes of water chemistry from rainfall to stream flow in Obagbile catchment, Southwest Nigeria. *Regional Sustainability*, *3*(2), 170–181. https://doi.org/10.1016/j.regsus.2022.07.006.

Orogade, S. A., Owoade, K. O., Hopke, P. K., Adie, D. B., Ismail, A., Okuofu, C. A. (2016). Source apportionment of fine and coarse particulate matter in industrial areas of Kaduna Northern Nigeria. Aerosol and Air Quality Research, 16, 1179–1190. https://doi.org/10.4209/aaqr.2015.11.0636

Owoade, K.O., Hopke, P.K., Olise, F.S., Adewole, O.O., Ogundele, L.T., & Fawole, O.G. (2016). Source apportionment analyses for fine (PM2.5) and coarse (PM2.5–10) mode particulate matter (PM) measured in an urban area in southwestern Nigeria. Atmos. Pollut. Res., 7, 843–857. DOI:10.1016/j.apr.2016.04.006

Pacyna, J., Pacyna, E. G., & Aas, W. (2009). Changes of emissions and atmospheric deposition of Mercury, lead, and Cadmium. *Atmospheric Environment*, *43*(1), 117–127. https://doi.org/10.1016/j.atmosenv.2008.09.066 .

Pardo, M., Qiu, X., Zimmermann, R., & Rudich, Y. (2020). Particulate matter toxicity is nrf2 and mitochondria-dependent: The roles of metals and polycyclic aromatic hydrocarbons. In *Chemical Research in Toxicology, 33*(5), 1110–1120. *American Chemical Society*. https://doi.org/10.1021/acs.chemrestox.0c00007.

Park, S., Im, J., Kim, J., Kim, S. (2022). Geostationary satellite-derived ground-level particulate matter concentrations using real-time machine learning in Northeast Asia. *Environmental Pollution, 306,* 119425. https://doi.org/10.1016/j.envpol.2022.119425.

Paull, B., & Nesterenkp, P.N. (2005). New possibilities in ion chromatography using porous monolithic stationary-phase media. Trends Anal. Chem., 24, 295. DOI:10.1016/j.trac.2004.11.018

Payus, C., Jikilim, C., & Sentian, J. (2020). Rainwater chemistry of acid precipitation occurrences due to long-range transboundary haze pollution and prolonged drought events during Southwest Monsoon season: Climate change driven. *Heliyon*, *6*(9). https://doi.org/10.1016/j.heliyon.2020.e04997.

Pehnec, G., Jakovljevic´, I., Godec, R., Sever Štrukil, Z., Žero, S., Huremovic´, J., & Džepina, K. (2020). Carcinogenic organic content of particulate matter at urban locations with different pollution sources. Sci. Total Environ., 734. DOI:10.1016/j.scitotenv.2020.139414Pelfrêne, A., Cave, M., Wragg, J., & Douay, F. (2017). *In vitro* investigations of human bioaccessibility from reference materials using simulated lung fluids. *International Journal of Environmental Research and Public Health*, *14*(2). https://doi.org/10.3390/ijerph14020112.

Peltier, R., Cromar, K., Ma, Y., Fan, Z., & Lippmann, M. (2011). Spatial and seasonal distribution of aerosol chemical components in New York City: (2) road dust and other tracers of traffic-generated air pollution. *Journal of Exposure Science and Environmental Epidemiology*, *21*(5), 484–494. https://doi.org/10.1038/jes.2011.15.

Popoola, L.T., Adebanjo, S.A., & Adeoye, B.K. (2018). Assessment of atmospheric particulate matter and heavy metals: A critical review. Int. J. Environ. Sci. Technol., 15, 935–948.

Prati, P., & Mazzei, F. (2009). Coarse particulate matter apportionment around a steel smelter plant. Journal of the Air & Waste Management Association, 59, 514–519. https://doi.org/10.3155/1047-3289.59.5.514

Priyamvada, H., Singh, R., Akila, M., Ravikrishna, R., Verma, R., & Gunthe, S. (2017). Seasonal variation of the dominant allergenic fungal aerosols – one year study from southern Indian region. Scientific Reports, 7(1). https://doi.org/10.1038/s41598-017-11727-7.

Pulles, T., Denier van der Gon, H., Appelman, W., & Verheul, M. (2012). Emission factors for heavy metals from diesel and petrol used in European vehicles. *Atmospheric Environment*, *61*, 641–651. https://doi.org/10.1016/j.atmosenv.2012.07.022.

Qian, X., Xu, G., Li, L., Shen, Y., He, T., Liang, Y., Yang, Z., Zhou, W., & Xu, J. (2016). Knowledge and perceptions of air pollution in Ningbo, China. *BMC Public Health*, *16*(1). https://doi.org/10.1186/s12889-016-3788-0.

Ramírez, O., Sánchez de la Campa, A., Sánchez-Rodas, D., & de la Rosa, J. (2020). Hazardous trace elements in thoracic fraction of airborne particulate matter: Assessment of temporal variations,

sources, and health risks in a megacity. *Science of the Total Environment*, *710*. https://doi.org/10.1016/j.scitotenv.2019.136344.

Rella, S., & Malitesta, C. (2015). X-ray photoelectron spectroscopy characterization of aerosol particles in Antarctica. Antarctic Science, 27, 493–499. DOI: https://doi.org/10.1017/S0954102015000176

Ren, H., Lu, J., Ning, J., Su, X., Tong, Y., Chen, J., & Ding, Y. (2020). Exposure to fine particulate matter induces self-recovery and susceptibility of oxidative stress and inflammation in rat lungs. Environ. Sci. Pollut. Res. 27, 40262–40276. DOI: 10.1007/s11356-020-10029-2

Ren, H., Yu, Y., & An, T. (2020). Bioaccessibilities of metal(loid)s and organic contaminants in particulates measured in simulated human lung fluids: A critical review. Environmental Pollution, 265, 115070. DOI: 10.1016/j.envpol.2020.115070

Ren, Helong, Yu, Y., & An, T. (2020). Bioaccessibilities of metal(loid)s and organic contaminants in particulates measured in simulated human lung fluids: A critical review. In *Environmental Pollution*, *265*. https://doi.org/10.1016/j.envpol.2020.115070.

Ren, M., Sun, W., & Chen, S. (2021). Combining machine learning models through multiple data division methods for $PM_{2.5}$ forecasting in Northern Xinjiang, China. *Environmental Monitoring Assessment, 193,* 476. https://doi.org/10.1007/s10661-021-09233-5.

Roy, D., Singh, G., & Gosai, N. (2015). Identification of possible sources of atmospheric PM10 using particle size, SEM-EDS and XRD analysis, Jharia Coalfield Dhanbad, India. Environmental Monitoring and Assessment, 187, 680. DOI: 10.1007/s10661-015-4853-3

Roy, R., Jan, R., Gunjal, G., Bhor, R., Pai, K., & Satsangi, P.G. (2019). Particulate matter bound polycyclic aromatic hydrocarbons: Toxicity and health risk assessment of exposed inhabitants. Atmos. Environ., 210, 47–57. DOI:10.1016/j.atmosenv.2019.04.034

Sairanen, M., & Rinne, M. (2019). Dust emission from crushing of hard rock aggregates. *Atmospheric Pollution Research*, *10*(2), 656–664. https://doi.org/10.1016/j.apr.2018.11.007.

Sánchez-Piñero, J., Moreda-Piñeiro, J., Concha-Graña, E., Fernández-Amado, M., Muniategui-Lorenzo, S., & López-Mahía, P. (2021). Inhalation bioaccessibility estimation of polycyclic aromatic hydrocarbons from atmospheric particulate matter (PM_{10}): Influence of PM_{10} composition and Health Risk Assessment. *Chemosphere*, *263*, 127847. https://doi.org/10.1016/j.chemosphere.2020.127847.

Sánchez, E. P., Sánchez-Guijarro, M., Sánchez-Soberón, F., Rovira, J., Sierra, J., Schuhmacher, M., ... Soler, A. (2018). Particulate matter source apportionment in complex urban and industrial cities: The case of Tarragona, Spain. WIT Transactions on Ecology and the Environment, 230, 511–518. https://www.witpress.com/elibrary/wit-transactions-on-ecology-and-the-environment/230/36786

Sara, Y.Y., Rashid, M., Chuah, T.G., Suhaimi, M., & Mohamed, N.N. (2013). Characteristics of airborne Pm2.5 and Pm2.5-10 in the urban environment of Kuala Lumpur. Adv. Mater. Res., 620, 502–510.

Satsangi, P.G., & Yadav, S. (2014). Characterization of PM2.5 by X-ray diffraction and scanning electron microscopy-energy dispersive spectrometer: Its relation with different pollution sources. Int. J. Environ. Sci. Technol., 11, 217–232. DOI 10.1007/s13762-012-0173-0

Schulz, F., Commodo, M., Kaiser, K., DeFalco, G., Minutolo, P., Meyer, G., ... Gross, L. (2019). Insights into incipient soot formation by atomic force microscopy. Proceedings of the Combustion Institute, 37, 885–892. https://doi.org/10.1016/j.proci.2018.06.100

Serikov, D. (2018). *Coal consumption in CHP has increased by 16%.* In business. Retrieved September 24, 2021, from https://inbusiness.kz/ru/last/potreblenie-bogatyrskogo-uglya-na-tec-astany-vyroslo-na-16.

Shao, S., Tian, Z., & Fan, M. (2018). Do the rich have stronger willingness to pay for environmental protection? New evidence from a survey in China. *World Development*, *105*, 83–94. https://doi.org/10.1016/j.worlddev.2017.12.033.

Sharma, S., & Mandal, T. (2017). Chemical composition of fine mode particulate matter ($PM_{2.5}$) in an urban area of Delhi, India and its source apportionment. *Urban Climate*, *21*, 106–122. https://doi.org/10.1016/j.uclim.2017.05.009.

Shaziayani, W., Ul-Saufie, A., Mutalib, S., Noor, N., & Zainordin, N. (2022). Classification Prediction of PM_{10} Concentration Using a Tree-Based Machine Learning Approach. *Atmosphere, 13*, 538. https://doi.org/10.3390/atmos13040538.

Shim, I., Kim, W., Kim, H., Lim, Y., Shin, H., & Park, K. (2021). Comparative cytotoxicity study of PM2.5 and TSP collected from urban areas. *Toxics*, 9(7), 167. https://doi.org/10.3390/toxics9070167.

Sielicki, P., Janik, H., Guzman, A., & Namies´nik, J. (2011). The progress in electron microscopy studies of particulate matters to be used as a standard monitoring method for air dust pollution. Crit. Rev. DOI: 10.1080/10408347.2011.607076

Smith, D. K. (1997). Evaluation of the detectability and quantification of respirable crystalline silica by X-ray powder diffraction methods. Powder Diffraction, 12, 200–227. DOI: https://doi.org/10.1017/S0885715600009775

Soleimani, M., Amini, N., Sadeghian, B., Wang, D., & Fang, L. (2018). Heavy metals and their source identification in particulate matter ($PM_{2.5}$) in Isfahan City, Iran. *Journal of Environmental Sciences (China)*, *72*, 166–175. https://doi.org/10.1016/j.jes.2018.01.002.

Song, D., & Yang, C. (2011). Geochemistry and source apportionment of atmospheric particulate matter in Jiaozuo City. *Applied Mechanics and Materials*, *71–78*, 2867–2872. https://doi.org/10.4028/www.scientific.net/AMM.71-78.2867.

Song, D., & Yang, C. (2011). Geochemistry and source apportionment of atmospheric particulate matter in Jiaozuo City. Appl. Mech. Mater., 71–78, 2867–2872.

Song, J., & Peng, P. (2009). Surface characterization of aerosol particles in Guangzhou, China: A study by XPS. Aerosol Sci. Technol., 43, 1230–1242. https://doi.org/10.1080/02786820903325394

Sooktawee, S., Kanabkaew, T., Boonyapitak, S., Patpai, A., & Piemyai, N. (2020). Characterising particulate matter source contributions in the pollution control zone of mining and related industries using bivariate statistical techniques. *Scientific Reports*, *10*(1). https://doi.org/10.1038/s41598-020-78445-5.

Sudarmadi, S., Suzuki, S., Kawada, T., Netti, H., Soemantri, S., & Tri Tugaswati, A. (2001). A Survey of perception, knowledge, awareness, and attitude in regard to environmental problems in a sample of two different social groups in Jakarta, Indonesia. *Environment, Development and Sustainability*, *3*(2), 169–183. https://doi.org/10.1023/a:1011633729185.

Tabernero, C., Hernández, B., Cuadrado , E., Luque, B., Pereira, C. (2015). A multilevel perspective to explain recycling behaviour in communities. *Journal of Environmental Management, 159,* 192–201. https://doi.org/10.1016/j.jenvman.2015.05.024.

Tang, C. Y., & Yang, Z. (2017). Transmission Electron Microscopy (TEM). In Membrane Characterization, 145–159. Elsevier Inc.: Amsterdam, The Netherlands. DOI:10.1016/B978-0-444-63776-5.00008-5

Tang, Z., Hu, X., Chen, Y., Qiao, J., & Lian, H. (2019). Assessment of in vitro inhalation bioaccessibility of airborne particle-bound potentially toxic elements collected using quartz and PTFE filter. Atmospheric Environment, 196, 118–124. https://doi.org/10.1016/j.atmosenv.2018.09.045

The World Bank. (2021). (rep.). *Cost-Effective Air Quality Management in Kazakhstan and Its Impact on Greenhouse Gas Emissions*, (Report No. AUS0002588). International Bank for Reconstruction and Development. https://documents1.worldbank.org/curated/en/099345012232191779/pdf/P1708700d2bd3a09093fa0cd27991d0662.pdf.

Thongthammachart, T., & Jinsart, W. (2019). Estimating $PM_{2.5}$ concentrations with statistical distribution techniques for health risk assessment in Bangkok. *Human and Ecological Risk Assessment: An International Journal*, 26, 1848–1863. https://doi.org/10.1080/10807039.2019.1613630.

Tian, H., Lu, L., Cheng, K., Hao, J., Zhao, D., Wang, Y., Jia, W., & Qiu, P. (2012). Anthropogenic atmospheric nickel emissions and its distribution characteristics in China. Science of The Total Environment, 417-418, 148–157. https://doi.org/10.1016/j.scitotenv.2011.11.069.

Tudu, P., Gaine, T., Mahanty, S., Mitra, S., Bhattacharyya, S., & Chaudhuri, P. (2022). Impact of covid‐19 lockdown on the elemental profile of PM10 present in the ambient aerosol of an educational institute in Kolkata, India. *Environmental Quality Management*, *32*(3), 79–96. https://doi.org/10.1002/tqem.21862.

U.S. EPA. (2010). *Environmental Protection Agency 40 CFR Parts 50 and 58 Primary National Ambient Air Quality Standards for Nitrogen Dioxide; Final Rule*. http://www.regulations.gov

U.S. EPA. (2019a). Regional Screening Levels (RSLs)-Generic Tables. *National Center for Environmental Assessment c/o-Risk Website. https://www. epa. gov/risk/regional-screening-levels-rsls-users-guide# special*.

U.S. EPA. (2019b). Regional Screening Levels (RSLs)-User's Guide. *National Center for Environmental Assessment c/o-Risk Website. https://www. epa. gov/risk/regional-screening-levels-rsls-users-guide# special*.

U.S. EPA. (2021). *Particulate Matter (PM) Pollution. EPA*. Retrieved February 20, 2022, from https://www.epa.gov/pm-pollution/particulate-matter-pm-basics#PM.

Ul-Saufie, A., Yahaya, A., Ramli, N., & Hamid, H. (2012). Performance of Multiple Linear Regression Model for Long-term PM_{10} Concentration Prediction Based on Gaseous and Meteorological Parameters. *Journal of Applied Sciences, 12,* 1488–1494. https://doi.org/10.3923/jas.2012.1488.14.94.

Uria-Tellaetxe, I., & Carslaw, D. C. (2014). Conditional bivariate probability function for source identification. *Environmental Modelling and Software*, *59*, 1–9. https://doi.org/10.1016/j.envsoft.2014.05.002.

Vardoulakis, S., Giagloglou, E., Steinle, S., Davis, A., Sleeuwenhoek, A., Galea, K.S., Dixon, K., & Crawford, J.O. (2020). Indoor exposure to selected air pollutants in the home environment: A systematic review. Int. J. Environ. Res. Public Health, 17, 8972. DOI: 10.3390/ijerph17238972

Vargas Buonfiglio, L., & Comellas, A. (2020). Mechanism of ambient particulate matter and respiratory infections. In *Journal of Thoracic Disease, 12*(3), 134–136. AME Publishing Company. https://doi.org/10.21037/jtd.2019.12.33.

Vattanasit, U., Navasumrit, P., Khadka, M. B., Kanitwithayanun, J., Promvijit, J., Autrup, H., Ruchirawat, M. (2014). Oxidative DNA damage and inflammatory responses in cultured human cells and in humans exposed to traffic-related particles. International Journal of Hygiene and Environmental Health, 217, 23–33. DOI: 10.1016/j.ijheh.2013.03.002

Vicente, P., Marques, C., & Reis, E. (2021). Willingness to pay for environmental quality: The effects of pro-environmental behavior, perceived behavior control, environmental activism, and educational level. *SAGE Open*, *11*(4). https://doi.org/10.1177/21582440211025256.

Wang, F., Liu, J., & Zeng, H. (2020). Interactions of particulate matter and pulmonary surfactant: Implications for human health. Adv. Colloid Interface Sci., 284, 102244. doi: 10.1016/j.cis.2020.102244

Wang, S., Hu, G., Yu, R., Shen, H., & Yan, Y. (2021). Bioaccessibility and source-specific health risk of heavy metals in PM2.5 in a coastal city in China. *Environmental Advances*, *4*, 100047. https://doi.org/10.1016/j.envadv.2021.100047 .

Wang, W., Lin, Y., Yang, H., Ling, W., Liu, L., Zhang, W., Lu, D., Liu, Q., & Jiang, G. (2022). Internal exposure and distribution of airborne fine particles in the human body: Methodology, current understandings, and research needs. Environmental Science & Technology, 56(12), 6857–6869.

Wang, Xiaochen, Wang, Y., Guo, F., Wang, D., & Bai, Y. (2020). Physicochemical characteristics of particulate matter emitted by diesel blending with various aromatics. *Fuel*, *275*. https://doi.org/10.1016/j.fuel.2020.117928.

WHO. (2000). Chapter 5.5 Carbon Monoxide-World Health Organization. Available online: https://www.euro.who.int/__data/assets/pdf_file/0020/123059/AQG2ndEd_5_5carbonmonoxide.PDF (accessed on 20 February 2022).

WHO. (2000). *Chapter 5.5 Carbon Monoxide - World Health Organization*. Retrieved February 20, 2022, from https://www.euro.who.int/__data/assets/pdf_file/0020/123059/AQG2ndEd_5_5carbonmonoxide.PDF.

WHO. (2006). *WHO Air quality guidelines for particulate matter, ozone, nitrogen dioxide and sulfur dioxide.* Retrieved February 20, 2022, from http://apps.who.int/iris/bitstream/handle/10665/69477/WHO_SDE_PHE_OEH_06.02_eng.pdf?sequence=1.

WHO. (2006). WHO Air Quality Guidelines for Particulate Matter, Ozone, Nitrogen Dioxide and Sulfur Dioxide. Available online: http://apps.who.int/iris/bitstream/handle/10665/69477/WHO_SDE_PHE_OEH_06.02 eng.pdf?sequence=1 (accessed on 20 Feb- ruary 2022).

WHO. (2016). *WHO releases country estimates on air pollution exposure and Health Impact*. World Health Organization. Retrieved October 3, 2022, from https://www.who.int/news/item/27-09-2016-who-releases-country-estimates-on-air-pollution-exposure-and-health-impact.

WHO. (2016c). Ambient air pollution: A global assessment of exposure and burden of disease. Clean Air J. 26, 6. https://doi.org/10.17159/2410-972x/2016/v26n2a4.

WHO. (2018). World Health Organization. Ambient Air Pollution: Health Impacts. Available online: https://www.who.int/news- room/fact-sheets/detail/ambient-(outdoor)-air-quality-and-health (accessed on 19 February 2022).

WHO. (2020). Health impact assessment of air pollution: AirQ+ life table manual. WHO Regional Office for Europe. License: CC BY- NC-SA 3.0 IGO. Available online: https://apps.who.int/iris/bitstream/handle/10665/337683/WHO-EURO-2020-1559-41310-56212-eng.pdf?sequence=1&isAllowed=y (accessed on 13 April 2022).

WHO. (2022). (rep.). *WHO ambient air quality database* (1–28). Geneva, Switzerland.

Wiseman, C. L. S. (2015). Analytical methods for assessing metal bioaccessibility in airborne particulate matter: A scoping review. Analytica Chimica Acta, 877, 9–18. DOI: 10.1016/j.aca.2015.01.024

Wu, D., Li, Q., Ding, X., Sun, J., Li, D., Fu, H., Teich, M., Ye, X., & Chen, J. (2018). Primary Particulate Matter Emitted from Heavy Fuel and Diesel Oil Combustion in a Typical Container Ship: Characteristics and Toxicity. *Environmental Science and Technology*, *52*(21), 12943–12951. https://doi.org/10.1021/acs.est.8b04471.

Xiao, Z., Shao, L., Zhang, N., Wang, J., Chuang, H. C., Deng, Z., Wang, Z., & BéruBé, K. (2014). A toxicological study of inhalable particulates in an industrial region of Lanzhou City, northwestern China: Results from plasmid scission assay. *Aeolian Research*, *14*, 25–34. https://doi.org/10.1016/j.aeolia.2014.03.004.

Xie, W., You, J., Zhi, C., & Li, L. (2021). The toxicity of ambient fine particulate matter (PM2.5) to Vascular Endothelial Cells. *Journal of Applied Toxicology*, *41*(5), 713–723. https://doi.org/10.1002/jat.4138.

Xu, P., Xu, J., He, M., Song, L., Chen, D., Guo, G., & Dai, H. (2016). Morphology and chemical characteristics of micro- and Nano-particles in the haze in Beijing studied by XPS and TEM/EDX. Sci. Total Environ., 565, 827–832. DOI: 10.1016/j.scitotenv.2016.03.042

Xue, J., Hu, S., Quiros, D., Ayala, A., & Jung, H. (2019). How do particle number, surface area, and mass correlate with toxicity of diesel particle emissions as measured in chemical and cellular assays? *Chemosphere*, *229*, 559–569. https://doi.org/10.1016/j.chemosphere.2019.05.010.

Yadav, I., & Devi, N. (2019). Biomass Burning, Regional Air Quality, and Climate Change. *Encyclopedia of Environmental Health*, 386–391. https://doi.org/10.1016/B978-0-12-409548-9.11022-X.

Yang, C., Jiang, L., Zhang, H., Shimoda, L. A., Deberardinis, R. J., Semenza, G. L. (2014). Analysis of hypoxia-induced metabolic reprogramming. Methods in Enzymology, 542, 425–455. DOI: 10.1016/B978-0-12-416618-9.00022-4

Yang, J., Huo, T., Zhang, X., Ma, J., Wang, Y., Dong, F., & Deng, J. (2018). Oxidative stress and cell cycle arrest induced by short-term exposure to dustfall $PM_{2.5}$ in A549 cells. *Environmental Science and Pollution Research*, *25*(23), 22408–22419. https://doi.org/10.1007/s11356-017-0430-3.

Yang, J., Huo, T., Zhang, X., Ma, J., Wang, Y., Dong, F., Deng, J. (2018). Oxidative stress and cell cycle arrest induced by short-term exposure to dustfall PM2.5 in A549 cells. Environ. Sci. Pollut. Res. 25, 22408–22419. DOI: 10.1007/s11356-017-0430-3

Yang, Q., & Wu, S. (2019). How social media exposure to health information influences Chinese people's health-protective behavior during air pollution: A theory of planned behavior perspective. *Health Communication*, *36*(3), 324–333. https://doi.org/10.1080/10410236.2019.1692486.

Yang, S., Wang, X., Guo, H., Liu, J. & Wang, J. (2019). The Development and Application of the "DALY"-Based Environmental Risk Assessment Methods with a Case Study on the Impact of $PM_{2.5}$ in Beijing. IOP Conf. Series Mater. Sci. Eng., 484, 012055. https://doi.org/10.1088/1757-899x/484/1/012055.

Yao, L., Lu, N., Yue, X., Du, J., & Yang, C. (2015). Comparison of Hourly $PM_{2.5}$ Observations Between Urban and Suburban Areas in Beijing, China. International Journal of Environmental Research and Public Health*, 12,* 12264–12276. https://doi.org/10.3390/ijerph121012264.

Zeng, J., Ge, X., Wu, Q., & Zhang, S. (2021). Three-Year Variations in Criteria Atmospheric Pollutants and Their Relationship with Rainwater Chemistry in Karst Urban Region, Southwest China. *Atmosphere*, *12*, 1073. https://doi.org/10.3390/atmos12081073.

Zhai, Y., Fu, Z., Wang, L., Zeng, G., Li, C., Chen, H., ... Lu, P. (2012). Characteristic, composition, and sources of TSP investigated by HRTEM/EDS and ESEM/EDS. Environmental Monitoring and Assessment, 184, 6693–6707. DOI: 10.1007/s10661-011-2452-5

Zhang, R., Liu, C., Zhou, G., Sun, J., Liu, N., & Hsu, P. (2018). Morphology and property investigation of primary particulate matter particles from different sources. *Nano Research*, *11*(6), 3182–3192. https://doi.org/10.1007/s12274-017-1724-y.

Zheng, L., Lin, R., Wang, X., & Chen, W. The Development and Application of Machine Learning in Atmospheric Environment Studies. (2021). *Remote Sensing, 13*, 4839. https://doi.org/10.3390/rs13234839.

Zhong, Q., Tong, D., Crosson, C., & Zhang, Y. (2022). A GIS-based approach to assessing the capacity of rainwater harvesting for addressing outdoor irrigation. *Landscape and Urban Planning*, *223*, 104416. https://doi.org/10.1016/j.landurbplan.2022.104416.

Zierold, K. M., & Odoh, C. (2020). A review on fly ash from coal-heated power plants: Chemical Composition, regulations, and Health Evidence. *Reviews on Environmental Health*, *35*(4), 401–418. https://doi.org/10.1515/reveh-2019-0039 .

Zou, Y., Jin, C., Su, Y., Li, J., & Zhu, B. (2016). Water soluble and insoluble components of urban PM2.5 and their cytotoxic effects on epithelial cells (A549) in vitro. Environmental Pollution, 212, 627–635.

Appendix A

1) **Analytical Methods for Physicochemical Characterization and Toxicity Assessment of Atmospheric Particulate Matter: A Review** (Agibayeva, A.; Guney, M.; Karaca, F.; Kumisbek, A.; Kim, J.R.; Avcu, E.)

Sustainability,
Impact Factor 3.9, CiteScore 5.8, Q1
Volume 4,
2022,
13481,
https://doi.org/10.3390/su142013481.

2) **An Air Quality Modeling and Disability-Adjusted Life Years (DALY) Risk Assessment Case Study: Comparing Statistical and Machine Learning Approaches for $PM_{2.5}$ Forecasting** (Agibayeva, A.; Khalikhan, R.; Guney, M.; Karaca, F.; Torezhan, A.; Avcu, E.)

Sustainability,
Impact Factor 3.9, CiteScore 5.8, Q1
Volume 14,
2022,
16641,
https://doi.org/10.3390/su142416641.

3) **Annual and periodic variations of particulates and selected gaseous pollutants in Astana, Kazakhstan: Source identification via conditional bivariate probability function** (Agibayeva, A.; Karaca, F.; Guney, M.; Bex,T.; Avcu, E.)

Aerosol Science and Engineering,
Impact Factor 1.5, Q3,
2023,
Volume 7,
https://doi.org/10.1007/s41810-023-00194-5.

Appendix B

The survey questionnaire:

1. What is your age?
   [ ] less than 18
   [ ] 18-24
   [ ] 25-34
   [ ] 35-44
   [ ] 45-54
   [ ] 55-64
   [ ] 65+

2. What is your gender?
   [ ] Male
   [ ] Female
   [ ] Prefer not to answer

3. What is your highest qualification?
   [ ] Secondary school degree
   [ ] High school degree
   [ ] Specialized secondary education
   [ ] Bachelor's degree
   [ ] Master's degree or above

4. What is your current employment status?
   [ ] Full-time employment
   [ ] Part-time employment
   [ ] Self-employed
   [ ] Unemployed
   [ ] Student
   [ ] Retired

5. What is the environment that you spend most of your day in?
   [ ] Environment where air quality is not a concern (e.g., school office)
   [ ] Industrial environment where air quality is a concern (e.g., metal workshops, heating, and power plants, etc.)
   [ ] Urban environment where air quality is a concern (e.g., highway toll collection, truck driver, taxi driver, etc.)
   [ ] Another environment where air quality is a concern (please specify)
   [ ] Not working
   [ ] Home environment

6. What is your average monthly household income?
   [ ] <100,000 KZT
   [ ] 100,000-250,000 KZT
   [ ] 250,001-500,000 KZT
   [ ] 500,001-1,000,000 KZT
   [ ] >1,000,000 KZT

7. Please indicate if you have the following chronic conditions.

High blood pressure [Yes] [No]
Cardiovascular conditions [Yes] [No]
Diabetes [Yes] [No]
Asthma [Yes] [No]
Chronic Obstructive Pulmonary Disease (COPD) [Yes] [No]

8. Overall, how would you rate the atmospheric condition at the region you live in?
   [ ] Highly polluted
   [ ] Moderately polluted and causes harm
   [ ] Moderately polluted but causes no harm
   [ ] Not polluted at all

9. What is your source of information about air quality and air pollution-related topics? (Select all that apply)
   [ ] Online media (e.g., social networks, websites)
   [ ] Printed media (e.g., books, brochures, magazines)
   [ ] Friends and Family
   [ ] Scientific Journals
   [ ] TV

10. Please select all that you think contributes to ambient air pollution.
    [ ] Industrial emissions
    [ ] Motor vehicle emissions
    [ ] Coal burnings
    [ ] Woodburning
    [ ] Construction and Demolition
    [ ] Wildfires
    [ ] Wind-blown dust
    [ ] Power/heating plants

Below are a number of statements. Please select whether you believe the statement is more likely to be TRUE or FALSE. If you really have no idea, only then you can proceed to choose I don't know.

11. The National Hydrometeorological Service of Kazakhstan "Kazhydromet" measures ambient air quality continuously in Nur-Sultan
    [ ] True [ ] False [ ] I don't know.

12. Nur-Sultan is currently ranked the number one most polluted city in the country according to the Air Pollution Index (API)
    [ ] True [ ] False [ ] I don't know.

13. The major cause of respiratory and cardiovascular conditions is air pollution.
    [ ] True [ ] False [ ] I don't know

14. Nitrogen oxides (NO_x) which are serious air pollutants are mainly emitted by vehicles.
    [ ] True [ ] False [ ] I don't know

15. Poor air quality with an Air Pollution Index (API) of 100 is not likely to cause adverse human health effects to the general public.
    [ ] True [ ] False [ ] I don't know

16. Sulfur dioxide (SO_2) which is a serious air pollutant is mainly coming from coal-heated power plants and residential heating.
[ ] True [ ] False [ ] I don't know

Please use the following scale to indicate your level of agreement or disagreement with each statement.

1-Strongly disagree	2-Disagree	3-Neutral	4-Agree	5-Strongly agree

17	Taking care of the environment is something I really care about.	1	2	3	4	5
18	In order to protect the environment, Kazakhstan needs economic growth.	1	2	3	4	5
19	I would contribute part of my income if I were certain that the money would be used to prevent atmospheric pollution.	1	2	3	4	5
20	Nothing can be done by me or my family / friends to improve the current atmospheric situation.	1	2	3	4	5
21	I do not mind an increase in taxes if the extra money is used to prevent further atmospheric pollution.	1	2	3	4	5
22	There is no point in doing what I can for the environment unless everyone does the same.	1	2	3	4	5
23	Air pollution is a fair price to pay for economic development.	1	2	3	4	5
24	Kazakhstan government has to reduce atmospheric pollution, but it should not cost me any money.	1	2	3	4	5
25	The air quality in Kazakhstan is getting better because of modern science and technology	1	2	3	4	5
26	Kazakhstani worry too much about industrial development polluting the atmosphere and degrading human health	1	2	3	4	5
27	Educating the younger generation about the knowledge of environmental protection is important	1	2	3	4	5
28	Protecting the environment should be given priority, even if it causes slower economic growth	1	2	3	4	5
29	I do not mind paying more money to use better quality gasoline which leads to less pollution	1	2	3	4	5
30	The economic growth of Kazakhstan is currently more important than environmental protection	1	2	3	4	5
31	I am willing to accept cuts in my standards of living in order to protect the environment	1	2	3	4	5
32	Air pollution caused by cars is extremely dangerous for health	1	2	3	4	5